Aus dem Institut für Prophylaxe und Epidemiologie der Kreislaufkrankheiten
des Klinikums der Ludwig-Maximilians-Universität München
Direktor: Univ.-Prof. Dr. med. Christian Weber

The regulation of microRNAs and their role in atherosclerosis

Dissertation
zum Erwerb des Doktorgrades der Naturwissenschaften
an der Medizinischen Fakultät der
Ludwig-Maximilians-Universität zu München

vorgelegt von
Dipl.-troph. Petra Hartmann
aus
Illertissen

2016

Gedruckt mit Genehmigung der Medizinischen Fakultät
der Universität München

Betreuerin: Prof. Dr. rer. nat. Sabine Steffens

Zweitgutachter: Prof. Dr. rer. nat. Jürgen Bernhagen

Dekan: Prof. Dr. med. dent. Reinhard Hickel

Tag der mündlichen Prüfung: 25.10.2016

Eidesstattliche Versicherung

Hartmann, Petra

Name, Vorname

Ich erkläre hiermit an Eides statt, dass ich die vorliegende Dissertation mit dem Thema

The regulation of microRNAs and their role in atherosclerosis

selbständig verfasst, mich außer der angegebenen keiner weiteren Hilfsmittel bedient und alle Erkenntnisse, die aus dem Schrifttum ganz oder annähernd übernommen sind, als solche kenntlich gemacht und nach ihrer Herkunft unter Bezeichnung der Fundstelle einzeln nachgewiesen habe.

Ich erkläre des Weiteren, dass die hier vorgelegte Dissertation nicht in gleicher oder in ähnlicher Form bei einer anderen Stelle zur Erlangung eines akademischen Grades eingereicht wurde.

_____ _____

Ort, Datum Unterschrift Doktorandin

Contents

1 Abbreviations

3` UTR	3` untranslated region
AGO	Argonaute
AKT1	Thymoma viral proto-oncogene 1
Apoe	Apolipoprotein e
ATP	Adenosine triphosphate
BCL6	B-cell lymphoma 6
C. elegans	Caenorhabditis elegans
CCL2	C-C motif chemokine 2
CVD	Cardiovascular disease
CX_3CL1	C-X_3-C motif chemokine 1
CXCL1	C-X-C motif chemokine 1
DGCR8	DiGeorge syndrome critical region 8 protein
dsRNA	Double-stranded RNA
EC	Endothelial cell
ER	Endoplasmatic reticulum
GTP	Guanosine triphosphate
HAEC	Human aortic endothelial cell
HIF-1α	Hypoxia-inducible factor-1α
HuR	ELAV-like protein 1
IPOA3	Importin α_3
KLF2	Krüppel-like factor 2
KLF4	Krüppel-like factor 4
LDL	Low-density lipoprotein
LPA	Lysophosphatidic acid
miR	MicroRNA
miRNA	MicroRNA
miRNA*	Passenger microRNA
moxLDL	Mildly-oxidized low-density lipoprotein
mRNA	Messenger RNA
NF-κB	Nuclear factor-κB
NO	Nitric oxide
NOS2	Nitric oxide synthase 2
NOS3	Nitric oxide synthase 3
oxLDL	Oxidized low-density lipoprotein
PAZ	PIWI–AGO–ZWILLE
pre-miRNA	Precursor microRNA
pre-RISC	Precursor RNA-induced silencing complex
pri-miRNA	Primary microRNA
R&D	Research and development
RISC	RNA-induced silencing complex
SHIP-1	Src homology 2 domain-containing inositol-5-phosphatase
SMC	Smooth muscle cell

SOCS1	Suppressor of cytokine signaling 1
TAK1	Transforming growth factor β-activated kinase 1
TLR4	Toll-like receptor 4
TNF-α	Tumor-necrosis factor-α
TSB	Target site blocker oligonucleotides
VEGF	Vascular endothelial growth factor
XPO5	Exportin 5
YY1	Yin Yang 1
β-TRC	β-transducin repeat-containing gene

2 Introduction

2.1 Cardiovascular diseases

Cardiovascular diseases (CVDs) are responsible for 30 % of all deaths worldwide, being the leading cause of death and loss of productive life years among Europeans and around the world[1,2]. Although novel treatments of CVDs in the past 30 years increased life expectancy by almost 4 years, more than 4 million Europeans still die from CVDs per year, mainly due to coronary heart disease or cerebrovascular disease[3,4]. The incidence of CVDs in Europe is rising due to an increased prevalence of cardiovascular risk factors, such as obesity and diabetes, in an aging population[5]. Despite of the increased demand for new CVD treatments, pharmaceutical innovations are reducing due to the low priority status of CVDs in the R&D strategies of pharmaceutical companies[6]. Thus, R&D activity in the area of CVDs is strongly needed to discover novel treatment strategies for controlling the epidemic of CVDs.

2.2 Pathogenesis of atherosclerosis

2.2.1 Physiological and pathological stages of atherosclerotic lesions

Atherosclerosis, the main cause of CVDs, is a chronic inflammatory disease of blood vessels characterized by the formation of lesions due to the accumulation of lipids, inflammatory cells and extracellular matrix in the subendothelial space of arteries[7]. Atherosclerotic lesions have been histologically classified into six major types, representing the early, developing and advanced stage of atherosclerosis (Figure 1)[8]. The initiation of atherosclerosis is mediated by the recruitment of circulating monocytes to inflammatory activated endothelial cells (ECs) that predominantly occurs at arterial branching points, where blood flow is naturally disturbed[9]. Monocytes transmigrate into the intima of arteries, where they differentiate into macrophages for phagocytic clearance of cholesterol-rich lipoproteins[10]. Increased intracellular accumulation of lipids transforms macrophages into foam cells, which leads to intimal thickening and to the formation of fatty streaks[7]. Over time, this process continues and multiple foam cell layers are formed[8]. In addition, impaired lipoprotein clearance induces extracellular lipid deposition, thereby developing fatty streaks into preatheromas[7]. Intimal thickening, fatty streaks, and preatheromas are physiological stages that remain clinically silent and are potentially reversible[8]. These early atherosclerotic lesions are detectable in every human, including children and in various free-living animals, such as elephants or birds[7,11-13]. The progression of atherosclerosis and the formation of pathological lesions is driven by the inflammatory activation of lipid-laden macrophages due to ongoing lipid accumulation, which triggers macrophage apoptosis[10]. Impaired phagocytosis of apoptotic cells contributes to the formation of a highly thrombogenic, lipid-rich necrotic core in the lesions, which is a hallmark of atheromas[10]. These vulnerable plaques are prone for rupture and thrombosis. A fibrous cap consisting of smooth muscle cells (SMCs) and collagen fibrils can cover the lipid core in advanced lesions, which may provide plaque stability and protect from plaque rupture[14,15]. Over time, complicated lesions with thin fibrous caps can develop, which can narrow the arterial lumen, resulting in impaired blood flow and reduced oxygen supply to organs, such as heart and brain[7]. Moreover, disruption of complicated lesions can result in the complete occlusion of arteries due to thrombus formation, causing life-threatening complications such as myocardial infarctions[15].

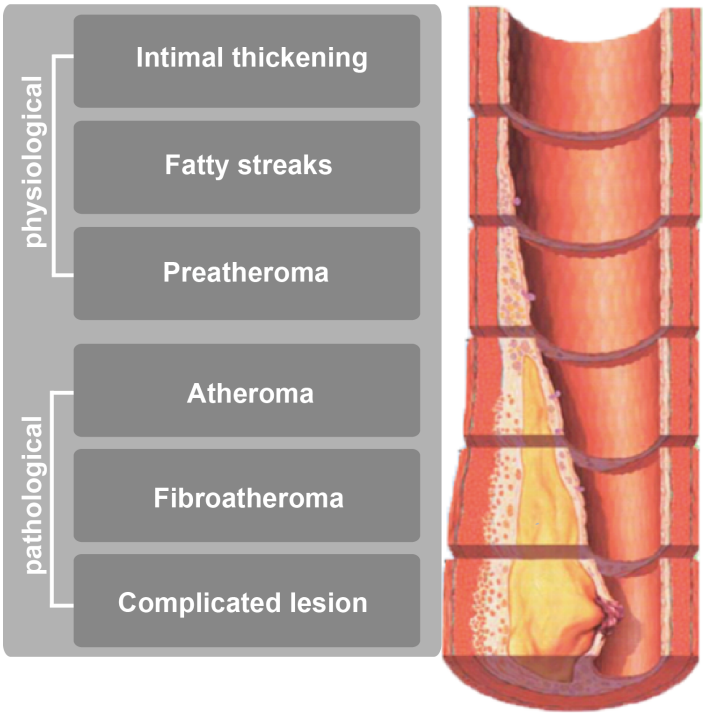

Figure 1: Histological classification of atherosclerotic lesions. Atherosclerotic lesions have been classified into six major types, representing physiological and pathological lesion stages[8]. Image is modified from Schober *et al.* (unpublished) and from Wikimedia Commons (permission to copy and modify is granted under the terms of the GNU Free Documentation License).

2.2.2 Maladaption of endothelial cells to disturbed flow

ECs form a thin monolayer at the luminal side of blood or lymphatic vessels and regulate many physiological processes, including vascular tone, permeability and maintenance of blood fluidity[16]. In contrast to veins, arterial ECs are exposed to hemodynamic forces characterized by high-pressure and high-shear stress, which is generated by laminar blood flow (Figure 2)[17]. ECs sense and convert hemodynamic forces by mechanotransduction of high-shear stress into cellular signaling, such as activation of the transcription factors Krüppel-like factor (KLF) 2 and 4, which provide a quiescent EC phenotype characterized by low turnover rates, tight intercellular junctions with low permeability, anti-inflammatory and anti-thrombogenic properties[18-20]. Therefore, arterial ECs are perfectly adapted to the mechanical stress, which promotes EC quiescence. However, the circulatory system requires branching of the arteries to conduct blood flow throughout the body, which causes permanent disturbed flow and low shear stress[17]. Disturbed blood flow induces chronic EC injury, characterized by the upregulation of adhesion molecules and increased EC apoptosis, indicating a maladaption of ECs to flow conditions at arterial branching points (Figure 2)[21,22]. Chronic EC injury at bifurcations is a physiological event, which might trigger the formation of early and reversible atherosclerotic lesions even under normal lipid levels[10].

Additional EC damage by hyperlipidemia induces endothelial inflammation at sites of disturbed flow owing to the suppression of KLF4, which promotes the activation of the proinflammatory transcription factor nuclear factor-κB (NF-κB) due to their mutual regulation via competitive binding to the coactivator p300 (Figure 2)[18,21,23]. Endothelial NF-κB activation promotes atherosclerosis in mice, whereas KLF4 is atheroprotective by reducing EC inflammation[24,25]. In contrast to KLF4, endothelial hypoxia-inducible factor (HIF)-1α promotes NF-κB activation in a positive feedback loop[26]. In contrast to the activation by hypoxia via increased HIF-1α protein stabilization, HIF-1α activation in

ECs occur rather by non-hypoxic stimuli such as Angiotensin II, which increases the expression of HIF-1α in a NF-κB-dependent manner[26,27]. In arterial ECs, HIF-1α regulates the expression of more than 5 % of all human genes, such as angiopoietin 1 and vascular endothelial growth factor (VEGF)[28].

Activation of endothelial NF-κB triggers the expression and secretion of endothelial chemokines such as C-X-C motif chemokine 1 (CXCL1) and C-C motif chemokine 2 (CCL2)[25,29,30]. CXCL1 is immobilized on the EC surface and triggers monocyte adhesion by activating integrins on the monocyte surface (Figure 2), whereas CCL2 promotes the monocytosis during hyperlipidemia and contributes to the transmigration of adherent monocytes into the subendothelial space[29,31-34]. Disturbed flow enhances EC apoptosis, which increases the permeability of the endothelium and promotes the influx of lipoproteins, such as the cholesterol-rich low-density lipoprotein (LDL) into the vessel wall during hyperlipidemia (Figure 2)[35-37]. Lipoproteins are retained in the subendothelial space by binding to proteoglycans, thereby accumulating in the intima[38]. Retained lipoproteins can undergo oxidative modification to different degrees by oxidation of proteins and polyunsaturated fatty acids mediated by ECs, SMCs or macrophages[39]. Compared to extensively oxidized LDL (oxLDL), mildly-oxidized LDL (moxLDL) is still recognized by the LDL receptor, but induces inflammation in ECs and in macrophages by releasing active phospholipids[40]. The generation of lysophosphatidic acid (LPA) during mild oxidation of LDL further promotes the recruitment of monocytes to the endothelium through the release of endothelial CXCL1[29]. Concurrently, increased accumulation of lipoproteins enhances endothelial apoptosis, thereby perpetuating the influx of lipoproteins into the vessel wall, concomitant with the subsequent recruitment of monocytes to the inflammatory endothelium[41].

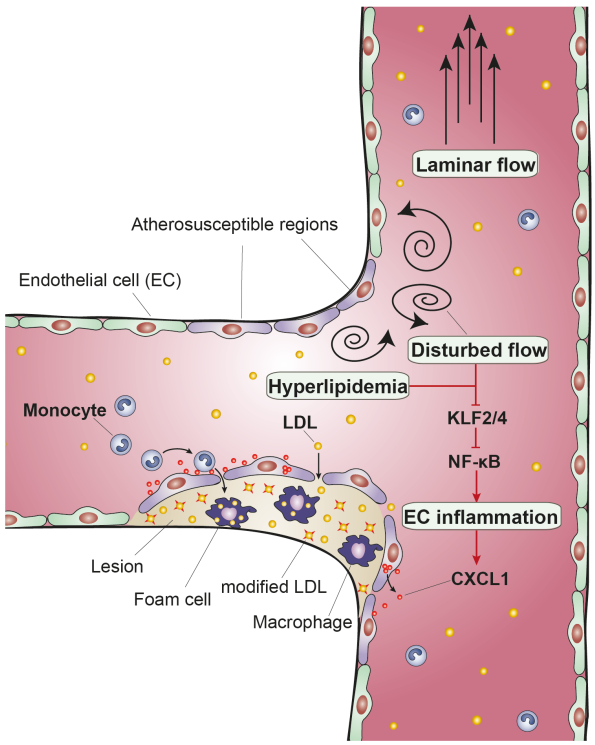

Figure 2: Atherosclerotic lesion formation at arterial bifurcations. Atherosclerosis preferentially develops at arterial branching points, where blood flow is disturbed. Hyperlipidemia induces endothelial inflammation at sites of disturbed flow due to the suppression of KLF2/4 and activation of NF-κB. Induced NF-κB activation promotes the expression and release of CXCL1 from intracellular storage of ECs, which immobilizes on the EC surface. CXCL1 mediates the adhesion of monocytes to the endothelium, which transmigrate into the vessel wall and differentiate into macrophages. Disturbed flow increases EC apoptosis, which triggers an increased influx of LDL into the subendothelial space due to an increased permeability of the EC monolayer. In the intima, LDL undergoes oxidative modification. Macrophages ingest the oxidative modified LDL in an unrestricted manner, thereby developing into lipid-laden foam cells and promoting lesion progression[10]. Abbreviations: CXCL1, C-X-C motif chemokine 1; EC, endothelial cell; KLF42/4, Krüppel-like factor 2 and 4; LDL, low-density lipoprotein; NF-κB, nuclear factor-κB.

2.2.3 Inflammatory activation of macrophages during atherosclerosis

Intimal macrophages recognize and ingest the retained lipoproteins for clearance from the extracellular space (Figure 2). OxLDL is no longer able to efficiently interact with the LDL receptor, instead they are recognized and internalized by scavenger receptors, mainly scavenger receptor-AI and cluster of differentiation 36 antigen on macrophages[42]. In contrast to LDL receptors, scavenger receptors take up oxLDL in an unrestricted manner, which is not inhibited by the cellular cholesterol content[40]. Internalized lipoproteins are digested in the lysosomes, which results in the release of free cholesterol and fatty acids and subsequent accumulation in cytosolic lipid droplets as cholesteryl esters and triglycerides, respectively[43]. Due to intracellular lipid accumulation, macrophages become lipid-laden foam cells[43]. Excessive free cholesterol can be removed from macrophages to the liver via high-density lipoproteins (HDLs) or lipid-free apolipoproteins (such as apoA-I), a process termed cholesterol efflux[43]. However, continuous influx of lipoproteins during the progression of atherosclerosis overwhelms the cholesterol efflux capacity of macrophages, causing the accumulation of free cholesterol in the endoplasmatic reticulum (ER) and plasma membrane of macrophages, which induces ER stress and activation of the proinflammatory Toll-like receptor 4 (TLR4)[44-46]. This process induces macrophage apoptosis and the inflammatory activation of macrophages, which is characterized by the upregulation of proinflammatory mediators such as nitric oxide synthase 2 (NOS2) and CCL2[47-49]. The proatherogenic effect of NOS2 is characterized by the generation of the oxidant species, such as peroxynitrite, which strongly promotes LDL oxidation[50]. The inflammatory activation of macrophages persistently induces monocyte recruitment, lipoprotein oxidation and impairs cholesterol efflux, thus promoting the ongoing inflammatory process[51-53]. The failure to resolve this chronic inflammation results in the progression of atherosclerotic lesions. Efficient clearance of apoptotic macrophages by efferocytosis at an early stage of atherosclerosis limits lesion formation, whereas in advanced lesions impaired phagocytic clearance of apoptotic cells results in secondary necrosis[53]. This process contributes to the formation of a lipid-rich necrotic core, which consists of cholesterol crystals and extracellular lipids and contributes to the vulnerability of advanced atherosclerotic lesions[53]. During lesion progression, SMCs migrate into the intima, which encapsulate and stabilize the highly thrombogenic necrotic core by building a fibrous cap together with collagen fibrils[14]. However, persistent infiltration of macrophages into the lesions causes thinning of the fibrous cap due to the secretion of proteases, thereby increasing the risk for plaque rupture and thrombosis[54].

2.3 MicroRNA biogenesis and function

In 1993, Ambros *et al.* discovered a small non-coding RNA located in the *lin-4* gene in nematodes, which controls the development of *Caenorhabditis elegans (C. elegans)* by inhibiting the translation of target messenger RNAs (mRNAs)[55]. Around eight years later, the discovery of the evolutionary conservation of microRNAs (miRNAs; miR) and the identification of an extensive set of new miRNAs introduced miRNAs as important posttranscriptional gene regulators and emerged the field of miRNA biology[56-58]. MiRNAs are 21–23 nucleotide long, single-stranded RNA molecules that are derived from a hairpin-loop-structured primary miRNA[59]. Following two maturation steps mediated by the RNase III endonucleases Drosha and Dicer, miRNAs repress the expression of their target mRNAs by mRNA degradation or translational repression[59].

2.3.1 Transcription and nuclear processing of primary miRNAs

Many miRNA genes (~70 %) are encoded within annotated transcription units, predominantly located within intronic regions of protein-coding genes or non-coding genes[60,61]. MiRNA genes can be transcribed together with their host genes, like miR-103, which expression is regulated by the promoter of its host gene pantothenate kinase[62]. Alternatively, miRNAs can reside in exonic or intergenic regions and are expressed by their own promoters[60]. The majority of miRNA genes is transcribed by the RNA Poylmerase II into a primary miRNA transcript (pri-miRNA) with a poly(A)-tail and 5`cap (Figure 3)[59]. A typical pri-miRNA transcript contains approximately thousand bases and is folded into a double-stranded hairpin structure composed of a hairpin stem (33-35 base pairs), a terminal loop and two single-stranded flanking segments[59]. The mature miRNA sequence is embedded in the stem of this hairpin structure[59]. Approximately 50 % of miRNA genes are located as clusters in introns or intergenic regions, which are usually co-transcribed as one long polycistronic transcript[63]. During transcription and before splicing, pri-miRNAs undergo the first maturation step by the nuclear Microprocessor complex composed of Drosha and its cofactor DiGeorge syndrome critical region 8 protein (DGCR8) (Figure 3)[64,65]. DGCR8-mediated positioning of the pri-miRNA hairpin to the RNase III domains of Drosha is essential for the correct cleavage at the site approximately 11 base pairs away from the basal junction, which produces the precursor miRNA (pre-miRNA) hairpin with a length of ~60-70 nucleotides and a 2 nucleotide overhang at the 3` end (Figure 3)[64,66]. The 2 nucleotide overhang is recognized by the nuclear export factor Exportin 5, which translocates the pre-miRNA into the cytoplasm through a nuclear pore complex in a GTP-dependent manner[67].

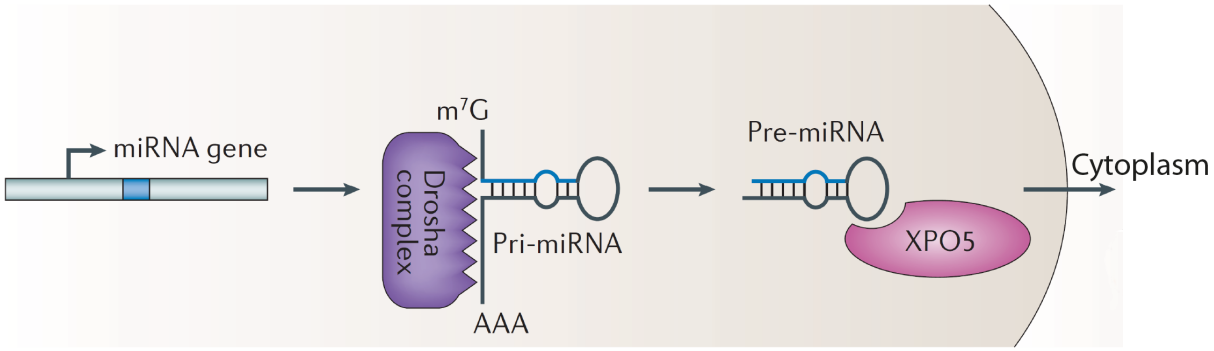

Figure 3: Transcription and nuclear processing of pri-miRNAs. In the nucleus, miRNA genes are transcribed by the RNA Polymerase II into pri-miRNA transcripts, which are cleaved into pre-miRNAs by the Drosha complex composed of Drosha and DGCR8. Pre-miRNAs are transported from the nucleus into the cytoplasm by Exportin 5 (XPO5) through the nuclear pore complex in a GTP-dependent manner[68]. Image is modified from[68].

2.3.2 Processing of precursor miRNAs by Dicer in the cytoplasm

In the cytoplasm, Dicer cleaves the pre-miRNA into a short miRNA duplex[69]. The precise processing by Dicer is crucial since alterations in the cleavage site may change the target recognition sequence of mature miRNAs[69]. The tertiary L-shaped structure of Dicer contains the PAZ (PIWI–AGO–ZWILLE) and Platform domains at the head of the L, the helicase domain at the base and the two catalytic cores RNase IIIa and IIIb at the lower half of the L-like structure (Figure 4)[69]. Dicer recognizes the terminal loop of the pre-miRNA through its helicase domain, and the 3` and 5` end of the double-stranded RNA (dsRNA) by its PAZ and Platform domain, respectively[70]. The 3` pocket binds the 2 nucleotide 3` overhang structure, whereas the 5` pockets anchors the 5`-phosphorylated end of the pre-miRNA[70]. The positioning locates the pre-miRNA to the catalytic center of Dicer and helps to

determine the precise cleavage site by measuring a fixed distance from either the 3` overhang or the 5`-phosphorylated end of the dsRNA terminus (molecular ruler function of Dicer) (Figure 4)[70,71]. According to the 3` counting rule, Dicer typically cleaves the pre-miRNAs 21–25 nucleotides from the 3` overhang of the dsRNA terminus[59]. Moreover, Dicer can use the 5` end of the pre-miRNA as a reference point to locate the cleavage site ~22 nucleotides from the 5` end of the dsRNA (5` counting rule)[70]. The 5` counting mechanism requires a phosphate group to efficiently recognize the 5` end and occurs mainly when the pre-miRNA end is thermodynamically unstable[70]. In either case, Dicer generates a double-stranded miRNA duplex with a length of approximately 22 nucleotides (Figure 5)[68]. In humans, Dicer associates with two dsRNA-binding proteins TAR RNA-binding protein 2 and PKR-associated protein X, which help to determine the length of mature miRNAs[72]. Currently only pre-miR-451 is processed in a Dicer-independent manner by the catalytic center of an Argonaute (AGO) protein[73].

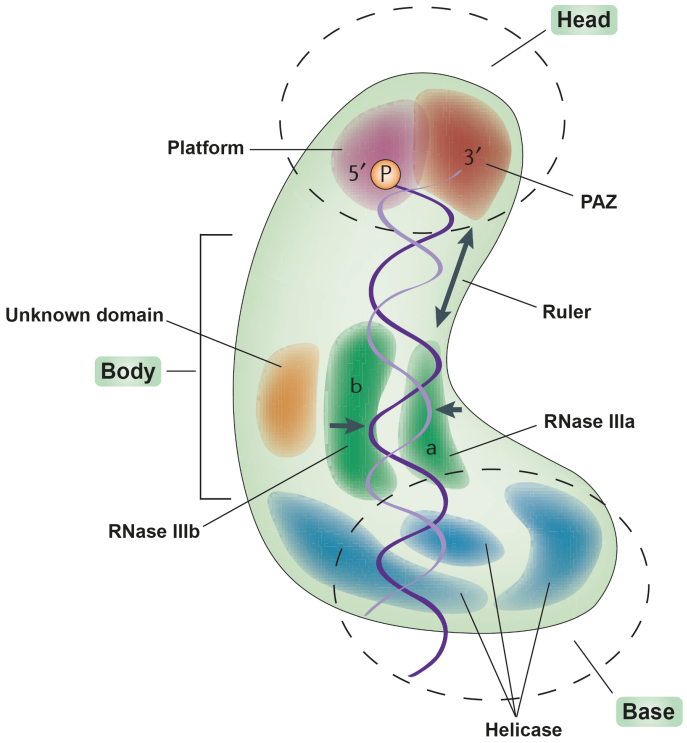

Figure 4: Structure and domains of Dicer. The tertiary structure of Dicer is L-shaped including a head, body and base region. The PAZ and Platform domains are located in the head of the L-shape, containing binding pockets for the 5`-phosphorylated and 3` overhang ends of the pre-miRNA. The linker sequence between PAZ and RNase III domains aligns the stem of the pre-miRNA along the axis of the protein and functions as a ruler by precisely positioning the pre-miRNA over the catalytic centers for cleavage. Thereby, the catalytic domains RNase IIIa and IIIb cleave approximately 22 nucleotides in distance of the dsRNA ends of the pre-miRNA. Arrows indicate the cleavage sites of the RNase IIIa and IIIb domains. The helicase domain in the base forms a clamp-like structure and helps to reorganize the substrate[69]. Image is modified from[69].

Following Dicer-mediated cleavage, the miRNA duplex is loaded onto AGO proteins in an ATP-dependent manner, thereby generating the precursor RNA-induced silencing complex (pre-RISC)[74]. During duplex unwinding, the two strands of the miRNA duplex are separated and the guide strand remains bound to the AGO protein, which results in the formation of the mature RISC (Figure 5)[68]. The other strand of the previous miRNA duplex, termed passenger miRNA or miRNA*, is mostly degraded, but can be also functional[59]. In general, the strand with the lower thermodynamic stability at its 5` terminus is selected as the guide strand, although strand selection is not always completely strict[59].

Binding to AGO proteins stabilizes miRNAs by protecting against exonucleolytic degradation[75]. Whereas a subset of miRNAs is highly stable, the expression of some miRNAs is strongly dependent on continuous biogenesis due to their fast turnover rates[76,77]. In quiescent cells, the majority of miRNAs is stable and functionally silent probably owing to their sequestering in polysomes[78-80]. In contrast, miRNA turnover and functional activity is enhanced in proliferating cells[78,80].

MiRNAs bound to AGO proteins recognize their target mRNAs by base pairing between the miRNA

seed sequence (nucleotide 2–8 in the 5` end of the miRNA) and the complementary miRNA response elements, which are predominantly located in the 3` untranslated region (3` UTR) of the target mRNA[81]. Targeting of the mRNA in the RISC leads to the recruitment of deadenylation factors, which remove the poly(A)-tail of the target mRNA and thus promote mRNA degradation by exonucleases[68]. In addition, the miRNA-target interaction can also induce translational repression without affecting the mRNA stability by blocking translational initiation or elongation[68]. In addition to direct target suppression, miRNAs can indirectly regulate gene expression owing to the competition of transcripts sharing the same miRNA binding sites, termed competing endogenous RNAs[82]. Therefore, the suppression of one miRNA target may result in the upregulation of other targets of the same miRNA[82].

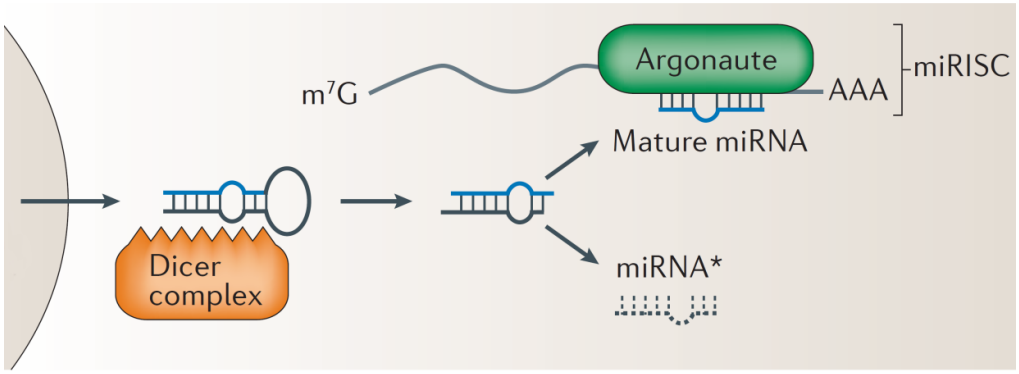

Figure 5: Dicer-mediated processing of pre-miRNAs in the cytoplasm. Dicer cleaves the pre-miRNA near the terminal loop, thereby generating a miRNA duplex. The miRNA duplex is loaded onto Argonaute proteins. Following duplex unwinding, the guide strand (mature miRNA) remains bound to the Argonaute protein, thereby forming the mature RNA-induced silencing complex (miRISC). The miRISC binds to the target mRNA and regulates its expression by mRNA degradation or translational repression. The passenger strand (miRNA*) is usually degraded[68]. Image is modified from[68].

2.3.3 The regulatory function of miRNAs

More than 60 % of human protein-coding genes are predicted to be conserved miRNA targets, indicating the enormous regulatory potential of miRNAs[83,84]. One miRNA can theoretically target several mRNAs and conversely, one mRNA can be regulated by multiple miRNAs, thus constituting a complex gene regulatory network with up to 18,500 miRNA-mRNA interactions in on cell type[84,85]. In general, miRNAs can act as off-switches or fine-tuners of gene expression, thereby conferring robustness to biological processes such as cell fate switches during development[85,86]. MiRNAs can control the development of a specific cell phenotype by switching-off transcripts that should not be expressed in a particular cell type, to inconsequential levels[85,87]. Moreover, miRNAs can act as fine-tuners to reduce the protein expression of their target mRNAs to a more optimal level, but which is still functional[85]. Thereby, miRNAs can buffer fluctuations in gene expression[86]. In contrast, so-called neutral repressions of the protein expression by miRNAs have no effect in the cell[85]. In general, the degree of target repression by miRNAs is modest, usually less than 2-fold[86]. However, miRNAs can amplify small changes in the target protein output by the regulation of regulatory proteins, which are components of feedback or feedforward loops[86].

2.3.4 Role of Dicer in the regulation of cell functions

Dicer knock-out in mice causes embryonic lethality at an early stage of development most likely due to an impaired blood vessel formation, demonstrating a key role of miRNAs during development[88,89]. Moreover, miRNAs are required for maintenance of organ function by regulating processes in various cell types. In adult mice, somatic Dicer deletion results in abnormalities of intestine and bone marrow, combined with a substantial reduction of the survival rate[90]. Deficiency of Dicer in pancreatic beta cells causes diabetes in mice, whereas Dicer deletion in cardiomyocytes results in severe hypertrophic heart failure[91,92]. Notably, only a small fraction of miRNAs was downregulated and even some miRNAs were upregulated in the heart following Dicer deletion[92].

Whereas deficiency of Dicer in SMCs causes embryonic lethality due to internal hemorrhage, EC-specific Dicer deletion does not affect the development of mice or induce an overt phenotype, indicating that permanent miRNA biogenesis is of less importance in EC than in SMC homeostasis[93-95]. However, knock-out of endothelial Dicer severely impairs angiogenesis, resulting in diminished EC proliferation and migration[93,96,97]. *In vitro*, knock-down of Dicer in ECs diminishes the expression of only a subset of miRNAs, probably owing to differences in the stability between miRNAs[80,97]. Moreover, silencing of endothelial Dicer reduces the expression of CXCL1, promotes the expression of endothelial nitric oxide synthase (eNOS) and increases nitric oxide (NO) production, indicating that Dicer generates miRNAs that promote endothelial inflammation[96]. However, the role of Dicer in endothelial inflammation during atherosclerosis is unclear.

2.4 Role of miRNAs in atherosclerosis

2.4.1 Role of miRNAs in endothelial inflammation during atherosclerosis

ECs at arterial bifurcations are primed by disturbed flow for inflammatory activation in response to hyperlipidemia, which triggers monocyte recruitment and atherosclerosis[23,98]. The miRNA expression profile in ECs differs between atheroprone and atherosusceptible arterial regions characterized by downregulation of atheroprotective miRNAs such as miR-10a and upregulation of proatherogenic miRNAs such as miR-92a or miR-103 in atheroprone regions[99]. Hyperlipidemia further increases the disturbed flow-induced expression of miR-92a, indicating that hyperlipidemia and disturbed flow can have additive effects on miRNA expression[100,101]. MiR-92a induces NF-κB-dependent chemokine expression and monocyte adhesion most likely by suppressing KLF2 and KLF4 in ECs, both of which inhibit NF-κB activation (Figure 6)[100]. In addition, miR-712 promotes endothelial NF-κB activation by inducing tumor necrosis factor-α (TNF-α) release from the endothelium (Figure 6)[102]. In contrast to miR-92a and miR-712, miR-181b and miR-10a inhibit NF-κB activation in ECs by impairing nuclear translocation of NF-κB, thereby contributing to an anti-inflammatory EC phenotype (Figure 6)[99,103,104]. In particular, miR-181b, which is downregulated by hyperlipidemia and TNF-α, reduces the expression of inflammatory chemokines such as CXCL1 and C-X_3-C motif chemokine 1 (CX_3CL1) in TNF-α-stimulated ECs[103,104]. To resolve prolonged EC inflammation, NF-κB-induced miR-146a negative feedbacks to NF-κB by stabilizing the KLF2 mRNA (Figure 6)[105]. By regulating EC inflammation, miRNAs might contribute to the formation of atherosclerotic lesions. For instance, systemic inhibition of miR-92a or overexpression of miR-181b in mice reduces atherosclerosis by limiting NF-κB activation; these effects are most likely attributed to reduced EC inflammation[100,104]. Although individual miRNAs have been implicated in endothelial inflammation during atherosclerosis, the effect of miRNA biogenesis on endothelial inflammation and atherosclerosis is unclear.

The molecular mechanisms by which disturbed flow and hyperlipidemia control the expression of endothelial miRNAs is incompletely understood. The transcription factor HIF-1α can regulate the expression of miRNAs, thus termed hypoxia-responsive miRNAs[106]. For instance, HIF-1α induces the expression of miR-107, which promotes VEGF-mediated angiogenesis during hypoxia[106]. Moreover, HIF-1α and miR-429 constitute in a negative feedback loop that limits VEGF expression in ECs[107]. During atherosclerosis the expression of HIF-1α is associated with lesion progression and lesional inflammation[108,109]. Endothelial HIF-1α and NF-κB reciprocally amplify each other, thereby regulating EC function[26]. However, it is unclear whether HIF-1α-regulated miRNAs are involved in the mutual activation of HIF-1α and NF-κB in infammatory ECs during atherosclerosis.

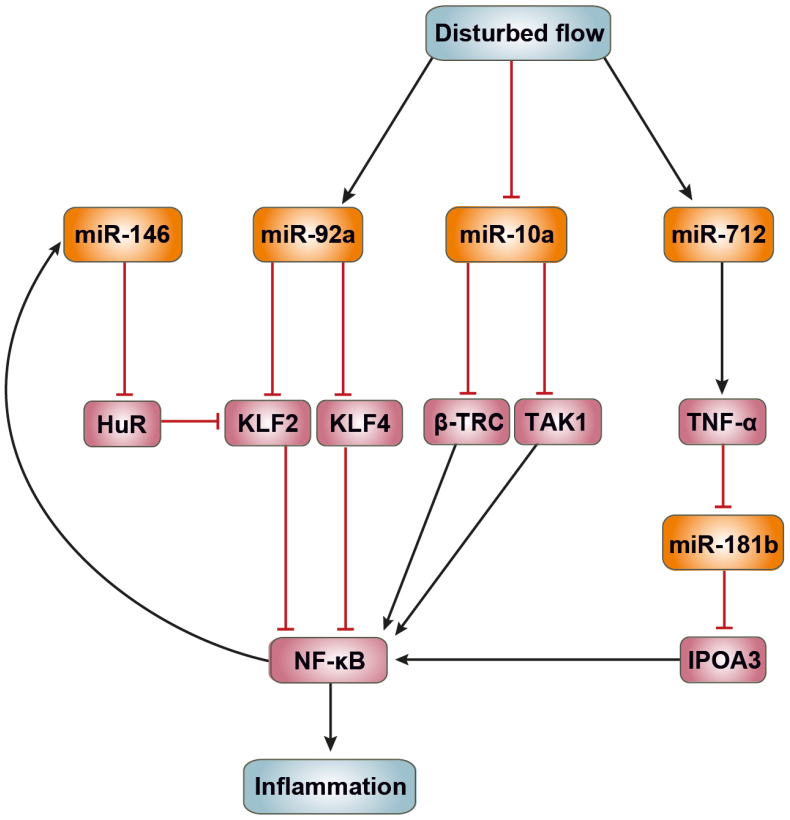

Figure 6: MiRNAs control the inflammatory activation in ECs. Individual miRNAs control NF-κB-mediated endothelial inflammation in response to atherogenic stimuli, such as disturbed flow. Disturbed flow upregulates the expression of miR-92a and miR-712 in ECs. MiR-92a promotes NF-κB activation by suppressing KLF4/2 expression and miR-712 induces the release of soluble TNF-α from the endothelium. In turn, TNF-α represses the expression of miR-181b in the endothelium, which limits the nuclear translocation of NF-κB by targeting importin α_3 (IPOA3). Moreover, NF-κB promotes miR-146a expression, which restrains endothelial inflammation. Disturbed flow promotes the proatherogenic phenotype in ECs by suppressing miR-10a that acts as a negative regulator of NF-κB[10]. Abbreviations: miR, microRNA; NF-κB, nuclear factor-κB; TNF-α, Tumor-necrosis factor-α; KLF2/4, Krüppel-like factor 2 and 4; β-TRC, β-transducin repeat-containing gene; TAK1, Transforming growth factor β-activated kinase 1; IPOA3, Importin α_3; HuR, ELAV-like protein 1.

2.4.2 Role of miRNAs in macrophage function during atherosclerosis

Several miRNAs, such as miR-155, -147 and -342-5p, are upregulated in macrophage-rich atherosclerotic lesions[110]. Whereas hyperlipidemia and oxLDL increase the expression of miR-155 in macrophages, the kinase thymoma viral proto-oncogene 1 (AKT1) and the transcriptional repressor Yin Yang1 (YY1) negatively regulate the expression of miR-155[111-113]. MiR-155 promotes macrophage inflammation by upregulating inflammatory mediators, like CCL2, NOS2, TNF-α and interleukin-6, by

targeting negative feedback mediators, such as B-cell lymphoma 6 (BCL6), Src homology 2 domain-containing inositol-5-phosphatase (SHIP-1) and suppressor of cytokine signaling 1 (SOCS1) (Figure 7)[110,112,114,115]. Suppression of BCL6 by miR-155 induces NF-κB-dependent expression of CCL2 and TNF-α in macrophages, thereby promoting atherosclerosis[110]. Moreover, miR-155 induces the expression of miR-147 in macrophages, indicating that miRNAs can regulate their expression reciprocally[116]. MiR-155 plays a crucial role in macrophages during atherosclerosis; however, the function of miR-342-5p, which is also upregulated during atherosclerosis, in the formation of atherosclerotic lesions is unknown. Moreover, it is unclear whether these upregulated miRNAs promote their expression reciprocally during the progression of atherosclerosis.

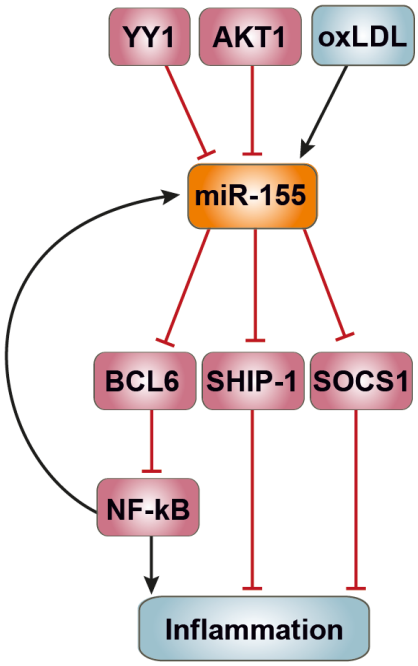

Figure 7: MiR-155 regulates macrophage inflammation during atherosclerosis. YY1 and AKT1 downregulate the expression of miR-155, whereas oxLDL upregulates the expression of miR-155. MiR-155 promotes macrophage inflammation through the inhibition of several negative regulators, such as BCL6, SHIP-1 and SOCS1[10]. Abbreviations: AKT1, thymoma viral proto-oncogene 1; BCL6, B-cell lymphoma 6; miRNA, microRNA; NF-κB, Nuclear factor-κB; oxLDL, oxidized low-density lipoprotein; SHIP-1, Src homology 2 domain-containing inositol-5-phosphatase; SOCS1, Suppressor of cytokine signaling 1; YY1, Yin Yang1.

2.5 Aims of the studies

2.5.1 Role of endothelial Dicer in atherosclerosis

Inflammatory activation of ECs triggers the adhesion of monocytes at arterial bifurcations. Endothelial miRNAs have been implicated in endothelial inflammation during atherosclerosis. Dicer processes almost all mature miRNAs and promotes the expression of proinflammatory genes in ECs *in vitro*. Although individual miRNAs affect endothelial inflammation, the role of Dicer in ECs during atherosclerosis is unclear. We hypothesized that endothelial Dicer affects the inflammatory activation of ECs during atherosclerosis by processing miRNAs.

Therefore, we investigated the role of endothelial Dicer on monocyte adhesion and atherosclerosis. We studied the effect of endothelial Dicer deletion on miRNA expression in the arteries of atherosclerotic mice. We investigated whether the effects of endothelial Dicer on EC function during atherosclerosis are mediated by miRNAs to assess the potential of miRNA-based therapy in atherosclerosis.

2.5.2 Effect of endothelial HIF-1α on miRNA expression in atherosclerosis

HIF-1α is expressed in atherosclerotic lesions and correlates with inflammation during atherosclerosis. In ECs, HIF-1α and NF-κB activate each other through a positive feedback loop. However, the exact mechanism of the interaction between HIF-1α and NF-κB is incompletely understood. In addition to the transcriptional regulation of protein-coding genes, HIF-1α mediates its effects through the regulation of miRNAs. We hypothesized that endothelial HIF-1α plays a role in atherosclerosis by regulating miRNAs, which induce NF-κB activation.

Therefore, we investigated the role of endothelial HIF-1α in EC inflammation during atherosclerosis. We studied the role of HIF-1α-regulated miRNAs in the mutual activation of HIF-1α and NF-κB in ECs during atherosclerosis.

2.5.3 Role of miR-342-5p in atherosclerosis

Macrophages promote the progression of atherosclerotic lesions by driving a chronic inflammatory response. Upregulated miRNAs during atherosclerosis, such as miR-155, play a crucial role in atherosclerosis. In addition to miR-155, miRNA expression profiles identified a selective upregulation of miR-342-5p in atherosclerotic lesions. We hypothesized that miR-342-5p plays a role in atherosclerosis, probably via an interaction with miR-155.

Therefore, we studied the function of miR-342-5p in atherosclerosis and characterized its potential effect as a therapeutic approach to treat atherosclerotic lesion formation.

3 Publications for cumulative dissertation

3.1 Endothelial Dicer in atherosclerosis

Nature communications. 2016 Feb; 3(7):10521. doi: 10.1038/ncomms10521.

Endothelial Dicer promotes atherosclerosis and vascular inflammation by miRNA-103-mediated suppression of KLF4

Petra Hartmann, Zhe Zhou, Lucia Natarelli, Yuanyuan Wei, Maliheh Nazari-Jahantigh, Mengyu Zhu, Jochen Grommes, Sabine Steffens, Christian Weber, Andreas Schober.

nature COMMUNICATIONS

ARTICLE

Received 26 Oct 2015 | Accepted 22 Dec 2015 | Published 3 Feb 2016

DOI: 10.1038/ncomms10521 OPEN

Endothelial Dicer promotes atherosclerosis and vascular inflammation by miRNA-103-mediated suppression of KLF4

Petra Hartmann[1], Zhe Zhou[2], Lucia Natarelli[1], Yuanyuan Wei[1,3], Maliheh Nazari-Jahantigh[1,3], Mengyu Zhu[1], Jochen Grommes[4,5], Sabine Steffens[1,3], Christian Weber[1,3] & Andreas Schober[1,2,3]

MicroRNAs regulate the maladaptation of endothelial cells (ECs) to naturally occurring disturbed blood flow at arterial bifurcations resulting in arterial inflammation and atherosclerosis in response to hyperlipidemic stress. Here, we show that reduced endothelial expression of the RNAse Dicer, which generates almost all mature miRNAs, decreases monocyte adhesion, endothelial C–X–C motif chemokine 1 (CXCL1) expression, atherosclerosis and the lesional macrophage content in apolipoprotein E knockout mice (*Apoe*$^{-/-}$) after exposure to a high-fat diet. Endothelial Dicer deficiency reduces the expression of unstable miRNAs, such as miR-103, and promotes Krüppel-like factor 4 (KLF4)-dependent gene expression in murine atherosclerotic arteries. MiR-103 mediated suppression of KLF4 increases monocyte adhesion to ECs by enhancing nuclear factor-κB-dependent CXCL1 expression. Inhibiting the interaction between miR-103 and KLF4 reduces atherosclerosis, lesional macrophage accumulation and endothelial CXCL1 expression. Overall, our study suggests that Dicer promotes endothelial maladaptation and atherosclerosis in part by miR-103-mediated suppression of KLF4.

[1] Institute for Cardiovascular Prevention, Ludwig-Maximilians University Munich, Pettenkoferstrasse 9, 80336 Munich, Germany. [2] Institute for Molecular Cardiovascular Research, RWTH Aachen University, Pauwelsstrasse 30, 52074 Aachen, Germany. [3] DZHK (German Centre for Cardiovascular Research), Partner Site Munich Heart Alliance, Biedersteiner Strasse 29, 80802 Munich, Germany. [4] European Vascular Center Aachen-Maastricht, Medical University Maastricht, P. Debyelaan 25, 6229 HX Maastricht, The Netherlands. [5] European Vascular Center Aachen-Maastricht, RWTH Aachen University, Pauwelsstrasse 30, 52074 Aachen, Germany. Correspondence and requests for materials should be addressed to A.S. (email: aschober@med.lmu.de).

Endothelial cells (ECs) are perfectly adapted to conduct blood through high-shear stress, high-pressure environment in unbranched segments of arteries[1]. High-shear stress at the endothelial surface induces the transcription factors Krüppel-like factors (KLF) 2 and KLF4, which promote a quiescent EC phenotype characterized by a low turnover rate, tight intercellular junctions with low permeability, reduced inflammatory activation and antithrombotic properties[2–4]. However, distribution of blood throughout the body requires branching of arteries where blood flow is naturally disturbed and consequently shear stress is low[5]. Disturbed flow at arterial bifurcations constantly damages the endothelium by activating the endoplasmic reticulum stress response, suppresses EC-specific transcriptional programmes by downregulating KLF2/4, and increases the activity of the proinflammatory transcription factor nuclear factor-κB (NF-κB)[6–8]. Moreover, the deposition of chemically modified lipoproteins in the subendothelial space aggravates the maladaptive response of ECs and results in the accumulation of macrophages derived from circulating monocytes in the arterial wall during atherosclerosis[9–11]. Inflammatory activation of macrophages triggers the secretion of inflammatory cytokines, such as tumour necrosis factor-α (TNF-α) and interleukin-1, which further promotes endothelial maladaptation by activating NF-κB[12,13]. Endothelial chemokines, such as chemokine (C–X–C motif) ligand 1 (CXCL1), chemokine (C–C motif) ligand 2 (CCL2) and chemokine (C–X3–C) ligand 1 (CX_3CL1), have key roles in the accumulation of macrophages in atherosclerotic lesions[14–17]. ECs secrete CXCL1 and CCL2 from intracellular storage compartments upon activation by thrombin or lipoprotein oxidation products[15,18]. Whereas CXCL1 is immobilized on the endothelial surface and triggers monocyte adhesion by activating integrins on the monocyte surface[15,19], CCL2 contributes to macrophage infiltration probably by regulating hypercholesterolemia-induced monocytosis[17,20]. The membrane-bound chemokine CX_3CL1 is upregulated in inflamed ECs and promotes atherogenic monocyte adhesion by activating platelets[21]. Constitutive and induced expression of CXCL1, CCL2 and CX_3CL1 are controlled by the activity of NF-κB[22,23].

MicroRNAs (miRNAs) are small noncoding RNAs of ~22 nucleotides that regulate a number of processes related to atherogenesis, such as macrophage activation and the phenotype of vascular smooth muscle cells (SMCs), by translational repression or degradation of their target mRNAs[24–26]. Mature miRNA sequences are embedded in the stem-loop structure of their primary miRNA (pri-miRNA) transcripts. The nuclear RNAse III Drosha crops the pri-miRNA stem at the 5′ and 3′ sides to release a ~65-nucleotide-long, hairpin-shaped precursor miRNA (pre-miRNA). In the cytoplasm, the RNAse III endonuclease Dicer cleaves all pre-miRNAs, except pre-miR-451, near the terminal loop of the hairpin into 21 to 25-nucleotide-long miRNA duplexes, which are subsequently loaded onto Argonaut proteins[27]. Although one strand of the miRNA duplex is selected during the loading step to generate the RNA-induced silencing complex (RISC), the second strand is usually removed and degraded. Binding to Argonaut proteins protects miRNAs from degradation by exonucleases and thus greatly increases their stability compared with that of mRNAs. However, the expression level of a small subset of miRNAs is highly dependent on continuous biogenesis because of a fast turnover rate[28,29].

Deletion of the gene encoding Dicer in mice compromises blood vessel formation and causes embryonic lethality, indicating an essential role of this endonuclease in vertebrate development[30,31]. In adults, Dicer is essential for the function of various cell types, such as pancreatic beta cells and cardiomyocytes[32,33], and reduced Dicer expression contributes to aging and promotes cancer development[34,35]. Although deletion of Dicer in SMCs results in embryonic lethality[36], mice with deficiency of Dicer in ECs develop normally and have no overt phenotype[37]. However, reduced endothelial Dicer expression severely impairs postnatal angiogenesis and limits the proliferation and migration of ECs[37–39]. Notably, knockdown of Dicer induces upregulation of EC-specific genes, such as endothelial nitric oxide synthase (eNOS), Angiopoietin-1 receptor (Tie2) and vascular endothelial growth factor receptor 2 (KDR), indicating that Dicer generates miRNAs that impair endothelial differentiation[38]. Disturbed blood flow increases the expression of several endothelial miRNAs, including miR-92a and miR-712, which promote atherosclerosis by targeting KLF2/4 and by increasing shedding of membrane-bound TNF-α, respectively[7,40,41]. Moreover, several miRNAs have been implicated in NF-κB pathway regulation in ECs. For example, miR-10a, miR-146a and miR-181b promote an anti-inflammatory phenotype in ECs by inhibiting the NF-κB pathway, whereas miR-19a has a proinflammatory role in ECs[42–45]. Although individual miRNAs affect endothelial inflammation, it is unclear which role Dicer-dependent miRNA biogenesis in ECs plays in atherosclerosis.

Here, we investigated the role of endothelial Dicer in monocyte adhesion and atherosclerosis. EC-specific deletion of Dicer in apolipoprotein E-knockout ($Apoe^{-/-}$) mice reduced monocyte adhesion to the early atherosclerotic endothelium by downregulating CXCL1, resulting in diminished lesion formation. MiR-103 is downregulated in Dicer-deficient ECs and promoted CXCL1-mediated monocyte adhesion by targeting KLF4. Blocking the interaction between miR-103 and KLF4 in arteries reduced atherosclerosis, lesional macrophage accumulation and CXCL1 expression, similar as the deletion of Dicer in ECs. Overall, these data indicate that Dicer can enhance atherosclerosis and endothelial inflammation by increasing miR-103 expression.

Results

Endothelial Dicer regulates miRNAs during atherosclerosis. Although many miRNAs are downregulated in atherosclerotic arteries[26], *Dicer* expression in the aortas of $Apoe^{-/-}$ mice was not affected by 12 weeks of high-fat diet (HFD) feeding compared with mice fed a normal diet (Supplementary Fig. 1a), indicating that miRNA biogenesis by Dicer is not generally impaired during early atherosclerosis. Moreover, the expression of *Dicer* in ECs was not affected by low-shear stress and did not differ between the aortic arch and thoracic aorta, indicating that Dicer is not regulated by blood flow (Supplementary Fig. 1b,**c**). To study the role of endothelial Dicer in atherosclerosis, we generated $Apoe^{-/-}$ mice containing a loxP site-flanked *Dicer* sequence ($Dicer^{flox}$) and a transgene with Tamoxifen (TMX) inducible Cre recombinase under control of the EC-specific VE-cadherin (Cdh5) promoter. TMX administration reduced aortic *Dicer* mRNA expression in EC-$Dicer^{flox}$ mice by 66% and 58% compared with EC-$Dicer^{WT}$ mice after 4 and 12 weeks of HFD feeding, respectively (Fig. 1a). In ECs isolated from the aortas of EC-$Dicer^{flox}$ mice injected with TMX, *Dicer* mRNA expression was decreased by 87% compared with ECs isolated from EC-$Dicer^{WT}$ mice (Fig. 1b), whereas the expression of *Dicer* was not affected in myeloid cells from EC-$Dicer^{flox}$ mice (Supplementary Fig. 1d). These results indicate that TMX treatment of EC-$Dicer^{flox}$ mice effectively reduced Dicer expression in ECs.

To determine the effect of endothelial Dicer deficiency on miRNA biogenesis during atherosclerosis, the miRNA expression profile was determined in aortas from HFD-fed EC-$Dicer^{flox}$ and EC-$Dicer^{WT}$ mice by quantitative real-time PCR (qRT–PCR) arrays. After 4 weeks of HFD feeding, 14 miRNAs were downregulated and 9 miRNAs were upregulated in EC-$Dicer^{flox}$

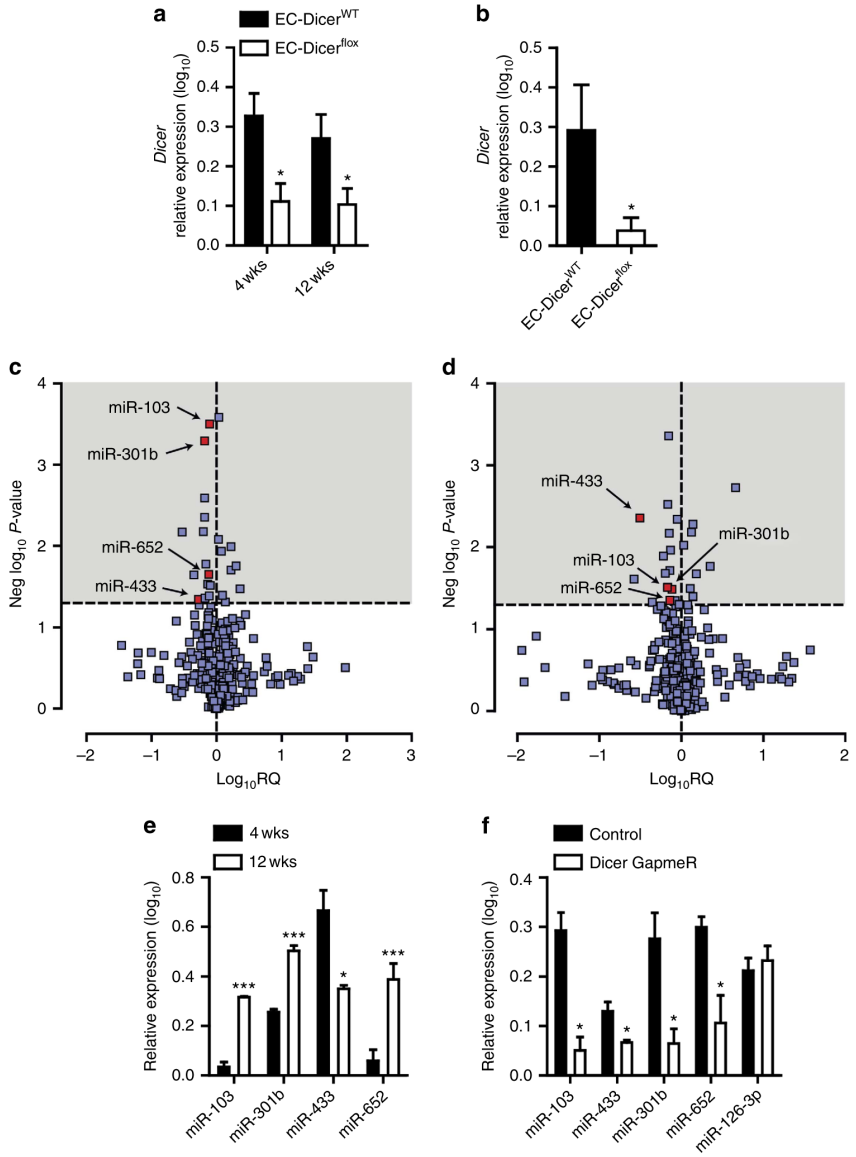

Figure 1 | Effect of endothelial Dicer on miRNA expression during atherosclerosis. (**a**) Quantitative RT-PCR analyses of *Dicer* mRNA expression in the aortas from TMX-treated EC-Dicer^{WT} and EC-Dicer^{flox} mice fed a HFD for 4 or 12 weeks (wks; $n=5$ mice per group). (**b**) *Dicer* mRNA expression levels in aortic ECs isolated from EC-Dicer^{WT} and EC-Dicer^{flox} mice 2 weeks after TMX injection ($n=3$ per group). (**c**,**d**) Differentially expressed miRNAs (grey areas) in the aortas of EC-Dicer^{flox} mice compared with EC-Dicer^{WT} mice ($n=3$ mice per group) after exposure to a HFD for 4 (**c**) or 12 weeks (**d**). The expression profiles were determined using qRT-PCR arrays. RQ, relative quantification. (**e**) The expression levels of miR-103, miR-301b, miR-433 and miR-652 in the aortas of EC-Dicer^{WT} mice fed a HFD for 4 or 12 weeks ($n=3$ mice per group). (**f**) Quantitative RT-PCR analyses of miR-103, miR-301b, miR-433, miR-652 and miR-126-3p expression in human aortic ECs (HAECs) treated with Dicer-specific LNA-GapmeRs or non-targeting control LNA-GapmeRs ($n=3$–4 per group). The data are represented as the mean ± s.e.m. of the indicated number (n) of repeats. $^{*}P<0.05$; $^{**}P<0.01$ and $^{***}P<0.001$ by Student's *t*-test.

mice compared with EC-Dicer^{WT} mice (Fig. 1c and Supplementary Table 1). After 12 weeks of HFD exposure, 18 miRNAs and 8 miRNAs were down- and upregulated in EC-Dicer^{flox} mice, respectively (Fig. 1d and Supplementary Table 2). Notably, the expression levels of miR-103, miR-301b, miR-433 and miR-652 were downregulated in EC-Dicer^{flox} mice at the 4- and 12-week time points. In contrast to miR-301b, endothelial Dicer deficiency reduced the expression levels of miR-103, miR-433 and miR-652 in both aortic arch and thoracic aorta (Supplementary Fig. 2), indicating that the effect of endothelial Dicer on these miRNAs is independent of disturbed flow. Moreover, the expression levels of miR-103, miR-652 and miR-301b in EC-Dicer^{WT} mice were higher at the 12-week time point than the 4-week time point (Fig. 1e). In human aortic ECs

(HAECs), silencing of Dicer using GapmeRs diminished the expression levels of miR-103, -301b, -652 and -433, but not that of miR-126-3p, after 24 h (Fig. 1f and Supplementary Fig. 3). In summary, these results suggest that endothelial Dicer deficiency selectively lowers the expression levels of unstable miRNAs, most of which are upregulated during atherosclerosis.

Endothelial Dicer promotes atherosclerosis. To determine the role of Dicer in endothelial inflammation, monocytic cell arrest was studied *ex vivo* using perfused carotid arteries from EC-Dicer^{flox} and EC-Dicer^{WT} mice that were fed a HFD for 4 weeks. Monocyte adhesion (Fig. 2a) and the expression levels of the *Cxcl1, Cx$_3$cl1* and *Ccl2* mRNAs (Fig. 2b) were significantly lower in carotid arteries from EC-Dicer^{flox} mice than in those from EC-Dicer^{WT} mice. Reduced endothelial expression of CXCL1 in EC-Dicer^{flox} mice was identified by dual immunostaining of CXCL1 and the endothelial marker CD31 (Fig. 2c). These results suggest that endothelial Dicer enhances chemokine expression and may promote monocyte adhesion during the early stages of atherosclerosis. After 12 weeks of HFD feeding, atherosclerosis in the aortic roots (Fig. 3a) and thoracoabdominal aortas (Fig. 3b) of EC-Dicer^{flox} mice was 58% and 41% lower than that in EC-Dicer^{WT} mice, respectively. The distribution of atherosclerotic lesions in the aorta did not differ between EC-Dicer^{flox} and EC-Dicer^{WT} mice (Supplementary Fig. 4). The number of macrophages per lesion (Fig. 3c) and the SMC content (Fig. 3d) were diminished in EC-Dicer^{flox} mice. Deletion of the endothelial *Dicer* gene did not affect serum cholesterol levels (Supplementary Fig. 5). Taken together, these findings indicate that the expression of Dicer in ECs enhances atherosclerotic lesion formation.

miR-103 induces endothelial inflammation. Among the miRNAs downregulated in the aorta of EC-Dicer^{flox} mice, miR-103 was expressed most abundantly in human ECs (Fig. 4a) and was highly enriched in the RISCs of these cells, as determined using anti-argonaute 2 (AGO2)-immunoprecipitation, suggesting a prominent role for miR-103 in the regulation of EC function (Fig. 4b). Notably, the expression of miR-107, which shares the same seed sequence with miR-103, was not affected by endothelial *Dicer* deletion (Fig. 1c,d and Supplementary Tables 1 and 2). Stimulation of HAECs with TNF-α moderately induced miR-103 and suppressed miR-433 expression, whereas blocking of NF-κB reduced only the expression of miR-103 and -301b (Fig. 4c,d). In addition, the expression of miR-103 was upregulated in HAECs upon stimulation with native low-density lipoprotein (LDL) and further increased by mildly oxidized LDL treatment (Fig. 4e). These data suggest that NF-κB activity and hyperlipidemia drive the expression of miR-103 in atherosclerotic ECs, which may in turn indirectly regulate the chemokine expression.

In addition, miR-103 was highly expressed in the aortic endothelium after 4 and 12 weeks of HFD feeding in EC-Dicer^{WT} mice, whereas endothelial miR-103 expression was not detectable by *in situ* PCR in EC-Dicer^{flox} mice (Fig. 4f and Supplementary Fig. 6). Similarly, combined *in situ* PCR and immunostaining of von Willebrand factor (vWF) revealed prominent miR-103 expression in ECs covering human atherosclerotic lesions (Fig. 4g,h). These results suggest that Dicer-mediated generation of endothelial miRNAs, in particular miR-103, may play a crucial role in lesion formation.

Overexpression of miR-103 was sufficient to upregulate the expression levels of the *CXCL1*, *CX$_3$CL1* and *CCL2* mRNAs after

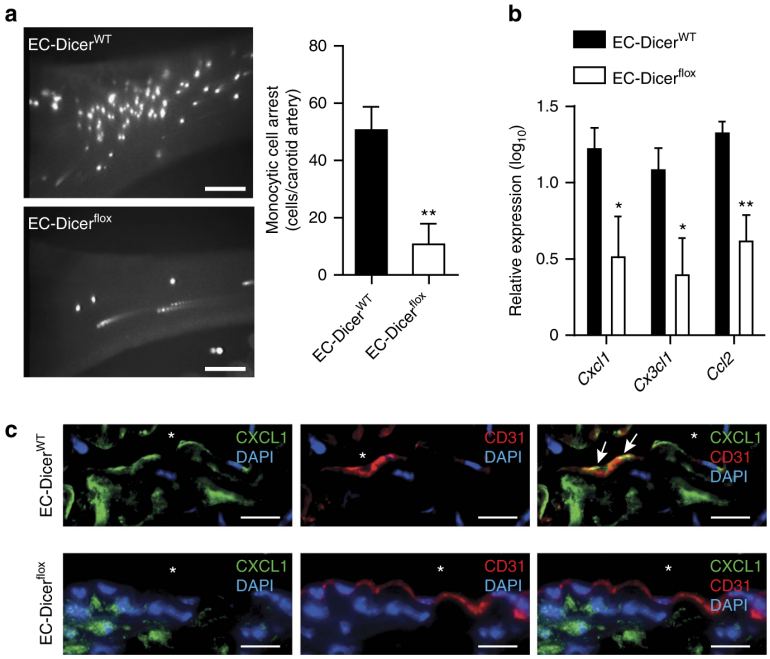

Figure 2 | Role of endothelial Dicer in atherogenic monocyte adhesion. (**a**) *Ex vivo* perfusion assays showing monocytic cell arrest on the endothelia of the left carotid arteries of mice ($n=4$–5 mice per group) fed a HFD for 4 weeks. (**b**) Quantitative RT-PCR analyses of the mRNA expression levels of chemokines in carotid arteries of mice ($n=3$–4 mice per group) fed a HFD for 4 weeks. (**c**) Immunostaining of CXCL1 and the endothelial marker CD31 in carotid artery sections after 4 weeks of HFD feeding. Arrows indicate CXCL1 expressing ECs. Representative images of three independent experiments are shown. The nuclei were stained with 4′,6-diamidino-2-phenylindole (DAPI). Scale bars, 30 μm (**a**), 12 μm (**c**). Asterisks indicate the lumen. The data are represented as the mean ± s.e.m. of the indicated number (n) of repeats. *$P<0.05$ and **$P<0.01$ by Student's t-test.

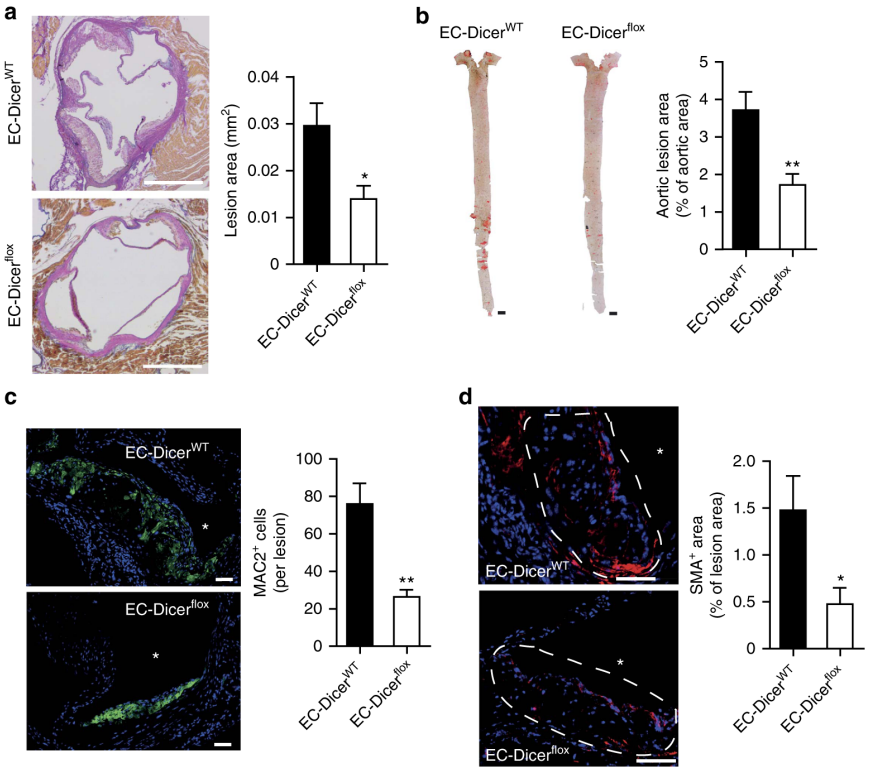

Figure 3 | Loss of endothelial Dicer limits atherosclerosis. (**a**,**b**) Atherosclerotic lesion formation in mice fed a HFD for 12 weeks analysed in aortic root sections stained with elastic van Gieson stain (a; $n=8$ mice per group) and in *en face* prepared aortas stained with Oil red O stain (b; $n=9$–10 mice per group). (**c**,**d**) Macrophage and smooth muscle cell accumulation in aortic root lesions determined by immunostaining of MAC2 (**c**, green; $n=7$–9 mice per group) and smooth muscle actin (**d**, red; $n=8$ mice per group), respectively. The nuclei were counterstained with 4′,6-diamidino-2-phenylindole (DAPI; blue). Scale bars, 500 μm (**a**), 50 μm (**c**,**d**) and 1 mm (**b**). Asterisks indicate the lumen. Dashed lines encircle atherosclerotic lesions. The data are represented as the mean ± s.e.m. of the indicated number (n) of repeats. $^*P<0.05$ and $^{**}P<0.01$ by Student's t-test.

silencing Dicer in HAECs (Fig. 5a). Furthermore, treatment of HAECs with a specific locked nucleic acid (LNA)-inhibitor, which reduced miR-103 expression by 70% (Fig. 5b), also reduced the expression of the *CXCL1*, *CX$_3$CL1* and *CCL2* mRNAs significantly (Fig. 5c). Downregulation of CXCL1 was also confirmed at the protein level (Fig. 5d). Next, *in vitro* flow chamber assays were used to examine the effect of miR-103 on monocyte adhesion to ECs. Unlike non-targeting LNA-oligonucleotides, LNA-inhibitors of miR-103 attenuated the adhesion of monocytic cells to HAECs (Fig. 5e). Conversely, transfection of HAECs with miR-103 mimics, which increased miR-103 expression by 22-fold (Fig. 5f), upregulated the expression levels of *CXCL1* and *CX$_3$CL1*, but had only a slight effect on the expression of *CCL2* (Fig. 5g). Furthermore, overexpression of miR-103 in HAECs increased monocytic cell adhesion, and this effect was reversed by blocking the CXCL1 receptor C–X–C chemokine receptor type 2 on monocytes (Fig. 5h). These findings suggest that reduced expression of miR-103 in EC-Dicer^{flox} mice results in diminished adhesion of monocytes to the carotid arteries.

Endothelial Dicer regulates KLF4-dependent gene expression. To study the mechanism by which deficiency of endothelial Dicer reduced lesion formation, genome-wide microarray analyses of atherosclerotic arteries from EC-Dicer^{WT} and EC-Dicer^{flox} mice fed a HFD for 12 weeks were performed ($n=2$ mice per group; $P<0.05$ by a moderated t-test (Limma); fold change cutoff = 1.2). Overall, 469 transcripts were upregulated and 652 transcripts were downregulated in EC-Dicer^{flox} mice compared with EC-Dicer^{WT} mice. In addition to the transcription factor *c-Myb*, the Wnt pathway members *transcription factor 7 (Tcf7)* and *lymphoid enhancer-binding factor 1* (*Lef1)* and the expression of EC-specific genes, such as *Cadherin 5* (*Cdh5;* also known as VE-Cadherin), *Claudin-5 (Cldn5)*, *BMX non-receptor tyrosine kinase (Bmx)* and *SRY (sex-determining region Y)-box 17 (Sox17),* were increased in EC-Dicer^{flox} mice (Fig. 6a). By contrast, the expression level of proinflammatory genes, like *Ccl2*, *CD44 antigen (CD44)*, *Rho-associated coiled-coil containing protein kinase 1* (*Rock1)* and *Nfkb1,* was reduced in the aortas of EC-Dicer^{flox} mice (Fig. 6a). We confirmed by qRT–PCR in a larger number of mice that endothelial Dicer deficiency increases the expression level of *c-Myb*, *Tcf7*, *dickkopf homolog 2* (*Dkk2)* and *Sox17*; however, the expression of *Lef-1* only tended to be increased in EC-Dicer^{flox} mice (Fig. 6b). Next, we analysed the differentially expressed genes using Ingenuity Pathway Analysis software. Genes related to biological processes such as development of blood vessels, inflammatory response, chemotaxis and immune cell adhesion were enriched among the differentially expressed genes in EC-Dicer^{flox} mice (Fig. 6c). Moreover, the expression levels of genes related to the KLF4 pathway were also differentially expressed in EC-Dicer^{flox} mice and were indicative of increased KLF4 signalling (Fig. 6d). KLF4 has been implicated in the regulation of *TCF7*

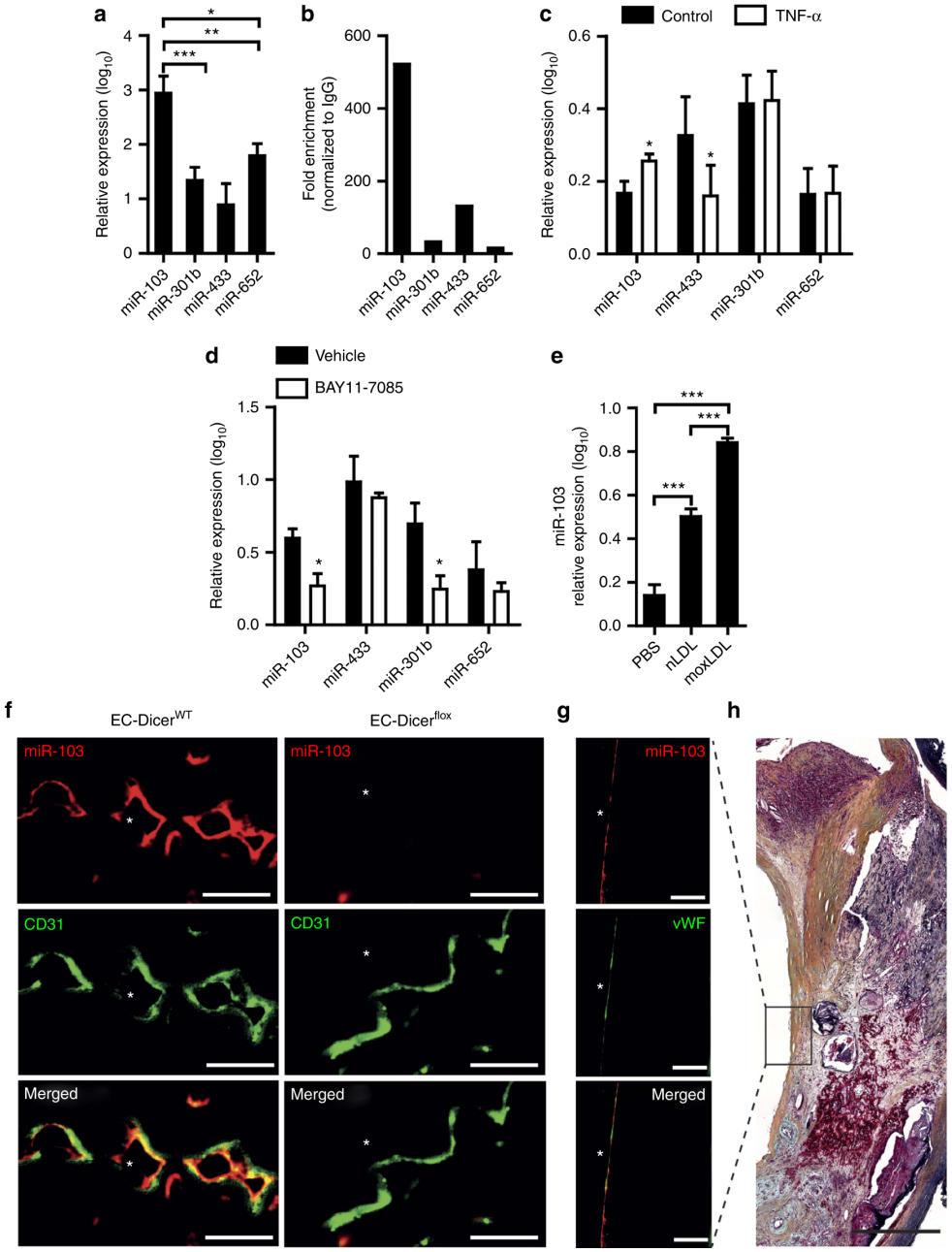

Figure 4 | Expression of miR-103 in ECs during atherosclerosis. (**a**,**b**) The expression levels of miR-103, miR-301b, miR-433 and miR-652 (a; $n=5$ per group) and their enrichment in AGO2-IPs of human ECs (**b**). The results of **b** are expressed as the fold enrichment of miRNAs in AGO2-IP samples compared with control IgG-IP samples. Results of one representative experiment are shown in **b**. (**c**) Quantitative RT-PCR analyses of the expression levels of miR-103, miR-301b, miR-433 and miR-652 in HAECs with and without TNF-α stimulation ($n=3$–4 per group). (**d**) MiRNA expression level in HAECs treated with vehicle or the NF-κB-inhibitor BAY11-7085 ($n=4$–5 per group). (**e**) Expression levels of miR-103 in HAECs treated with PBS, native low-density lipoprotein (nLDL) or mildly oxidized-low-density lipoprotein (moxLDL; $n=4$ per group). (**f**) Combined *in situ* PCR detection of miR-103 and immunostaining of the endothelial marker CD31 in carotid sections from EC-Dicer^{WT} and EC-Dicer^{flox} mice fed a HFD for 4 weeks. Representative images of three independent experiments are shown. (**g**) Endothelial miR-103 expression in human atherosclerotic plaques determined by *in situ* PCR and immunostaining of von Willebrand factor (vWF). (**h**) Movat's pentachrome staining of a human atherosclerotic plaque section located adjacent to that used for the *in situ* detection of miR-103. The region of the plaque used for miR-103 expression analysis is indicated. Scale bars, 12 μm (**f**), 25 μm (**g**) and 500 μm (**h**). Asterisks indicate the lumen. The data are represented as the mean ± s.e.m. of the indicated number (n) of repeats. $^{*}P<0.05$, $^{**}P<0.01$ and $^{***}P<0.001$ by Student's *t*-test and one-way analysis of variance.

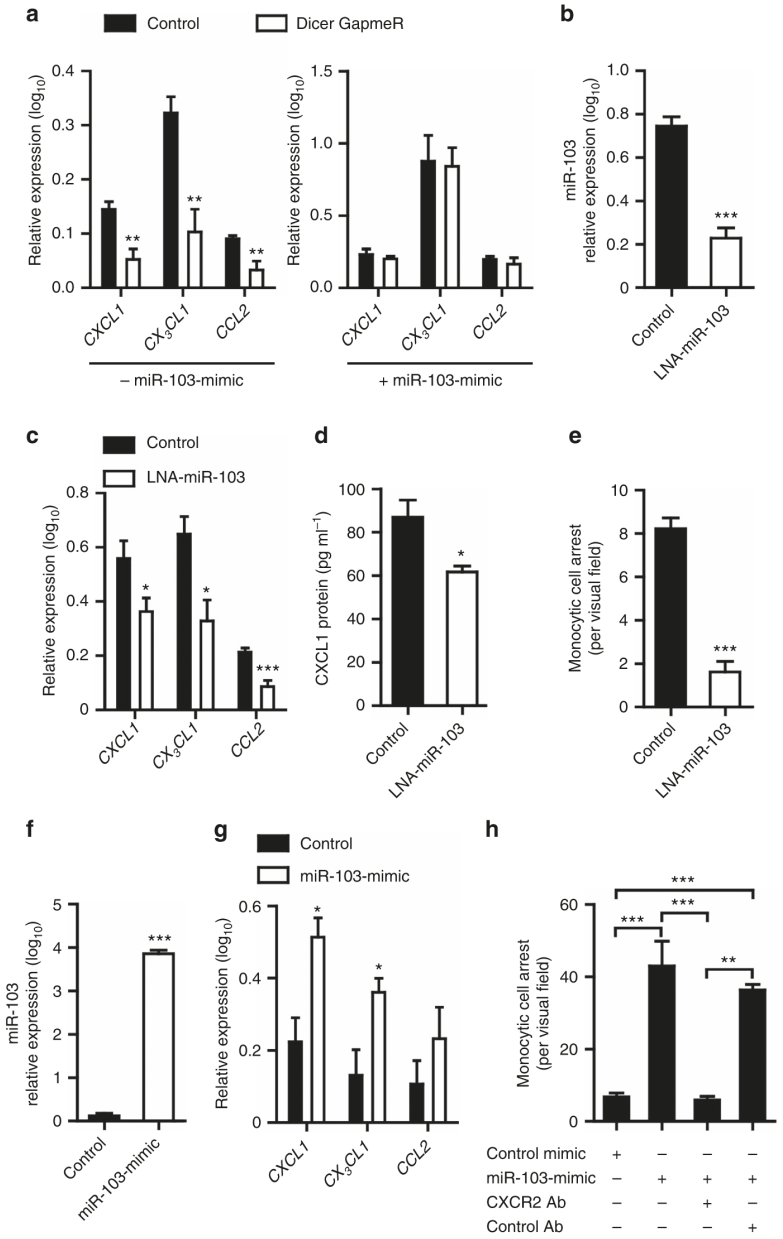

Figure 5 | Effects of miR-103 on chemokine expression in ECs and monocyte adhesion. (**a**) Chemokine mRNA expression in HAECs treated with Dicer-specific LNA-GapmeRs or control LNA-GapmeRs with (right) or without (left) miR-103-mimic treatment ($n=4$–6 per group). (**b**,**c**) Quantitative RT-PCR analyses of miR-103 (**b**) and chemokine mRNA (**c**) expression levels in HAECs ($n=5$–6 per group) treated with LNA-inhibitors of miR-103 or non-targeting LNA-oligonucleotides. (**d**) ELISA of CXCL1 protein expression in HAEC lysates ($n=3$–4 per group) with and without miR-103 inhibition. (**e**) Flow chamber assays to determine monocyte adhesion to HAECs treated with LNA-inhibitors of miR-103 or control oligonucleotides ($n=3$ per group). (**f**,**g**) The expression of miR-103 (**f**) or chemokine mRNAs (**g**) in HAECs treated with miR-103-specific or negative control mimics ($n=3$–4 per group). (**h**) Adhesion of monocytes to HAECs treated with miR-103-mimics or control oligonucleotides under flow conditions. Monocytic cells were pretreated with or without an antibody to block CXCR2 or non-targeting control IgG ($n=3$ per group). The data are represented as the mean ± s.e.m. of the indicated number (n) of repeats. $^{*}P<0.05$, $^{**}P<0.01$ and $^{***}P<0.001$ by Student's t-test (**b**–**d**) and one-way analysis of variance (**a**,**e**).

and *MYB* expression[46,47]. Overexpression and silencing of *KLF4* in HAECs increased and reduced the expression of *c-MYB*, respectively, whereas the expression of *TCF7* mRNA was not affected (Supplementary Figs 7 and 8). Accordingly, knockout of *Dicer* in ECs resulted in *c-MYB* expression in ECs covering aortic root lesions, which was not detectable in ECs from EC-Dicer^{WT} mice by dual immunostaining of c-MYB and vWF (Supplementary Fig. 9). Overall, these data demonstrate that

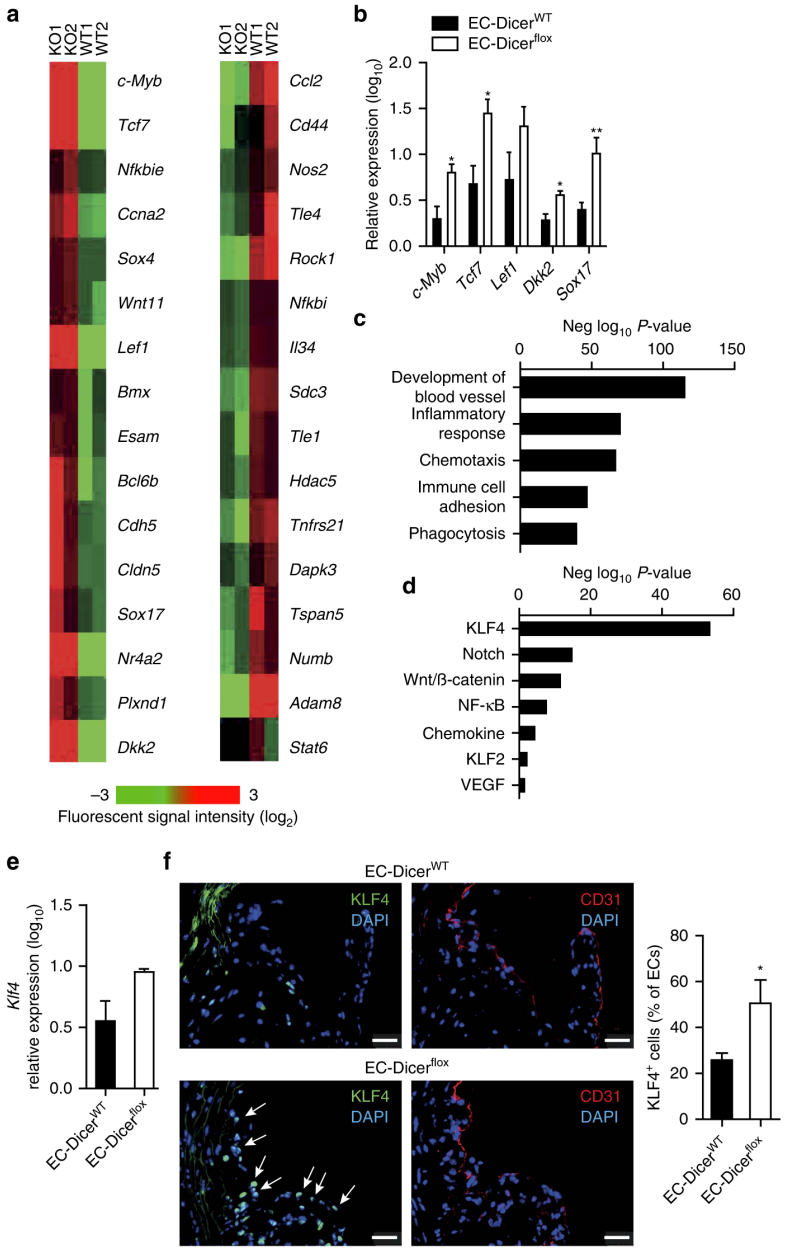

Figure 6 | Effect of endothelial Dicer deletion on arterial gene expression. (**a**) Heat map of genes differentially expressed in the aortas of EC-Dicer^{flox} mice compared with EC-Dicer^{WT} mice ($n=2$ mice per group; $P<0.05$; fold change cutoff = 1.2) after 12 weeks HFD feeding. (**b**) Quantitative RT-PCR analyses of the *c-Myb, Tcf7, Lef1, Dkk2* and *Sox17* expression levels in the aortas of EC-Dicer^{WT} and EC-Dicer^{flox} mice after 12 weeks HFD feeding ($n=4$–7 mice per group). (**c**,**d**) Significant enriched biological processes (**c**) and signalling pathways (**d**) among the genes differentially regulated in EC-Dicer^{flox} mice as compared with EC-Dicer^{WT} mice using Ingenuity Pathway Analysis software. (**e**) Quantitative RT-PCR analyses of *Klf4* mRNA expression in the aortas of EC-Dicer^{WT} and EC-Dicer^{flox} mice after 12 weeks of HFD feeding ($n=4$ mice per group). (**f**) KLF4$^+$ ECs in aortic root sections of EC-Dicer^{WT} and EC-Dicer^{flox} mice identified by immunostaining of KLF4 and the endothelial marker CD31. The arrows indicate ECs with nuclear KLF4 staining. The nuclei were counterstained with 4′,6-diamidino-2-phenylindole (DAPI). Representative images are shown ($n=3$–4 mice per group). Scale bar, 25 μm. The data are represented as the mean ± s.e.m. of the indicated number (n) of repeats. $^*P<0.05$; $^{**}P<0.01$ by Student's t-test.

loss of Dicer upregulates the expression of KLF4-regulated genes in ECs, such as *c-MYB*.

Although deficiency of endothelial Dicer preferentially regulated KLF4-dependent genes, KLF4 mRNA expression levels in the aortic wall were not different between EC-Dicer^{flox} and EC-Dicer^{WT} mice (Fig. 6e). However, the number of KLF4-expressing arterial ECs was increased in EC-Dicer^{flox} compared with EC-Dicer^{WT} mice (Fig. 6f), compatible with

translational inhibition of KLF4 expression by miR-103. These results suggest that activation of the KLF4 pathway in ECs contributes to the atheroprotective effect of endothelial Dicer deficiency by reducing arterial inflammation and increasing endothelial differentiation.

miR-103 induces endothelial inflammation by targeting KLF4. Notably, miR-103 can directly target the *KLF4* mRNA by binding to a conserved site in its 3′ untranslated region (UTR; Supplementary Fig. 10)[48]. Overexpressing a mutant GW182 protein in murine (Fig. 7a) and human ECs (Fig. 7b) enabled the locking of miRNAs and their targets in the RISC[49]. MiR-103-mimic treatment in these cells enriched *KLF4* mRNA but not *c-MYB* mRNA in the GW182-IPs, demonstrating that miR-103 targets *KLF4*, but not *c-MYB* mRNA in ECs (Fig. 7a,b). Moreover, treatment of HAECs with LNA inhibitors of miR-103 increased KLF4 protein expression (Fig. 7c) but did not affect *KLF4* mRNA levels (Fig. 7d). By contrast, the expression of KLF2 protein was not affected by treatment of HAECs with LNA inhibitors of miR-103 (Supplementary Fig. 11). Taken together, these results suggest that reduced endothelial miR-103 expression due to Dicer deficiency results in increased KLF4 protein expression in atherosclerotic endothelium.

Silencing of KLF4 in HAECs upregulated the expression level of miR-103 (Fig. 7e), as well as those of the *CXCL1*, *CX_3CL1* and *CCL2* mRNAs in both the presence and absence of miR-103 inhibition (Fig. 7f). Conversely, overexpression of KLF4 downregulated the expression levels of miR-103 (Fig. 7g) and the *CXCL1*, *CX_3CL1* and *CCL2* mRNAs (Fig. 7h) in HAECs, and treatment with miR-103 mimics prevented the suppression of chemokine expression by KLF4 (Fig. 7h). These data suggest that KLF4 affects chemokine expression downstream of miR-103, but may also act upstream of this miRNA in a negative feedback loop. TNF-α stimulation and blockage of NF-κB reduced and increased the expression of *KLF4*, respectively (Supplementary Fig. 12). Moreover, inhibition of the interaction between miR-103 and its binding site in the 3′UTR of *KLF4* using LNA-modified target site blockers (KLF4-TSBs) reduced the expression levels of chemokine mRNAs (Fig. 7i) and diminished monocyte adhesion (Fig. 7j), demonstrating that miR-103 regulates the adhesive properties of ECs by targeting KLF4. Overall, these results indicate that miR-103 induces chemokine expression in ECs by translational repression of the anti-inflammatory transcription factor KLF4.

Targeting of KLF4 by miR-103 promotes atherosclerosis. To study the effect of the interaction between miR-103 and KLF4 on atherosclerosis, *$Apoe^{-/-}$* mice were treated with KLF4-TSBs or control LNA-modified oligonucleotides during the last 4 weeks of an 8-week HFD feeding programme. Increased endothelial expression of KLF4 in *$Apoe^{-/-}$* mice treated with KLF4-TSBs was detected by dual immunostaining of KLF4 and vWF (Fig. 8a). Treatment with KLF4-TSBs reduced the aortic lesion area (by 53%; Fig. 8b) and the lesional macrophage number (by 30%; Fig. 8c) compared with the treatment with control oligonucleotides. Moreover, inhibition of the interaction between miR-103 and KLF4 reduced the number of CXCL1-expressing ECs (Fig. 8d) and downregulated the *Cxcl1* mRNA expression in carotid arteries (Fig. 8e). By contrast, the expression level of *Cxcl1* was not affected in other tissues, like the liver, spleen and heart, following KLF4-TSBs treatment (Fig. 8e). Treatment with KLF4-TSBs induced endothelial expression of eNOS in aortic root lesions and the expression of *Nos3* in carotid arteries (Fig. 8f,g). Serum cholesterol levels were similar between control mice and mice treated with KLF4-TSBs (Supplementary Fig. 13). Taken together, these findings indicate that miR-103 enhances atherosclerotic lesion formation by suppressing KLF4.

Discussion

Here, we demonstrate that deficiency of Dicer in the endothelium of *$Apoe^{-/-}$* mice diminishes endothelial inflammation, which reduces monocyte adhesion to atherosclerosis-prone endothelium and the development of atherosclerotic lesions. Deletion of *Dicer* in ECs primarily decreased the expression of a small subset of unstable miRNAs, including miR-103, and promoted KLF4-dependent gene expression. MiR-103 expression was upregulated by NF-κB and mildly oxidized LDL in human ECs and increased the expression of CXCL1 by targeting KLF4, thereby enhancing monocyte adhesion to ECs. Inhibition of the miR-103-KLF4 interaction reduced atherosclerosis, lesional macrophage accumulation and endothelial CXCL1 expression in the arteries of *$Apoe^{-/-}$* mice, indicating a proinflammatory and proatherogenic role of miR-103 by targeting KLF4.

The normal functions of various differentiated cell types, such as cardiomyocytes, pancreatic beta cells and SMCs, requires Dicer activity and fully functioning miRNA biogenesis[32,33,50]. However, mice with a deletion of the *Dicer* gene in ECs develop normally, indicating that permanent Dicer activity is of less importance in EC homeostasis[37]. Notably, knockdown of Dicer in ECs *in vitro* reduces the expression of CXCL1 and upregulates endothelial genes, like *eNOS* and *Tie2*, indicating that Dicer promotes inflammatory activation and impairs endothelial differentiation[38,51]. ECs at arterial bifurcations are primed by disturbed flow for inflammatory activation in response to hyperlipidemic stress, which results in NF-κB-dependent upregulation of CXCL1 and atherogenic monocyte adhesion[8,15]. Accordingly, we found that endothelial Dicer deficiency downregulates CXCL1 in murine arteries and reduces the adhesion of monocytes to the endothelium during the early stage of atherosclerosis. In line with its effect on monocyte adhesion, deficiency of Dicer in ECs reduced the development of atherosclerosis and the accumulation of lesional macrophages, suggesting that the generation of miRNAs in ECs during atherosclerosis promotes lesion formation by increasing CXCL1-dependent monocyte adhesion. The detrimental role of endothelial Dicer during atherogenesis may be due to the key role of miRNAs in the maladaptive response of ECs to disturbed flow. The miRNA expression profile in ECs exposed to disturbed blood flow at arterial bifurcations differs substantially from that in ECs at unbranched arterial segments[42] and is characterized by downregulation of atheroprotective (such as miR-126-5p)[52] and upregulation of pro-atherogenic miRNAs (such as miR-92a)[41]. Moreover, ECs at arterial bifurcations proliferate more frequently than quiescent ECs at unbranched segments[52]. In contrast to proliferating cells, the majority of miRNAs in quiescent cells is stable (persistence of miRNAs up to 2 months following Dicer ablation in neurons *in vivo* have been reported)[53], stored in Argonaut complexes and functionally silent probably due to their sequestration by polysomes[29,54–56]. Therefore, reduced endothelial miRNA biogenesis at predilection sites of atherosclerosis may cause the protective effects of endothelial Dicer deficiency on lesion formation.

Although miRNAs are generally stable, a small subset of miRNAs that associates with Argonaut proteins demonstrates fast turnover rates in a highly dynamic and cell type-specific manner[28,29,57]. After silencing of Dicer in ECs, let-7 family miRNAs, miR-103, miR-221 and miR-27b have a higher turnover rate than miR-126-3p, miR-21, miR-23a and miR-26a[39]. We found that the expression levels of four miRNAs, including miR-103, were highly dependent on endothelial Dicer activity.

Hence, downregulation of unstable miRNAs, like miR-103, following *Dicer* deletion may limit monocyte adhesion and atherosclerosis in mice. MiR-103 has a key role in regulating insulin sensitivity in adipocytes by targeting caveolin-1, and in cancer cell growth and metastasis by repressing different targets, including KLF4 (refs 48,58,59). MiR-103 is one of the most highly expressed miRNA in ECs cultured under static conditions and downregulated by high-shear stress[38,60]. *In vivo*, miR-103 is upregulated at predilection sites for the development of atherosclerosis characterized by disturbed flow-induced

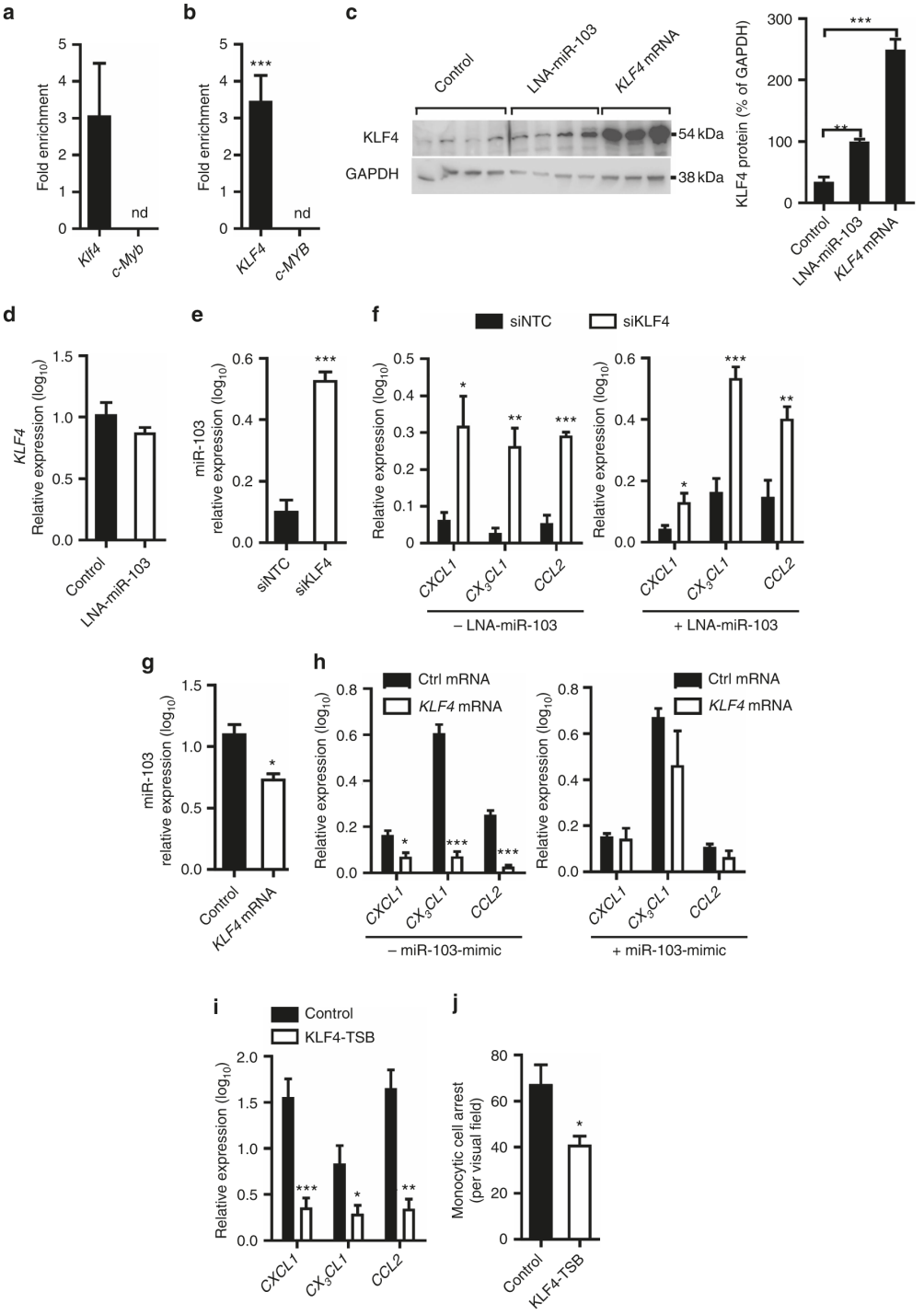

endothelial NF-κB activation[42]. The results presented here show that NF-κB activation upregulates miR-103 and thereby promotes the expression of chemokines, such as CXCL1, CCL2 and CX_3CL1. MiR-103 increased CXCL1-dependent monocyte adhesion and rescued the decreased chemokine expression caused by knockdown of *Dicer* in ECs, indicating that reduced endothelial miR-103 levels limit monocyte adhesion and atherosclerosis in EC-Dicer^{flox} mice by downregulating CXCL1.

The reduced endothelial inflammation in atherosclerotic arteries of EC-Dicer^{flox} mice was associated with enhanced KLF4 activity. Although KLF4 is closely related to KLF2, only 30% of the KLF4-regulated genes in ECs are also controlled by KLF2, indicating non-redundant roles of KLF2 and KLF4 in endothelial function[46]. For example, KLF4 but not KLF2 upregulates Cdh5 and Claudin-5 by direct interaction with their promoter and thus reduces endothelial permeability[61–63]. By contrast, both KLF4 and KLF2 attenuate endothelial inflammation by inhibiting NF-κB activation through competitive binding to the p300 coactivator[2]. An atheroprotective role of endothelial KLF4 was demonstrated by gain-an-loss-function studies in mice[64]. The expression of KLF2 and KLF4 is transcriptionally upregulated by the MEK5/Erk5/MEF2 signalling pathway and posttranscriptionally silenced by disturbed flow-induced miR-92a[3,65]. In accordance with previous reports in cancer cells, we found that miR-103 represses the translation of KLF4 mRNA by direct interaction with a conserved binding site in its 3′UTR, which results in NF-κB-mediated upregulation of CXCL1 in ECs[48]. Hence, miR-103 might act as a molecular switch for the inflammatory activation of arterial ECs by fine-tuning the functional antagonism between KLF4 and NF-κB. The findings that inhibition of the interaction between miR-103 and KLF4 reduced atherosclerosis and increased endothelial KLF4 expression in *Apoe*$^{-/-}$ mice demonstrates a proatherogenic role of this interaction and suggests that derepression of KLF4 due to downregulation of miR-103 contributes to the atheroprotective effect of Dicer deficiency in ECs.

In conclusion, deficiency of Dicer in the endothelium of *Apoe*$^{-/-}$ mice reduced monocyte adhesion to the early atherosclerotic endothelium by downregulating CXCL1, and thereby diminished lesion formation. Thus, endothelial Dicer activity at arterial sites predisposed to atherosclerosis may play a pro-atherogenic role by generating proinflammatory miRNAs. This effect of Dicer is attributable to reduced endothelial miR-103 expression and the subsequent restoration of *KLF4* expression. Moreover, selective inhibition of the targeting of KLF4 by miR-103 using antisense oligonucleotides may represent a novel approach to treat atherosclerosis.

Methods

Animal models. Cdh5-CreER^{T2} mice (kindly provided by Dr Iruela-Arispe, UCLA, Los Angeles, CA, USA) were crossed with Dicer1$^{flox/flox}$/*Apoe*$^{-/-}$ mice (Jackson Laboratory) to obtain Cdh5-CreER^{T2}Dicer1$^{WT/flox}$/*Apoe*$^{-/-}$ mice[66,67]. Cdh5-CreER^{T2}Dicer1$^{flox/flox}$/*Apoe*$^{-/-}$ (EC-Dicer^{flox}) and Cdh5-CreER^{T2}Dicer1$^{WT/WT}$/*Apoe*$^{-/-}$ (EC-Dicer^{WT}) littermates were used for experiments. Cre recombinase activity was induced by intraperitoneal injection of the mice with TMX (2 mg per 20 g body weight; Sigma-Aldrich) dissolved in neutral oil (Migyol; Sasol) for 5 consecutive days. Deletion of the conditional *Dicer* allele after TMX injection was verified in the aortas of EC-Dicer^{flox} mice by PCR[67]. One week after the last TMX injection, 6- to 8-week-old female mice were fed a HFD consisting of 21% crude fat, 0.15% cholesterol and 19.5% casein (Altromin, Lage, Germany) for the indicated time points. For immunohistochemistry, the aortas and carotid arteries were harvested after *in situ* perfusion fixation with 4% paraformaldehyde (Carl Roth) or PAXgene (Qiagen). For purification of mRNAs or miRNAs, the arteries were perfused with RNAlater (Life Technologies). All animal experiments were reviewed and approved by the local authorities (State Agency for Nature, Environment and Consumer Protection of North Rhein-Westphalia and District Government of Upper Bavaria) in accordance with the German animal protection laws.

Histology and immunostaining. Thoracoabdominal aortas were prepared *en face* and stained with Oil Red O stain. The Oil Red O-positive area was quantified from digital images of the aorta using image analysis software (ImageJ). Serial sections (5 μm thick) from carotid arteries and aortic roots were stained with Movat's pentachrome or Elastic van Gieson stain. A bright-field microscope (Leica DM6000B; Leica Microsystems) connected to a CCD camera (Leica DFC365FX) was used to obtain the images. The lesion area was quantified using planimetry (Leica LAS software). Immunostaining of CXCL1 (1:25; rabbit polyclonal antibody, PeproTech), macrophage-specific Mac2 (MAC2; 1:400; clone M3/38, Cedarlane), α-smooth muscle actin (1:200; clone 1A4, Dako), CD31 (1:75; goat polyclonal antibody, Santa Cruz Biotechnology), vWF (1:1,000; rabbit polyclonal antibody, Abcam), KLF4 (1:200; rabbit polyclonal antibody, Abcam), eNOS (1:100; purified mouse antibody, BD Bioscience) and c-MYB (1:300, rabbit polyclonal antibody, Hölzel Diagnostika Handels GmbH) was performed in carotid arteries or aortic root sections. The staining of KLF4 and CD31 was performed separately on adjacent sections. Cell nuclei were counterstained with 4′,6-diamidino-2-phenylindole (Vectashield, Vector Laboratories). The positively stained area or the number of positive cells was normalized to the lesion area or lesional cell number, respectively, using ImageJ. Non-specific primary antibodies were used as negative controls (Santa Cruz Biotechnology). The background of the negative control defined the threshold. The analysis of the stainings was performed in blinded manner.

Human carotid lesion samples. Human atherosclerotic lesion samples were obtained during carotid endarterectomy and fixed with 4% paraformaldehyde (Carl Roth). The Ethics Committee of the Medical Faculty at RWTH Aachen University approved the study protocol for the collection of human atherosclerotic plaque specimens and all participants gave their written informed consent.

Blood chemistry. Serum cholesterol levels were measured by dry chemistry using a Vitros 250 Analyzer (Ortho Clinical 10 Diagnostics).

***Ex vivo* perfusion of carotid arteries.** The left carotid arteries were isolated from EC-Dicer^{flox} and EC-Dicer^{WT} mice after 4 weeks of HFD feeding and were mounted onto a microscopic stage. Monocytic Mono Mac6 cells (MM6; 10^6 cells per ml; Leibniz Institute DSMZ-German Collection of Microorganisms and Cell Cultures, Braunschweig, Germany) labelled with calcein AM (1 μM; Life Technologies), were perfused at a flow rate of 4 μl min^{-1} and monocytic cell adhesion was recorded using stroboscopic epifluorescence illumination[15].

Figure 7 | miR-103 promotes inflammatory activation of ECs by targeting KLF4. (**a**,**b**) Enrichment of *Klf4* and *c-Myb* transcripts in the miRNA-induced silencing complex (RISC) of mouse aortic ECs (**a**) and human aortic ECs (HAECs, **b**) treated with miR-103-mimics as determined by GW182-IP. The results are expressed as the fold enrichment of the mRNAs in GW182-IP samples compared with the input samples. Results of two independent experiments are shown. ND indicates not detected. (**c**) Immunoblot analyses of KLF4 protein expression in HAECs treated with LNA-inhibitors of miR-103, non-targeting control LNA-oligonucleotides or premade *KLF4* mRNA ($n=3$–4 per group). The KLF4 protein levels were normalized to those of GAPDH. Full scans of western blots are provided in Supplementary Fig. 14. (**d**) *KLF4* mRNA levels in HAECs treated with LNA-inhibitors of miR-103 or control LNA-oligonucleotides ($n=4$–5 per group). (**e**) MiR-103 expression after silencing KLF4 using siRNA (siKLF4) in HAECs. A non-targeting siRNA (siNTC) was used in the control group ($n=4$–5 per group). (**f**) The expression of *CXCL1*, *CX_3CL1* and *CCL2* after silencing KLF4 (siKLF4) in HAECs treated with (right) or without (left) LNA-inhibitors of miR-103 ($n=4$–5 per group). siNTCs were used in the control group. (**g**,**h**) The effect of transfection with *GFP* mRNAs (Ctrl) or premade *KLF4* mRNAs on miR-103 (**g**) and chemokine expression (**h**) in HAECs treated with (**h**, right) or without (**g**; **h**, left) miR-103-mimics ($n=3$–5 per group). (**i**) Expression of *CXCL1*, *CX_3CL1* and *CCL2* in HAECs treated with LNA-oligonucleotides (KLF4-target site blockers; KLF4-TSBs) designed to inhibit the interaction between miR-103 and the 3′UTR of KLF4 ($n=6$ per group). Non-targeting LNA-oligonucleotides were used in the control group. (**j**) Flow chamber assays to determine monocyte adhesion to HAECs treated with KLF4-TSBs or non-targeting oligonucleotides ($n=4$ per group). The data are represented as the mean ± s.e.m. of the indicated number (n) of repeats. *$P<0.05$, ** $P<0.01$ and *** $P<0.001$ by Student's *t*-test (**a**,**b**,**d**–**j**) and one-way analysis of variance (**c**).

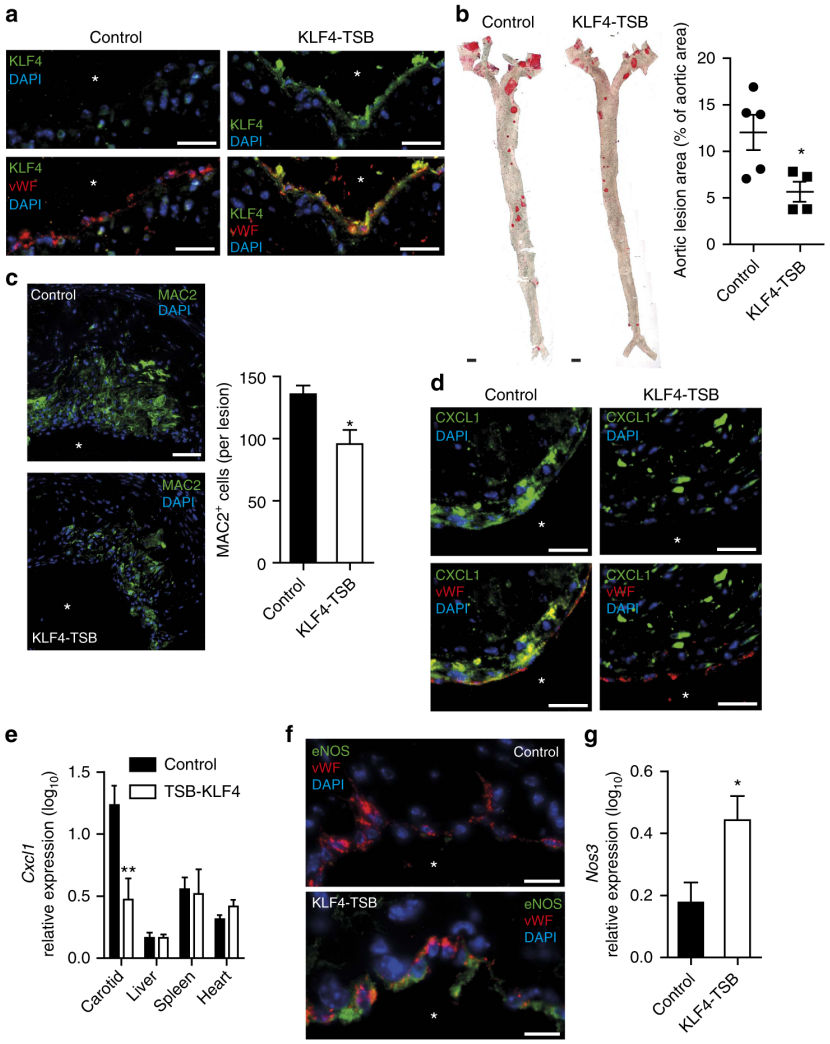

Figure 8 | Inhibition of the interaction between miR-103 and KLF4 limits atherosclerosis. (**a**) Immunostaining of KLF4 and von Willebrand factor (vWF) in aortic root sections of *Apoe*$^{-/-}$ mice treated with KLF4-TSBs or non-targeting LNA-oligonucleotides (control). Representative images are shown. Atherosclerosis (**b**) quantified in Oil red O-stained, *en face* prepared aortas and the lesional macrophage cell number (**c**) determined by MAC2 immunostaining in aortic root lesions from *Apoe*$^{-/-}$ mice treated with KLF4-TSBs or control oligonucleotides ($n=4$–6 mice per group). (**d**) Dual immunostaining of CXCL1 and vWF in aortic root sections of *Apoe*$^{-/-}$ mice treated with KLF4-TSBs or control oligonucleotides. (**e**) The expression levels of *Cxcl1* in the carotid, liver, spleen and heart of KLF4-TSB-treated *Apoe*$^{-/-}$ mice compared with control mice ($n=4$–7 mice per group). (**f**) Dual immunostaining of eNOS and vWF in aortic root sections of *Apoe*$^{-/-}$ mice treated with KLF4-TSBs or control oligonucleotides. (**g**) *Nos3* mRNA expression in the carotid arteries of KLF4-TSB-treated *Apoe*$^{-/-}$ mice compared with control mice ($n=5$–6 mice per group). The nuclei were counterstained with 4′,6-diamidino-2-phenylindole (DAPI). Asterisks indicate the lumen. Representative images of three independent experiments are shown. Scale bars, 10 μm (**f**), 25 μm (**a**,**d**), 50 μm (**c**) and 1 mm (**b**). The data are represented as the mean ± s.e.m. of the indicated number (n) of repeats. *$P<0.05$ and **$P<0.01$ by Student's t-test.

***In vivo* target site blocker treatment.** Following 4 weeks of HFD feeding, *Apoe*$^{-/-}$ mice were randomized to the different experimental groups and injected once weekly via the tail vein with KLF4 LNA-target site blocker oligonucleotides (5′-GTATGCAGCAGTTGG-3′) or control LNA-target site blocker oligonucleotides (5′-GCTCCCTTCAATCCAA-3′; 0.4 mg per 20 kg; miRCURY LNA Target Site Blocker, *in vivo* use; Exiqon). During the injection period, mice were fed with a HFD. The tissues were harvested 1 week after the last injection.

MiRNA real-time PCR array. After reverse transcription and pre-amplification of total RNA using the Megaplex RT & Preamp Rodent Pool Set (Life Technologies), the samples were loaded onto preconfigured 384-well microfluidic TaqMan Array MicroRNA Cards for real-time PCR (RT–PCR) analyses of 641 mouse miRNAs, using the 7900HT Real-Time PCR System (all from Life Technologies). Data analysis was performed using StatMiner software (Integromics) along with multiple internal control genes and the cycle threshold (CT) method. After 4 and 12 weeks HFD feeding, a total of 428 and 458 miRNAs, respectively, were detected according to the detection limit (defined as a CT = 40) of the individual assays.

Global gene expression analysis. Global gene expression analysis was performed using Agilent 8 × 60 K SurePrint G3 Mouse Gene Expression in combination with a one-colour-based hybridization protocol (IMGM Laboratories GmbH). Fluorescent signals on the microarrays were detected using the Agilent DNA Microarray Scanner (Agilent Technologies Germany GmbH). Flagged genes were removed from the analysis. Probe set intensities were summarized and normalized

using robust multi-array average, and significant differential expression was determined by moderated *t*-test (Limma) using a *P*-value cutoff of 0.05 and a fold change cutoff of 1.2 (GeneSpring GX Software, Agilent). Differentially regulated genes were analysed by Ingenuity Pathway Analysis (Qiagen). The Fisher's exact *t*-test was selected for the function and pathway analysis.

Preparation of moxLDL. Human native low-density lipoprotein (nLDL; 1 mg ml^{-1}, Calbiochem, Millipore) was incubated with 5 μM $CuSO_4$ at 37 °C for 4 h to prepare mildly oxidized-low-density lipoprotein (moxLDL). The LDL oxidation was stopped by adding 10 μM EDTA and the LDL was passed through PD-10 desalting column (GE Healthcare). To prepare nLDL for experimental use as a negative control, all the above steps were performed except the addition of $CuSO_4$. The moxLDL and nLDL were used within 14 days after preparation and stored at 4 °C.

Cell culture. HAEC (Cat. # C-12271; PromoCell), umbilical vein ECs (HUVEC; Cat. # CC-2517; Lonza) and mouse aortic ECs (Pelobiotech) were cultured in collagen-coated dishes (Millipore) using EC-growth medium (PromoCell). HAECs were stimulated for 6 h with TNF-α (10 ng ml^{-1}; R&D Systems), nLDL (50 μg ml^{-1}; Calbiochem, Millipore) or moxLDL (50 μg ml^{-1}, Calbiochem, Millipore). HAECs were incubated for 30 min with 5 μM BAY11-7085 (Millipore) to block NF-κB activation. Subsequently, the medium was replaced and RNA was isolated after 24 h. HAECs were cultured in collagen-coated perfusion chambers (μ-Slides VI$^{0.4}$, ibidi GmbH) and exposed to high-shear stress (15 dyne cm^{-2}) or low-shear stress (4 dyne cm^{-2}) for 48 h generated by perfusion with medium (ibidi Pump System, ibidi GmbH).

Gram-negative endotoxin levels were tested in the medium of HAECs und HUVECs using the LAL Chromogenic Endotoxin Quantitation Kit (Thermo Scientific). The endotoxin concentration was consistently less than 0.1 Endotoxin Units (EU)/ml.

MM6 cells (Mono Mac 6; Leibniz Institute DSMZ-German Collection of Microorganisms and Cell Cultures) were cultured in RPMI medium (with L-Glutamine; GE Healthcare Life Sciences) containing 10% FBS, OPI media supplement (1 mM oxaloacetate, 0.45 mM pyruvate, 0.2 U ml^{-1} insulin; Sigma-Aldrich), 1 × MEM non-essential amino acids (Life Technologies), 2.5 μg ml^{-1} Plasmocin (InvivoGen), 100 μg ml^{-1} streptomycin and 100 U ml^{-1} penicillin (Life Technologies).

To isolate ECs, the periadventitial fat and connective tissue was removed from the aortas of EC-Dicer^{WT} and EC-Dicer^{flox} mice 2 weeks after TMX injection. The tissue was cut into 1–2 mm^2 sections, which were cultured in endothelial growth medium (PromoCell) for 7 days to allow the outgrowth of ECs. Subconfluent ECs of passage 3–5 were used for experiments. The EC phenotype was confirmed by lectin staining (*Lycopersicon esculentum*; Sigma)[15].

Myeloid cells were isolated from the blood of EC-Dicer^{WT} and EC-Dicer^{flox} mice 4 weeks after TMX injection and HFD feeding by magnetic cell sorting using CD11b$^+$ microbeads (MACS Miltenyi Biotec GmbH).

Treatment of HAECs. Lipofectamine RNAiMAX (Life Technologies) was used to transfect HAECs with a LNA-miR-103 inhibitor (50 nM, miRCURY LNA microRNA Inhibitors; Exiqon), a miR-103 mimic (15 nM, *mir*Vana mimics; Life Technologies), Dicer GapmeRs (10 nM, LNA GapmeRs; Exiqon), miR-103-KLF4 target site blockers (50 nM miRCURY LNA microRNA Target Site Blockers; Exiqon), premade *KLF4* mRNA (2 μg, mRNAExpress Human KLF4 Transcript; BioCat GmbH) or scrambled controls. Total RNA was isolated after 24 or 48 h using the RNeasy Mini Kit (Qiagen) or mirVana Isolation Kit (Life Technologies). HAECs were transfected with a small interfering RNA (siRNA) against KLF4 or a non-targeting siRNA (1 μM Accell siRNA in Accell Delivery Cell Culture Medium; Thermo Scientific) for 72 h. Additional treatment with the LNA-miR-103 inhibitor was performed as described above.

Quantitative real-time PCR. Total RNA was isolated from carotid arteries, aortas or cultured ECs using the mirVana miRNA Isolation Kit (Life Technologies), the RNeasy Mini Kit (Qiagen) or NucleoSpin microRNA Kit (Macherey-Nagel GmbH & Co. KG) and reverse-transcribed with a TaqMan microRNA reverse transcription kit or a high-capacity cDNA reverse transcription kit (both from Life Technologies). MiRNA qRT-PCR was performed using TaqMan microRNA assays and TaqMan Universal PCR Master Mix (both from Life Technologies). qRT–PCR assays for mRNAs were performed either with TaqMan gene expression assays and TaqMan Universal PCR Master Mix (both from Life Technologies) or with gene-specific primers (Sigma-Aldrich; Supplementary Table 3) and a SYBR Green Master Mix (Thermo Scientific). All qRT–PCR experiments were run on a 7900HT real-time PCR system (Life Technologies). The data were normalized to single or multiple reference genes (sno-135, RNU44 and U6 for miRNAs; *GAPDH* and *B2M* for mRNAs) and scaled to the sample with of the lowest expression using Qbase^{PLUS} software (Biogazelle NV).

***In situ* reverse transcriptase PCR.** Sections (5 μm thick) of carotid arteries and aortic roots were treated with DNase (Roche) for 15–17 h at 37 °C. One-step reverse transcriptase *in situ* PCR was performed using gene-specific Taq *in situ* primers (Sigma-Aldrich; Supplementary Table 3), SuperScript One-Step RT–PCR with PlatinumTaq (Life Technologies), and digoxigenin-11-dUTPs (Roche)[68]. After two washes with saline-sodium citrate buffer buffer and blocking of biotin/avidin-binding sites (Blocking Kit; Vector Laboratories), the sections were incubated with horseradish peroxidase-conjugated anti-digoxigenin sheep F'ab fragments (Roche) for 1 h at 37 °C. The probes were visualized using a tyramide-based amplification system (TSA Plus Biotin; Perkin Elmer) and DyLight 549-labelled streptavidin (Kirkegaard & Perry Laboratories)[52].

Argonaute 2 immunoprecipitation. ECs were harvested and washed in ice-cold phosphate-buffered saline (GE Healthcare Life Sciences), and then incubated in lysis buffer containing 400 μM vanadyl ribonucleoside complexes (New England Biolabs) and protease inhibitors (Complete Protease Inhibitor Cocktail Tablets; Roche).[26] The cell lysates were centrifuged and the input RNA was extracted from the supernatant using TRIzol reagent (Life Technologies). A human monoclonal AGO2 Ab (5 μg per 1,000 μl; clone 2E12-1C9; Abnova) or control IgG (5 μg per 1,000 μl; Millipore) was pre-incubated with protein A/G-conjugated magnetic beads (Millipore), and then incubated with the cell extract for 7 h at 4 °C. The precipitate was immobilized with a magnetic separator (Millipore). RNA was isolated from the precipitate using TRIzol reagent, reverse-transcribed using a high-capacity cDNA reverse transcription kit (Life Technologies), and amplified with gene-specific primers (Supplementary Table 3) and SYBR Green PCR Master Mix (Thermo Scientific). The fold enrichment of target genes in AGO2-immunoprecipitates (AGO2-IPs) over IgG-immunoprecipitates (IgG-IPs) was calculated as follows: $\Delta CT_{AGO2\text{-}IP} = CT_{input} - CT_{AGO2\text{-}IP}$, $\Delta CT_{IgG\text{-}IP} = CT_{input} - CT_{IgG\text{-}IP}$, $\Delta\Delta CT = \Delta CT_{AGO2\text{-}IP} - \Delta CT_{IgG\text{-}IP}$; and fold enrichment $= 2^{\Delta\Delta CT}$.

MiRNA target identification and quantification system (MirTrap). HAECs and mouse aortic ECs were co-transfected with miR-103-mimics and pMirTrap Vector using the Xfect MicroRNA Transfection Reagent in combination with Xfect Polymer for 24 h (all from Clontech). The pMirTrap Vector expressed a DYKDDDDK-tagged GW182 protein, which enabled locking of the miRNA/mRNA complex into the RISC[49]. After 24 h, ECs were harvested and washed in ice-cold × 1 phosphate-buffered saline (GE Healthcare Life Sciences), and then incubated in lysis buffer (MirTrap System, Clontech) supplemented with protease inhibitors (Complete Protease Inhibitor Cocktail Tablets; Roche). The cell lysates were centrifuged and part of the input RNA was extracted from the supernatant using the NucleoSpin RNA XS Kit (Macherey-Nagel GmbH & Co. KG). Anti-DYKDDDDK-conjugated magnetic beads were washed twice with lysis/wash buffer containing 1 mM dithiothreitol, 0.1 U μl^{-1} RNase inhibitor and protease inhibitors (Complete Protease Inhibitor Cocktail Tablets; Roche) and blocked for 3 h at 4 °C with 1.25 mg ml^{-1} tRNA solution and 1.25 mg ml^{-1} BSA. To immunoprecipitate the DYKDDDDK-tagged RISC complex, blocked anti-DYKDDDDK beads were incubated with the cell extract for 2 h at 4 °C. Immobilization of the precipitates and subsequent RNA isolation was performed using the NucleoSpin RNA XS Kit (Macherey-Nagel GmbH & Co. KG). Reverse transcription of input and IP samples were performed using a high-capacity cDNA reverse transcription kit (Life Technologies), followed by the amplification with gene-specific primers (Supplementary Table 3) using the SYBR Green PCR Master Mix (Thermo Scientific). The fold enrichment was calculated according to the manufacturer's protocol. Efficiency of transfection has been determined by performing a control transfection using miR-132-mimic, the pMirTrap Vector and the pMirTrap Control Vector, which express an AcGFP1 fluorescein protein containing a miR-132 target sequence. The efficient enrichment of AcGFP1 fluorescein protein in the RISC was confirmed and compared to that of a non-miR-132 target gene, such as *Lef1* mRNA transcript.

Flow adhesion assay. Mono Mac6 cells (MM6; 0.5 × 10^6 cells per ml) were labelled with calcein AM (1 μM) and, for some experiments, were treated with an antibody against C–X–C chemokine receptor type 2 (20 μg ml^{-1}, clone 48311) or an isotype control IgG (20 μg ml^{-1}, clone 20102; both from R&D Systems). HAECs were cultured in collagen-coated cell culture dishes (35 × 10 mm^2; Becton Dickinson) and transfected with LNA-miR-103, miR-103 mimic, KLF4 target site blockers or scrambled controls for 24 h. MM6 cells were resuspended in medium containing 1 × Hank's Balanced Salt Solution (Life Technologies), 1 M HEPES (Thermo Scientific) and 0.5% bovine serum albumin, and then perfused in a parallel plate flow chamber over a confluent monolayer of HAECs at a flow rate of 0.1 ml min^{-1}. Monocytic cell arrest on the endothelial monolayer was visualized by videomicroscopy at × 10 magnifications. After a 2-min observation period, cells adhering to the HAEC monolayer were counted in at least ten different microscopic view fields within 8 min.

Enzyme-linked immunosorbent assay. The CXCL1 protein concentration was determined in HAEC cell lysates with the GRO/MGS ELISA Development Kit (PeproTech). The absorbances were measured at 450 and 405 nm, respectively, on a microplate reader (Tecan).

Western blot analysis. HAECs were lysed in RIPA buffer (Sigma-Aldrich) including protease inhibitors (Complete Protease Inhibitor Cocktail, Roche). Cell lysates were resolved on SDS–PAGE gels and then transferred to nitrocellulose membranes. Proteins were detected using primary antibodies against KLF4 (1:1,000, EPR3550(2)ABC, Abcam), KLF2 (1:75, ab139699, Abcam) and GAPDH (1:1,000, clone 6C5, Millipore), and horseradish peroxidase (HRP)-conjugated secondary antibodies (1:1,000, Goat Anti-Mouse IgG HRP Affinity Purified PAb, R&D Systems; Goat Anti-Rabbit IgG HRP Affinity Purified PAb, Santa Cruz). Protein bands were visualized using an enhanced chemiluminescence detection system (ECL Advance, GE Healthcare Life Sciences) and an LAS 3000 Imager (Fuji Photo Film Co., Ltd.) and were quantified using Multigauge software (Fuji Photo Film). Intensities of the KLF4 and KLF2 bands were expressed as a percentage of those of the GAPDH bands.

Statistical analysis. The miRNA real-time PCR array data were analysed using StatMiner 4.2 software (Integromics) and are presented as mean values. All other data represent the mean ± s.e.m. Student's *t*-tests and one-way analysis of variance followed by the Newman–Keuls *post-hoc* test were used for statistical comparisons between groups using Prism 6 software (GraphPad Software Inc.). Sample size was estimated using StatMate software (GraphPad Software Inc.). $P<0.05$ was considered statistically significant.

References

1. Aird, W. C. Phenotypic heterogeneity of the endothelium: I. Structure, function, and mechanisms. *Circ. Res.* **100,** 158–173 (2007).
2. Hamik, A. *et al.* Kruppel-like factor 4 regulates endothelial inflammation. *J. Biol. Chem.* **282,** 13769–13779 (2007).
3. Parmar, K. M. *et al.* Integration of flow-dependent endothelial phenotypes by Kruppel-like factor 2. *J. Clin. Invest.* **116,** 49–58 (2006).
4. Jain, M. K., Sangwung, P. & Hamik, A. Regulation of an inflammatory disease: Kruppel-like factors and atherosclerosis. *Arterioscler. Thromb. Vasc. Biol.* **34,** 499–508 (2014).
5. Kwak, B. R. *et al.* Biomechanical factors in atherosclerosis: mechanisms and clinical implicationsdagger. *Eur. Heart J.* (2014).
6. Zeng, L. *et al.* Sustained activation of XBP1 splicing leads to endothelial apoptosis and atherosclerosis development in response to disturbed flow. *Proc. Natl Acad. Sci. USA* **106,** 8326–8331 (2009).
7. Fang, Y. & Davies, P. F. Site-specific microRNA-92a regulation of Kruppel-like factors 4 and 2 in atherosusceptible endothelium. *Arterioscler. Thromb. Vasc. Biol.* **32,** 979–987 (2012).
8. Hajra, L. *et al.* The NF-kappa B signal transduction pathway in aortic endothelial cells is primed for activation in regions predisposed to atherosclerotic lesion formation. *Proc. Natl Acad. Sci. USA* **97,** 9052–9057 (2000).
9. Gareus, R. *et al.* Endothelial cell-specific NF-kappaB inhibition protects mice from atherosclerosis. *Cell. Metab.* **8,** 372–383 (2008).
10. Aikawa, M. *et al.* Lipid lowering reduces oxidative stress and endothelial cell activation in rabbit atheroma. *Circulation* **106,** 1390–1396 (2002).
11. Schober, A., Nazari-Jahantigh, M. & Weber, C. MicroRNA-mediated mechanisms of the cellular stress response in atherosclerosis. *Nat. Rev. Cardiol.* **12,** 361–374 (2015).
12. Shemesh, S. *et al.* Interleukin-1 receptor type-1 in non-hematopoietic cells is the target for the pro-atherogenic effects of interleukin-1 in apoE-deficient mice. *Atherosclerosis* **222,** 329–336 (2012).
13. Ohta, H. *et al.* Disruption of tumor necrosis factor-alpha gene diminishes the development of atherosclerosis in ApoE-deficient mice. *Atherosclerosis* **180,** 11–17 (2005).
14. Combadiere, C. *et al.* Combined inhibition of CCL2, CX3CR1, and CCR5 abrogates Ly6C(hi) and Ly6C(lo) monocytosis and almost abolishes atherosclerosis in hypercholesterolemic mice. *Circulation* **117,** 1649–1657 (2008).
15. Zhou, Z. *et al.* Lipoprotein-derived lysophosphatidic acid promotes atherosclerosis by releasing CXCL1 from the endothelium. *Cell. Metab.* **13,** 592–600 (2011).
16. Boisvert, W. A. *et al.* Up-regulated expression of the CXCR2 ligand KC/GRO-alpha in atherosclerotic lesions plays a central role in macrophage accumulation and lesion progression. *Am. J. Pathol.* **168,** 1385–1395 (2006).
17. Gu, L. *et al.* Absence of monocyte chemoattractant protein-1 reduces atherosclerosis in low density lipoprotein receptor-deficient mice. *Mol. Cell* **2,** 275–281 (1998).
18. Oynebraten, I. *et al.* Characterization of a novel chemokine-containing storage granule in endothelial cells: evidence for preferential exocytosis mediated by protein kinase A and diacylglycerol. *J. Immunol.* **175,** 5358–5369 (2005).
19. Huo, Y. *et al.* The chemokine KC, but not monocyte chemoattractant protein-1, triggers monocyte arrest on early atherosclerotic endothelium. *J. Clin. Invest.* **108,** 1307–1314 (2001).
20. Tsou, C.-L. *et al.* Critical roles for CCR2 and MCP-3 in monocyte mobilization from bone marrow and recruitment to inflammatory sites. *J. Clin. Invest.* **117,** 902–909 (2007).
21. Schulz, C. *et al.* Chemokine fractalkine mediates leukocyte recruitment to inflammatory endothelial cells in flowing whole blood: a critical role for P-selectin expressed on activated platelets. *Circulation* **116,** 764–773 (2007).
22. Denk, A. *et al.* Activation of NF-kappa B via the Ikappa B kinase complex is both essential and sufficient for proinflammatory gene expression in primary endothelial cells. *J. Biol. Chem.* **276,** 28451–28458 (2001).
23. Hartmann, P., Schober, A. & Weber, C. Chemokines and microRNAs in atherosclerosis. *Cell. Mol. Life Sci.* **72,** 3253–3266 (2015).
24. Wei, Y., Nazari-Jahantigh, M., Neth, P., Weber, C. & Schober, A. MicroRNA-126, -145, and -155: a therapeutic triad in atherosclerosis? *Arterioscler. Thromb. Vasc. Biol.* **33,** 449–454 (2013).
25. Nazari-Jahantigh, M., Wei, Y. & Schober, A. The role of microRNAs in arterial remodelling. *Thromb. Haemost.* **107,** 611–618 (2012).
26. Wei, Y. *et al.* The microRNA-342-5p fosters inflammatory macrophage activation through an Akt1- and microRNA-155-dependent pathway during atherosclerosis. *Circulation* **127,** 1609–1619 (2013).
27. Ha, M. & Kim, V. N. Regulation of microRNA biogenesis. *Nat. Rev. Mol. Cell. Biol.* **15,** 509–524 (2014).
28. Guo, Y. *et al.* Characterization of the mammalian miRNA turnover landscape. *Nucleic Acids Res.* **43,** 2326–2341 (2015).
29. Gantier, M. P. *et al.* Analysis of microRNA turnover in mammalian cells following Dicer1 ablation. *Nucleic Acids Res.* (2011).
30. Bernstein, E. *et al.* Dicer is essential for mouse development. *Nature Genet.* **35,** 215–217 (2003).
31. Yang, W. J. *et al.* Dicer is required for embryonic angiogenesis during mouse development. *J. Biol. Chem.* **280,** 9330–9335 (2005).
32. da Costa Martins, P. A. *et al.* Conditional dicer gene deletion in the postnatal myocardium provokes spontaneous cardiac remodeling. *Circulation* **118,** 1567–1576 (2008).
33. Melkman-Zehavi, T. *et al.* miRNAs control insulin content in pancreatic beta-cells via downregulation of transcriptional repressors. *EMBO J.* **30,** 835–845 (2011).
34. Mori, M. A. *et al.* Role of microRNA processing in adipose tissue in stress defense and longevity. *Cell Metab.* **16,** 336–347 (2012).
35. Kumar, M. S., Lu, J., Mercer, K. L., Golub, T. R. & Jacks, T. Impaired microRNA processing enhances cellular transformation and tumorigenesis. *Nature Genet.* **39,** 673–677 (2007).
36. Albinsson, S. *et al.* MicroRNAs are necessary for vascular smooth muscle growth, differentiation, and function. *Arterioscler. Thromb. Vasc. Biol.* **30,** 1118–1126 (2010).
37. Suarez, Y. *et al.* Dicer-dependent endothelial microRNAs are necessary for postnatal angiogenesis. *Proc. Natl Acad. Sci. USA* **105,** 14082–14087 (2008).
38. Suarez, Y., Fernandez-Hernando, C., Pober, J. S. & Sessa, W. C. Dicer dependent microRNAs regulate gene expression and functions in human endothelial cells. *Circ. Res.* **100,** 1164–1173 (2007).
39. Kuehbacher, A., Urbich, C., Zeiher, A. M. & Dimmeler, S. Role of Dicer and Drosha for endothelial microRNA expression and angiogenesis. *Circ. Res.* **101,** 59–68 (2007).
40. Son, D. J. *et al.* The atypical mechanosensitive microRNA-712 derived from pre-ribosomal RNA induces endothelial inflammation and atherosclerosis. *Nat. Commun.* **4,** 3000 (2013).
41. Loyer, X. *et al.* Inhibition of microRNA-92a prevents endothelial dysfunction and atherosclerosis in mice. *Circ. Res.* **114,** 434–443 (2014).
42. Fang, Y., Shi, C., Manduchi, E., Civelek, M. & Davies, P. F. MicroRNA-10a regulation of proinflammatory phenotype in athero-susceptible endothelium in vivo and in vitro. *Proc. Natl Acad. Sci. USA* **107,** 13450–13455 (2010).
43. Cheng, H. S. *et al.* MicroRNA-146 represses endothelial activation by inhibiting pro-inflammatory pathways. *EMBO Mol. Med.* **5,** 949–966 (2013).
44. Sun, X. *et al.* Systemic delivery of microRNA-181b inhibits nuclear factor-kappaB activation, vascular inflammation, and atherosclerosis in apolipoprotein E-deficient mice. *Circ. Res.* **114,** 32–40 (2014).
45. Akhtar, S. *et al.* Endothelial hypoxia-inducible factor-1 alpha promotes atherosclerosis and monocyte recruitment by upregulating microRNA-19a. *Hypertension* **66,** 1220–1226 (2015).
46. Villarreal, Jr G. *et al.* Defining the regulation of KLF4 expression and its downstream transcriptional targets in vascular endothelial cells. *Biochem. Biophys. Res. Commun.* **391,** 984–989 (2010).
47. Chen, X. *et al.* Integration of external signaling pathways with the core transcriptional network in embryonic stem cells. *Cell* **133,** 1106–1117 (2008).
48. Chen, H. Y. *et al.* miR-103/107 promote metastasis of colorectal cancer by targeting the metastasis suppressors DAPK and KLF4. *Cancer Res.* **72,** 3631–3641 (2012).
49. Cambronne, X. A., Shen, R., Auer, P. L. & Goodman, R. H. Capturing microRNA targets using an RNA-induced silencing complex (RISC)-trap approach. *Proc. Natl Acad. Sci. USA* **109,** 20473–20478 (2012).

50. Albinsson, S. *et al.* Smooth muscle miRNAs are critical for post-natal regulation of blood pressure and vascular function. *PLoS ONE* **6,** e18869 (2011).
51. Wu, W. *et al.* Flow-dependent regulation of kruppel-like factor 2 is mediated by MicroRNA-92a. *Circulation* **124,** 633–641 (2011).
52. Schober, A. *et al.* MicroRNA-126-5p promotes endothelial proliferation and limits atherosclerosis by suppressing Dlk1. *Nature Med.* **20,** 368–376 (2014).
53. Schaefer, A. *et al.* Cerebellar neurodegeneration in the absence of microRNAs. *J. Exp. Med.* **204,** 1553–1558 (2007).
54. La Rocca, G. *et al. In vivo*, Argonaute-bound microRNAs exist predominantly in a reservoir of low molecular weight complexes not associated with mRNA. *Proc. Natl Acad. Sci. USA* **112,** 767–772 (2015).
55. Olejniczak, S. H., La Rocca, G., Gruber, J. J. & Thompson, C. B. Long-lived microRNA-Argonaute complexes in quiescent cells can be activated to regulate mitogenic responses. *Proc. Natl Acad. Sci. USA* **110,** 157–162 (2013).
56. Ghosh, S., Bose, M., Ray, A. & Bhattacharyya, S. N. Polysome arrest restricts miRNA turnover by preventing exosomal export of miRNA in growth-retarded mammalian cells. *Mol. Biol. Cell* **26,** 1072–1083 (2015).
57. Li, Y. *et al.* Genome-wide analysis of human microRNA stability. *Biomed. Res. Int.* **2013,** 368975 (2013).
58. Martello, G. *et al.* A MicroRNA targeting dicer for metastasis control. *Cell* **141,** 1195–1207 (2010).
59. Trajkovski, M. *et al.* MicroRNAs 103 and 107 regulate insulin sensitivity. *Nature* **474,** 649–653 (2011).
60. Qin, X. *et al.* MicroRNA-19a mediates the suppressive effect of laminar flow on cyclin D1 expression in human umbilical vein endothelial cells. *Proc. Natl Acad. Sci. USA* **107,** 3240–3244 (2010).
61. Cowan, C. E. *et al.* Kruppel-like factor-4 transcriptionally regulates VE-cadherin expression and endothelial barrier function. *Circ. Res.* **107,** 959–966 (2010).
62. Dekker, R. J. *et al.* KLF2 provokes a gene expression pattern that establishes functional quiescent differentiation of the endothelium. *Blood* **107,** 4354–4363 (2006).
63. Ma, J. *et al.* Kruppel-like factor 4 regulates blood-tumor barrier permeability via ZO-1, occludin and claudin-5. *J. Cell Physiol.* **229,** 916–926 (2014).
64. Zhou, G. *et al.* Endothelial Kruppel-like factor 4 protects against atherothrombosis in mice. *J. Clin. Invest.* **122,** 4727–4731 (2012).
65. Ohnesorge, N. *et al.* Erk5 activation elicits a vasoprotective endothelial phenotype via induction of Kruppel-like factor 4 (KLF4). *J. Biol. Chem.* **285,** 26199–26210 (2010).
66. Monvoisin, A. *et al.* VE-cadherin-CreERT2 transgenic mouse: a model for inducible recombination in the endothelium. *Dev. Dyn.* **235,** 3413–3422 (2006).
67. Harfe, B. D., McManus, M. T., Mansfield, J. H., Hornstein, E. & Tabin, C. J. The RNaseIII enzyme Dicer is required for morphogenesis but not patterning of the vertebrate limb. *Proc. Natl Acad. Sci. USA* **102,** 10898–10903 (2005).
68. Nuovo, G., Lee, E. J., Lawler, S., Godlewski, J. & Schmittgen, T. *In situ* detection of mature microRNAs by labeled extension on ultramer templates. *BioTechniques* **46,** 115–126 (2009).

Acknowledgements

This work was supported by the Deutsche Forschungsgemeinschaft (DFG FOR809, SCHO1056/3-2, LMUexcellent and SFB 1123-B4) and by the German Centre for Cardiovascular Research (MHA VD 1.2). We thank Kathrin Heyll, Claudia Geißler, Farima Zahedi, Judit Corbalán Campos and Lourdes Ruiz-Heinrich for their technical assistance.

Author contributions

A.S. conceived and designed the experiments. P.H. and Z.Z. carried out all experiments. L.N. helped in the immunoprecipitation experiments and M.Z. contributed to *in situ* PCRs. J.G. helped with the human plaque specimen. M.N-J. and Y.W. assisted with the data analysis and the mouse experiments. S.S. and C.W. helped in performing the statistical and microarray data analysis. P.H. and A.S. wrote the manuscript, which was read, edited and approved by all the authors.

Additional information

Accession codes: The microarray data have been deposited in the National Center for Biotechnology Information Gene Expression Omnibus database (http://www.ncbi.nlm.nih.gov/geo/) under accession numbers GSE53433 and GSE53435.

Supplementary Information accompanies this paper at http://www.nature.com/naturecommunications

Competing financial interests: The authors declare no competing financial interests.

Reprints and permission information is available online at http://npg.nature.com/reprintsandpermissions/

How to cite this article: Hartmann, P. *et al.* Endothelial Dicer promotes atherosclerosis and vascular inflammation by miRNA-103-mediated suppression of KLF4. *Nat. Commun.* 7:10521 doi: 10.1038/ncomms10521 (2016).

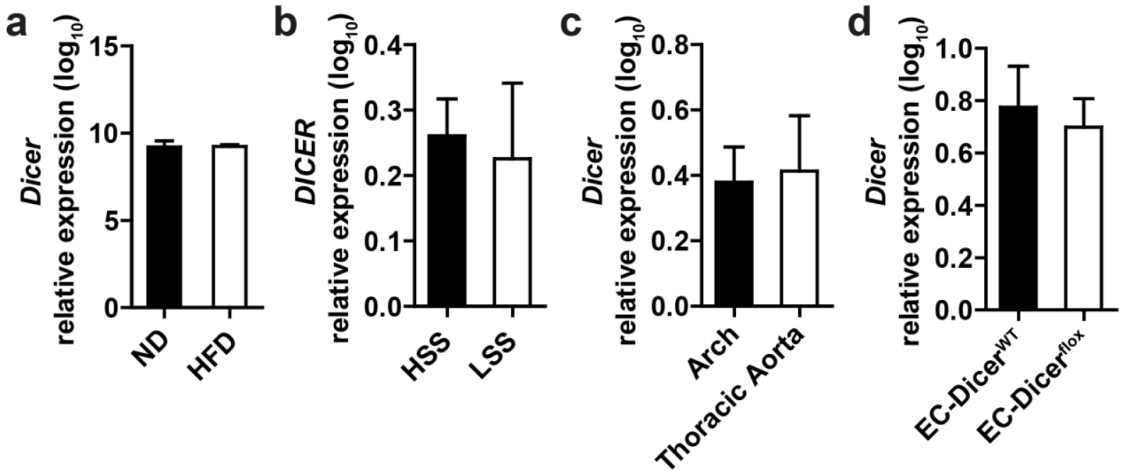

Supplementary Figure 1. Regulation of *Dicer* expression. (a) Quantitative RT-PCR analyses of *Dicer* mRNA expression in aortas of *Apoe*$^{-/-}$ mice fed a normal diet (ND) or a high fat diet (HFD) for 12 weeks (n = 3–4 mice per group). (b) Quantitative RT-PCR analyses of *Dicer* mRNA expression in human aortic ECs (HAECs) exposed to high shear stress (HSS) compared to low shear stress (LSS) for 48 h (n = 3–4 per group). (c) The expression levels of *Dicer* in the aortic arch and thoracic aorta of *Apoe*$^{-/-}$ mice fed a HFD (n = 4 mice per group). (d) *Dicer* mRNA expression in CD11b^{+} peripheral blood cells isolated from EC-Dicer^{WT} and EC-Dicer^{flox} mice fed a HFD for 4 weeks (n = 6 mice per group). The data are represented as the mean ± s.e.m. of the indicated number (n) of repeats. Student *t*-test was used to compare the groups.

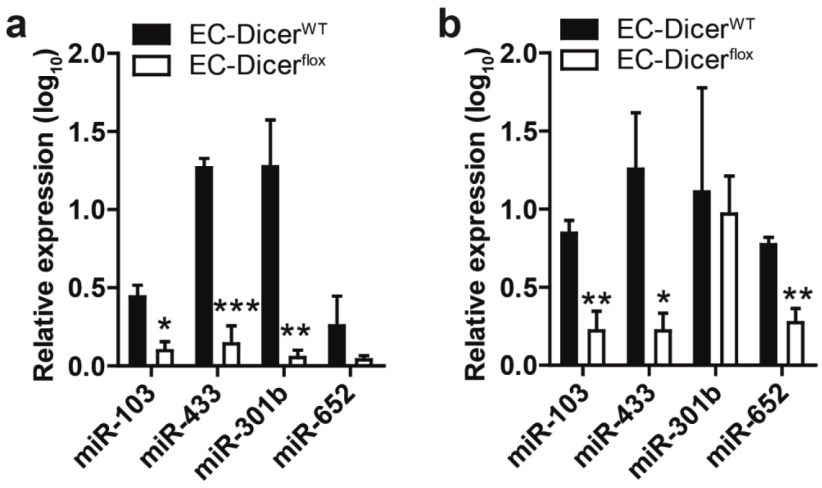

Supplementary Figure 2. Effects of endothelial Dicer deficiency on miRNA expression in different parts of the aorta. (a, b) The expression levels of miR-103, miR-301b, miR-433, and miR-652 in the aortic arch (a) and descending thoracic aorta (b) from EC-Dicer^{WT} compared to EC-Dicer^{flox} mice after HFD feeding (n = 3–4 mice per group). The data are represented as the mean ± s.e.m. of the indicated number (n) of repeats. **P* < 0.05, ***P* < 0.01, and ****P* < 0.001. Student *t*-test was used to compare the groups.

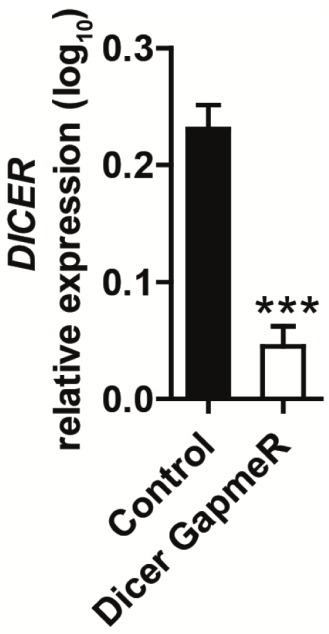

Supplementary Figure 3. Silencing of Dicer in ECs. Quantitative RT-PCR analyses of *DICER* mRNA expression in human aortic ECs (HAECs) treated with Dicer-specific LNA-GapmeRs or non-targeting control LNA-GapmeRs (n = 5 per group). The data are represented as the mean ± s.e.m. of the indicated number (n) of repeats. ***$P < 0.001$. Student *t*-test was used to compare the groups.

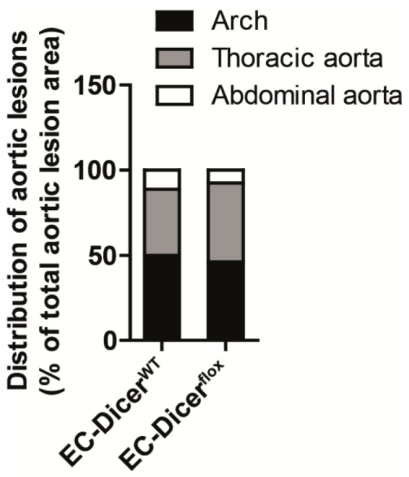

Supplementary Figure 4. Effects of endothelial Dicer deletion on the distribution of aortic lesions. Distribution of atherosclerotic lesions between the arch, thoracic aorta and abdominal aorta of EC-Dicer^{WT} and EC-Dicer^{flox} mice fed a HFD for 12 weeks (n = 5 mice per group). P = not significant. Student *t*-test was used to compare the groups.

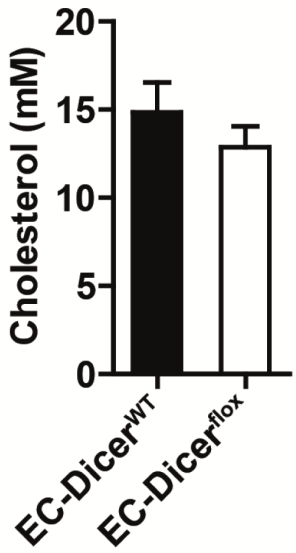

Supplementary Figure 5. Effect of endothelial Dicer knockout on serum cholesterol levels. Cholesterol levels were analyzed in the serum of EC-Dicer^{WT} and EC-Dicer^{flox} mice after 12 weeks of HFD feeding (n = 4–5 mice per group). The data are represented as the mean ± s.e.m. of the indicated number (n) of repeats. Student *t*-test was used to compare the groups.

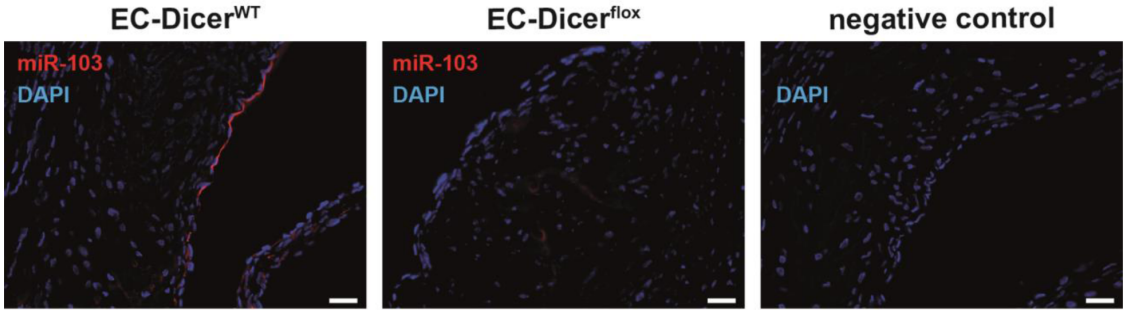

Supplementary Figure 6. MiR-103 expression in aortic root lesions. MiR-103 expression in aortic root lesions after 12 weeks of HFD feeding, as determined by *in situ* PCR. The nuclei were counterstained with DAPI. Negative control staining was performed without reverse transcription. Scale bar, 25 µm.

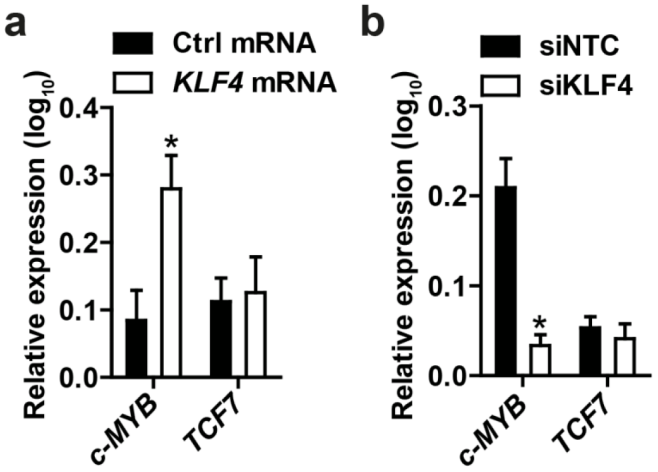

Supplementary Figure 7. Effects of KLF4 on the expression of *c-MYB* and *TCF7* in ECs. (a) Expression of *c-MYB* and *TCF7* mRNAs in HAECs treated with *GFP* control mRNA (Ctrl mRNA) or premade KLF4 mRNAs (n = 3–4 per group). (b) Expression of *c-MYB* and *TCF7* mRNAs in HAECs treated with siRNA against KLF4 (n = 4–5 per group). Non-targeting oligonucleotides were used as control. The data are represented as the mean ± s.e.m. of the indicated number (n) of repeats. *$P < 0.05$. Student *t*-test was used to compare the groups.

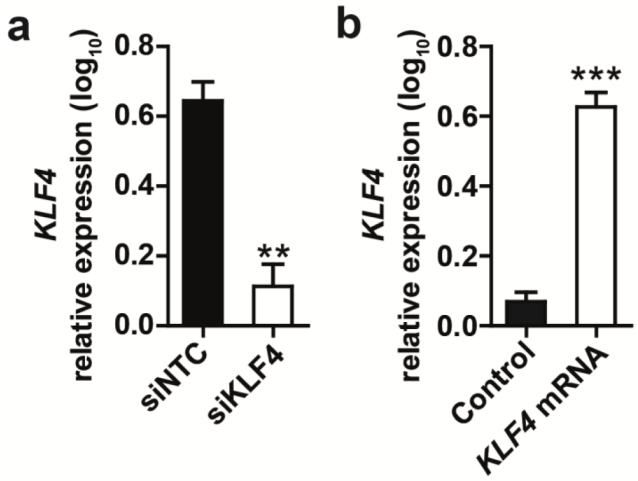

Supplementary Figure 8. Silencing and overexpression of KLF4 in ECs. (a) Quantitative RT-PCR analyses of *KLF4* mRNA expression levels in HAECs after silencing KLF4 (siKLF4). A non-targeting siRNA (siNTC) was used in the control group (n = 3–4 per group). (b) The effect of transfection with *GFP* mRNA (control) or premade *KLF4* mRNA on *KLF4* mRNA expression levels in HAECs (n = 3–5 per group). The data are represented as the mean ± s.e.m. of the indicated number (n) of repeats. $^{**}P < 0.01$, and $^{***}P < 0.001$. Student *t*-test was used to compare the groups.

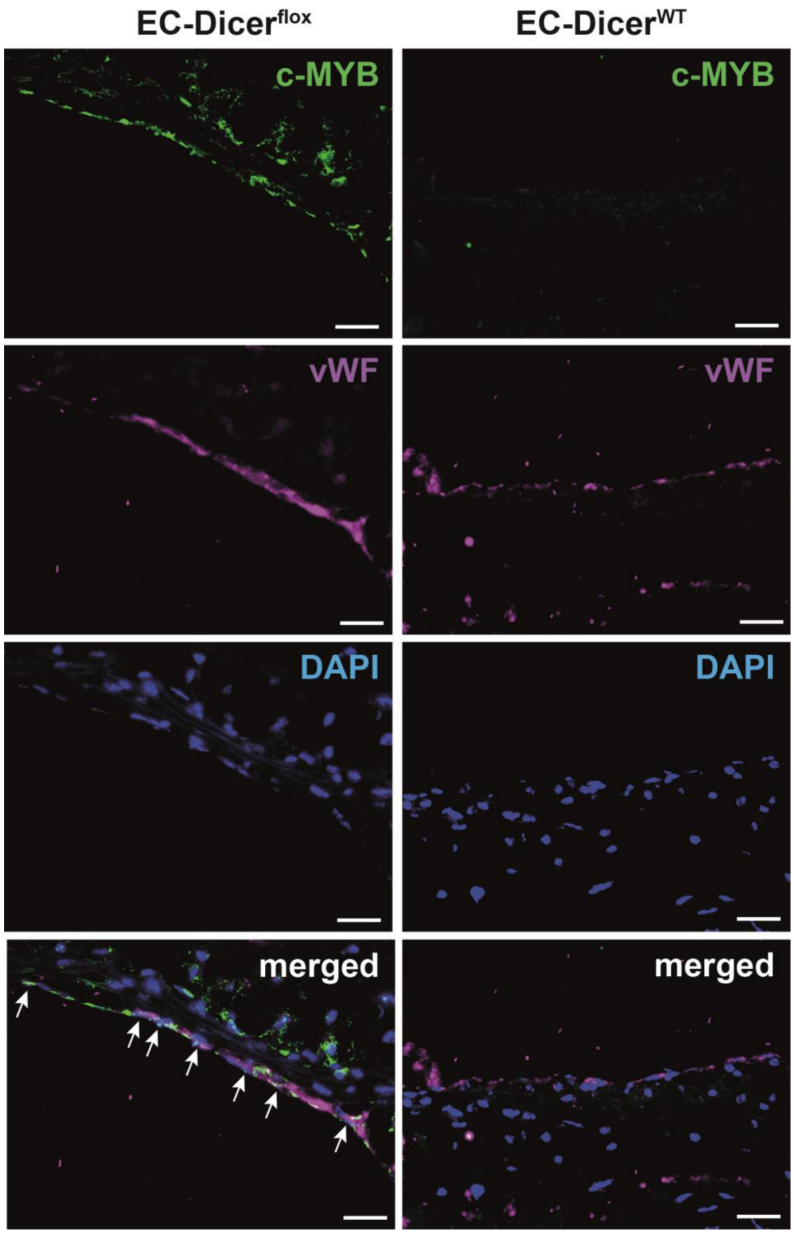

Supplementary Figure 9. c-Myb expression in ECs. Immunostaining of c-MYB and von Willebrand factor (vWF) in aortic root sections after 12 weeks of HFD feeding. Arrows indicate c-MYB expressing ECs. The nuclei were stained with DAPI. Scale bar, 25 µm.

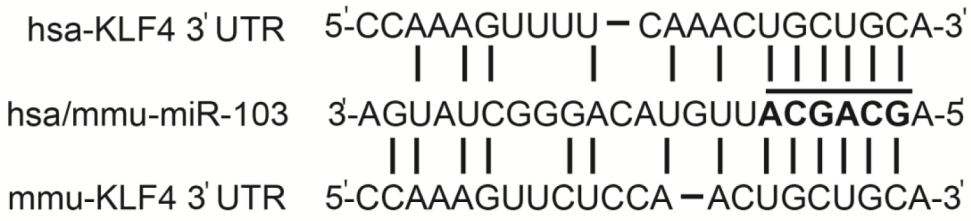

Supplementary Figure 10. Target site for human and murine (hsa/mmu) miR-103 in the 3′ untranslated region (UTR) of *KLF4* mRNA[1]. The seed sequence of miR-103 is highlighted in bold.

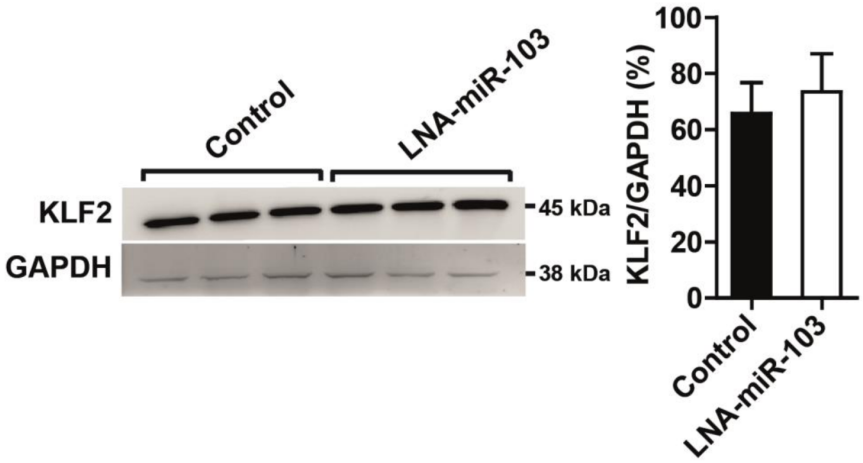

Supplementary Figure 11. Effects of miR-103 on KLF2 protein expression. Western blot analyses of KLF2 in HAECs treated with LNA-inhibitors of miR-103 or non-targeting control oligonucleotides. The expression levels were normalized to those of GAPDH (n = 3 per group). Full scans of Western Blots are provided in Supplementary Figure 15. The data are represented as the mean ± s.e.m. of the indicated number (n) of repeats. Student *t*-test was used to compare the groups.

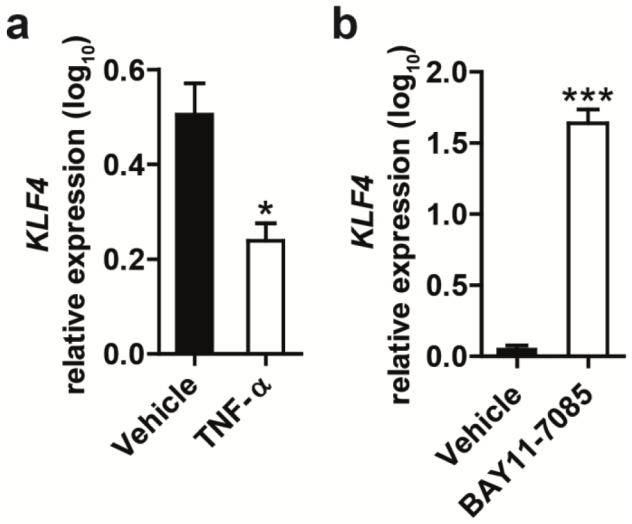

Supplementary Figure 12. NF-κB reduces *KLF4* expression in ECs. (a) Quantitative RT-PCR analyses of *KLF4* mRNA expression in HAECs with TNF-α stimulation (n = 4 per group). (b) *KLF4* mRNA expression in HAECs treated with vehicle or the NF-κB-inhibitor BAY11-7085 (n = 5 per group). The data are represented as the mean ± s.e.m. of the indicated number (n) of repeats. **P* < 0.05 and ****P* < 0.001. Student *t*-test was used to compare the groups.

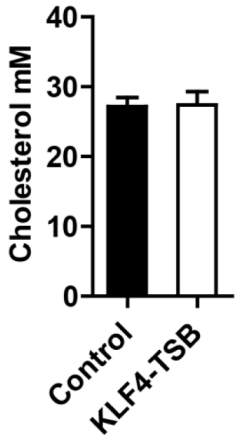

Supplementary Figure 13. Effect of KLF4-Target Site Blockers (KLF4-TSBs) treatment on serum cholesterol levels. Cholesterol levels were analyzed in the serum of Apoe$^{-/-}$ mice treated with KLF4-TSBs or control oligonucleotides after 8 weeks HFD feeding (n = 6–7 mice per group). The data are represented as the mean ± s.e.m. of the indicated number (n) of repeats. Student *t*-test was used to compare the groups.

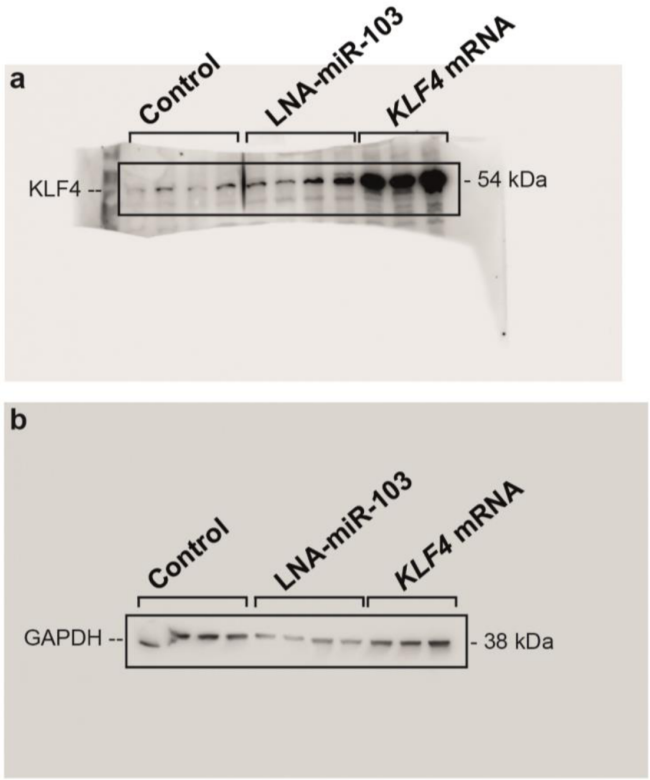

Supplementary Figure 14. Full scans of the Western Blots for KLF4 and GAPDH.

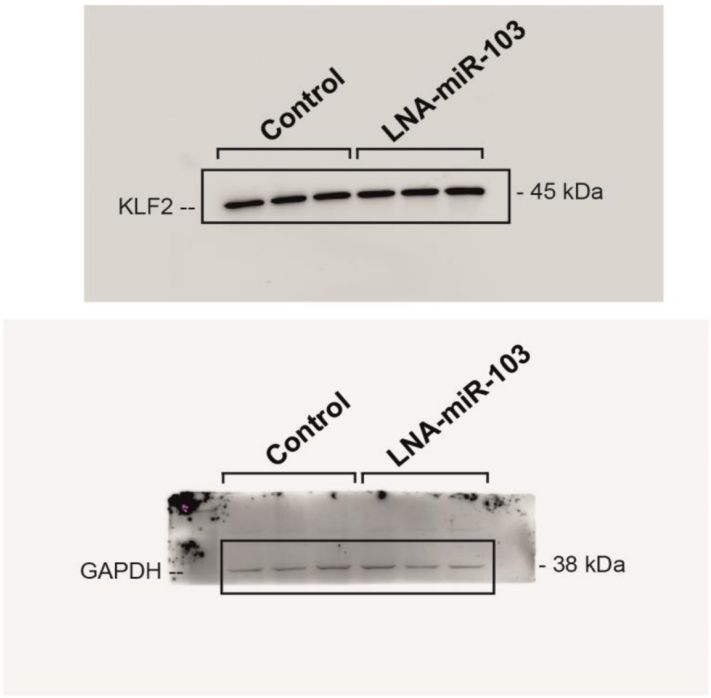

Supplementary Figure 15. Full scans of the Western Blots for KLF2 and GAPDH.

Supplementary Tables

Supplementary Table 1. Significantly downregulated miRNAs in EC-Dicer^{flox} compared with EC-Dicer^{WT} mice after 4 weeks of HFD feeding (n = 3 mice per group).

miRNAs	log_{10} RQ	neg log_{10} *P*-value
miR-465C-5p	−0.52	2.17
miR-142-5p	−0.34	1.64
miR-433	−0.27	1.34
miR-495	−0.20	2.17
miR-331-3p	−0.18	2.35
miR-301b	−0.18	3.29
miR-301a	−0.18	2.59
miR-615-3p	−0.18	1.35
miR-487b	−0.17	1.77
miR-425	−0.13	1.53
miR-652	−0.11	1.65
miR-18a*	−0.11	1.38
miR-103	−0.10	3.50
miR-1191	−0.09	1.51

Supplementary Table 2. Significantly downregulated miRNAs in EC-Dicer^{flox} compared with EC-Dicer^{WT} mice after 12 weeks of HFD feeding (n = 3 mice per group).

miRNAs	log_{10} RQ	neg log_{10} *P*-value
miR-183	−0.57	1.60
miR-433	−0.50	2.35
let-7d*	−0.35	1.32
miR-669D	−0.21	1.51
miR-1198	−0.21	1.89
miR-667	−0.19	1.68
miR-103	−0.17	1.50
miR-106b*	−0.16	2.52
miR-301b	−0.16	1.50
miR-99b	−0.15	3.36
let-7i	−0.14	2.16
miR-324-3p	−0.13	1.71
miR-652	−0.13	1.35
miR-136	−0.13	1.96
miR-384-3p	−0.11	1.48
miR-434-3p	−0.07	1.34
let-7b	−0.04	2.34
miR-872*	−0.02	1.30

Supplementary Table 3. PCR primer sequences

Gene	Primer Sequence
Human:	
CX_3CL1	sense 5'-GCAAACGCGCAATCATCTTG-3'
	antisense 5'-TTGACCCATTGCTCCTTCGG-3'
CXCL1	sense 5'-CCCAAACCGAAGTCATAGCCA-3'
	antisense 5'-GATGCAGGATTGAGGCAAGC-3'
CCL2	sense 5'-CGCTCAGCCAGATGCAATCAA-3'
	antisense 5'-GACACTTGCTGCTGGTGATTC-3'
KLF4	sense 5'-ATCTCAAGGCACACCTGCG-3'
	antisense 5'-CCTGGTCAGTTCATCTGAGCG-3'
GAPDH	sense 5'-AGGGCTGCTTTTAACTCTGGT-3'
	antisense 5'-CCCCACTTGATTTTGGAGGGA-3'
c-MYB	sense 5'-AAGCTACTGCCTGGACGAAC-3'
	antisense 5'-TTCCTGTTCGACCTTCCGAC-3'
TCF7	sense 5'-TGCTCCAAGTGGTGGGAATC-3'
	antisense 5'-GCAGGCAGCCATAGGTACAA-3'
Mouse:	
Dicer1	sense 5'-GAATAAGGCTTATCTTCTGCAGG-3'
	antisense 5'-CATAAAGGTGCTTGGTTATGAGG-3'
Klf4	sense 5'-GACTAACCGTTGGCGTGAGG-3'
	antisense 5'-CGGGTTGTTACTGCTGCAAG-3'
c-Myb	sense 5'-CGTACCTAAGAACAGGCCCC-3'
	antisense 5'-GCGTTCACGTATTTCCGAGC-3'
Tcf7	sense 5'-AGGTGGCATGCACTATCTCG-3'
	antisense 5'-TTTCCCTTGACCGCCTCTTC-3'
Lef1	sense 5'-GATCCTGGGCAGAACATGGC-3'
	antisense 5'-GCTGTCTCTCTTTCCGTGCT-3'
Dkk2	sense 5'-TCTAGGAAGGCCACACTCCA-3'
	antisense 5'-TGGGTCTCCTTCATGTCCTTT-3'
Sox17	sense 5'-TTCCATCTCCACCTCCGACC-3'
	antisense 5'-GTCGATTGGCACCTTTCACC-3'
B2m	sense 5'-TCGGTGACCCTGGTCTTTCT-3'
	antisense 5'-TTTGAGGGGTTTTCTGGATAGCA-3'
Mouse/Human:	
Taq-in situ-miR-103 RT	5'-GTCGTATCCAGTGCAGGGTCCGAGGTAT TCGCACTGGATACGACTCATA-3'
Taq-in situ-miR-103	sense 5'-GCCCAGCAGCATTGTACAG-3'
	antisense 5'-GTGCAGGGTCCGAGGT-3'
C. elegans:	
Taq-in situ-cel-miR-39 RT	5'-GTCGTATCCAGTGCAGGGTCCGAGGTAT TCGCACTGGATACGACCAAGC-3'
Taq-in situ-cel-miR-39	sense 5'-GCCCTCACCGGGTGTAAAT-3'
	antisense 5'-GTGCAGGGTCCGAGGT-3'

Supplementary Reference

1 Chen, H. Y. *et al.* miR-103/107 promote metastasis of colorectal cancer by targeting the metastasis suppressors DAPK and KLF4. *Cancer research* **72**, 3631-3641, doi:10.1158/0008-5472.CAN-12-0667 (2012).

3.2 Endothelial HIF-1α in atherosclerosis

Hypertension. 2015 Dec; 66(6):1220-6. doi: 10.1161/HYPERTENSIONAHA.115.05886.

Endothelial Hypoxia-Inducible Factor-1α Promotes Atherosclerosis and Monocyte Recruitment by Upregulating MicroRNA-19a

Shamima Akhtar*, **Petra Hartmann*,** Ela Karshovska, Fatuma-Ayaan Rinderknecht, Pallavi Subramanian, Felix Gremse, Jochen Grommes, Michael Jacobs, Fabian Kiessling, Christian Weber, Sabine Steffens, Andreas Schober.

*These authors contributed equally to this work[1].

[1] Reason for shared first authorship: The first authorship of the publication "Endothelial Hypoxia-Inducible Factor-1α Promotes Atherosclerosis and Monocyte Recruitment by Upregulating MicroRNA-19a" is shared between Shamima Akhtar and Petra Hartmann, as both scientists contributed to a similar extent to the realization of this publication. Both scientists designed experiments, performed data analysis and data interpretation. Shamima Akhtar contributed to the data of Figure 1, 2 and 3 of the publication. Petra Hartmann contributed to the data of Figure 4 and 5 of the publication and wrote the manuscript.

Vascular Biology

Endothelial Hypoxia-Inducible Factor-1α Promotes Atherosclerosis and Monocyte Recruitment by Upregulating MicroRNA-19a

Shamima Akhtar,* Petra Hartmann,* Ela Karshovska, Fatuma-Ayaan Rinderknecht, Pallavi Subramanian, Felix Gremse, Jochen Grommes, Michael Jacobs, Fabian Kiessling, Christian Weber, Sabine Steffens, Andreas Schober

Abstract—Chemokines mediate monocyte adhesion to dysfunctional endothelial cells (ECs) and promote arterial inflammation during atherosclerosis. Hypoxia-inducible factor (HIF)-1α is expressed in various cell types of atherosclerotic lesions and is associated with lesional inflammation. However, the impact of endothelial HIF-1α in atherosclerosis is unclear. HIF-1α was detectable in the nucleus of ECs covering murine and human atherosclerotic lesions. To study the role of endothelial HIF-1α in atherosclerosis, deletion of the *Hif1*a gene was induced in ECs from apolipoprotein E knockout mice (EC-*Hif1a*$^{-/-}$) by Tamoxifen injection. The formation of atherosclerotic lesions, the lesional macrophage accumulation, and the expression of CXCL1 in ECs were reduced after partial carotid ligation in EC-*Hif1a*$^{-/-}$ compared with control mice. Moreover, the lesion area and the lesional macrophage accumulation were decreased in the aortas of EC-*Hif1a*$^{-/-}$ mice compared with control mice during diet-induced atherosclerosis. In vitro, mildly oxidized low-density lipoprotein or lysophosphatidic acid 20:4 increased endothelial CXCL1 expression and monocyte adhesion by inducing HIF-1α expression. Moreover, endothelial *Hif1a* deficiency resulted in downregulation of miR-19a in atherosclerotic arteries determined by microRNA profiling. In vitro, HIF-1α–induced miR-19a expression mediated the upregulation of CXCL1 in mildly oxidized low-density lipoprotein–stimulated ECs. These results indicate that hyperlipidemia upregulates HIF-1α expression in ECs by mildly oxidized low-density lipoprotein–derived unsaturated lysophosphatidic acid. Endothelial HIF-1α promoted atherosclerosis by triggering miR-19a–mediated CXCL1 expression and monocyte adhesion, indicating that inhibition of the endothelial HIF-1α/miR-19a pathway may be a therapeutic option against atherosclerosis. (***Hypertension***. **2015;66:1220-1226. DOI: 10.1161/HYPERTENSIONAHA.115.05886.)**
● **Online Data Supplement**

Key Words: atherosclerosis ■ chemokines ■ endothelial cells ■ microRNAs

The adhesion of circulating monocytes to dysfunctional endothelial cells (ECs) results in the accumulation of macrophages in the subendothelial space and the formation of atherosclerotic lesions.[1] Disturbed blood flow at arterial bifurcations primes the endothelium for inflammatory activation by modified lipoproteins, such as mildly oxidized low-density lipoproteins (moxLDLs).[2–4] The oxidation of LDL leads to the generation of lysophosphatidic acid (LPA), which increases atherogenic monocyte adhesion by upregulating (C–X–C motif) ligand 1 (CXCL1) expression in ECs.[5–7] Accordingly, CXCL1 and its receptor CXCR2 play key roles in the accumulation of macrophages in atherosclerotic lesions.[8] In addition to proinflammatory nuclear factor-κB (NF-κB) signaling, the transcription factor hypoxia-inducible factor (HIF)-1α has been implicated in the regulation of CXCL1 expression.[9,10]

Endothelial HIF-1α activity mediates transendothelial glucose transport and hypoxia-induced angiogenesis.[11,12] In addition to the upregulation of proangiogenic genes, such as vascular endothelial growth factor, the effects of endothelial HIF-1α on angiogenesis are mediated by microRNAs (miRNAs).[13–15] For example, HIF-1α induces the expression of miR-107 in ECs, which promotes neoangiogenesis.[15] By contrast, HIF-1α and miR-429 constitute a negative feedback loop that limits vascular endothelial growth factor expression

Received May 26, 2015; first decision June 5, 2015; revision accepted September 25, 2015.

From the Institute for Cardiovascular Prevention, Ludwig-Maximilians-University Munich, Munich, Germany (S.A., P.H., E.K., F.-A.R., P.S., C.W., S.S., A.S.); Institute for Molecular Cardiovascular Research (S.A., A.S.), Department of Experimental Molecular Imaging (F.G., F.K.), and European Vascular Center Aachen-Maastricht (J.G., M.J.), RWTH Aachen University, Aachen, Germany; European Vascular Center Aachen-Maastricht, University Maastricht Medical Center, Maastricht, The Netherlands (J.G., M.J.); Cardiovascular Research Institute Maastricht, University Maastricht, Maastricht, The Netherlands (C.W.); and DZHK (German Centre for Cardiovascular Research), Partner Site Munich Heart Alliance, Munich, Germany (C.W., S.S., A.S.).
*These authors contributed equally to this work.

The online-only Data Supplement is available with this article at http://hyper.ahajournals.org/lookup/suppl/doi:10.1161/HYPERTENSIONAHA.115.05886/-/DC1.

Correspondence to Andreas Schober, Experimental Vascular Medicine, Institute for Cardiovascular Prevention, Ludwig-Maximilians University Munich, Pettenkoferstr. 9b, 80336 Munich, Germany. E-mail aschober@med.lmu.de

Hypertension **is available at http://hyper.ahajournals.org** **DOI: 10.1161/HYPERTENSIONAHA.115.05886**

in hypoxic ECs.[13] In atherosclerosis, HIF-1α activation correlates with disease progression and lesional inflammation.[16,17] Vascular injury induces HIF-1α activation in smooth muscle cells and promotes neointima formation by upregulating CXCL12.[18]

Here, we investigated the role of endothelial HIF-1α in atherosclerosis. We found that HIF-1α is activated in atherosclerotic ECs and deletion of endothelial HIF-1α reduces atherosclerosis, the lesional macrophage content, and the expression of CXCL1 and miR-19a in apolipoprotein E knockout (*Apoe*$^{-/-}$) mice. In ECs, moxLDL and LPA upregulated HIF-1α, which increased CXCL1-mediated monocyte adhesion by inducing miR-19a expression. These findings indicate that hyperlipidemia-induced HIF-1α in ECs promotes atherosclerosis by upregulating a proinflammatory miRNA.

Materials and Methods

Materials and Methods are available in the online-only Data Supplement.

Results

HIF-1α Expression in Atherosclerosis

HIF-1α expression was detectable in the nuclei of ECs covering human atherosclerotic lesions (Figure S1A in the online-only Data Supplement). In *Apoe*$^{-/-}$ mice, nuclear HIF-1α expression was found in atherosclerotic ECs after 12 weeks of high fat diet (HFD) feeding but not in ECs from mice fed a normal diet (Figure S1B). These findings indicate that HIF-1α is activated in ECs during atherosclerosis. HFD feeding increased the *Hif1a* mRNA expression in the aortic arch, the thoracic and abdominal aorta, and the carotid artery of *Apoe*$^{-/-}$ mice (Figure S2A). In the aortic root, however, HFD feeding did not increase the expression of *Hif1a* (Figure S2A) and nuclear HIF-1α accumulation was found in the majority of vascular cells in *Apoe*$^{-/-}$ mice fed a normal diet (Figure S2B).

Disturbed blood flow is essential for hyperlipidemia-induced endothelial inflammation and atherosclerosis. After a decline of the *Hif1a* mRNA expression at 1 day and 1 week after induction of blood flow disturbances in the carotid artery of *Apoe*$^{-/-}$ mice by partial ligation, the *Hif1a* transcript levels were increased after 2 and 4 week when compared with unligated carotid arteries (Figure S2C). Nuclear HIF-1α signals were detectable by immunostaining in ECs from partially ligated carotid arteries (Figure 1A).

HIF-1α Promotes Endothelial Inflammation

To investigate the role of HIF-1α on endothelial inflammation, EC-specific knockout of the *Hif1a* gene was induced

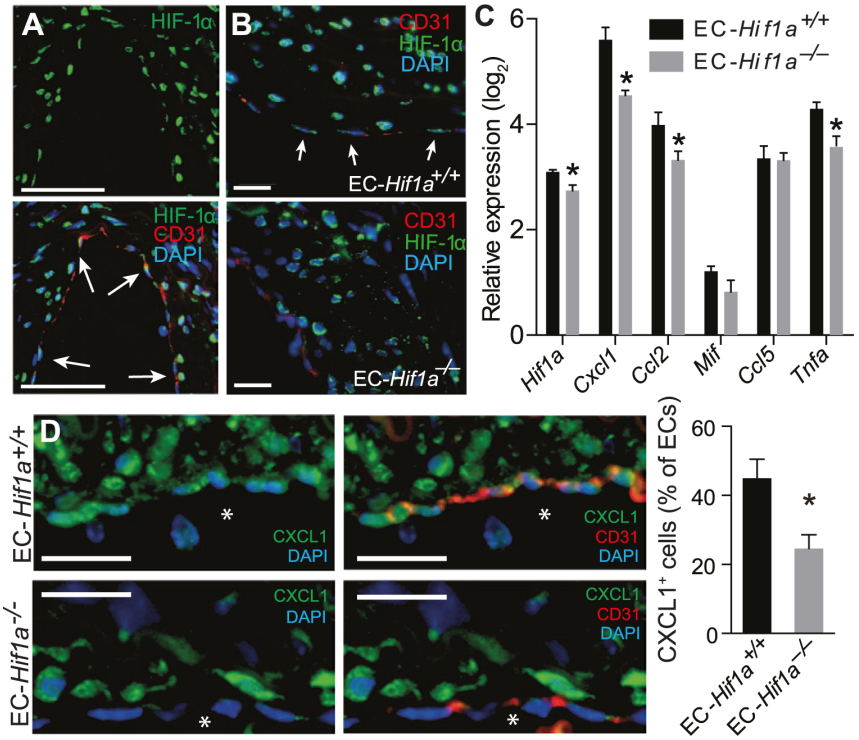

Figure 1. Endothelial hypoxia-inducible factor (HIF)-1α induces proinflammatory gene expression. Dual HIF-1α and CD31 immunostaining in carotid arteries from *Apoe*$^{-/-}$ mice (**A**) or from endothelial cell (EC)-*Hif1a*$^{+/+}$ and EC-*Hif1a*$^{-/-}$ mice (**B**) 6 weeks after partial ligation and feeding a high fat diet (HFD). Arrows indicate HIF-1α^{+} ECs. **C**, Gene expression in the carotid arteries 2 weeks after partial ligation and HFD feeding determined by quantitative reverse transcription polymerase chain reaction. **D**, Dual immunostaining for CXCL1 and CD31 in partially ligated carotid arteries. Nuclei were stained with 4′,6-diamidino-2-phenylindole (DAPI). Stars indicate the lumen. Scale bars, 50 μm (**A** and **B**) and 25 μm (**D**). *P<0.05, n=5 to 8 mice per group.

in *Apoe*$^{-/-}$ (EC-*Hif1a*$^{-/-}$) mice using the Cre-lox system. Endothelial HIF-1α immunostaining (Figure 1B) and *Hif1a* mRNA expression (Figure 1C) were reduced in partially ligated carotid arteries from EC-*Hif1a*$^{-/-}$ mice when compared with EC-*Hif1a*$^{+/+}$ mice. Moreover, the expression level of *Cxcl1, Ccl2,* and *Tnfa* but not those of *Ccl5* and *Mif* were reduced in the carotid arteries of EC-*Hif1a*$^{-/-}$ mice compared with EC-*Hif1a*$^{+/+}$ mice 2 weeks after partial ligation (Figure 1C). CXCL1 expressing ECs were reduced in partially ligated carotid arteries from EC-*Hif1a*$^{-/-}$ mice, as identified by dual immunofluorescence staining of CXCL1 and CD31 (Figure 1D). A similar effect of HIF-1α on CXCL1 expression was observed in atherosclerotic lesions in the aorta after feeding EC-*Hif1a*$^{-/-}$ mice and EC-*Hif1a*$^{+/+}$ mice an HFD for 12 weeks (Figure S3). These results indicate that activation of HIF-1α in atherosclerotic ECs enhances the expression of proinflammatory cytokines.

Endothelial HIF-1α Increases Atherosclerosis

To study the effect of endothelial HIF-1α on atherosclerosis, lesion formation was determined in EC-*Hif1a*$^{-/-}$ mice and EC-*Hif1a*$^{+/+}$ mice. The lesion area was reduced in carotid arteries from EC-*Hif1a*$^{-/-}$ mice at 6 weeks after partial ligation and feeding an HFD (Figure 2A). Moreover, the lesional accumulation of macrophages was lower in EC-*Hif1a*$^{-/-}$ mice than in EC-*Hif1a*$^{+/+}$ mice (Figure 2B). The lesional smooth muscle cell and collagen type I content were similar in both groups (Figure S4). To investigate whether HIF-1α in ECs contributes to vascular stenosis, the lumen of the partially ligated carotid arteries was quantified by computed tomographic angiography in vivo. The luminal volume was significantly reduced in the carotid arteries from EC-*Hif1a*$^{-/-}$ mice compared with EC-*Hif1a*$^{+/+}$ mice (Figure S5). Moreover, the lesion area and the lesional macrophage content were reduced in the aortas of EC-*Hif1a*$^{-/-}$ mice compared with EC-*Hif1a*$^{+/+}$ mice after feeding an HFD for 12 weeks (Figure S6). Deletion of the *Hif1a* gene in ECs did not affect serum cholesterol and triglyceride levels (Tables S2 and S3). Taken together, these results indicate that activation of HIF-1α in ECs enhances atherosclerotic lesion formation.

Endothelial HIF-1α Regulates CXCL1-Mediated Monocyte Adhesion

MoxLDL releases unsaturated LPA species, such as LPA20:4, which promote atherosclerosis by upregulating endothelial CXCL1 expression.[6] Accordingly, blocking LPA receptors using Ki16425 inhibited the moxLDL-induced release of CXCL1 from mouse aortic ECs (MAECs; Figure S7A). In contrast to LPA18:0, treatment with LPA20:4 induced the expression of *Cxcl1* and its secretion from MAECs through the activation of LPA receptors (Figure S7B and S7C). Moreover, moxLDL or LPA20:4 stimulation induced *Hif1a* at the mRNA and protein level in MAECs (Figure 3A and 3B; Figure S8). Treatment with Ki16425 diminished both moxLDL- and LPA20:4-induced *Hif1a* expression in MAECs (Figure 3A and 3B). Silencing of *Hif1a* in MAECs using siRNA (Figure S9) decreased moxLDL- or LPA 20:4-induced *Cxcl1* mRNA expression and CXCL1 protein secretion compared with nontargeting control siRNAs (Figure 3C and 3D). Knockdown of *Hif1a* reduced the expression of *Tnfa* in moxLDL-stimulated MAECs, but not in LPA20:4-stimulated MAECs (Figure 3C). The role of endothelial HIF-1α in monocyte adhesion was studied using in vitro flow chamber assays. Treatment with moxLDL or LPA20:4 increased monocyte adhesion compared with native LDL and LPA18:0 (Figure S10). The moxLDL- and LPA20:4-induced monocyte adhesion was abolished by silencing *Hif1a* in MAECs (Figure 3E and 3F). These results suggest that moxLDL-derived unsaturated LPAs promote CXCL1-dependent monocyte adhesion by upregulation HIF-1α.

HIF-1α Increases Endothelial Chemokine Expression by Upregulating MiR-19a

To study the effect of endothelial HIF-1α on the expression of miRNAs during atherosclerosis, miRNA expression profiling was performed in partially ligated carotid arteries from EC-*Hif1a*$^{-/-}$ and EC-*Hif1a*$^{+/+}$ mice fed an HFD for 2 weeks using quantitative reverse transcription polymerase chain reaction arrays. Six miRNAs, including miR-19a and miR-9, were downregulated in EC-*Hif1a*$^{-/-}$ mice compared with EC-*Hif1a*$^{+/+}$ mice (Figure 4A; Table S4). The downregulation of miR-19a in EC-*Hif1a*$^{-/-}$ mice occurred mainly in ECs as determined by combined in situ polymerase chain reaction

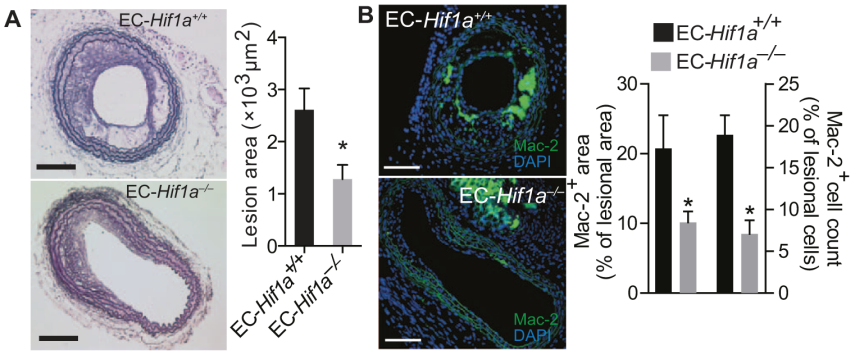

Figure 2. Endothelial *Hif1a* deficiency reduces disturbed flow-induced atherosclerosis. **A**, Lesional area was quantified in elastic van Gieson–stained sections of carotid arteries 6 weeks after partial ligation. **B**, Lesional macrophage accumulation was determined in partially ligated carotid arteries by Mac-2 immunostaining. Nuclei were stained with 4′,6-diamidino-2-phenylindole (DAPI). Scale bars, 100 µm. *P<0.05, n=5 to 8 mice per group.

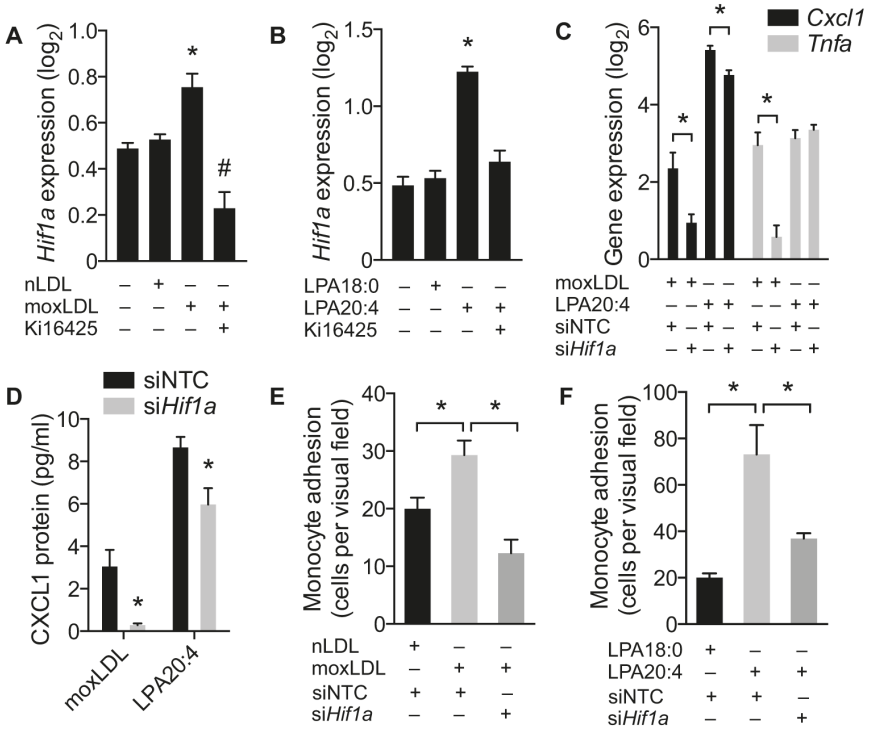

Figure 3. Endothelial hypoxia-inducible factor (HIF)-1α promotes CXCL1-mediated monocyte adhesion. **A** and **B**, *Hif1a* expression in mouse aortic endothelial cells (MAECs) treated with native low-density lipoprotein (nLDL), mildly oxidized LDL (moxLDL), lysophosphatidic acid (LPA)18:0, or LPA20:4 with or without the LPA receptor antagonist Ki16425. Effect of *Hif1a* silencing on *Cxcl1* and *Tnfa* mRNA expression (**C**) and CXCL1 protein secretion (**D**) in moxLDL- or LPA20:4-stimulated MAECs treated with siRNA against *Hif1a* (si*Hif1a*) or nontargeting control siRNAs (siNTCs). MoxLDL- (**E**) or LPA20:4-induced (**F**) monocyte adhesion to MAECs treated with si*Hif1a* or siNTC. **P*<0.05, n=3 to 5.

for miR-19a and CD31 immunostaining (Figure 4A and 4B). Moreover, partial ligation increased the miR-19a expression in carotid arteries of *Apoe*$^{-/-}$ mice (Figure 4C).

In vitro, stimulation with moxLDL increased the expression of miR-19a and *HIF1a* in human aortic ECs (Figure 5A; Figure S11). Silencing *Hif1a* using siRNAs reduced the

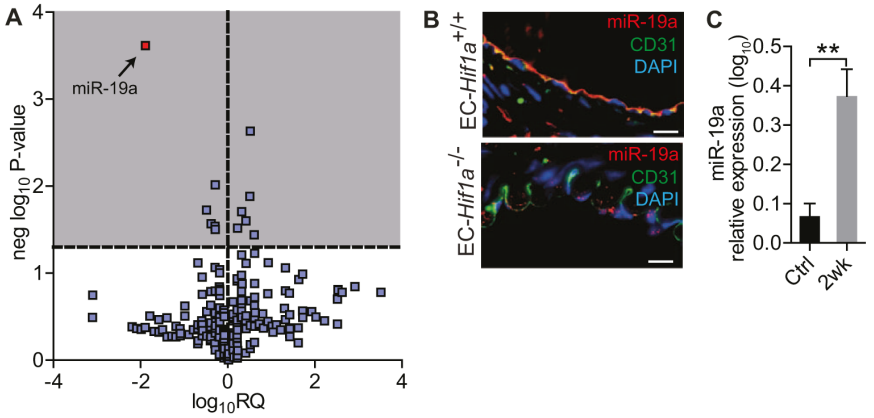

Figure 4. Effect of endothelial hypoxia-inducible factor (HIF)-1α on microRNA (miRNA) expression. **A**, The expression of miRNAs was determined by quantitative reverse transcription polymerase chain reaction (PCR) arrays in partially ligated left carotid arteries from endothelial cell (EC)-*Hif1a*$^{-/-}$ mice and compared with that from EC-*Hif1a*$^{+/+}$ mice fed a high fat diet for 2 weeks. The gray area indicates differentially regulated miRNAs; n=3 mice per group. **B**, Combined in situ PCR detection of miR-19a and immunostaining for CD31 in sections from partially ligated carotid arteries. Scale bars, 10 μm. **C**, MiR-19a expression in carotid arteries from *Apoe*$^{-/-}$ mice at 2 weeks after partial ligation compared with that in nonligated carotid arteries (Ctrl). ***P*<0.01, n=4 mice per group. RQ indicates relative quantification.

expression of miR-19a in moxLDL-stimulated human aortic ECs (Figure 5B; Figure S12). Inhibition of miR-19a using antisense oligonucleotides diminished moxLDL-induced expression of *CXCL1* and *CCL2* mRNAs in human aortic ECs (Figure 5C). Conversely, transfection of human aortic ECs with miR-19a mimics substantially increased the expression of *CXCL1* and *CCL2* (Figure 5D), triggered nuclear translocation of the NF-κB protein p65 (Figure S13), and enhanced monocyte adhesion to ECs (Figure 5E). Blocking the CXCL1 receptor CXCR2 on monocytes abrogated the effect of miR-19a on monocyte adhesion (Figure 5E). These findings suggest that reduced expression of miR-19a diminishes endothelial Cxcl1 expression and NF-κB activation in EC-*Hif1a*$^{-/-}$ mice, and thereby limits atherogenic monocyte adhesion.

Discussion

We found that enhanced HIF-1α activation in atherosclerotic ECs promotes the expression of CXCL1 and increases atherosclerosis. MoxLDL and its derivative LPA induced CXCL1 expression and monocyte adhesion by upregulating *Hif1a* expression in ECs. This effect of HIF-1α was because of increased expression of miR-19a, which triggers NF-κB activation, CXCL1 expression, and CXCL1-dependent monocyte adhesion. Taken together, our findings indicate that hyperlipidemia-induced HIF-1α activation in ECs contributes to atherogenic monocyte recruitment by upregulating miR-19a, which increases NF-κB activation and CXCL1 expression.

Hyperlipidemia increased HIF-1α expression and activation in atherosclerotic ECs. HIF-1α accumulates in hypoxic cells mainly because of increased protein stabilization. However, ECs produce ATP mainly by glycolysis, and oxygen supply via the blood stream to atherosclerotic ECs is not limited.[19] Therefore, nonhypoxic stimuli of HIF-1α activation, such as tumor necrosis factor-α and angiotensin II, which increase *Hif1a* transcription, may be more important for the activation of HIF-1α in ECs.[20] Unsaturated LPAs are produced during mild oxidation of LDL and induce the upregulation of *Hif1a* expression by activating LPA receptors in cancer cells and in smooth muscle cells.[21,22] In line with these reports, our findings indicate that hyperlipidemia-induced endothelial HIF-1α activation is because of LPA receptor signaling triggered by moxLDL-derived LPAs.[6] In addition, LPAs activate proatherogenic NF-κB signaling in ECs.[6] Endothelial NF-κB activation may upregulate HIF-1α expression, which reciprocally amplifies NF-κB signaling and enhances angiotensin II–induced hypertensive kidney injury.[23] In quiescent ECs, the anti-inflammatory transcription factor Krüpple-like factor 2 limits NF-κB activation and HIF-1α accumulation.[24] However, disturbed flow downregulates endothelial Krüpple-like factor 2 expression and primes the endothelium for inflammatory activation by hyperlipidemia.[3] Accordingly, our findings indicate that disturbed flow is a prerequisite for hyperlipidemia-induced HIF-1α expression in ECs; however, the effect of disturbed flow alone on endothelial HIF-1α activation need to be studied in more detail.

The deletion of the *Hif1a* gene in ECs reduced the expression of proinflammatory cytokines, such as CXCL1 and tumor necrosis factor-α. HIF-1α transcriptional activity is also required for CXCL1 expression in myeloid cells, which mediates the survival of neutrophils in mycosis.[9] In ECs, preformed CXCL1 is stored in vesicles and released on activation by LPA.[6] CXCL1 is immobilized on the endothelial surface and induces proatherogenic monocyte adhesion by binding to its receptor CXCR2.[5,6] LPA also increases *CXCL1* mRNA expression in ECs by activating NF-κB.[6] Our results indicate that HIF-1α activation is essential for LPA-induced CXCL1 expression and monocyte adhesion, suggesting that HIF-1α amplifies NF-κB signaling in lipid-induced endothelial inflammation.

We found that *Hif1a* deletion selectively reduces the expression miR-19a in atherosclerotic ECs. In contrast to short-term exposure of ECs to high shear stress, which upregulates miR-19a expression, chronic high shear stress did not affect miR-19a expression levels.[25–27] Low shear stress upregulates the expression of miR-19a in oxLDL-stimulated ECs.[27] Consistently, our data show that stimulation with moxLDL increases the expression of miR-19a in ECs cultured under static conditions by inducing *Hif1a* expression. Moreover, overexpression of miR-19a promoted CXCR2-dependent adhesion of monocytes by upregulating endothelial *CXCL1*

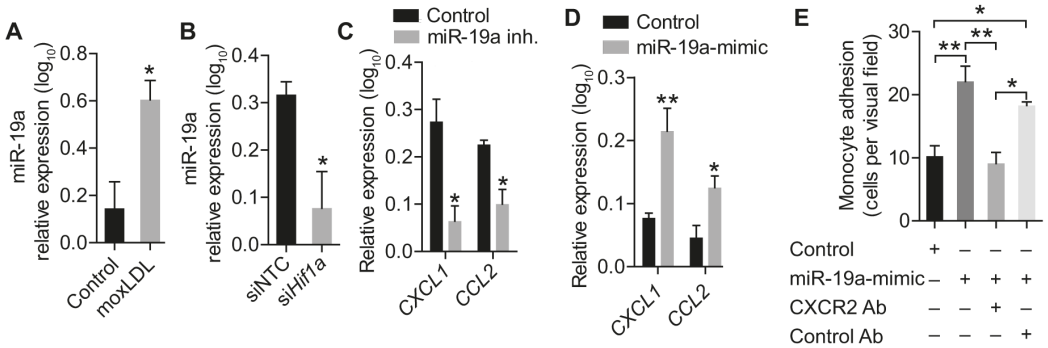

Figure 5. MiR-19a promotes endothelial inflammation. **A**, MiR-19a expression levels in mildly oxidized low-density lipoprotein (moxLDL)- and buffer (control)-treated human aortic endothelial cells (HAECs). **B**, Expression levels of miR-19a in HAECs after treatment with *Hif1a* siRNA (si*Hif1a*) or a nontargeting control siRNA (siNTC). *CXCL1* and *CCL2* mRNA expression in moxLDL-stimulated HAECs treated with inhibitors (**C**) or mimics (**D**) of miR-19a, or nontargeting oligonucleotides (control). **E**, Adhesion of monocytes to HAECs treated with miR-19a-mimics or control oligonucleotides. Monocytes were untreated or pretreated with CXCR2 antibodies or isotype control antibodies (control Ab). *P<0.05, **P<0.01; n=2 to 5.

expression, indicating that miR-19a plays a key role in HIF-1α–induced endothelial inflammation. MiR-19a promotes NF-κB signaling by targeting several negative regulators of NF-κB, such as NF-κB inhibitor α, and may thereby increase CXCL1 expression.[28–30] Accordingly, we found that miR-19a increases NF-κB activation in ECs, indicating that HIF-1α upregulates CXCL1 expression via miR-19a–induced NF-κB activation. In line with a proatherogenic role of miR-19a, the second miR-19 family member miR-19b, which differs only in 1 nucleotide from miR-19a, increases atherosclerosis.[31]

In conclusion, we found that endothelial HIF-1α promotes the development of atherosclerosis by mediating the effects of unsaturated LPA on endothelial inflammation and monocyte recruitment through upregulation of miR-19a.

Perspectives

Our finding that endothelial HIF-1α activation in ECs by hyperlipidemia promotes atherosclerosis provides further insights in the transcriptional regulation of endothelial inflammation. HIF-1α promoted NF-κB activation by upregulating miR-19a, which in turn may enhance HIF-1α activation. Therefore, targeting this mutual activation of NF-κB and HIF-1α by inhibiting miR-19a in ECs may provide a novel approach in the treatment of atherosclerosis.

Acknowledgments

We thank Melanie Garbe, Stephanie Elbin, Kathrin Heyll, and Claudia Geißler for their technical assistance.

Sources of Funding

This work was supported by the German Research Foundation (Deutsche Forschungsgemeinschaft [DFG]) as part of the Collaborative Research Center 1123 (B04 and B08), by the German Centre for Cardiovascular Research, and by a DAAD-Siemens scholarship (to S. Akhtar)

Disclosures

None.

References

1. Natarelli L, Schober A. MicroRNAs and the response to injury in atherosclerosis. *Hamostaseologie*. 2015;35:142–150. doi: 10.5482/HAMO-14-10-0051.
2. Hajra L, Evans AI, Chen M, Hyduk SJ, Collins T, Cybulsky MI. The NF-kappa B signal transduction pathway in aortic endothelial cells is primed for activation in regions predisposed to atherosclerotic lesion formation. *Proc Natl Acad Sci U S A*. 2000;97:9052–9057.
3. Schober A, Nazari-Jahantigh M, Weber C. MicroRNA-mediated mechanisms of the cellular stress response in atherosclerosis. *Nat Rev Cardiol*. 2015;12:361–374. doi: 10.1038/nrcardio.2015.38.
4. Schober A, Nazari-Jahantigh M, Wei Y, Bidzhekov K, Gremse F, Grommes J, Megens RT, Heyll K, Noels H, Hristov M, Wang S, Kiessling F, Olson EN, Weber C. MicroRNA-126-5p promotes endothelial proliferation and limits atherosclerosis by suppressing Dlk1. *Nat Med*. 2014;20:368–376. doi: 10.1038/nm.3487.
5. Huo Y, Weber C, Forlow SB, Sperandio M, Thatte J, Mack M, Jung S, Littman DR, Ley K. The chemokine KC, but not monocyte chemoattractant protein-1, triggers monocyte arrest on early atherosclerotic endothelium. *J Clin Invest*. 2001;108:1307–1314. doi: 10.1172/JCI12877.
6. Zhou Z, Subramanian P, Sevilmis G, Globke B, Soehnlein O, Karshovska E, Megens R, Heyll K, Chun J, Saulnier-Blache JS, Reinholz M, van Zandvoort M, Weber C, Schober A. Lipoprotein-derived lysophosphatidic acid promotes atherosclerosis by releasing CXCL1 from the endothelium. *Cell Metab*. 2011;13:592–600. doi: 10.1016/j.cmet.2011.02.016.
7. Schober A, Siess W. Lysophosphatidic acid in atherosclerotic diseases. *Br J Pharmacol*. 2012;167:465–482. doi: 10.1111/j.1476-5381.2012.02021.x.
8. Boisvert WA, Rose DM, Johnson KA, Fuentes ME, Lira SA, Curtiss LK, Terkeltaub RA. Up-regulated expression of the CXCR2 ligand KC/GRO-alpha in atherosclerotic lesions plays a central role in macrophage accumulation and lesion progression. *Am J Pathol*. 2006;168:1385–1395.
9. Shepardson KM, Jhingran A, Caffrey A, Obar JJ, Suratt BT, Berwin BL, Hohl TM, Cramer RA. Myeloid derived hypoxia inducible factor 1-alpha is required for protection against pulmonary *Aspergillus fumigatus* infection. *PLoS Pathog*. 2014;10:e1004378. doi: 10.1371/journal.ppat.1004378.
10. Semenza GL. Oxygen sensing, hypoxia-inducible factors, and disease pathophysiology. *Annu Rev Pathol*. 2014;9:47–71. doi: 10.1146/annurev-pathol-012513-104720.
11. Huang Y, Lei L, Liu D, Jovin I, Russell R, Johnson RS, Di Lorenzo A, Giordano FJ. Normal glucose uptake in the brain and heart requires an endothelial cell-specific HIF-1α-dependent function. *Proc Natl Acad Sci U S A*. 2012;109:17478–17483. doi: 10.1073/pnas.1209281109.
12. Tang N, Wang L, Esko J, Giordano FJ, Huang Y, Gerber HP, Ferrara N, Johnson RS. Loss of HIF-1alpha in endothelial cells disrupts a hypoxia-driven VEGF autocrine loop necessary for tumorigenesis. *Cancer Cell*. 2004;6:485–495. doi: 10.1016/j.ccr.2004.09.026.
13. Bartoszewska S, Kochan K, Piotrowski A, Kamysz W, Ochocka RJ, Collawn JF, Bartoszewski R. The hypoxia-inducible miR-429 regulates hypoxia-inducible factor-1α expression in human endothelial cells through a negative feedback loop. *FASEB J*. 2015;29:1467–1479. doi: 10.1096/fj.14-267054.
14. Manalo DJ, Rowan A, Lavoie T, Natarajan L, Kelly BD, Ye SQ, Garcia JG, Semenza GL. Transcriptional regulation of vascular endothelial cell responses to hypoxia by HIF-1. *Blood*. 2005;105:659–669. doi: 10.1182/blood-2004-07-2958.
15. Chen Z, Lai TC, Jan YH, et al. Hypoxia-responsive miRNAs target argonaute 1 to promote angiogenesis. *J Clin Invest*. 2013;123:1057–1067. doi: 10.1172/JCI65344.
16. Vink A, Schoneveld AH, Lamers D, Houben AJ, van der Groep P, van Diest PJ, Pasterkamp G. HIF-1 alpha expression is associated with an atheromatous inflammatory plaque phenotype and upregulated in activated macrophages. *Atherosclerosis*. 2007;195:e69–e75. doi: 10.1016/j.atherosclerosis.2007.05.026.
17. Sluimer JC, Gasc JM, van Wanroij JL, Kisters N, Groeneweg M, Sollewijn Gelpke MD, Cleutjens JP, van den Akker LH, Corvol P, Wouters BG, Daemen MJ, Bijnens AP. Hypoxia, hypoxia-inducible transcription factor, and macrophages in human atherosclerotic plaques are correlated with intraplaque angiogenesis. *J Am Coll Cardiol*. 2008;51:1258–1265. doi: 10.1016/j.jacc.2007.12.025.
18. Karshovska E, Zernecke A, Sevilmis G, Millet A, Hristov M, Cohen CD, Schmid H, Krotz F, Sohn HY, Klauss V, Weber C, Schober A. Expression of HIF-1alpha in injured arteries controls SDF-1alpha mediated neointima formation in apolipoprotein E deficient mice. *Arterioscler Thromb Vasc Biol*. 2007;27:2540–2547. doi: 10.1161/ATVBAHA.107.151050.
19. Eelen G, de Zeeuw P, Simons M, Carmeliet P. Endothelial cell metabolism in normal and diseased vasculature. *Circ Res*. 2015;116:1231–1244. doi: 10.1161/CIRCRESAHA.116.302855.
20. Kuschel A, Simon P, Tug S. Functional regulation of HIF-1α under normoxia–is there more than post-translational regulation? *J Cell Physiol*. 2012;227:514–524. doi: 10.1002/jcp.22798.
21. Lee SJ, No YR, Dang DT, Dang LH, Yang VW, Shim H, Yun CC. Regulation of hypoxia-inducible factor 1α (HIF-1α) by lysophosphatidic acid is dependent on interplay between p53 and Krüppel-like factor 5. *J Biol Chem*. 2013;288:25244–25253. doi: 10.1074/jbc.M113.489708.
22. Subramanian P, Karshovska E, Reinhard P, Megens RT, Zhou Z, Akhtar S, Schumann U, Li X, van Zandvoort M, Ludin C, Weber C, Schober A. Lysophosphatidic acid receptors LPA1 and LPA3 promote CXCL12-mediated smooth muscle progenitor cell recruitment in neointima formation. *Circ Res*. 2010;107:96–105. doi: 10.1161/CIRCRESAHA.109.212647.
23. Luo R, Zhang W, Zhao C, Zhang Y, Wu H, Jin J, Zhang W, Grenz A, Eltzschig HK, Tao L, Kellems RE, Xia Y. Elevated endothelial hypoxia-inducible factor-1α contributes to glomerular injury and promotes hypertensive chronic kidney disease. *Hypertension*. 2015;66:75–84. doi: 10.1161/HYPERTENSIONAHA.115.05578.
24. Kawanami D, Mahabeleshwar GH, Lin Z, Atkins GB, Hamik A, Haldar SM, Maemura K, Lamanna JC, Jain MK. Kruppel-like factor 2 inhibits hypoxia-inducible factor 1alpha expression and function in the endothelium. *J Biol Chem*. 2009;284:20522–20530. doi: 10.1074/jbc.M109.025346.
25. Qin X, Wang X, Wang Y, Tang Z, Cui Q, Xi J, Li YS, Chien S, Wang N. MicroRNA-19a mediates the suppressive effect of laminar flow on cyclin D1 expression in human umbilical vein endothelial cells. *Proc Natl Acad Sci U S A*. 2010;107:3240–3244. doi: 10.1073/pnas.0914882107.

26. Hergenreider E, Heydt S, Tréguer K, Boettger T, Horrevoets AJ, Zeiher AM, Scheffer MP, Frangakis AS, Yin X, Mayr M, Braun T, Urbich C, Boon RA, Dimmeler S. Atheroprotective communication between endothelial cells and smooth muscle cells through miRNAs. *Nat Cell Biol*. 2012;14:249–256. doi: 10.1038/ncb2441.
27. Loyer X, Potteaux S, Vion AC, Guérin CL, Boulkroun S, Rautou PE, Ramkhelawon B, Esposito B, Dalloz M, Paul JL, Julia P, Maccario J, Boulanger CM, Mallat Z, Tedgui A. Inhibition of microRNA-92a prevents endothelial dysfunction and atherosclerosis in mice. *Circ Res*. 2014;114:434–443. doi: 10.1161/CIRCRESAHA.114.302213.
28. Gantier MP, Stunden HJ, McCoy CE, Behlke MA, Wang D, Kaparakis-Liaskos M, Sarvestani ST, Yang YH, Xu D, Corr SC, Morand EF, Williams BR. A miR-19 regulon that controls NF-κB signaling. *Nucleic Acids Res*. 2012;40:8048–8058. doi: 10.1093/nar/gks521.
29. Hartmann P, Schober A, Weber C. Chemokines and microRNAs in atherosclerosis. *Cell Mol Life Sci*. 2015;72:3253–3266. doi: 10.1007/s00018-015-1925-z.
30. Yang F, Wang H, Jiang Z, Hu A, Chu L, Sun Y, Han J. MicroRNA-19a mediates gastric carcinoma cell proliferation through the activation of nuclear factor-κB. *Mol Med Rep*. 2015;12:5780–5786. doi: 10.3892/mmr.2015.4151.
31. Lv YC, Tang YY, Peng J, et al. MicroRNA-19b promotes macrophage cholesterol accumulation and aortic atherosclerosis by targeting ATP-binding cassette transporter A1. *Atherosclerosis*. 2014;236:215–226. doi: 10.1016/j.atherosclerosis.2014.07.005.

Novelty and Significance

What Is New?

- Enhanced hypoxia-inducible factor (HIF)-1α activation in atherosclerotic ECs promotes the expression of CXCL1 and increases atherosclerosis. Endothelial HIF-1α induces lysophosphatidic acid–mediated CXCL1 expression and monocyte adhesion by upregulating miR-19a.

What Is Relevant?

- Inhibition of the endothelial HIF-1α/miR-19a pathway may be a therapeutic option against atherosclerosis.

Summary

Our results indicate that hyperlipidemia upregulates endothelial HIF-1α expression by mildly oxidized low-density lipoprotein–derived unsaturated lysophosphatidic acid, which induces CXCL1 expression and monocyte adhesion. The effects of HIF-1α are mediated by miR-19a, which triggers nuclear factor-κB activation, and CXCL1-dependent monocyte adhesion. Taken together, our findings indicate that hyperlipidemia-induced HIF-1α activation in endothelial cells contributes to atherogenic monocyte recruitment by upregulating miR-19a.

ONLINE SUPPLEMENT

Endothelial hypoxia-inducible factor-1α promotes atherosclerosis and monocyte recruitment by upregulating miRNA-19a

Shamima Akhtar[1,2]*, Petra Hartmann[1]*, Ela Karshovska[1], Fatuma-Ayaan Rinderknecht[1], Pallavi Subramanian[1], Felix Gremse[3], Jochen Grommes[4,5], Michael Jacobs[4,5], Fabian Kiessling[3], Christian Weber[1,6,7], Sabine Steffens[1,7], Andreas Schober[1,2,7]

[1]Institute for Cardiovascular Prevention, Ludwig-Maximilians-University Munich, Germany, Munich;
[2]Institute for Molecular Cardiovascular Research, [3]Department of Experimental Molecular Imaging, and [4]European Vascular Center Aachen-Maastricht, RWTH Aachen University, Aachen, Germany;
[5]European Vascular Center Aachen-Maastricht, University Maastricht Medical Center, Maastricht, The Netherlands;
[6]Cardiovascular Research Institute Maastricht, University Maastricht, Maastricht, The Netherlands;
[7]DZHK (German Centre for Cardiovascular Research), partner site Munich Heart Alliance, Munich, Germany;
* These authors contributed equally to this work.

Supplemental Methods

Animal model

Hif1a$^{flox/flox}$*Apoe*$^{-/-}$ mice were generated by crossing mice carrying a floxed *Hif1a* allele (The Jackson Laboratories, Bar Harbor, USA) with *Apoe*$^{-/-}$ mice. VE-Cad-Cre-ER^{T2} mice[1], which express a Tamoxifen (TMX)-inducible Cre recombinase under the endothelial specific VE-Cadherin promoter, were mated with the *Hif1a*$^{flox/flox}$ *Apoe*$^{-/-}$ mice to generate VE-Cad-Cre-ER^{T2}/*Hif1a*$^{flox/flox}$/*Apoe*$^{-/-}$ mice. VE-Cad-Cre-ER^{T2}/*Hif1a*$^{flox/flox}$/*Apoe*$^{-/-}$ mice (EC-*Hif1a*$^{-/-}$) and VECad-Cre-ER^{T2}/*Hif1a*$^{WT/WT}$/*Apoe*$^{-/-}$ mice (EC-*Hif1a*$^{+/+}$) were used throughout this study. Cre recombinase activity was induced by intraperitoneal injection of the mice with Tamoxifen (2 mg/20 g body weight; Sigma-Aldrich, Munich, Germany) dissolved in neutral oil (Migyol; Sasol, Hamburg, Germany) for 5 consecutive days. One week after the last injection, mice were either subjected to partial carotid ligation (PL) and fed a high fat diet (HFD, 0.15% cholesterol, Altromin, Lage, Germany) for 2, 4 or 6 weeks or fed the HFD for 12 weeks without partial ligation. All of the animal experiments were reviewed and approved by the local authorities in accordance with German animal protection law.

Partial ligation of carotid arteries

The left carotid arteries of 6–8-weeks old EC-*Hif1a*$^{-/-}$ and EC-*Hif1a*$^{+/+}$ mice were partially ligated and the mice were fed a HFD for the indicated time-points. Briefly, mice were anesthetized by injection with ketamine (80 mg/kg, i.p.) and xylazine (10 mg/kg, i.p.) and the external, the internal and the occipital artery were ligated allowing blood outflow only via the superior thyroid artery. Two or six weeks after the partial ligation, the carotid arteries were harvested after perfusion fixation with 4% paraformaldehyde (PFA, Sigma-Aldrich) and embedded in paraffin. The first 200 µm of the ligated carotid artery starting from bifurcation were analyzed.

Diet-induced atherosclerosis

Female EC-*Hif1a*$^{+/+}$ and EC-*Hif1a*$^{-/-}$ mice (age 6–8-weeks) were fed a HFD for 12 weeks. Mice were anesthetized by injection with ketamine (80 mg/kg, i.p.) and xylazine (10 mg/kg, i.p.). The carotid arteries, aortic roots, and thoracoabdominal aorta were harvested after perfusion fixation with 4% PFA (Sigma-Aldrich). The tissues were embedded in paraffin.

Micro-computed tomography (CT) angiography

Micro-CT (TomoScope DUO, CT Imaging, Erlangen, Germany) scans was performed on partially ligated mice, as described previously[2]. A blood-pool contrast agent was intravenously injected and the luminal diameter of the common carotid artery was quantified within a distance of 1 mm from the bifurcation with the Imalytics Research workstation (Philips Technologie GmbH, Aachen, Germany). Three dimensional (3D) renderings of the carotid artery were created using the Definiens Developer XD software (Definiens, Munich, Germany).

Lesion quantification

Thoracoabdominal aortas were prepared *en face* and stained with Oil Red O stain. The Oil Red O-positive area was quantified from digital images of the aorta using image analysis software (ImageJ). The lesion area was analyzed in the carotid

arteries by elastic van Gieson (EVG) staining of serial sections (4–5 µm thick) at an interval of 100 µm.

Immunostaining

Consecutive sections at an interval of 120 µm were immunostained for SM22 (rabbit polyclonal antibody, Abcam, Cambridge, UK), Mac-2 (clone M3/38 antibody, Cedarlane, Ontario, Canada) and collagen type-1 (rabbit polyclonal antibody, Cedarlane). The SM22, Mac-2 and collagen type-1 positive area in the lesion was quantified using ImageJ software.

Expression of HIF-1α was determined by immunostaining using a mouse monoclonal antibody against HIF-1α (Novus Biologicals, Cambridge, UK). Double immunostaining for Hif-1α or CXCL1 (rabbit polyclonal, Abcam) and CD31 (goat polyclonal, Santa Cruz, Heidelberg, Germany) or von Willebrand factor (vWF; rabbit polyclonal Ab, Abcam, Cambridge, UK) was performed in carotid artery sections or aortic root sections by sequential incubation of primary antibodies. Non-specific IgG served as a negative control. Primary antibodies were detected using fluorescently labelled secondary antibodies. The double immunostainings were analyzed by counting the number of CD31 and HIF-1α or CD31 and CXCL1 double positive cells in the lesions according to the presence of DAPI-(4'6-diamidino-2-phenylindole) stained nuclei and expressed as percentage of the total number of $CD31^+$ cells.

Human atherosclerotic lesion specimens were obtained during carotid endarterectomy and fixed in PFA. The expression of endothelial specific HIF-1α was determined by double immunostaining for vWF (rabbit polyclonal, Abcam) and Hif-1α (mouse monoclonal, Novus Biologicals). The study protocol for the collection of human plaque samples was approved by the Ethics Committee of the Medical Faculty (RWTH Aachen University). Written informed consent was obtained from all participants.

Cell Culture

To obtain mouse aortic ECs (MAECs), the aortic arch and the thoracic aorta were cut into small pieces, which were aseptically placed on collagen gel. The ECs that migrated onto the gel after 5–6 days were isolated by digesting the gel with 0.3% collagenase and cultured in a tissue culture flask with endothelial cell growth medium (PAA, Pasching, Austria). The purity of the ECs was determined at passage 3 by lectin staining (*Lycopersicon esculentum*; Sigma). MAECs were seeded into collagen-coated 6-well plates (Millipore, Billerica, MA, USA) and grown to appropriate density in complete growth medium.

Human aortic ECs (HAEC; PromoCell, Heidelberg, Germany) were cultured in collagen-coated dishes (Millipore) using EC growth medium (PromoCell).

Following serum starvation for 18–20 h, the culture medium was replaced with fresh growth medium. LPA20:4 (Echelon, Salt Lake City, USA, 10 µmol/L), LPA18:0 (Avanti Polar Lipids, Alabaster, USA, 10 µmol/L), mildly-oxidized LDL (moxLDL; 50 µg/ml), native LDL (nLDL; 50 µg/ml) dissolved in PBS were added to the medium and incubated at 37°C for 4–6 h. MAECs/HAECs were also treated with LPA20:4 (10 µmol/L) and the LPA receptor antagonist Ki16425 (Cayman Chemical, 100 µmol/L) or moxLDL (50 µg/ml) and Ki16425 (100 µmol/L) for 4–6 h. The medium was collected and stored at -80°C until measurement. The cells were harvested for RNA isolation.

Transfection of MAECs and HAECs

MAECs/HAECs were transfected with a small interfering RNA (siRNA) against *Hif1a* (Thermo Scientific, Braunschweig, Germany; Accell Mouse Hif1a (15251), Cat. # 040638-00-0002; Accell Human HIF1A (3091), Cat. # 004018-00-0005; 1µM) or a non-targeting siRNA for 72 h. MAECs were additionally incubated with or without LPA20:4 (10 µmol/L) or moxLDL (50 µg/ml) for 4 h. Cell culture medium was collected and stored at -80°C until measurement and the cells were harvested for RNA or protein isolation. Lipofectamine 2000 (Life Technologies, Darmstadt, Germany) was used to transfect HAECs with a locked nucleic acid (LNA)-miR-19a inhibitor (50 nM, miRCURY LNA^{TM} microRNA Inhibitors; Exiqon, Vedbaek, Denmark), a miR-19a mimics (50 nM, *mir*VanaTM mimics; Life Technologies) or scrambled controls for 24h. Additional treatment with moxLDL (50 µg/ml) was performed for 6h, before the RNA was isolated.

For the p65 staining, HAECs were cultured in chamber slides (NuncTM Lab-TekTM; Thermo Scientific) and transfected with miR-19a-mimics or scrambled controls for 24h. HAECs were fixed with aceton/methanol (1:1) and p65 was determined using a polyclonal antibody against p65 (ab7970, Abcam).

Quantitative real time polymerase chain reaction (qRT-PCR)

Total RNA was isolated from carotid arteries and from cultured ECs using the RNA easy mini kit (Qiagen, Hilden, Germany) or NucleoSpin microRNA Kit (Macherey-Nagel GmbH & Co. KG, Düren, Germany). Reverse transcription was performed using M-MLV reverse transcriptase (Promega, Mannheim, Germany), TaqMan microRNA reverse transcription kit or high-capacity cDNA reverse transcription kit (both from Life Technologies). *Hif1a* mRNA and transcripts of proinflammatory cytokines were quantified by SYBR green PCR amplification in 7900HT fast real-time PCR system (Applied Biosystems, Darmstadt, Germany) (Table S1). *Gapdh* and *Actb* were used as reference genes. MiR-19a (Cat. # 000395) expression levels were quantified using TaqMan microRNA assays and TaqMan Universal PCR Master Mix (all from Life Technologies). RNU44 (Cat. # 001094) or sno135 (Cat. # 001230) were used as reference genes. The relative expression levels were normalized to a single or multiple reference genes scaled to the sample with the lowest expression and logarithmically transformed using Qbase^{PLUS} software (Biogazelle NV, Zwijnaarde, Belgium).

MiRNA Real-time PCR Array

After reverse transcription and pre-amplification of total RNA using the Megaplex RT & Preamp Rodent Pool Set (Life Technologies), the samples were loaded onto preconfigured 384-well microfluidic TaqMan Array MicroRNA Cards for real-time polymerase chain reaction (RT-PCR) analyzing 641 mouse miRNAs, using the 7900HT Real-Time PCR System (all from Life Technologies). Data analysis was performed using Qbase^{PLUS} software (Biogazelle NV) along with multiple internal control genes. The detection limit of the individual assays was defined as a CT < 40.

Flow Chamber Assay

Monocyte adhesion to MAECs stimulated with LPA20:4 (10 µmol/L), LPA18:0 (10 µmol/L), moxLDL (50 µg/ml) or nLDL (50 µg/ml) was measured using a parallel plate

flow chamber, as described previously[3]. MonoMac6 cells (MM6; 0.5 × 10^6 cells/ml; Leibniz Institute DSMZ-German Collection of Microorganisms and Cell Cultures, Braunschweig, Germany) were suspended in HBSS-medium (1× Hanks Balanced Salt Solution, 1% FCS, 0.5% BSA) and labeled with calcein AM (1 µM; Life Technologies) for 30 min. For some experiments MM6 cells were treated with an antibody against C-X-C chemokine receptor type 2 (CXCR2; 20 µg/ml, clone 48311) or an isotype control IgG (20 µg/ml, clone 20102) (both from R&D Systems, Minneapolis, MN, USA). MM6 cells were perfused over MAECs in the lower chamber using a perfusion pump (WPI-SP100I, Berlin, Germany, shear rate of 1.5 dyn/cm^2). Monocyte-endothelial interactions were visualized by video-microscopy using a 10x magnification. For each experiment, recordings were made for 15 sec in one visual field and 5 random microscopic visual fields were analyzed for each experiment. After a 5 min observation period, monocytes that firmly attached to the MAECs were manually counted per visual field. Each experiment was repeated at least 3 times.

Lipid Analysis

The serum samples were analyzed for total cholesterol and triglycerides by dry chemistry using a Vitros 250 Analyzer (Ortho Clinical Diagnostics, Neckargemuend, Germany).

Preparation of mildly-oxidized LDL (moxLDL)

Human native LDL (1 mg/ml, Calbiochem, Darmstadt, Germany) was incubated with 5 µM CuSO4 at 37°C for 4 hours to prepare moxLDL. The LDL oxidation was stopped by adding 10 µM EDTA and the LDL was passed through PD-10 desalting column (GE Healthcare, Uppsala, Sweden). To prepare native LDL (nLDL) for experimental use as a negative control, all the above steps were performed except the addition of CuSO4. The protein concentration was measured using DC protein assay kit (Bio-Rad Laboratories GmbH, Munich, Germany) with BSA as a standard. The level of oxidation was evaluated by spectrophotometrically quantification the formation of thiobarbituric acid-reactive species (TBARS) at 532 nm (TBARS assay kit, Cayman Chemical, Michigan, USA). The moxLDL and nLDL were used within 14 days after preparation and stored at 4°C.

Enzyme-linked Immunosorbent Assay (ELISA)

The level of CXCL1 protein in the cell culture medium of MAECs was determined by a mouse CXCL1/KC ELISA kit (Ray Biotech, Inc, Norcross, USA) according to the manufacturer's protocol. The absorbance was measured at 450 nm with a microplate reader (SPECTRA Fluor Plus, Tecan).

Western Blot Analysis

The level of HIF-1α protein was determined in the cell lysate of MAECs or HAECs. ECs were lysed in RIPA buffer (Sigma-Aldrich) including protease inhibitors (CompleteProtease Inhibitor Cocktail, Roche, Basel, Switzerland). The cell lysate was resolved on SDS-PAGE gels and then transferred to nitrocellulose membranes. Proteins were detected using primary antibodies against HIF-1α (clone H-206, Santa Cruz Biotechnology, CA, USA), and GAPDH (clone 6C5, Millipore), and horse radish peroxidase conjugated (HRP)-conjugated secondary antibodies (Goat Anti-Mouse IgG HRP Affinity Purified PAb, R&D Systems; Goat Anti-Rabbit IgG HRP Affinity Purified PAb, Santa Cruz). Protein bands were visualized using an enhanced chemiluminescence detection system (ECL Advance, GE Healthcare Life Sciences)

and a LAS 3000 Imager (Fuji Photo Film Co., Ltd., Tokyo, Japan) and were quantified using Multigauge software (Fuji Photo Film). Intensities of the HIF-1α bands were expressed as a percentage of those of the GAPDH bands.

In Situ Reverse Transcriptase PCR

Sections (5 µm thick) of carotid arteries were cooked in citrate buffer for 20 min using a microwave (600 W). One-step reverse transcriptase *in situ* PCR was performed using gene-specific Taq *in situ* primers (Sigma-Aldrich) (Table S1), SuperScript One-Step RT-PCR with PlatinumTaq (Life Technologies), and digoxigenin-11-dUTPs (Roche). After washing with SSC buffer and blocking of biotin/avidin binding sites (Blocking Kit; Vector Laboratories, Peterborough, UK), the sections were incubated with HRP anti-digoxigenin sheep F'ab fragments (Roche) for 1 h at 37°C. The probes were visualized using a tyramide-based amplification system (TSA Plus Biotin; Perkin Elmer, Waltham, MA, USA) and DyLight 549-labeled streptavidin (Kirkegaard & Perry Laboratories, Gaithersburg, MD, USA[4].

Statistical Analysis

The miRNA real-time PCR array data were analyzed using Qbase^{PLUS} software (Biogazelle NV) and are presented as mean values. All other data represent the mean ± SEM and were compared by either a 1-way or 2-way ANOVA followed by the Newman-Keuls or Bonferroni post-test, respectively, or an unpaired two-tailed Student *t*-test (Prism 6 software; Inc., La Jolla, CA, USA). $P < 0.05$ was considered to be statistically significant.

References

1. Monvoisin A, Alva JA, Hofmann JJ, Zovein AC, Lane TF, Iruela-Arispe ML. VE-cadherin-CreERT2 transgenic mouse: a model for inducible recombination in the endothelium. *Dev Dyn*. 2006;235:3413-3422.
2. Gremse F, Grouls C, Palmowski M, Lammers T, de Vries A, Grull H, Das M, Muhlenbruch G, Akhtar S, Schober A, Kiessling F. Virtual elastic sphere processing enables reproducible quantification of vessel stenosis at CT and MR angiography. *Radiology*. 2011;260:709-717.
3. Schober A, Zernecke A, Liehn E, von Hundelshausen P, Knarren S, Kuziel W, Weber C. Crucial role of the CCL2/CCR2 axis in neointimal hyperplasia after arterial injury in hyperlipidemic mice involves early monocyte recruitment and CCL2 presentation on platelets. *Circ Res*. 2004;95:1125-1133.
4. Nuovo GJ, Elton TS, Nana-Sinkam P, Volinia S, Croce CM, Schmittgen TD. A methodology for the combined in situ analyses of the precursor and mature forms of microRNAs and correlation with their putative targets. *Nat Protoc*. 2009;4:107-115.

Supplemental Tables

Table S1: PCR primer sequences

Gene	Primer Sequence
Mouse:	
Hif1a	sense 5'-AGAAACGACCACTGCTAAGGC-3'
	antisense 5'-GTGGCAGACAGGTTAAGGCTC3-3'
Cxcl1	sense 5'-ACCGAAGTCATAGCCACACTC-3'
	antisense 5'-TCTCCGTTACTTGGGGACAC-3'
Ccl5	sense 5'-CTGCTGCTTTGCCTACCTCT-3'
	antisense 5'-TCCTTCGAGTGACAAACACG-3'
Mif	sense 5'-TTTAGCGGCACGAACGATCC-3'
	antisense 5'-CGTTGGCAGCGTTCATGTC-3'
Ccl2	sense 5'-CTTCTGGGCCTGCTGTTCA-3'
	antisense 5'-CCAGCCTACTCATTGGGATC-3'
Tnfa	sense 5'-CCACCACGCTCTTCTGTCTA-3'
	antisense 5'-AGGGTCTGGGCCATAGAACT-3'
Gapdh	sense 5'-CACTCAAGATTGTCAGC-3'
	antisense 5'-CCACAGCCTTGGCAGC-3'
Actb	sense 5'-CAACGAGCGGTTCCGATG-3'
	antisense 5'-GCCACAGGATTCCATACCCAA-3'
Taq-*in situ*-miR-19 RT	5'-GTCGTATCCAGTGCAGGGTCCGAGGTA TTCGCACTGGATACGACTCAGTT-3'
Taq-*in situ*-miR-19	sense 5'-GCCCTGTGCAAATCTATGCA-3'
	antisense 5'-GTGCAGGGTCCGAGGT-3'
Human:	
HIF1a	sense 5'-CCCATTTTCTACTCAGGACACAG-3'
	antisense 5'-TGAGGACTTGCGCTTTCAGG-3'
CXCL1	sense 5'-CCCAAACCGAAGTCATAGCCA-3'
	antisense 5'-GATGCAGGATTGAGGCAAGC-3'
CCL2	sense 5'-CGCTCAGCCAGATGCAATCAA-3'
	antisense 5'-GACACTTGCTGCTGGTGATTC-3'
GAPDH	sense 5'-AGGGCTGCTTTTAACTCTGGT-3'
	antisense 5'-CCCCACTTGATTTTGGAGGGA-3'

Table S2: Serum cholesterol and triglyceride levels in EC-*Hif1a*$^{+/+}$ and EC-*Hif1a*$^{-/-}$ mice after partial ligation and 6 weeks HFD feeding (N=8 mice per group).

Serum levels (mmol/L)	EC-*Hif1a*$^{+/+}$	EC-*Hif1a*$^{-/-}$	P-value
Cholesterol	18.16 ± 1.409	16.64 ± 1.880	0.5268
Triglycerides	0.97 ± 0.098	0.84 ± 0.101	0.3770

Table S3: Serum cholesterol and triglyceride levels in EC-*Hif1a*$^{+/+}$ and EC-*Hif1a*$^{-/-}$ mice after 12 weeks HFD feeding (N=5–7 mice per group).

Serum levels (mmol/L)	EC-*Hif1a*$^{+/+}$	EC-*Hif1a*$^{-/-}$	P-value
Cholesterol	18.74 ± 0.623	16.80 ± 0.730	0.1123
Triglycerides	0.81 ± 0.143	0.80 ± 0.075	0.9655

Table S4: Significantly downregulated miRNAs in partially ligated LCs from EC-*Hif1a*$^{-/-}$ compared to EC-*Hif1a*$^{+/+}$ mice after 2 weeks of HFD feeding (N=3 mice per group).

miRNAs	log_{10} RQ	neg log_{10} P-value
miR-19a	-1.89	3.62
miR-9	-0.28	2.02
miR-10a	-0.49	1.73
miR-142-3p	-0.38	1.57
miR-410	-0.29	1.54
miR-30c	-0.29	1.50

Table S5: Significantly upregulated miRNAs in partially ligated LCs from EC-*Hif1a*$^{-/-}$ compared to EC-*Hif1a*$^{+/+}$ mice after 2 weeks of HFD feeding (N=3 mice per group).

miRNAs	log_{10} RQ	neg log_{10} P-value
miR-101a	0.52	2.63
miR-542-5p	0.51	1.88
miR-500	0.32	1.71
miR-345-5p	0.42	1.60
miR-542-3p	0.23	1.52
miR-339-3p	0.61	1.44

Supplemental Figures

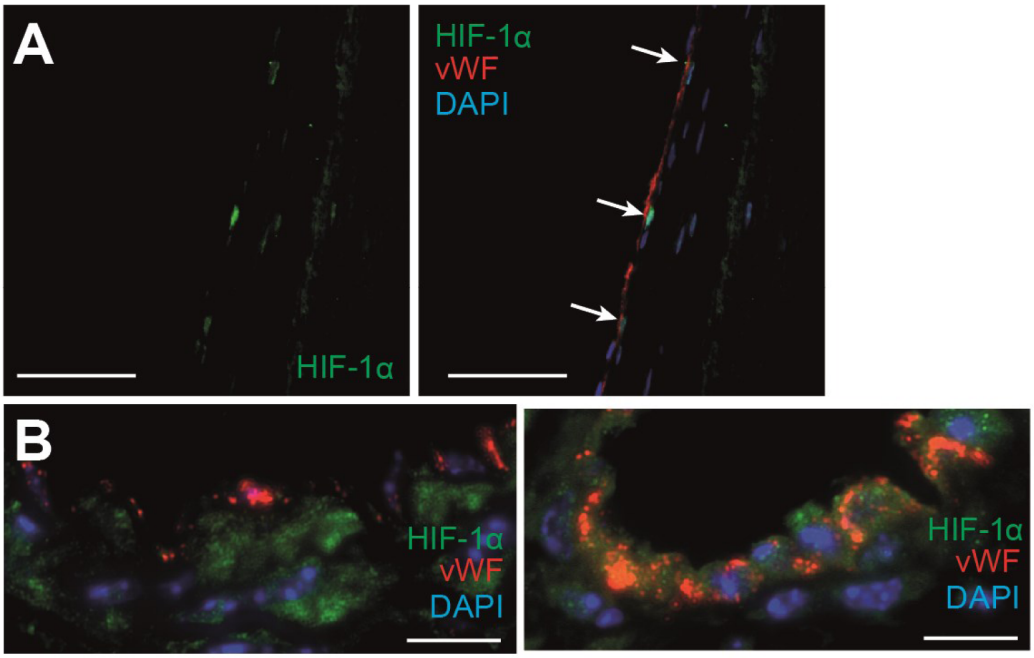

Figure S1: Endothelial HIF-1α expression in atherosclerotic lesions. (A) Dual immunostaining for HIF-1α and von Willebrand factor (vWF) in human carotid lesions. (B) Dual HIF-1α and vWF immunostaining in normal (left) and atherosclerotic aortas (right) from *Apoe*$^{-/-}$ mice. Arrows indicate HIF-1α^{+} ECs. Nuclei were stained with DAPI. Scale bars, 25 μm (A), 10 μm (B).

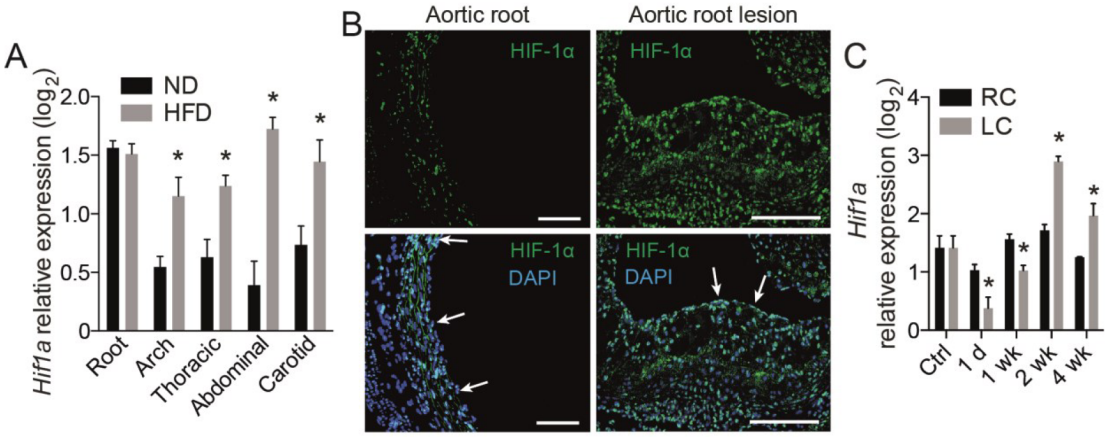

Figure S2: HIF-1α expression in murine arteries. (A) *Hif1a* mRNA expression in different aortic regions and carotid arteries of *Apoe*$^{-/-}$ mice fed a normal diet (ND) or a high-fat diet (HFD) for 12 weeks. (B) HIF-1α immunostaining in normal aortic roots and in the lesions of the aortic roots from *Apoe*$^{-/-}$ mice fed a HFD for 12 weeks. Arrows indicate HIF-1α^{+} ECs. Nuclei were stained with DAPI. Scale bars, 100 µm. (C) *Hif1a* mRNA expression in partially ligated left carotid arteries (LC) and non-ligated right carotid arteries (RC). *P<0.05, N=4-5 mice per group.

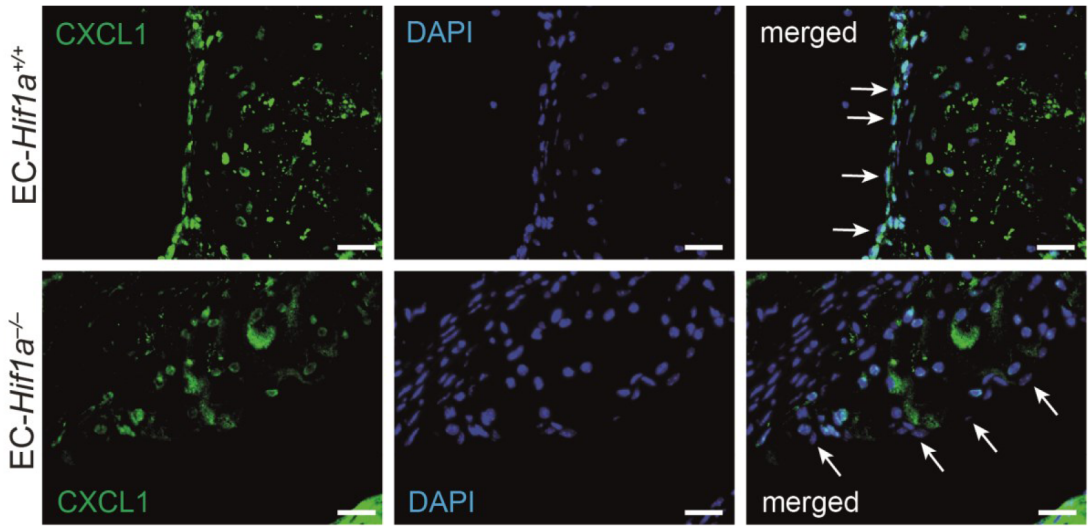

Figure S3: Effect of endothelial *Hif1a* deficiency on CXCL1 expression. Immunostaining for CXCL1 in the aortas of EC-*Hif1a*$^{+/+}$ and EC-*Hif1a*$^{-/-}$ mice fed a HFD for 12 weeks. Nuclei were stained with DAPI. Arrows indicate cells at the luminal site. Scale bars, 25 µm.

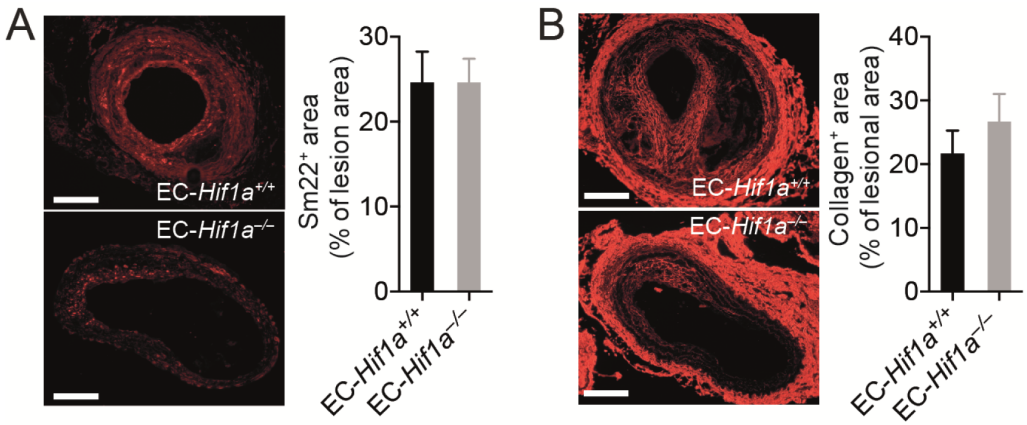

Figure S4: Effect of endothelial *Hif1a* deficiency on disturbed flow-induced plaque composition. Representative images and quantification of Sm22 (A) and Collagen type I (B) immunostaining in EC-*Hif1a*$^{+/+}$ and EC-*Hif1a*$^{-/-}$ mice 6 weeks following partial carotid ligation and HFD feeding. Scale bars, 200 µm. N=5-7 mice per group.

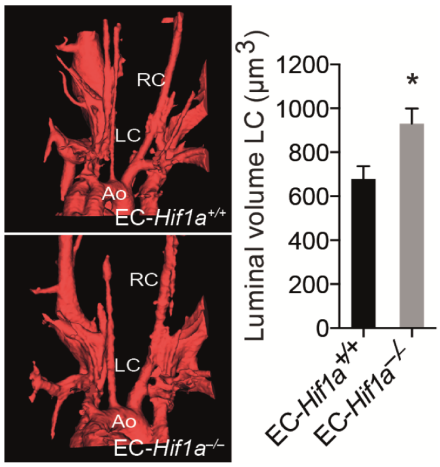

Figure S5: Effect of endothelial *Hif1a* deficiency on the luminal volume in carotid arteries. The luminal volume of the partially ligated carotid arteries from EC-*Hif1a*$^{+/+}$ and EC-*Hif1a*$^{-/-}$ mice was determined by micro-CT angiography. Representative three-dimensional reconstructions of the micro-CT angiograms are shown. LC, left carotid; RC, right carotid; Ao, Aorta. *P<0.05, N=5-8 mice per group.

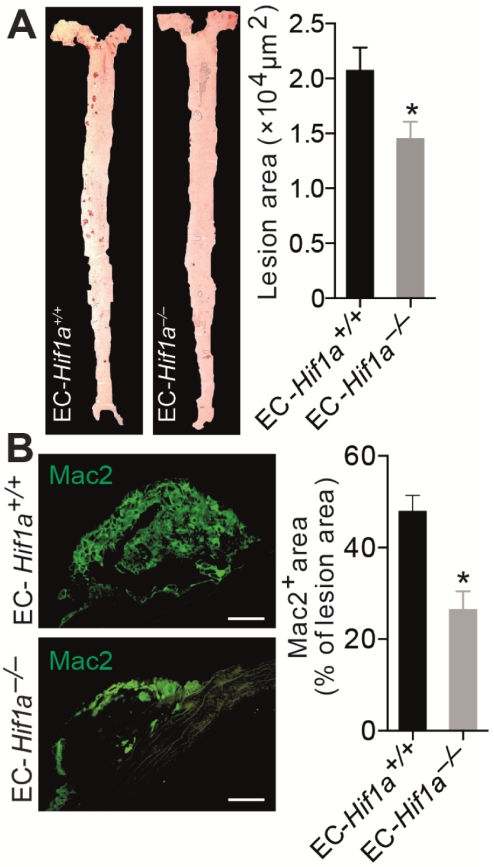

Figure S6: Effect of endothelial *Hif1a* deficiency on diet-induced atherosclerosis. (A) Atherosclerotic lesion area was quantified by Oil red O staining in the aortas from EC-*Hif1a*$^{+/+}$ and EC-*Hif1a*$^{-/-}$ mice fed a HFD for 12 weeks. (B) The lesional macrophage accumulation was determined by Mac-2 immunostaining and expressed as percentage of the lesion area. Scale bars, 100 µm (B). *P<0.05, N=8-10 mice per group.

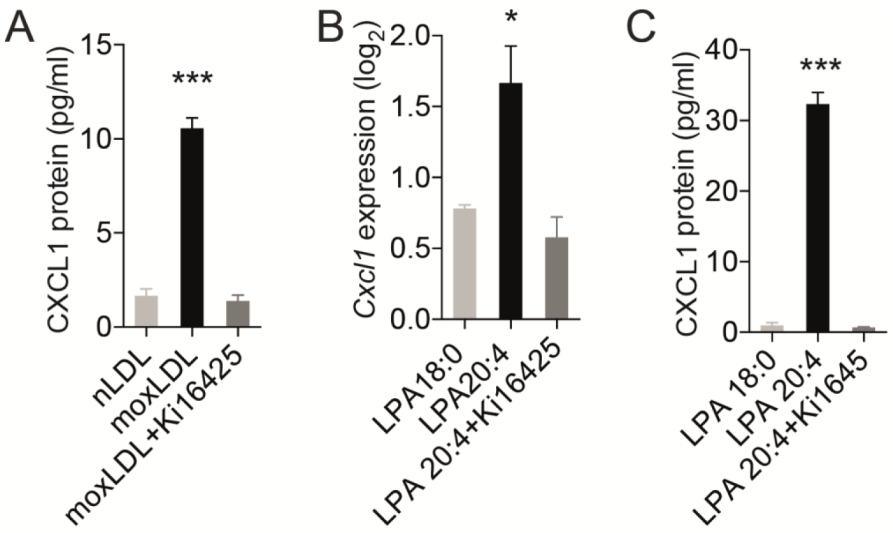

Figure S7: Regulation of CXCL1 expression by moxLDL and LPA. (A) CXCL1 protein was quantified in the medium of MAECs treated with nLDL or moxLDL with or without LPA1/3 receptor antagonist Ki16425. (B) *Cxcl1* mRNA expression was quantified in MAECs treated with LPA18:0 or LPA20:4 with or without Ki16425. (C) CXCL1 protein was quantified in medium of MAECs treated with LPA18:0 or LPA20:4 with or without Ki16425. *P<0.05 versus all other groups, ***P<0.0001 versus all other groups. N=3-4.

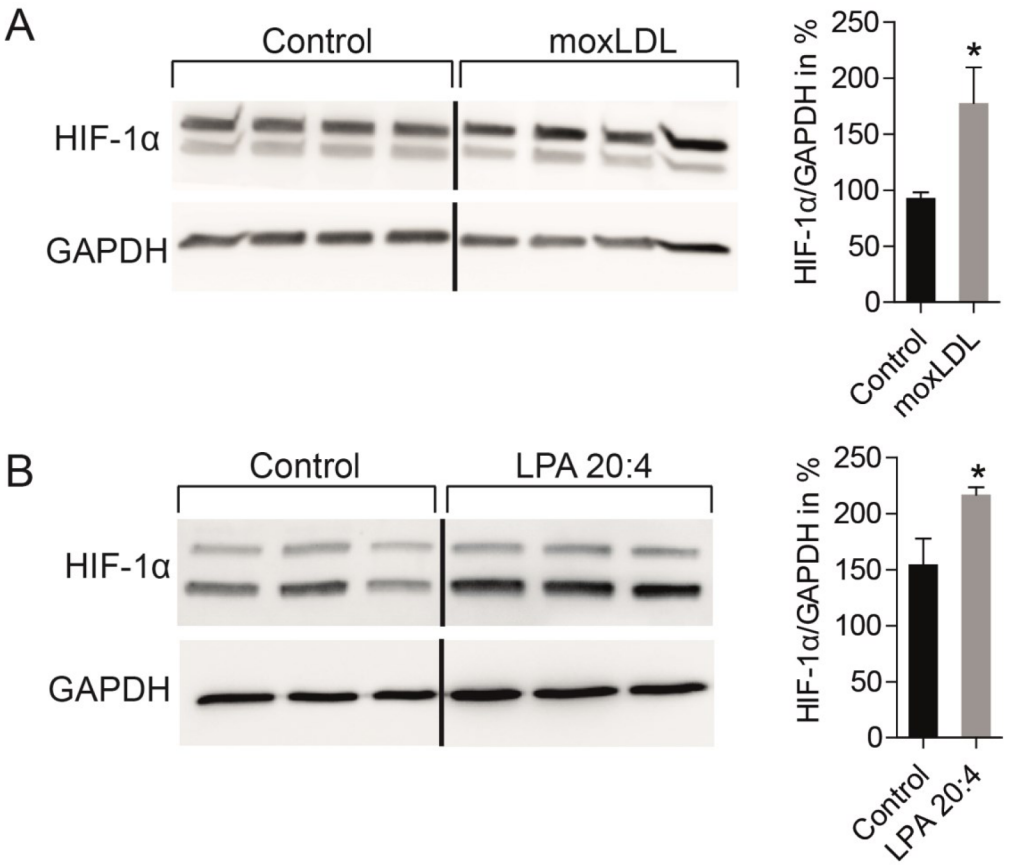

Figure S8: Effect of moxLDL and LPA 20:4 on HIF-1α protein expression. (A, B) Western blot of HIF-1α and GAPDH in MAECs stimulated with moxLDL (A) or LPA 20:4 (B). The expression levels were normalized to those of GAPDH. Unstimulated MAECs were used as a control. Samples were run on the same gel but were noncontiguous (black line). Representative blots are shown. *P<0.05, N=3-4.

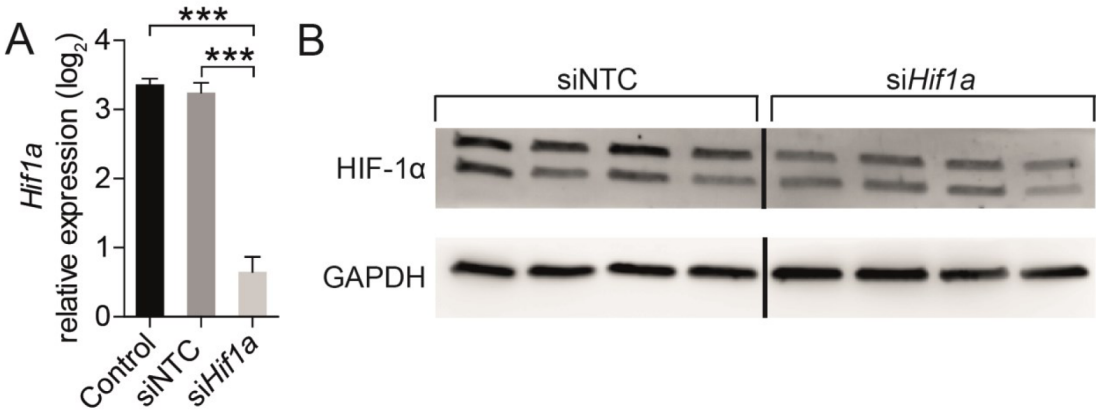

Figure S9: Efficiency of HIF-1α knockdown in MAECs. (A) Expression level of *Hif1a* in MAECs treated with siRNA against *Hif1a*. An untransfected control (Control) or a non-targeting control siRNA (siNTC) was used as control. (B) Western blots of HIF-1α and GAPDH in MAECs transfected with siRNA against *Hif1a* or a non-targeting control siRNA (siNTC). Samples were run on the same gel but were noncontiguous (black line). Representative blots are shown. ***P<0.0001, N=3-4.

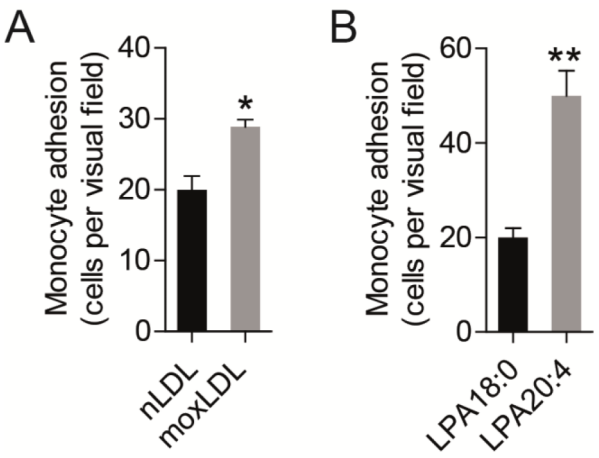

Figure S10: Effects of moxLDL or LPA20:4 on monocyte adhesion under flow conditions. Monocyte adhesion to MAECs treated with moxLDL (A) or unsaturated LPA20:4 (B) as compared to nLDL or LPA18:0. *P<0.05, **P<0.01, N=3.

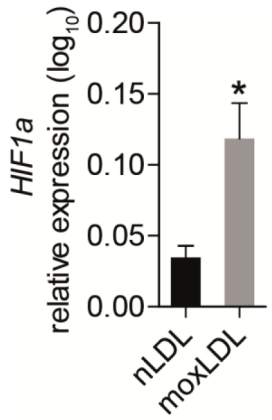

Figure S11: Effects of moxLDL on HIF-1α expression in HAECs. (A) *Hif1a* expression in HAECs treated with moxLDL as compared to nLDL. *P<0.05, N=3-4.

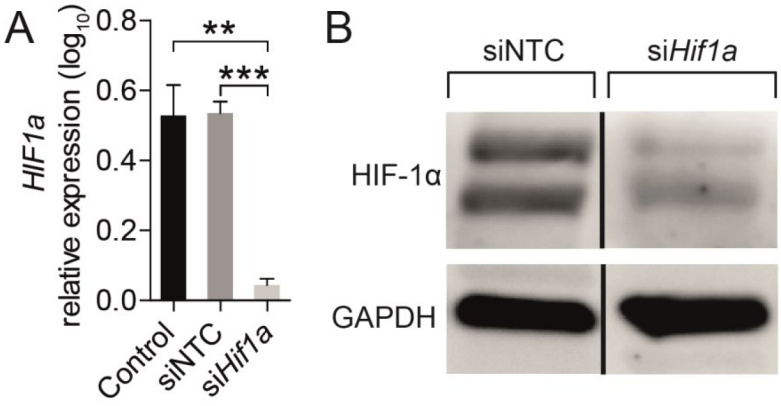

Figure S12: Efficiency of HIF-1α knockdown in HAECs. (A) Expression level of *HIF1a* mRNA in HAECs treated with siRNA against *Hif1a*. An untransfected control (Control) or a non-targeting control siRNA (siNTC) was used as control. (B) Western blots of HIF-1α and GAPDH in HAECs transfected with siRNA against *Hif1a* or a non-targeting control siRNA (siNTC). Samples were run on the same gel but were noncontiguous (black line). Representative blots are shown. **P<0.01,***P<0.0001. N=2-5.

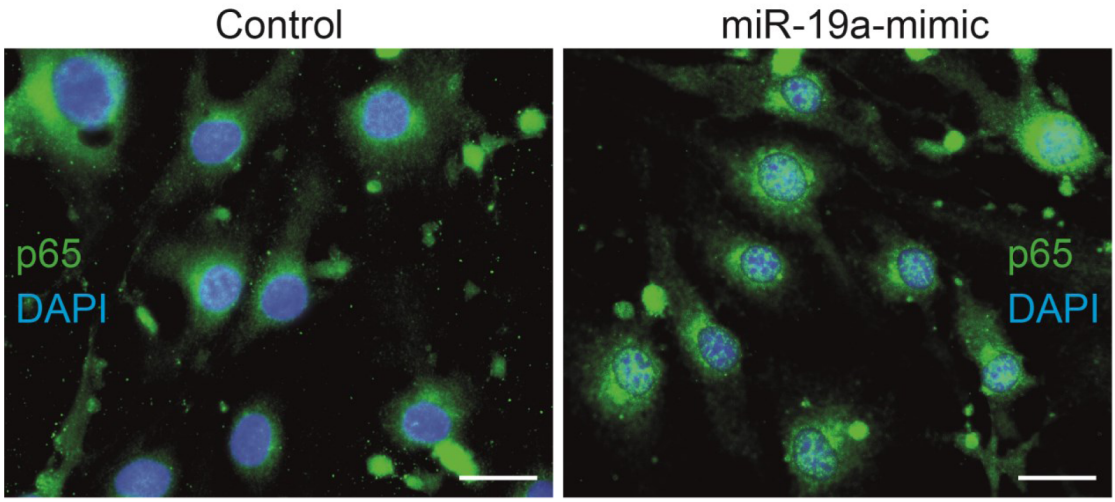

Figure S13: Effect of miR-19a-mimic treatment on p65 localization in HAECs. Immunostaining of p65 (green) in HAECs treated with miR-19a-mimics or control oligonucleotides (control). The nuclei were counterstained with DAPI (blue). Representative images are shown. Scale bars, 25µm.

Hypertension
Journal of the American Heart Association

Endothelial Hypoxia-Inducible Factor-1α Promotes Atherosclerosis and Monocyte Recruitment by Upregulating MicroRNA-19a

Shamima Akhtar, Petra Hartmann, Ela Karshovska, Fatuma-Ayaan Rinderknecht, Pallavi Subramanian, Felix Gremse, Jochen Grommes, Michael Jacobs, Fabian Kiessling, Christian Weber, Sabine Steffens and Andreas Schober

Hypertension. 2015;66:1220-1226; originally published online October 19, 2015;
doi: 10.1161/HYPERTENSIONAHA.115.05886
Hypertension is published by the American Heart Association, 7272 Greenville Avenue, Dallas, TX 75231

Print ISSN: 0194-911X. Online ISSN: 1524-4563

3.3 MiRNA-342-5p in atherosclerosis

Circulation. 2013 Apr; 127(15):1609-19. doi: 10.1161/CIRCULATIONAHA.112.000736.

The microRNA-342-5p Fosters Inflammatory Macrophage Activation Through an Akt1- and microRNA-155–Dependent Pathway During Atherosclerosis

Yuanyuan Wei, Maliheh Nazari-Jahantigh, Lily Chan, Mengyu Zhu, Kathrin Heyll, Judit Corbalán-Campos, **Petra Hartmann,** Anna Thiemann, Christian Weber, Andreas Schober.

Vascular Medicine

The *microRNA-342-5p* Fosters Inflammatory Macrophage Activation Through an Akt1- and *microRNA-155*–Dependent Pathway During Atherosclerosis

Yuanyuan Wei, PhD*; Maliheh Nazari-Jahantigh, MSc*; Lily Chan, BSc; Mengyu Zhu, MSc; Kathrin Heyll, BSc; Judit Corbalán-Campos, MSc; Petra Hartmann, MSc; Anna Thiemann, BSc; Christian Weber, MD; Andreas Schober, MD

Background—Atherosclerosis is a chronic inflammatory vascular disease driven by the subendothelial accumulation of macrophages. The mechanism regulating the inflammatory response in macrophages during atherogenesis remains unclear. Because microRNAs (miRNAs) play a crucial role in cellular signaling by posttranscriptional regulation of gene expression, we studied the miRNA expression profiles during the progression of atherosclerosis.

Methods and Results—Using an miRNA real-time polymerase chain reaction array, we found that macrophage-derived *miR-342-5p* and *miR-155* are selectively upregulated in early atherosclerotic lesions in *Apoe*$^{-/-}$ mice. *miR-342-5p* directly targets *Akt1* through its 3′-untranslated region. *Akt1* suppression by *miR-342-5p* induces proinflammatory mediators such as *Nos2* and *Il6* in macrophages via the upregulation of *miR-155*. The local application of an *miR-342-5p* antagomir inhibits the development of atherosclerosis in partially ligated carotid arteries. In atherosclerotic lesions, the *miR-342-5p* antagomir upregulated *Akt1* expression and suppressed the expression of *miR-155* and *Nos2*. This reduced *Nos2* expression was associated with a diminished generation of nitrotyrosine in the plaques. Furthermore, systemic treatment with an inhibitor of *miR-342-5p* reduced the progression of atherosclerosis in the aorta of *Apoe*$^{-/-}$ mice.

Conclusions—Macrophage-derived *miR-342-5p* promotes atherosclerosis and enhances the inflammatory stimulation of macrophages by suppressing the *Akt1*-mediated inhibition of *miR-155* expression. Therefore, targeting *miR-342-5p* may offer a promising strategy to treat atherosclerotic vascular disease. **(*Circulation*. 2013;127:1609-1619.)**

Key Words: atherosclerosis ■ macrophages ■ microRNAs

Macrophage function is of central importance for the initiation and progression of atherosclerosis.[1] Inflammatory monocytes are recruited primarily to the arterial wall after endothelial cells are activated by the products of oxidatively modified lipoproteins and/or low shear stress. These inflammatory monocytes will subsequently differentiate into macrophages and dendritic-like cells.[2] In early atherosclerosis, macrophages accumulate cholesterol through the uptake of cytotoxic, modified lipoproteins deposited in the subendothelial space and partly reallocate cholesterol from the vessel wall to high-density lipoproteins.[1,2] Minimally modified low-density lipoproteins, which can activate Toll-like receptor 4, induce the expression of inflammatory cytokines such as CCL2 in macrophages.[3] Moreover, in a mouse model of early atherosclerosis, the vascular expression of proinflammatory factors such as *Nos2*, *Il-12*, and *Ccl2* steadily increases concomitant with the accumulation of leukocytes.[4] Mechanistically, this inflammatory response amplifies monocyte recruitment, enhances the formation of oxidized lipoproteins, and may impair reverse cholesterol transport.[5–7] Thus, the transition of early atherosclerotic lesions, which are potentially reversible and clinically silent, into advanced lesions is thought to arise from a defective resolution of vascular inflammation.[8]

Clinical Perspective on p 1619

The various phases of inflammation are modulated by distinct sets of microRNAs (miRNAs) that negatively regulate posttranscriptional gene expression in leukocyte subtypes.[9,10] During the innate immune response, Toll-like receptor activation induces *miR-155* expression, which promotes inflammatory cytokine production by suppressing SOCS-1, as well as *miR-146a* and *miR-147*, which are involved in inflammation resolution.[11–14] Furthermore, miRNAs such as

Received July 15, 2012; accepted March 8, 2013.

From Experimental Vascular Medicine, Institute for Cardiovascular Prevention, Ludwig-Maximilians-University Munich, Munich (Y.W., M.N.-J., M.Z., K.H., J.C.-C., P.H., C.W., A.S.); Institute for Molecular Cardiovascular Research, RWTH Aachen University, Aachen (Y.W., M.-N.J., L.C., K.H., A.T., C.W., A.S.); and DZHK (German Centre for Cardiovascular Research), partner site Munich Heart Alliance, Munich (C.W., A.S.), Germany.

*Drs Wei and Nazari-Jahantigh contributed equally to this article.

The online-only Data Supplement is available with this article at http://circ.ahajournals.org/lookup/suppl/doi:10.1161/CIRCULATIONAHA.112.000736/-/DC1.

Correspondence to Andreas Schober, MD, Institute for Cardiovascular Prevention, Ludwig-Maximilians-University Munich, Pettenkoferstrasse 9, 80336 Munich, Germany. E-mail aschober@med.lmu.de

***Circulation* is available at http://circ.ahajournals.org** **DOI: 10.1161/CIRCULATIONAHA.112.000736**

miR-223, *miR-155*, and *miR-146a* govern the proinflammatory activation of macrophages by regulating the nuclear factor-κB signaling pathway.[9,15] The atherogenic stimulation of monocytes and macrophages by oxidized low-density lipoprotein also alters the miRNA expression profile, including the expression of *miR-155* and *miR-146a*; this, in turn, affects lipid uptake and inflammatory cytokine secretion.[16] Moreover, inhibition of *miR-33* causes an increase in reverse cholesterol transport, thereby reducing atherosclerosis and inflammatory gene expression.[17] Thus, miRNAs may be crucial for the regulation of inflammatory and lipid-handling functions in lesional macrophages. However, the miRNAs that control the inflammatory response during atherosclerosis have not been identified.

In this study, we generated stage-specific miRNA expression profiles in atherosclerotic lesions from *Apoe*$^{-/-}$ mice. During early atherosclerosis, the most prominently upregulated miRNA was *miR-342-5p*, which is expressed in lesional macrophages. On proinflammatory activation in macrophages in vitro, *miR-342-5p* promoted *Nos2* expression in an *miR-155*–dependent manner by targeting *Akt1*, an inhibitor of *miR-155* expression. Accordingly, the inhibition of *miR-342-5p* reduced atherosclerotic lesion formation and suppressed *Akt1*-dependent *Nos2* expression in lesional macrophages. Taken together, these data demonstrate a crucial role for *miR-342-5p* in the early inflammatory response in lesional macrophages.

Methods

Animal Models

Apoe$^{-/-}$ mice (age, 6–8 weeks; The Jackson Laboratory, Bar Harbor, ME) were fed a high-cholesterol diet (HCD; Altromin, Germany) comprising 21% crude fat, 0.15% cholesterol, and 19.5% casein for 3 or 10 months. *LysM-Cre* mice were mated with *Dicer*$^{flox/flox}$/*Apoe*$^{-/-}$ mice (The Jackson Laboratory) to generate *Apoe*$^{-/-}$ mice with a conditional deletion of *Dicer* in myeloid cells. Partial ligation of the carotid artery was performed as previously described.[18] Then, the mice were fed an HCD for 42 days. All animal experiments were approved by the local authorities (Landesamt für Natur, Umwelt und Verbraucherschutz, Nordrhein-Westfalen [LANUV NRW]) in accordance with German animal protection laws.

Laser Capture Microdissection

Serial sections (20 μm thick) of aortic roots were mounted on membrane-mounted metal frame slides (Molecular Machines and Industries [MMI], Glattburg, Switzerland). Laser capture microdissection was performed with a laser microdissection system (MMI CellCut Plus laser system, MMI) assembled onto an inverted microscope (Olympus IX71, Olympus Optical Co Ltd, Tokyo, Japan).

miRNA Real-Time Polymerase Chain Reaction Array

The samples were loaded onto preconfigured 384-well microfluidic cards (TaqMan Array MicroRNA Cards) for the real-time analysis (7900HT RT-PCR System, Applied Biosystems, Foster City, CA) of 518 mouse miRNAs (Sanger miRBase version 10). The data were analyzed with StatMiner software (Integromics, Philadelphia, PA) according to the ΔΔCt method, with multiple internal control genes.

Argonaut2 Immunoprecipitation

Unstimulated bone marrow–derived macrophages (BMDMs) were harvested and lysed 24 hours after the transfection of the *miR-342-5p* inhibitor. Protein A/G–conjugated magnetic beads (Millipore, Billerica, MA) were preincubated with a mouse monoclonal anti-argonaut2 antibody (clone 2E12-1C9, Abnova, Heidelberg, Germany) or mouse IgG (Millipore). The antibody-conjugated beads were subsequently incubated with cell lysates, and the precipitate was immobilized with a magnetic separator (Millipore).

Antagomir Treatment

A chemically modified antisense RNA oligonucleotide against *miR-342-5p* and a negative control antagomir were generated (Dharmacon, Inc, Chicago, IL).[19] Perivascular antagomir treatment of the carotid arteries was begun 3 weeks after the partial ligation of the carotid artery with 160 μg antagomir dissolved in 35% pluronic gel. The application was repeated twice at weekly intervals.[20]

Locked Nucleic Acid Inhibitor Treatment In Vivo

The locked nucleic acid (LNA) inhibitor of *miR-342-5p* (LNA-342-5p; ATCACAGATAGCACC) and the nonspecific control LNA oligonucleotide (LNA-control; ATCAAAGCTAGGACC) were synthesized by Exiqon, Inc (Vedbaek, Denmark). After 2 months of an HCD, *Apoe*$^{-/-}$ mice were injected 4 times with LNA-control or LNA-342-5p (25 mg/kg IV), once per week.[21] The aortas were harvested 1 week after the last injection.

Statistical Analysis

The data represent the mean±SEM and were compared by use of an unpaired or a paired *t* test or 1-way ANOVA followed by the Newman-Keuls post hoc test (StatMiner 4.2, Integromics; or Prism, GraphPad). A value of $P < 0.05$ was considered significant.

Results

miRNA Expression Profiles in Early and Advanced Atherosclerotic Lesions

During the HCD feeding period, atherosclerosis in the *Apoe*$^{-/-}$ mice increased steadily, resulting in a 2-fold increase in lesion size between 3 and 10 months (Figure IA in the online-only Data Supplement). This lesion progression was associated with the formation of a lipid core, demonstrating that early lesions (after 3 months) transformed into advanced lesions (after 10 months) in mice fed an HCD (Figure IA in the online-only Data Supplement). Concomitantly, the lesional macrophage content, as detected by Mac-2–specific immunostaining, decreased during this progression (Figure IB in the online-only Data Supplement). The smooth muscle cell content was marginal in both early and advanced lesions, as revealed by immunostaining for smooth muscle actin, and tended to decrease after 10 months of an HCD (Figure IC in the online-only Data Supplement). Therefore, our results show that early and advanced atherosclerotic lesions were generated in mice fed an HCD after 3 and 10 months, respectively.

The miRNA expression profiles of laser-microdissected samples from early and advanced lesions were studied with an miRNA real-time polymerase chain reaction array (Figure II in the online-only Data Supplement). To ensure a more complete detection of differentially expressed miRNAs, statistical analysis of the miRNA array was performed without correction for multiple comparisons.[22] In early lesions, 5 miRNAs (*miR-342-5p*, *miR-296-5p*, *miR-146b*, *miR-21**, and *miR-155*) were increased and 57 miRNAs were suppressed (Figure 1A and Table I in the online-only Data Supplement) compared

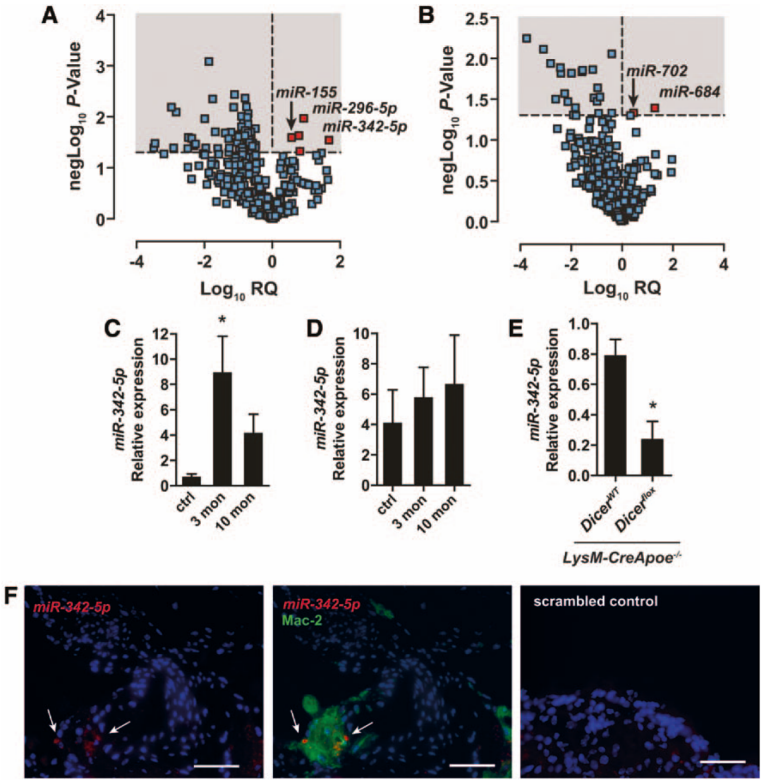

Figure 1. Increased expression of *miR-342-5p* in early atherosclerotic lesions is specific to macrophages. **A** and **B**, Differentially expressed miRNAs in lesions compared with healthy arterial tissue after (**A**) 3 months and (**B**) 10 months of a high-cholesterol diet (HCD; gray area). The upregulated miRNAs are labeled in red. n=3 or 4 mice per group. RQ indicates relative quantification value. **C** and **D**, Expression levels of *miR-342-5p* in (**C**) atherosclerotic lesions or (**D**) entire aorta after 3 months (3 mon) or 10 months (10 mon) on an HCD compared with levels in healthy vessel walls (control [ctrl]). **P*<0.05 vs control; n=3 or 4 mice from each group. **E**, Expression of *miR-342-5p* in the aortic walls of *LysM-CreDicer*^{flox}*Apoe*$^{-/-}$ mice maintained on an HCD for 3 months compared with that in *LysM-CreDicer*^{WT} *Apoe*$^{-/-}$ mice. **P*<0.05; n=4 or 5 mice from each group. **F**, In situ hybridization of *miR-342-5p* (red) combined with macrophage-specific Mac-2 staining (green) in atherosclerotic lesions from the aortic roots of *Apoe*$^{-/-}$ mice after 3 months on an HCD. Arrows indicate *miR-342-5p*–positive macrophages. Nuclei were counterstained with DAPI. Scale bars=25 μm.

with nonatherosclerotic areas in the arterial walls of the same mice. Moreover, in advanced lesions, only 2 miRNAs (*miR-684* and *miR-702*) were elevated over those in nonatherosclerotic walls, and 21 miRNAs were reduced (Figure 1B and Figure IIIA in the online-only Data Supplement). Between the early- and late-staged lesions, 8 miRNAs were either upregulated or downregulated (Figure IIIB in the online-only Data Supplement). Even in the nonatherosclerotic vessel wall, miRNA deregulation was detectable during the HCD feeding period. After 10 months, 9 miRNAs, including *miR-145**, *miR-871*, and *miR-465a-5p*, were increased, and 5 miRNAs, including *miR-377* and *miR-665*, were downregulated relative to the respective levels in mice fed an HCD for only 3 months (Figure IIIC in the online-only Data Supplement).

miR-342-5p Is Expressed in Lesional Macrophages

In early, macrophage-rich lesions, *miR-342-5p* was one of the most highly upregulated miRNAs and was barely detectable in nonatherosclerotic arteries compared with the other upregulated miRNAs (Figure 1C), indicating that *miR-342-5p* plays a role in macrophages during atherosclerosis. Accordingly, in advanced lesions with lower macrophage content, the *miR-342-5p* expression declined compared with early lesions (Figure 1C). This increased expression of *miR-342-5p* was specific to lesioned regions of the arteries because its expression did not change significantly throughout the entire length of the aortic wall during high-cholesterol feeding (Figure 1D).

In the aortic walls of *Apoe*$^{-/-}$ mice with a conditional knockout of the miRNA-processing enzyme *Dicer1* in myeloid cells (LysM-Cre/*Dicer*^{flox}), the expression of *miR-342-5p* was reduced in mice after 3 months on an HCD compared with LysM-Cre/*Dicer*^{WT}/*Apoe*$^{-/-}$ mice, indicating that macrophages were likely to be the primary cellular source of *miR-342-5p* in atherosclerotic lesions (Figure 1E). To confirm this, we next performed in situ hybridization combined with Mac-2 immunostaining and found *miR-342-5p* to be expressed in the macrophages of early plaques (Figure 1F). Furthermore, *miR-342-5p* expression was low in BMDM precursor cells but increased during their differentiation into macrophages (Figure 2A). Macrophage stimulation with lipopolysaccharide/interferon-γ (IFN-γ) or interleukin-4, however, did not differentially regulate *miR-342-5p* expression after 6 and 12 hours (Figure 2B and Figure IVA in the online-only Data Supplement), with increases noted after 48 hours. Interestingly, lipopolysaccharide/IFN-γ alone slightly upregulated *miR-342-5p* as soon as 24 hours (Figure IVA in the online-only Data Supplement), and treatment with highly oxidized low-density lipoprotein increased *miR-342-5p* after 48 hours (Figure IVB in the online-only Data Supplement). These findings indicate that *miR-342-5p* expression is associated with mature and activated macrophages during early atherosclerosis.

miR-342-5p Promotes the Proinflammatory Activation of Macrophages

Early atherosclerotic lesions in *Apoe*$^{-/-}$ mice are characterized by the increased expression of proinflammatory markers such as NOS2 and CCL2 and the enrichment of macrophages.[4] Therefore, we hypothesized a role for *miR-342-5p* in macrophage

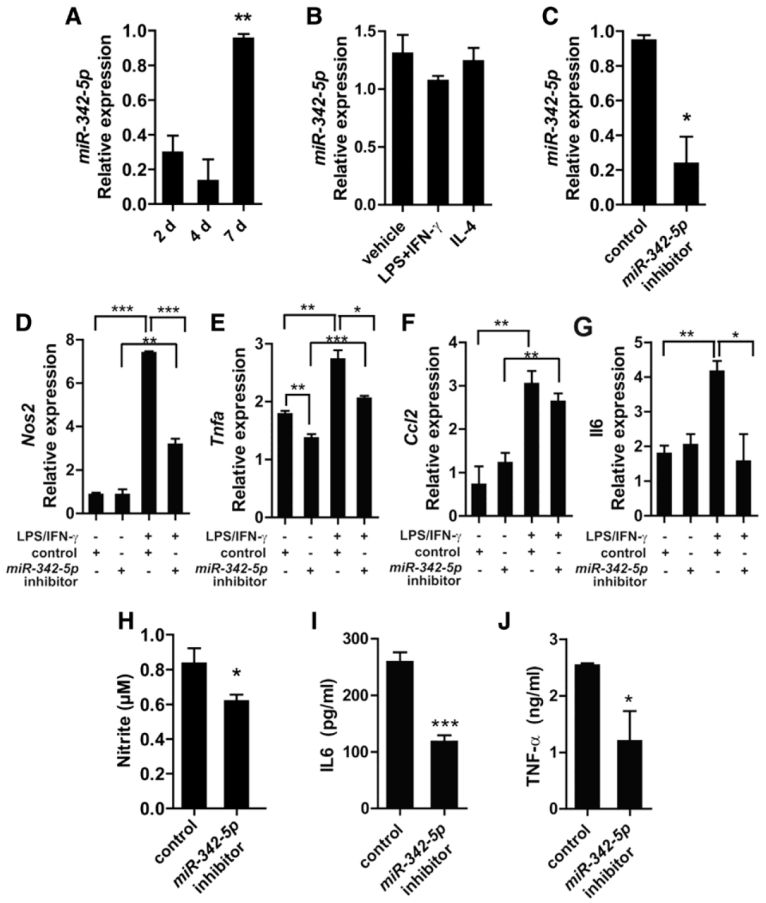

Figure 2. Effects of *miR-342-5p* on the proinflammatory activation of macrophages. **A**, The induction of *miR-342-5p* expression during the in vitro differentiation of murine bone marrow–derived macrophages (BMDMs) at days 2, 4, and 7. $^{**}P<0.01$ vs all other groups; n=3. **B**, Expression of *miR-342-5p* in BMDMs stimulated with lipopolysaccharide (LPS) and interferon-γ (IFN-γ) or interleukin (IL)-4. n=3. **C**, *miR-342-5p* expression after BMDM treatment with the locked nucleic acid (LNA)–*miR-342-5p* inhibitor or nontargeting LNA oligonucleotides. $^{*}P<0.05$; n=3 to 4. **D** through **G**, Effect of the *miR-342-5p* inhibitor on the mRNA expression of *Nos2* (**D**), *Tnfa* (**E**), *Ccl2* (**F**), and *Il6* (**G**) in unstimulated and LPS/IFN-γ–stimulated BMDMs. Nontargeting LNA oligonucleotides were used in the control group. $^{*}P<0.05$, $^{**}P<0.01$, $^{***}P<0.001$; n=3. **H** through **J**, Concentration of nitrite (**H**), tumor necrosis factor-α (TNF-α) protein (**I**), and IL6 protein (**J**) in the culture media of LPS/IFN-γ–stimulated BMDMs treated with the *miR-342-5p* LNA inhibitor or nontargeting LNA oligonucleotides. $^{*}P<0.05$, $^{***}P<0.005$ vs control; n=3 to 4.

activation. The expression of *miR-342-5p* in BMDMs was greatly reduced after transfection with an *miR-342-5p* inhibitor (Figure 2C). After lipopolysaccharide/IFN-γ stimulation, *Nos2* expression and nitrite generation by NOS2 were substantially reduced by the *miR-342-5p* inhibitor (Figure 2D and 2H and Figure VA in the online-only Data Supplement). The *miR-342-5p* inhibitor reduced *Tnfa* and *Il6* expression at both the mRNA and protein levels in lipopolysaccharide/IFN-γ–activated BMDMs, but a similar inhibition was not observed for *Ccl2* (Figure 2E–2G, 2I, and 2J and Figure V in the online-only Data Supplement). Interestingly, *Tnfa* expression was also decreased in unstimulated BMDMs by the *miR-342-5p* inhibitor (Figure 2E). The *miR-342-5p* inhibitor also diminished the degree of lipid accumulation in BMDMs incubated with acetylated low-density lipoprotein (Figure VI in the online-only Data Supplement). These results indicate that *miR-342-5p* promotes the proinflammatory activation of macrophages by enhancing nitric oxide production and the expression of *Tnfa* and *Il6*.

Bmpr2 and *Akt1* Are Direct Targets of *miR-342-5p*

To address the mechanism by which *miR-342-5p* affects macrophage activation, an in silico target prediction analysis was performed. Ten potential targets of *miR-342-5p* related to macrophage function were identified with 3 different target prediction algorithms. The expression of these potential *miR-342-5p* targets was quantified in unstimulated BMDMs transfected with either the *miR-342-5p* mimic or the inhibitor. Of the 10 selected targets, only *Bmpr2* and *Akt1* were significantly increased by the *miR-342-5p* inhibitor and suppressed by the *miR-342-5p* mimic (Figure 3A and 3B). *Foxo3* was significantly upregulated only in macrophages treated with the *miR-342-5p* inhibitor, whereas *Nfkb2* and *Rara* expression was decreased by the *miR-342-5p* mimic (Figure 3A and 3B). To verify the direct repression of the differentially regulated genes by *miR-342-5p*, argonaute2 immunoprecipitations were performed. Only the messages of *Bmpr2, Akt1,* and *Nfkb2* were reduced in the argonaute2 immunoprecipitates from BMDMs treated with the *miR-342-5p* inhibitor (Figure 3C), indicating that *miR-342-5p* directly suppresses these 3 targets in macrophages.

Using luciferase reporter assays, we examined the binding sites for *miR-342-5p* in the 3′-untranslated regions (3′-UTRs) of *Bmpr2*, *Akt1*, and *Nfkb2*. Transfection with the *miR-342-5p* mimic repressed the luciferase activity of the *Bmpr2* and *Akt1* 3′-UTRs (Figure 3D and 3E) but not that of the *Nfkb2* 3′-UTR (Figure VII in the online-only Data Supplement). In contrast, the luciferase activities of these constructs bearing mutations in the *miR-342-5p* target sites in the 3′-UTRs of *Bmpr2* and

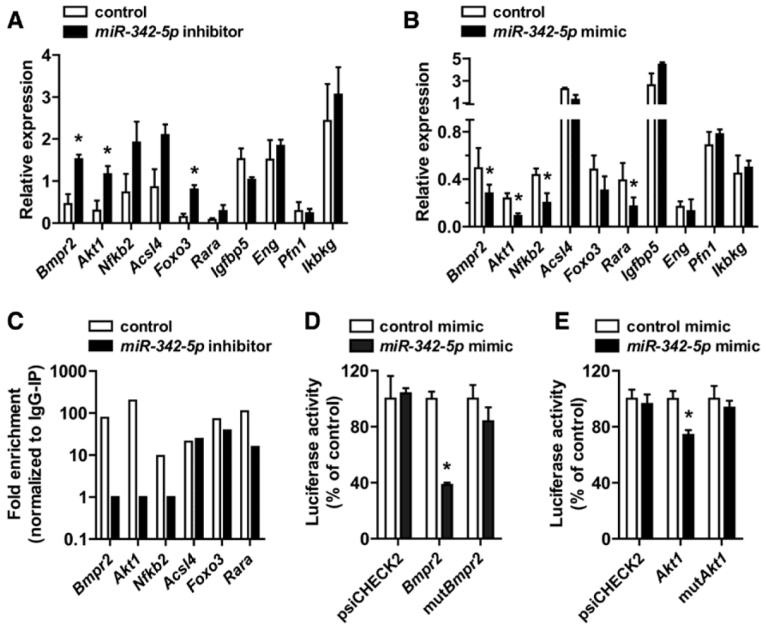

Figure 3. Identification of the mRNA targets of *miR-342-5p* in macrophages. **A** and **B**, Unstimulated bone marrow–derived macrophages (BMDMs) were transfected with the (**A**) *miR-342-5p* inhibitor or (**B**) an *miR-342-5p* mimic, and the mRNA expression of the predicted targets was quantified with quantitative real-time polymerase chain reaction 24 hours after transfection. Nontargeting locked nucleic acid (LNA) oligonucleotides and negative control mimic oligonucleotides were used in the control groups, respectively. **P*<0.05 vs control; n=3 to 4. **C**, Enrichment of the predicted targets of *miR-342-5p* in argonaut2-coimmunoprecipitated RNA in unstimulated BMDMs transfected with the *miR-342-5p* inhibitor or nontargeting LNA oligonucleotides (control). The data are from 1 experiment that is representative of 3 independent experiments. **D** and **E**, Normalized luciferase activity in HEK293 cells transfected with the psiCHECK2 vector containing the 3′-untranslated region (UTR) of (**D**) *Bmpr2* with (mut*Bmpr2*) or without (*Bmpr2*) the mutated binding site of *miR-342-5p* and (**E**) the 3′-UTR of *Akt1* with (mut*Akt1*) or without (*Akt1*) the mutated binding site of *miR-342-5p* 48 hours after treatment with an *miR-342-5p* mimic or a negative control mimic. **P*<0.05 vs control; n=4.

Akt1 were not affected by the *miR-342-5p* mimic (Figure 3D and 3E and Figure VIII in the online-only Data Supplement). Taken together, these results suggest that *miR-342-5p* directly targets *Bmpr2* and *Akt1* in macrophages via a recognition element in their 3′-UTRs. Although targeting of the 3′-UTR of *Nfkb2* by *miR-342-5p* was not observed, binding of *miR-342-5p* to the 5′-UTR or the coding region of the *Nfkb2* mRNA cannot be excluded.

Targeting of *Akt1* by *miR-342-5p* Mediates the Proinflammatory Activation of Macrophages

Next, we assessed the functional roles of *Akt1* and *Bmpr2* in *miR-342-5p*–mediated macrophage activation. In contrast to interleukin-4, lipopolysaccharide/IFN-γ treatment suppressed *Akt1* mRNA, which could be abolished with the *miR-342-5p* inhibitor (Figure 4A and Figure IX in the online-only Data Supplement). Accordingly, inhibition of *miR-342-5p* increased AKT1 protein expression and phosphorylation in lipopolysaccharide/IFN-γ–stimulated BMDMs (Figure 4B and 4C). Although treatment with an *miR-342-5p* inhibitor increased *Bmpr2* mRNA and protein expression in lipopolysaccharide/IFN-γ–stimulated macrophages, *Bmpr2* mRNA levels were still lower than those observed in unstimulated BMDMs (Figure 4A and 4D), suggesting additional mechanisms for *Bmpr2* suppression in inflammatory macrophages. This increase in *Akt1* and *Bmpr2* could be reduced by siRNAs specific to *Akt1* and *Bmpr2*, respectively (Figure X in the online-only Data Supplement). Furthermore, the silencing of *Akt1* but not *Bmpr2* in these macrophages treated with the *miR-342-5p* inhibitor upregulated *Nos2, Tnfa*, and *Il6* (Figure 4E). Overall, these results indicate that *miR-342-5p* primarily regulates the proinflammatory activation of macrophages by targeting *Akt1*.

Although *Akt1* suppression by *miR-342-5p* appeared to be enhanced after lipopolysaccharide/IFN-γ stimulation, the expression level of *miR-342-5p* was unaltered. To determine whether *Akt1* mRNA and *Bmpr2* mRNA compete for binding to *miR-342-5p* in unstimulated macrophages, we studied the effect of silencing *Bmpr2* on the expression of *Akt1*. Notably, *Bmpr2* silencing decreased *Akt1* mRNA expression in unstimulated macrophages (Figure 4F), which could be rescued by inhibiting *miR-342-5p* (Figure 4G). This indicated that an abundance of *Bmpr2* mRNA may regulate *Akt1* in unstimulated macrophages by competing with Akt1 for *miR-342-5p* binding.

Role of *miR-155* in the *Akt1*-Dependent Regulation of Macrophage Activation by *miR-342-5p*

Akt1 negatively regulates *miR-155* expression in macrophages, which, in turn, impairs macrophage response to lipopolysaccharide.[13] Therefore, we investigated the role of *miR-155* in *miR-342-5p*–mediated proinflammatory activation of macrophages. We found that lipopolysaccharide/IFN-γ stimulation increased *miR-155* expression (Figure 5A). This increase

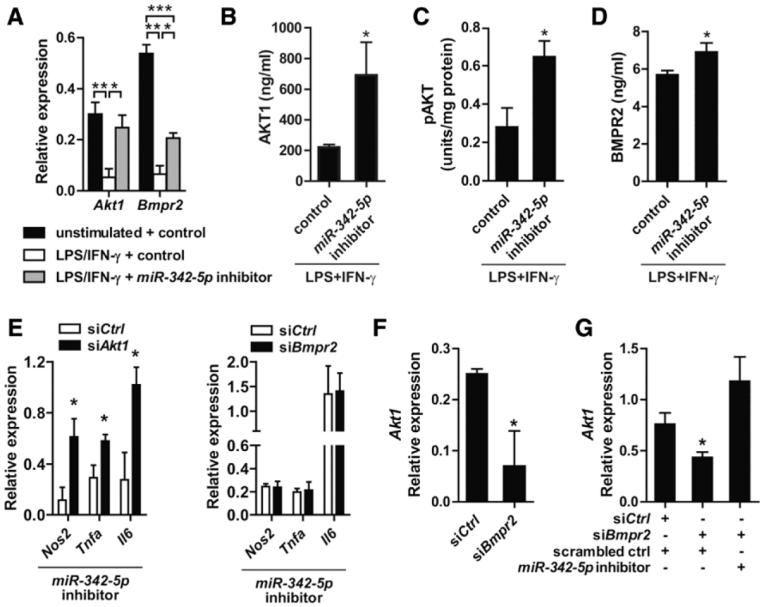

Figure 4. Roles of Akt1 and bone morphogenetic protein receptor, type II (Bmpr2) in *miR-342-5p*–mediated macrophage activation. **A**, *Akt1* and *Bmpr2* expression in bone marrow–derived macrophages (BMDMs) stimulated with or without lipopolysaccharide (LPS)/interferon-γ (IFN-γ) was analyzed after treatment with an *miR-342-5p* inhibitor or nontargeting locked nucleic acid (LNA; control) oligonucleotide. **P*<0.05, ***P*<0.01, ****P*<0.005; n=3 to 4. **B** through **D**, Effects of the *miR-342-5p* inhibitor or nontargeting LNA (control) on AKT1 and BMPR2 protein (**B** and **D**) expression and the phosphorylation of Akt (**C**) in LPS/IFN-γ–stimulated BMDMs. **P*<0.05 vs control; n=3 to 5. **E**, Effects of si*Akt1* or si*Bmpr2* treatment on *Nos2*, *Tnfa,* and *Il6* expression in LPS/IFN-γ–stimulated BMDMs treated with an *miR-342-5p* inhibitor or the nontargeting siRNA (siCtrl). **P*<0.05 vs siCtrl; n=3 to 4. **F**, *Akt1* mRNA expression was determined in BMDMs treated with si*Bmpr2* or si*Ctrl*. **P*<0.05; n=3. **G**, *Akt1* mRNA expression levels in BMDMs treated with si*Bmpr2* or siCtrl with either an *miR-342-5p* inhibitor or a nontargeting LNA control oligonucleotide (scrambled control). **P*<0.05 vs all other groups; n=3.

could be abolished by treatment with an *miR-342-5p* inhibitor (Figure 5B) but then subsequently restored by siRNA-mediated *Akt1* suppression (Figure 5C). These findings indicate that *miR-342-5p* upregulates *miR-155* via the suppression of *Akt1* in classically activated macrophages.

To verify the role of *miR-155* in this *miR-342-5p*–dependent proinflammatory pathway, we examined the effect of lipopolysaccharide/IFN-γ stimulation on BMDMs derived from *miR-155*$^{-/-}$ mice. We found a reduced expression of *Nos2*, *Tnfa*, and *Il6* after lipopolysaccharide/IFN-γ stimulation in *miR-155*$^{-/-}$ compared with *miR-155*$^{+/+}$ macrophages (Figure 5D). Interestingly, treatment of *miR-155*$^{-/-}$ macrophages with an *miR-342-5p* inhibitor increased *Nos2* expression after lipopolysaccharide/IFN-γ stimulation but had no effect on *Tnfa* and *Il6* expression (Figure 5E). This indicates that, in the absence of *miR*-155, miR-*342-5p* regulates *Nos2* via a different pathway. Bone morphogenetic protein 6 stimulation was previously shown to increase *Nos2* expression via Bmpr2 in macrophages.[23] Therefore, we studied whether *miR-342-5p* affects *Nos2* expression in the absence of *miR-155* by targeting *Bmpr2*. Indeed, the siRNA-mediated suppression of *Bmpr2* prevented *Nos2* upregulation in lipopolysaccharide/IFN-γ–stimulated *miR-155*$^{-/-}$ macrophages on treatment with the *miR-342-5p* inhibitor (Figure 5F). This suggests that the effect of *miR-342-5p* on *Nos2* expression in classically activated macrophages is reversed by targeting *Bmpr2* in the absence of the Akt1–*miR-155* pathway.

Inhibition of *miR-342-5p* Suppresses Atherosclerosis

To address the role of *miR-342-5p* in atherogenesis, atherosclerotic lesion formation was induced locally in the carotid artery 42 days after partial carotid ligation in hyperlipidemic *Apoe*$^{-/-}$ mice. In this model, *miR-342-5p* was upregulated in the carotid artery as early as 7 days, remaining high compared with nonligated carotid arteries, until 42 days after ligation (Figure 6A). Perivascular treatment of the carotid arteries with the *miR-342-5p* inhibitor (*miR-342-5p* antagomir) suppressed *miR-342-5p* at 42 days compared with the nontargeting control antagomir (Figure 6B). Furthermore, the mean lesion size in the carotid arteries was significantly decreased after *miR-342-5p* antagomir treatment (Figure 6C), diminishing the lesional content of the macrophages and smooth muscle cells in the *miR-342-5p* antagomir-treated carotid arteries (Figure 6D and 6E and Figure XI in the online-only Data Supplement). Local treatment with the *miR-342-5p* antagomir did not affect serum cholesterol levels (Figure XII in the online-only Data Supplement). The inhibition of *miR-342-5p* increased *Akt1* expression and diminished *miR-155*, *Nos2*, and *Il6* expression in atherosclerotic lesions at 42 days (Figure 7A). In addition, NOS2 expression in lesional macrophages (Figure 7B) and peroxynitrite production (Figure 7C) were reduced after *miR-342-5p* inhibition. These results demonstrate that *miR-342-5p* promotes atherogenesis by increasing the accumulation of macrophages and smooth muscle cells in the lesions. This effect might be due to the *miR-342-5p*–mediated upregulation

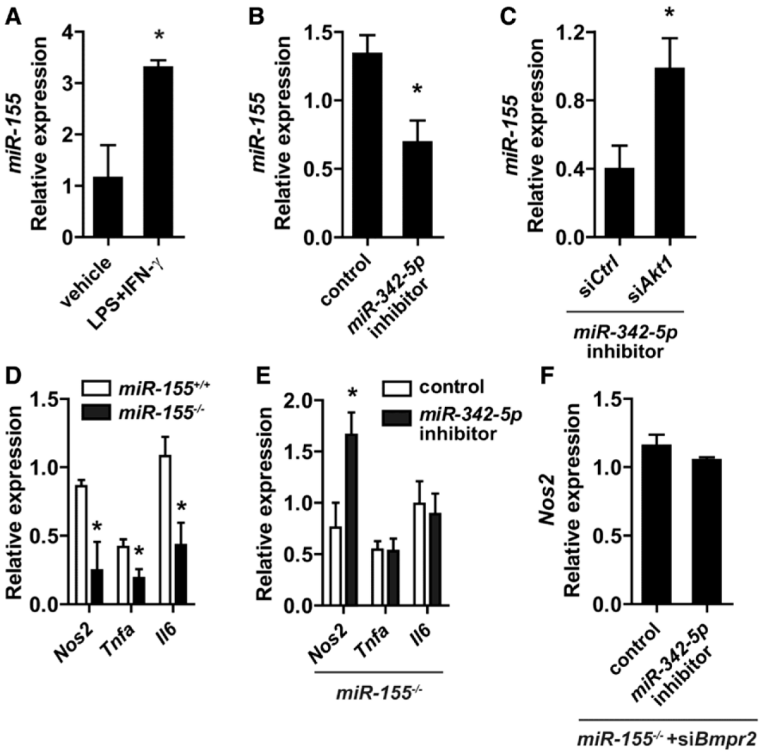

Figure 5. The role of *miR-155* in *miR-342-5p*–mediated macrophage activation. **A**, *miR-155* expression in bone marrow–derived macrophages (BMDMs) in response to lipopolysaccharide (LPS)/interferon-γ (IFN-γ) stimulation. **P*<0.05; n=3 to 4. **B**, Effects of an *miR-342-5p* inhibitor on *miR-155* expression in LPS/IFN-γ–stimulated BMDMs compared with the effects of a nontargeting locked nucleic acid (LNA) oligonucleotide (control). **P*<0.05; n=3 to 4. **C**, Silencing *Akt1* with RNA interference (si*Akt1*) increased the expression of *miR-155* in LPS/IFN-γ–stimulated BMDMs treated with an *miR-342-5p* inhibitor compared with those treated with a nontargeting siRNA (si*Ctrl*). **P*<0.05; n=3 to 4. **D**, Expression of *Nos2*, *Tnfa*, and *Il6* in *miR-155*$^{-/-}$ BMDMs compared with their expression in *miR-155*$^{+/+}$ LPS/IFN-γ–treated BMDMs. **P*<0.05; n=3 to 4. **E**, Effects of treatment with an *miR-342-5p* inhibitor on the expression of *Nos2*, *Tnfa*, and *Il6* in LPS/IFN-γ–stimulated *miR-155*$^{-/-}$ BMDMs compared with the effects of treatment with a nontargeting LNA oligonucleotide. **P*<0.05; n=4. **F**, Expression of *Nos2* after treatment with an *miR-342-5p* inhibitor or a control LNA oligonucleotide in LPS/IFN-γ–stimulated *miR-155*$^{-/-}$ BMDMs in which *Bmpr2* had been silenced by siRNA (si*Bmpr2*). n=3 to 4.

of *miR-155*, which, in turn, leads to an increase in Nos2 activity in atherosclerotic lesions via *Akt1* suppression.

We next administered LNA-342-5p to *Apoe*$^{-/-}$ mice fed an HCD for 2 months to investigate whether systemic treatment with the *miR-342-5p* inhibitor could inhibit the progression of atherosclerosis. One-month treatment with LNA-342-5p reduced lesion formation in both the aorta and the aortic root compared with a nontargeting control (LNA-control) (Figure 8A and 8B). Similar to the effect of local *miR-342-5p* inhibition on carotid lesion formation, systemic treatment with LNA-342-5p diminished the lesional macrophage and smooth muscle cell content (Figure 8C and 8D). Furthermore, silencing *miR-342-5p* enhanced AKT1 expression in lesional macrophages (Figure 8E) but reduced *miR-155*, *Nos2,* and *Il6* expression in the aortas of *Apoe*$^{-/-}$ mice compared with the control (Figure 8F).

Discussion

Atherosclerotic lesion formation is associated with a distinct miRNA expression profile, but the functions of individual miRNAs in atherogenesis are unknown.[24] We found that the miRNA expression profile of murine atherosclerotic lesions is stage specific and that early lesions are characterized by the increased expression of *miR-342-5p* in macrophages. In vitro, *miR-342-5p* targets *Akt1* and thus turns off the repression of *miR-155*; this, in turn, mediates the upregulation of proinflammatory mediators such as *Nos2* and *Tnfa* in activated macrophages. In flow-induced atherosclerosis, the inhibition of *miR-342-5p* reduced lesion formation by impairing the accumulation of macrophages and smooth muscle cells. Furthermore, blocking *miR-342-5p* in atherosclerotic lesions increased *Akt1* expression, suppressed the expression of *miR-155* and *Nos2*, and reduced protein nitrosylation. Systemic treatment with an inhibitor of *miR-342-5p* inhibited the progression of atherosclerosis in mice, demonstrating the therapeutic potential of oligonucleotide-based targeting of *miR-342-5p*.

During the progression of atherosclerosis, distinct, stage-specific lesional morphologies occur that range from early, macrophage-rich lesions to advanced lesions with extracellular lipid deposition and macrophage apoptosis. Whereas the inflammatory response driven by recruited macrophages prevails in early lesions, studies implicate impaired efferocytosis as the cause of defective resolution of inflammation in advanced atherosclerosis.[8] miRNAs play a crucial role in the innate immune response by positively or negatively regulating inflammatory signaling pathways. However, the effects of lesion-specific miRNAs in the macrophage response during atherosclerosis have not been determined. Therefore, in a murine model of experimental atherosclerosis, we compared the miRNA expression profiles in early and advanced lesions with the respective non–lesion-bearing arterial wall from the same mice. Because macrophages exist only in the lesions, we were able to identify miRNAs involved in the development of lesional macrophages by comparing these lesioned tissues with normal arteries.

Our miRNA profiling demonstrated increased expression of 5 miRNAs, including *miR-342-5p* and *miR-155*, in early

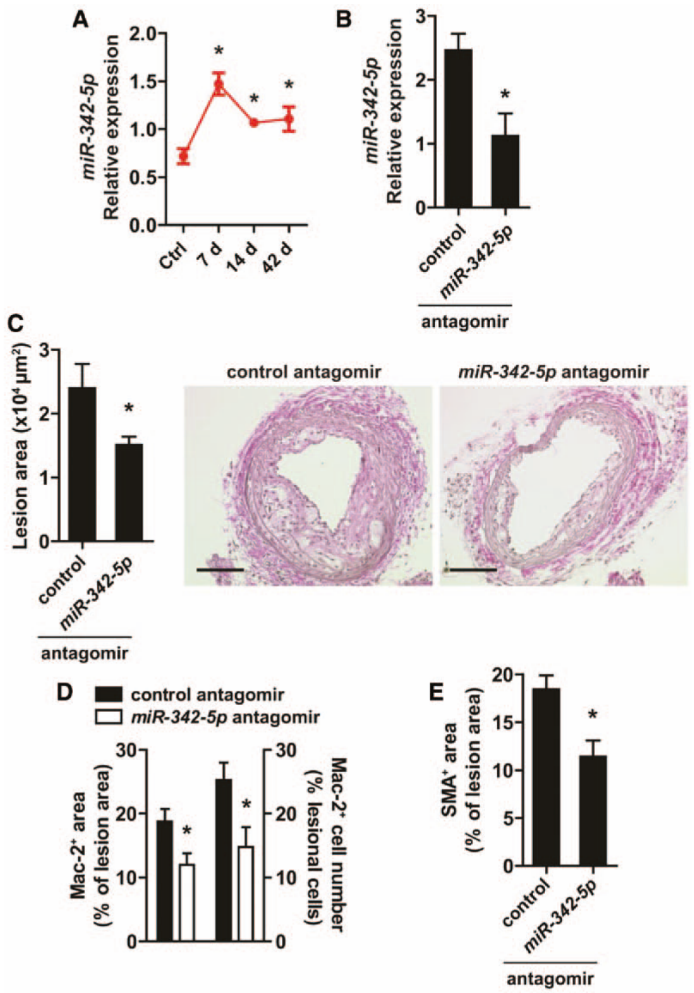

Figure 6. The role of *miR-342-5p* in atherosclerosis induced by acute flow disturbance. **A**, *miR-342-5p* expression during flow-induced lesion formation after the partial ligation of the carotid artery in *Apoe*$^{-/-}$ mice fed a high-cholesterol diet (HCD). Carotid arteries without partial ligation were studied in the control group (Ctrl). *P<0.05 vs control; n=4 to 5 mice from each group. **B**, *miR-342-5p* expression in carotid arteries from *Apoe*$^{-/-}$ mice perivascularly treated with an *miR-342-5p* inhibitor (antagomir) or a nontargeting (control) antagomir 42 days after partial ligation. *P<0.05; n=5 or 6 mice from each group. **C**, Effect of local treatment with the *miR-342-5p* antagomir or control antagomir on atherosclerotic lesion formation in the partially ligated carotid arteries of *Apoe*$^{-/-}$ mice fed an HCD 42 days after partial ligation. Representative sections of carotid arteries stained with Elastic van Gieson stain are shown. *P<0.05; n=5 or 6 mice per group. Scale bars=100 µm. **D**, Lesional macrophages accumulation, as determined by Mac-2 immunostaining, in partially ligated carotid arteries treated with the *miR-342-5p* antagomir or control antagomir. *P<0.05; n=5 or 6 mice per group. **E**, Smooth muscle cell accumulation as determined by smooth muscle actin (SMA) immunostaining in partially ligated carotid arteries treated with the *miR-342-5p* antagomir or control antagomir. *P<0.05; n=5 or 6 mice per group.

lesions. Although the sample size in this initial screening was limited and false discoveries were not controlled, we confirmed that *miR-342-5p* is expressed primarily in lesional macrophages and is a marker for mature macrophages. Moreover, miR-155 is induced by the proinflammatory stimulation of macrophages and upregulated in atherosclerotic lesions.[25] Although *miR-342-5p* might be upregulated during the differentiation of monocytes into macrophages in atherosclerotic lesions, the increased expression of *miR-342-5p* in early lesions compared with advanced lesions is more likely due to the higher macrophage content in early lesions rather than transcriptional upregulation.

Intronic *miR-342* is expressed together with its host gene, *Evl* (Ena-vasodilator stimulated phosphoprotein), and the sister strand of *miR-342-5p*, *miR-342-3p,* is highly upregulated by the transcription factor PU.1 during macrophage differentiation.[26,27] However, the functional role of *miR-342-5p* was unclear. We have shown that increased *miR-342-5p* expression sensitizes macrophages to proinflammatory stimulation by regulating Nos2. Lesional macrophages express high levels of Nos2 in human and murine atherosclerosis, and a genetic deficiency in *Nos2* in macrophages reduces atherogenesis in *Apoe*$^{-/-}$ mice.[28,29] Consistent with these results, we demonstrated that *miR-342-5p* inhibition in the vessel wall reduces atherosclerosis and inhibits the expression of Nos2 in lesional macrophages. The proatherogenic effect of Nos2 has been linked to the generation of peroxynitrite by the reaction of nitric oxide with superoxide in the vessel wall.[28,30,31] Peroxynitrite is a strong oxidant species that induces highly atherogenic lipoprotein modifications and the dysregulation of various signaling pathways by protein nitration.[32–34] Our findings suggest that *miR-342-5p* inhibition during atherosclerosis reduces Nos2-mediated peroxynitrite formation, which may be functionally linked to *miR-342-5p*–mediated lesion progression.

Several reports have demonstrated that Nos2 and other proinflammatory mediators are negatively regulated by the activated PI3-kinase/AKT1 pathway.[35–37] Accordingly, the serine/threonine kinase *Akt1* (also called protein kinase B) is essential for endotoxin tolerance and inhibits the expression of Nos2, CCL2, and tumor necrosis factor-α in lipopolysaccharide-stimulated macrophages.[13,37] Moreover, *Akt1* expression in macrophages prevents their polarization to a proinflammatory

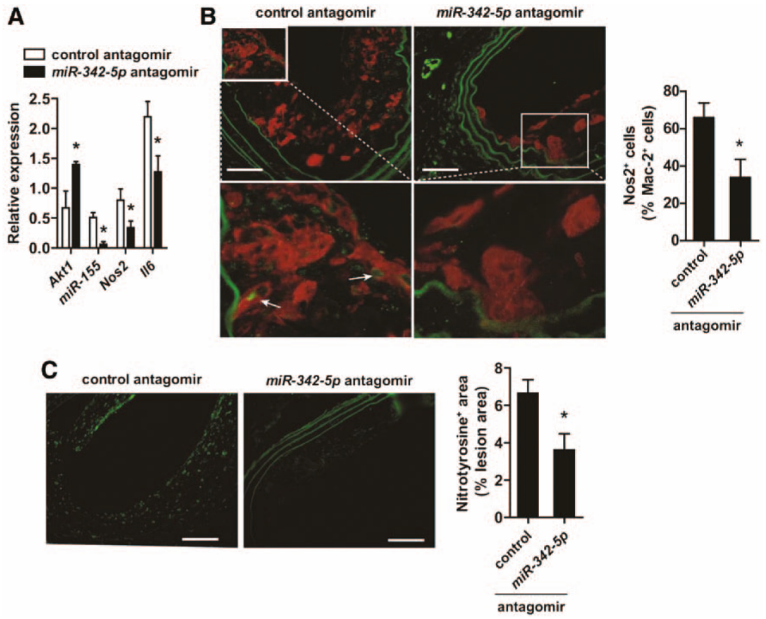

Figure 7. Effects of *miR-342-5p* inhibition on the expression of proinflammatory mediators in atherosclerotic lesions induced by acute flow disturbance. **A**, *Akt1*, *miR-155*, *Nos2,* and *Il6* expression was measured in carotid arteries treated with the *miR-342-5p* antagomir or the control antagomir 42 days after partial carotid ligation in *Apoe*$^{-/-}$ mice fed a high-cholesterol diet. For all figures, **P*<0.05; n=5 or 6 mice per group. **B**, Nos2 expression in lesional macrophages from partially ligated carotid arteries treated with the *miR-342-5p* antagomir or the control antagomir. Representative immunostaining shows combined immunostaining for NOS2 (green) and Mac-2 (red). Arrows indicate Nos2-expressing macrophages. Scale bars=50 μm. **C**, The nitrotyrosinylation in lesions of partially ligated carotid arteries treated with the *miR-342-5p* antagomir or the control antagomir. Representative immunostaining shows nitrotyrosine staining. Scale bars=50 μm.

M1 phenotype.[38] AKT1 also activates nuclear factor-κB, a key factor in the transcriptional regulation of Nos2, which appears, however, to be cell type specific and dependent on the availability of I kappa-B kinase alpha (IKKα).[39] Our results indicate that *miR-342-5p* suppresses *Akt1* in classically activated macrophages and thereby upregulates *Nos2,* supporting the concept of an anti-inflammatory role for Akt1 in macrophages. In addition to the regulation of AKT1 by PI3K-dependent phosphorylation, our data suggest that the posttranscriptional regulation of *Akt1* by miRNAs is crucial for the proinflammatory activation of macrophages. Compared with no stimulation, lipopolysaccharide/IFN-γ treatment enhanced the suppressive activity of *miR-342-5p* on *Akt1*. This "activation" of *miR-342-5p* appears to be due to the transcriptional downregulation of the alternative *miR-342-5p* target, *Bmpr2*, after stimulation, which might alleviate the competition between *Akt1* and *Bmpr2* for binding to *miR-342-5p* and thus promote the suppression of *Akt1* by *miR-342-5p*.[40]

The increase in *Akt1* expression during atherosclerotic lesion formation resulting from the inhibition of *miR-342-5p* indicates that *Akt1* plays a protective role in atherosclerosis by impairing Nos2-dependent peroxynitrite generation. These findings are in agreement with previous reports showing increased lesion development in *Akt1*$^{-/-}$ mice resulting from increased macrophage infiltration and enhanced expression of proinflammatory genes such as *Tnf*α.[41]

The effects of *Akt1* on lipopolysaccharide responsiveness are partly mediated by the suppression of *miR-155*, which targets SOCS1, an inhibitor of Toll-like receptor 4 signaling.[13] In macrophages, miR-155 expression is upregulated after the activation of various Toll-like receptors via either MyD88- or TRIF-dependent signaling pathways, which enhances the lipopolysaccharide-induced expression of Nos2.[11,42] Moreover, miR-155 can reduce macrophage apoptosis in infectious diseases, but only in stimulated macrophages.[25,43] Although *miR-155* is reduced in the circulation of patients with coronary heart disease, microarray analyses have demonstrated an increase in the expression of *miR-155* in human atherosclerotic lesions.[24,44] In line with a proatherogenic role of *miR-155*, the presence of advanced atherosclerotic lesions was reduced in *Apoe*$^{-/-}$ mice harboring *miR-155*-deficient macrophages by removing the repression to the anti-inflammatory transcription factor Bcl6.[25] Interestingly, our findings indicate that *miR-342-5p* positively regulates *miR-155* expression in atherosclerotic lesions via *Akt1* suppression. Moreover, this *Akt1–miR-155* pathway may mediate the effects of *miR-342-5p* on lesion formation and nitro-oxidative stress because the *miR-342-5p*–mediated upregulation of *Nos2* depends on the expression of *miR-155*. Notably, the role of *miR-342-5p* in *Nos2* regulation in macrophages that are genetically deficient in *miR-155* was completely reversed by the targeting of *Bmpr2*. Therefore, *miR-342-5p* and *miR-155* may form a functional miRNA pair that promotes lesion inflammation and nitro-oxidative stress in atherosclerosis.

Conclusions

We found that the most significantly upregulated miRNA in murine atherosclerotic lesions, *miR-342-5p*, promotes atherosclerosis and increases nitro-oxidative stress during lesion formation. This effect may be due to the upregulation of *Nos2* in proinflammatory macrophages by removing the repression of *miR-155* by the targeting of *Akt1*. Thus, targeting *miR-342-5p* in atherogenesis may be a promising therapeutic strategy because it prevents the initiation of a cascade of molecular events that sensitize macrophages to inflammatory stimulation.

Acknowledgments

We thank Stephanie Wilbertz, Melanie Garbe, Yuan Kong, and Roya Soltan for their excellent technical assistance.

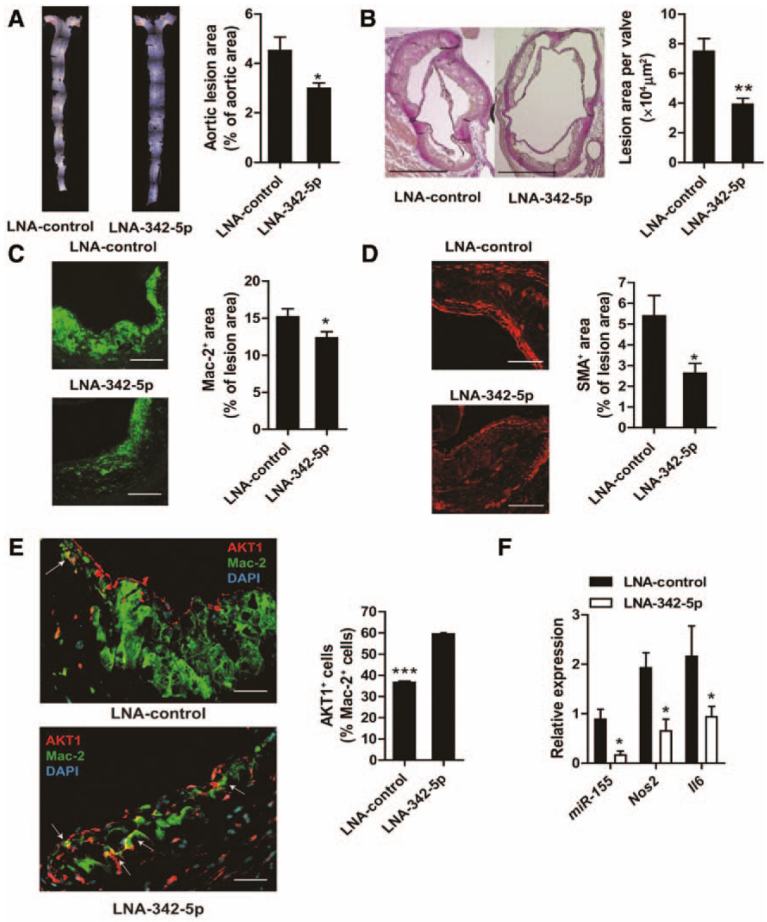

Figure 8. The effects of systemic administration of *miR-342-5p* inhibitors on diet-induced atherosclerosis. **A**, *Apoe*$^{-/-}$ mice fed a high-cholesterol diet (HCD) for 2 months were treated with locked nucleic acid (LNA)-342-5p or LNA-control for 4 weeks. Lesion formation was determined in Oil red O–stained, en face prepared aortas. For all figures, **P*<0.05; ***P*<0.01, and ****P*<0.005. n=6 mice per group unless otherwise indicated. **B**, Representative sections of aortic roots stained with Elastic van Gieson stain from mice treated with LNA-342-5p or LNA-control. The lesion area was quantified by planimetry. Scale bars=500 µm. **C**, Accumulation of lesional macrophages, as determined by Mac-2 immunostaining, in aortic roots in LNA-342-5p–treated and LNA-control–treated *Apoe*$^{-/-}$ mice. Scale bars=100 µm. **D**, Accumulation of smooth muscle cells in aortic root lesions after treatment with LNA-342-5p or LNA control as determined by smooth muscle actin (SMA) immunostaining. Scale bars=100 µm. **E**, Representative immunostaining for Akt1 in lesional macrophages in *Apoe*$^{-/-}$ mice treated with LNA-342-5p or LNA control, Akt1 (red), and Mac-2 (green). Scale bars=25 µm. **F**, *miR-155*, *Nos2,* and *Il6* expression was quantified in the aortas of *Apoe*$^{-/-}$ mice treated with LNA-342-5p or LNA control after 3 months of an HCD. n=3 or 4 mice per group.

Sources of Funding

This work was supported by the Deutsche Forschungsgemeinschaft (Scho1056/3-1 and FOR809) , by the DZHK (German Centre for Cardiovascular Research), by the BMBF (German Ministry of Education and Research), and by the Interdisciplinary Center for Clinical Research in the Faculty of Medicine at the RWTH Aachen University.

Disclosures

None.

References

1. Moore KJ, Tabas I. Macrophages in the pathogenesis of atherosclerosis. *Cell*. 2011;145:341–355.
2. Weber C, Noels H. Atherosclerosis: current pathogenesis and therapeutic options. *Nat Med*. 2011;17:1410–1422.
3. Miller YI, Viriyakosol S, Worrall DS, Boullier A, Butler S, Witztum JL. Toll-like receptor 4-dependent and -independent cytokine secretion induced by minimally oxidized low-density lipoprotein in macrophages. *Arterioscler Thromb Vasc Biol*. 2005;25:1213–1219.
4. Veillard NR, Steffens S, Burger F, Pelli G, Mach F. Differential expression patterns of proinflammatory and antiinflammatory mediators during atherogenesis in mice. *Arterioscler Thromb Vasc Biol*. 2004;24:2339–2344.
5. Aiello RJ, Bourassa PA, Lindsey S, Weng W, Natoli E, Rollins BJ, Milos PM. Monocyte chemoattractant protein-1 accelerates atherosclerosis in apolipoprotein E-deficient mice. *Arterioscler Thromb Vasc Biol*. 1999;19:1518–1525.
6. Carr AC, McCall MR, Frei B. Oxidation of LDL by myeloperoxidase and reactive nitrogen species: reaction pathways and antioxidant protection. *Arterioscler Thromb Vasc Biol*. 2000;20:1716–1723.
7. McGillicuddy FC, de la Llera Moya M, Hinkle CC, Joshi MR, Chiquoine EH, Billheimer JT, Rothblat GH, Reilly MP. Inflammation impairs reverse cholesterol transport in vivo. *Circulation*. 2009;119:1135–1145.
8. Tabas I. Macrophage death and defective inflammation resolution in atherosclerosis. *Nat Rev Immunol*. 2010;10:36–46.
9. O'Connell RM, Rao DS, Chaudhuri AA, Baltimore D. Physiological and pathological roles for microRNAs in the immune system. *Nat Rev Immunol*. 2010;10:111–122.
10. O'Neill LA, Sheedy FJ, McCoy CE. MicroRNAs: the fine-tuners of Toll-like receptor signalling. *Nat Rev Immunol*. 2011;11:163–175.
11. O'Connell RM, Taganov KD, Boldin MP, Cheng G, Baltimore D. MicroRNA-155 is induced during the macrophage inflammatory response. *Proc Natl Acad Sci USA*. 2007;104:1604–1609.
12. Liu G, Friggeri A, Yang Y, Park YJ, Tsuruta Y, Abraham E. miR-147, a microRNA that is induced upon Toll-like receptor stimulation, regulates murine macrophage inflammatory responses. *Proc Natl Acad Sci USA*. 2009;106:15819–15824.
13. Androulidaki A, Iliopoulos D, Arranz A, Doxaki C, Schworer S, Zacharioudaki V, Margioris AN, Tsichlis PN, Tsatsanis C. The kinase Akt1 controls macrophage response to lipopolysaccharide by regulating microRNAs. *Immunity*. 2009;31:220–231.
14. Taganov KD, Boldin MP, Chang KJ, Baltimore D. NF-kappaB-dependent induction of microRNA miR-146, an inhibitor targeted to signaling proteins of innate immune responses. *Proc Natl Acad Sci USA*. 2006;103:12481–12486.
15. Li T, Morgan MJ, Choksi S, Zhang Y, Kim Y-S, Liu Z-g. MicroRNAs modulate the noncanonical transcription factor NF-κb pathway by regulating expression of the kinase IKKα during macrophage differentiation. *Nat Immunol*. 2010;11:799–805.
16. Nazari-Jahantigh M, Wei Y, Schober A. The role of microRNAs in arterial remodelling. *Thromb Haemost*. 2012;107:611–618.
17. Rayner KJ, Sheedy FJ, Esau CC, Hussain FN, Temel RE, Parathath S, van Gils JM, Rayner AJ, Chang AN, Suarez Y, Fernandez-Hernando C,

Fisher EA, Moore KJ. Antagonism of miR-33 in mice promotes reverse cholesterol transport and regression of atherosclerosis. *J Clin Invest*. 2011;121:2921–2931.
18. Nam D, Ni CW, Rezvan A, Suo J, Budzyn K, Llanos A, Harrison D, Giddens D, Jo H. Partial carotid ligation is a model of acutely induced disturbed flow, leading to rapid endothelial dysfunction and atherosclerosis. *Am J Physiol Heart Circ Physiol*. 2009;297:H1535–H1543.
19. Krützfeldt J, Rajewsky N, Braich R, Rajeev KG, Tuschl T, Manoharan M, Stoffel M. Silencing of microRNAs in vivo with "antagomirs." *Nature*. 2005;438:685–689.
20. Subramanian P, Karshovska E, Reinhard P, Megens RT, Zhou Z, Akhtar S, Schumann U, Li X, van Zandvoort M, Ludin C, Weber C, Schober A. Lysophosphatidic acid receptors LPA1 and LPA3 promote CXCL12-mediated smooth muscle progenitor cell recruitment in neointima formation. *Circ Res*. 2010;107:96–105.
21. Boon RA, Seeger T, Heydt S, Fischer A, Hergenreider E, Horrevoets AJ, Vinciguerra M, Rosenthal N, Sciacca S, Pilato M, van Heijningen P, Essers J, Brandes RP, Zeiher AM, Dimmeler S. MicroRNA-29 in aortic dilation: implications for aneurysm formation. *Circ Res*. 2011;109:1115–1119.
22. Rothman KJ. No adjustments are needed for multiple comparisons. *Epidemiology*. 1990;1:43–46.
23. Hong JH, Lee GT, Lee JH, Kwon SJ, Park SH, Kim SJ, Kim IY. Effect of bone morphogenetic protein-6 on macrophages. *Immunology*. 2009;128(suppl):e442–e450.
24. Raitoharju E, Lyytikäinen LP, Levula M, Oksala N, Mennander A, Tarkka M, Klopp N, Illig T, Kähönen M, Karhunen PJ, Laaksonen R, Lehtimäki T. miR-21, miR-210, miR-34a, and miR-146a/b are up-regulated in human atherosclerotic plaques in the Tampere Vascular Study. *Atherosclerosis*. 2011;219:211–217.
25. Nazari-Jahantigh M, Wei Y, Noels H, Akhtar S, Zhou Z, Koenen RR, Heyll K, Gremse F, Kiessling F, Grommes J, Weber C, Schober A. MicroRNA-155 promotes atherosclerosis by repressing Bcl6 in macrophages. *J Clin Invest*. 2012;122:4190–4202.
26. Ghani S, Riemke P, Schönheit J, Lenze D, Stumm J, Hoogenkamp M, Lagendijk A, Heinz S, Bonifer C, Bakkers J, Abdelilah-Seyfried S, Hummel M, Rosenbauer F. Macrophage development from HSCs requires PU.1-coordinated microRNA expression. *Blood*. 2011;118:2275–2284.
27. Grady WM, Parkin RK, Mitchell PS, Lee JH, Kim YH, Tsuchiya KD, Washington MK, Paraskeva C, Willson JK, Kaz AM, Kroh EM, Allen A, Fritz BR, Markowitz SD, Tewari M. Epigenetic silencing of the intronic microRNA hsa-miR-342 and its host gene EVL in colorectal cancer. *Oncogene*. 2008;27:3880–3888.
28. Ponnuswamy P, Ostermeier E, Schröttle A, Chen J, Huang PL, Ertl G, Nieswandt B, Kuhlencordt PJ. Oxidative stress and compartment of gene expression determine proatherosclerotic effects of inducible nitric oxide synthase. *Am J Pathol*. 2009;174:2400–2410.
29. Wilcox JN, Subramanian RR, Sundell CL, Tracey WR, Pollock JS, Harrison DG, Marsden PA. Expression of multiple isoforms of nitric oxide synthase in normal and atherosclerotic vessels. *Arterioscler Thromb Vasc Biol*. 1997;17:2479–2488.
30. Buttery LD, Springall DR, Chester AH, Evans TJ, Standfield EN, Parums DV, Yacoub MH, Polak JM. Inducible nitric oxide synthase is present within human atherosclerotic lesions and promotes the formation and activity of peroxynitrite. *Lab Invest*. 1996;75:77–85.
31. Pacher P, Beckman JS, Liaudet L. Nitric oxide and peroxynitrite in health and disease. *Physiol Rev*. 2007;87:315–424.
32. Szabó C, Ischiropoulos H, Radi R. Peroxynitrite: biochemistry, pathophysiology and development of therapeutics. *Nat Rev Drug Discov*. 2007;6:662–680.
33. Graham A, Hogg N, Kalyanaraman B, O'Leary V, Darley-Usmar V, Moncada S. Peroxynitrite modification of low-density lipoprotein leads to recognition by the macrophage scavenger receptor. *FEBS Lett*. 1993;330:181–185.
34. White CR, Brock TA, Chang LY, Crapo J, Briscoe P, Ku D, Bradley WA, Gianturco SH, Gore J, Freeman BA. Superoxide and peroxynitrite in atherosclerosis. *Proc Natl Acad Sci USA*. 1994;91:1044–1048.
35. Díaz-Guerra MJ, Castrillo A, Martín-Sanz P, Boscá L. Negative regulation by phosphatidylinositol 3-kinase of inducible nitric oxide synthase expression in macrophages. *J Immunol*. 1999;162:6184–6190.
36. Fukao T, Koyasu S. PI3K and negative regulation of TLR signaling. *Trends Immunol*. 2003;24:358–363.
37. Guha M, Mackman N. The phosphatidylinositol 3-kinase-Akt pathway limits lipopolysaccharide activation of signaling pathways and expression of inflammatory mediators in human monocytic cells. *J Biol Chem*. 2002;277:32124–32132.
38. Arranz A, Doxaki C, Vergadi E, Martinez de la Torre Y, Vaporidi K, Lagoudaki ED, Ieronymaki E, Androulidaki A, Venihaki M, Margioris AN, Stathopoulos EN, Tsichlis PN, Tsatsanis C. Akt1 and Akt2 protein kinases differentially contribute to macrophage polarization. *Proc Natl Acad Sci USA*. 2012;109:9517–9522.
39. Gustin JA, Ozes ON, Akca H, Pincheira R, Mayo LD, Li Q, Guzman JR, Korgaonkar CK, Donner DB. Cell type-specific expression of the IkappaB kinases determines the significance of phosphatidylinositol 3-kinase/Akt signaling to NF-kappa B activation. *J Biol Chem*. 2004;279:1615–1620.
40. Salmena L, Poliseno L, Tay Y, Kats L, Pandolfi PP. A ceRNA hypothesis: the Rosetta Stone of a hidden RNA language? *Cell*. 2011;146:353–358.
41. Fernández-Hernando C, Ackah E, Yu J, Suárez Y, Murata T, Iwakiri Y, Prendergast J, Miao RQ, Birnbaum MJ, Sessa WC. Loss of Akt1 leads to severe atherosclerosis and occlusive coronary artery disease. *Cell Metab*. 2007;6:446–457.
42. Wang X, Zhao Q, Matta R, Meng X, Liu X, Liu CG, Nelin LD, Liu Y. Inducible nitric-oxide synthase expression is regulated by mitogen-activated protein kinase phosphatase-1. *J Biol Chem*. 2009;284:27123–27134.
43. Koch M, Mollenkopf HJ, Klemm U, Meyer TF. Induction of microRNA-155 is TLR- and type IV secretion system-dependent in macrophages and inhibits DNA-damage induced apoptosis. *Proc Natl Acad Sci USA*. 2012;109:E1153–E1162.
44. Fichtlscherer S, De Rosa S, Fox H, Schwietz T, Fischer A, Liebetrau C, Weber M, Hamm CW, Röxe T, Müller-Ardogan M, Bonauer A, Zeiher AM, Dimmeler S. Circulating microRNAs in patients with coronary artery disease. *Circ Res*. 2010;107:677–684.

CLINICAL PERSPECTIVE

Atherosclerosis is a chronic inflammatory vascular disease and the leading cause of death worldwide. Deciphering the mechanisms of atherosclerosis is essential for developing novel and effective therapeutic strategies. microRNAs (miRNAs) are small RNA molecules that can fine-tune inflammatory responses through negative regulation of mRNA expression and may thereby control the pathogenesis of vascular diseases. Hence, studying the functional roles of miRNAs during atherogenesis may provide clues for the development of miRNA-based therapeutic strategies. Here, we demonstrated that miR-342-5p facilitates the inflammatory activation of macrophages by targeting Akt1 and promotes atherosclerotic lesions progression in mice. The suppression of Akt1 by miR-342-5p upregulates miR-155, which leads to increased lesional nitro-oxidative stress. Inhibition of miR-342-5p by local administration of antagomirs or systematic administration of locked nucleic acid antisense oligonucleotides greatly reduced the progression of atherosclerosis in *Apoe*$^{-/-}$ mice. Thus, our data indicate that the progression of atherosclerosis can be suppressed by inhibiting miRNAs, which promote the inflammatory response in lesional macrophages. This treatment strategy may also be applied locally to the atherosclerotic vessel wall (eg, via drug-eluting stents) with presumably fewer side effects compared with systemic administration. Moreover, as a result of fine-tuning of the interactions of miRNAs in inflammatory macrophage activation, a more subtle manipulation of the chronic, nonresolving inflammation in atherosclerosis may be possible by inhibiting miRNAs without interfering with essential macrophage functions.

Circulation
JOURNAL OF THE AMERICAN HEART ASSOCIATION

American Heart Association®

The *microRNA-342-5p* Fosters Inflammatory Macrophage Activation Through an Akt1- and *microRNA-155*–Dependent Pathway During Atherosclerosis

Yuanyuan Wei, Maliheh Nazari-Jahantigh, Lily Chan, Mengyu Zhu, Kathrin Heyll, Judit Corbalán-Campos, Petra Hartmann, Anna Thiemann, Christian Weber and Andreas Schober

Circulation. 2013;127:1609-1619; originally published online March 19, 2013;
doi: 10.1161/CIRCULATIONAHA.112.000736
Circulation is published by the American Heart Association, 7272 Greenville Avenue, Dallas, TX 75231

Print ISSN: 0009-7322. Online ISSN: 1524-4539

SUPPLEMENTAL MATERIAL

Supplemental Methods

Animal models

Apoe$^{-/-}$ mice (6-8 weeks, Jackson Laboratory) were fed an HCD (21% crude fat, 0.15% cholesterol and 19.5% casein, Altromin, Germany) for 3 or 10 months. *Lysz-Cre* mice were mated with *Dicer*$^{flox/flox}$/*Apoe*$^{-/-}$ mice (all from Jackson Laboratory) to generate *Apoe*$^{-/-}$ mice with a conditional deletion of *Dicer* in myeloid cells. *Lysz-Cre/Apoe*$^{-/-}$ mice harboring the wildtype *Dicer* alleles were utilized as controls. Partial ligation of the carotid artery was performed as previously described[1]. In brief, the left carotid arteries of *Apoe*$^{-/-}$ mice anesthetized with xylazine (10 mg/kg) and ketamine (80 mg/kg) were exposed, and the external carotid, internal carotid, and occipital arteries were ligated. This ligation results in an acute reduction of the blood flow in the common carotid artery via the thyroid artery. Following this partial carotid ligation, the mice were fed an HCD for 42 days. *In situ* perfusion fixation was performed with paraformaldehyde. The animal experiments were approved by the local authorities (LANUV NRW) in accordance with German animal protection laws.

Histology and immunostaining

Serial sections (5 µm thick) of aortic roots (3-5 sections per mouse) or carotid arteries were stained with Movat's pentachrome or Elastic van Gieson stain. Images were obtained with a bright-field microscope (Leica DMLB) connected to a CCD camera (JVC). The lesion and the lipid core area, which was defined as the lipid-rich, acellular region within the lesion, were quantified using planimetry (Diskus software, Hilgers, Bonn). The quantitative immunostaining of α-SMA (clone1A4, Dako), Mac-2 (clone

M3/38, Cederlane), and nitrotyrosine (clone 39B6, Abcam), as well as the combined immunofluorescence staining of NOS2 (rabbit polyclonal, Abcam) and Mac-2, Akt1 (clone C73H10, Cell Signaling) and Mac-2 were performed. Non-specific primary antibodies were used as negative controls. The primary antibodies were detected with a fluorescently labeled secondary antibody (DyLight, KPL). Digital images were acquired with a fluorescence microscope (Leica, DMLB) that was connected to a CCD camera and Diskus software. The size of the positively stained area per lesion area (2-3 sections per mouse) was determined with image analysis software (ImageJ), and the threshold was set according to the background of the negative control staining.

Laser capture microdissection (LCM)

Serial sections (20 µm thick) of aortic roots were mounted on membrane-mounted metal frame slides (MMI), deparaffinized under RNase-free conditions, and completely dried. LCM was performed using a laser microdissection system (mmi CellCut Plus laser system, Molecular Machines and Industries, Switzerland) assembled onto an inverted microscope (Olympus IX71). Lesion tissue samples or samples of the non-atherosclerotic arterial walls (at least 40 sections per mouse) were collected. RNA was isolated with a RecoverAll total nucleic acid isolation kit (Applied Biosystems).

MiRNA real-time PCR array

Total RNA was reverse-transcribed and pre-amplified (Megaplex RT & Preamp

Primers, Rodent Pool Set, Applied Biosystems) according to the manufacturer's instructions. The samples were loaded onto preconfigured 384-well microfluidic cards (TaqMan Array MicroRNA Cards) for the real-time analysis (7900HT RT-PCR System, Applied Biosystems) of 518 mouse miRNAs (Sanger miRBase v10). The data were analyzed with StatMiner software (Integromics) according to the ΔΔCt method, with multiple internal control genes. The most stable combination of the internal controls was determined using the GeNorm algorithm. A cycle threshold value below 40 was defined as the detection limit of the assay. The time course analysis was performed with qbase software (Biogazelle). The array data have been deposited in the National Center for Biotechnology Information Gene Expression Omnibus (GEO; http://www.ncbi.nlm.nih.gov/geo/) and are accessible with GEO series accession numbers GSE34644, GSE34645, GSE34646, and GSE34647.

Quantitative real-time PCR

Total RNA was reverse-transcribed with a TaqMan microRNA RT kit or a high-capacity cDNA reverse transcription kit. The miRNA qRT-PCR assay was performed with TaqMan microRNA assays and the TaqMan universal PCR master mix on a 7900HT RT-PCR system (all from Applied Biosystems). The mRNA qRT-PCR assay was performed with gene-specific primers and a SYBR Green master mix (Fermentas). The data were normalized to a single or multiple reference genes (snoRNA-135, snoRNA-429, and U6 for miRNA and *gapdh* and *actb* for mRNA), scaled to the sample with the lowest expression (qbase software, Biogazelle), and logarithmically transformed (Log_2 or Log_{10}).

In situ hybridization

Sections (7 µm in thickness) from PAXgene (Qiagen)-fixed and paraffin-embedded aortic roots were hybridized with double digoxigenin (DIG)-labeled probes (50 nM *miR-342-5p* or 20 nM scrambled probes in hybridization buffer, Exiqon) at 56℃ for 1 hr in a thermoblock (Eppendorf). After stringent washes with SSC buffer and the blocking of nonspecific (TNB, Perkin Elmer) and biotin/avidin (Blocking Kit, Vector Lab) binding sites, the sections were incubated with a peroxidase-conjugated anti-DIG antibody (Fab fragments from sheep, Roche; 1:100 for 1 h at 37℃). A tyramide-based amplification system (TSA Plus Biotin, Perkin Elmer) and DyLight 549-conjugated streptavidin (KPL) were used to visualize the probes.

Cell culture

Bone marrow-derived cells from the femurs of C57BL/6, *miR-155*$^{-/-}$ or *miR-155*$^{+/+}$ mice were harvested and cultured in DMEM/F12 supplemented with 10% FBS and 10% L929-conditioned medium. After 7 days of culture, flow cytometry revealed that more than 96% of the cells expressed F4/80 and CD11b, confirming their macrophage phenotype. The macrophages were stimulated with either IL-4 (5 ng/ml, 6 h) or LPS (100 ng/ml, 14 h) and IFN-γ (10 ng/ml, 6 h). Oxidized LDL (oxLDL) was generated as previously described[2]. BMDMs were treated with native LDL, mildly oxidized LDL (moxLDL), or oxLDL (50 µg/ml) for 48 h.

To determine the effect of miR-342-5p on lipid accumulation, untreated BMDMs or BMDMs treated with acetylated LDL (acLDL; 50 µg/ml; Life Technologies) for 24 h, fixed with paraformaldehyde, and then stained with Oil red O stain. The Oil red

O-stained area was quantified in 5 visual fields (ImageJ) and normalized to the cell number. Transfection of the BMDMs was performed with a *miR-342-5p* LNA inhibitor or non-targeting LNA oligonucleotide (50 nM, Exiqon) for 24 h before the incubation with acLDL.

The total levels of nitrite in the culture media of the BMDMs were measured with the Griess reagent (G-7921, Invitrogen) according to the manufacturer's instructions. In brief, the Griess reagent and the culture medium were mixed with deionized water and incubated at room temperature for 30 min. The absorbance at 548 nm was measured with a microplate reader (Tecan). The absorbance was converted to the nitrite concentration using a standard curve.

Transfection of macrophages

Lipofectamine 2000 (Invitrogen) was used to transfect unstimulated bone marrow-derived macrophages (BMDMs) with a *miR-342-5p* mimic (30 nM, Pre-miR miRNA Precursor, Ambion), an *miR-342-5p* LNA inhibitor (50 nM, Exiqon), or scrambled controls. The BMDMs were subsequently stimulated with either LPS and IFN-γ or IL-4. Total RNA was isolated after 24 h with the RNeasy Mini Kit (Qiagen) or the mirVana miRNA Isolation Kit (Ambion).

The BMDMs were transfected with siRNAs against *Bmpr2*, *Akt1* or a non-targeting siRNA (1 μM, Accell siRNA in Accell delivery cell culture medium, Dharmacon) after 4 days in culture. Subsequent treatment with the *miR-342-5p* inhibitor and macrophage activation were performed as described above.

Target prediction

Potential miR-342-5p target genes were identified with the following miRNA target prediction algorithms: TargetScan (www.targetscan.org)[3], miRanda (www.microrna.org)[4], and MicroCosm Targets (www.ebi.ac.uk/enright-srv/microcosm/htdocs/targets/v5/)[5].

Argonaut2 (Ago2) immunoprecipitation

Unstimulated BMDMs were harvested 24 hours after the transfection of the miR-342-5p inhibitor by washing with ice-cold PBS, subsequent incubation for 15 min on ice in lysis buffer (100 mM KCl, 5 mM $MgCl_2$, 10 mM HEPES pH 7.0, 0.5% NP40, 5 mM DTT, 250 units/ml RNase OUT [Invitrogen], 400 µM vanadyl ribonucleoside complexes [New England Biolabs], and 1 tablet per 10 ml protease inhibitors [Complete Protease Inhibitor Cocktail Tablets, Roche]), and homogenized with a Dounce homogenizer. The lysates were centrifuged at 16,000 x *g* for 15 min at 4℃. The input RNA was extracted from the supernatant with TRIzol (Invitrogen). Prior to the IP, protein A/G-conjugated magnetic beads (Millipore) were incubated with a mouse monoclonal anti-Ago2 antibody (clone 2E12-1C9, Abnova) or mouse IgG (Millipore). The antibody-conjugated beads were subsequently incubated with the cell extracts in the supernatant for 7 hours at 4℃ befo re immobilization of the precipitate with a magnetic separator (Millipore). RNA was isolated from the precipitate with TRIzol (Invitrogen), reverse-transcribed with random primers, and amplified with SYBR Green PCR Master Mix (Fermentas). The fold-enrichment (FE) of the target genes in the Ago2-immunoprecipitated (Ago2-IP) RNA compared with the

IgG-immunoprecipitated (IgG-IP) RNA was calculated using the following equations: $\Delta CT_{Ago2\text{-}IP}=CT_{input}-CT_{Ago2\text{-}IP}$; $\Delta CT_{IgG\text{-}IP}=CT_{input}-CT_{IgG\text{-}IP}$; $\Delta\Delta CT=\Delta CT_{Ago2\text{-}IP}-\Delta CT_{IgG\text{-}IP}$; and $FE=2^{\Delta\Delta CT}$.

Luciferase assays

The full-length 3′-UTRs of murine *Bmpr2*, *Akt1* and *Nfkb2* were cloned into the psiCHECK-2 Vector (Promega) at the XhoI/NotI sites. Mutagenesis PCR at the *miR-342-5p* target sites of *Bmpr2* and *Akt1* was performed with the following sets of primers: *Bmpr2* mutagenic primers: 5' GCTTTAACCTCCTGTCAGGTGGCCTTCCCACCCCTGC 3′ and 5′ CCACCTGACAGGAGGTTAAAGCAGTTTTTTTTTTAAA 3′; *Akt1* mutagenic primers: 5′ GCAAGAAGGCACCAGAAGGTGGCCCCTGTGGTATGCT 3′ and 5′ CCACCTTCTGGTGCCTTCTTGCTGGACTTTGGCCCTG 3′. HEK293 cells were cultured in complete DMEM until subconfluency and cotransfected with 100 ng of luciferase reporter or empty vector and an *miR-342-5p* mimic or scrambled control (Ambion) using Lipofectamine 2000 (Invitrogen). The *Firefly* and *Renilla* luciferase activities were measured with the Dual-Glo Luciferase Assay System (Promega) using a microplate reader (Tecan) 48 h after transfection. The *Firefly* luciferase activity was normalized to the *Renilla* luciferase activity and expressed as a percentage of the activity following the transfection of the empty vector.

Enzyme linked immunosorbent assay (ELISA)

The concentration of Akt1, Bmpr2, Il6 and TNF-α was determined in BMDM cell

lysates or cell culture medium by ELISAs (mouse total Akt1 Elisa kit, Life technologies; Bmpr2 Elisa kit, MyBioSource; TNF-α and Il6 Elisa kit, Ray Biotech). The phosphorylation of Akt was measured using Akt [pS473] Elisa kit (Life technologies). The absorbance at 450 nm was measured with a microplate reader (Tecan).

Antagomir treatment

A chemically modified (6 phosphorothioate [*], all 2'Ome [m] and 3'-cholesterol modification) antisense RNA oligonucleotide against miR-342-5p (5'-mC(*)mU(*)mCmAmAmUmCmAmCmAmGmAmUmAmGmCmAmCmC(*)mC(*)mC(*)mU(*)-Chol-3′, Dharmacon), known as an antagomir, was designed[6]. The control antagomir contained a nucleotide sequence that was not complementary to any known miRNA[7]. Perivascular antagomir treatment of the carotid arteries began 3 weeks after the partial ligation (160 µg dissolved in 35% pluronic gel) and was repeated twice at weekly intervals[8]. Carotid arteries were harvested 42 days after the partial ligation and embedded in paraffin following perfusion with paraformaldehyde. After sectioning, RNA was isolated from some of the sections (RecoverAll Total RNA Isolation Kit, Applied Biosystems).

Locked nucleic acid (LNA) inhibitor treatment *in vivo*

The LNA inhibitor of *miR-342-5p* (LNA-342-5p, ATCACAGATAGCACC) and the non-specific control LNA oligonucleotide (LNA-control, ATCAAAGCTAGGACC) were synthesized by Exiqon, Inc. (Vedbaek, Denmark). After 2 months of feeding on an HCD, *Apoe*$^{-/-}$ mice were injected four times with LNA-control or LNA-342-5p (25

mg/kg, intravenously), once per week[9]. The aortas were harvested 1 week after the last injection. Following *en face* preparation, the aortas were stained with Oil red O stain. Cross sections of the aortic roots were stained with Verhoeff's elastic van Gieson stain. Oil red O and Verhoeff's staining methods were performed according to standard laboratory protocols.

Supplemental Tables

Supplemental Table 1. Differentially expressed miRNAs in early atherosclerotic plaques compared to non-diseased arterial tissues (n = 3-4 mice).

miRNA	$Log_{10}RQ$	$-Log_{10}p$ value	miRNA	$Log_{10}RQ$	$-Log_{10}p$ value
miR-342-5p	1.675	1.541	*miR-30d*	-0.874	1.323
miR-296-5p	0.933	1.968	*miR-206*	-0.884	1.399
miR-146b	0.817	1.324	*miR-26a*	-0.902	1.805
*miR-21**	0.788	1.632	*miR-99a*	-0.904	2.009
miR-155	0.574	1.594	*miR-181c*	-0.976	1.346
miR-30e	-0.485	1.442	*miR-301a*	-0.989	1.608
*miR-376b**	-0.490	1.397	*miR-26b*	-0.996	1.647
*miR-214**	-0.490	1.770	*let-7e*	-1.028	1.503
miR-152	-0.575	1.482	*miR-365*	-1.106	2.434
*miR-16**	-0.581	1.408	*miR-218*	-1.135	2.187
miR-92a	-0.588	1.429	*miR-18a*	-1.214	1.696
miR-140	-0.622	1.338	*miR-677*	-1.266	1.392
miR-195	-0.627	1.642	*miR-676**	-1.285	1.303
miR-30b	-0.631	1.705	*miR-329*	-1.288	1.571
miR-30a	-0.667	1.498	*miR-205*	-1.387	1.683
miR-23b	-0.684	1.570	*miR-301b*	-1.603	1.380
miR-193b	-0.700	1.468	*miR-708*	-1.683	1.704
miR-701	-0.710	2.062	*miR-143*	-1.754	2.350
miR-434-3p	-0.713	1.684	*miR-145*	-1.862	3.088
miR-127	-0.715	1.855	*miR-15a*	-1.959	1.389
miR-99b	-0.730	1.987	*miR-9**	-1.990	1.961
let-7d	-0.743	1.520	*miR-345-5p*	-2.259	1.469
miR-125b-5p	-0.756	2.195	*miR-124*	-2.308	1.432
miR-130a	-0.757	1.502	*miR-224*	-2.367	1.578
miR-181a	-0.761	1.568	*miR-187*	-2.472	1.593
let-7c	-0.791	1.792	*miR-382*	-2.490	1.376
let-7b	-0.793	1.874	*miR-129-3p*	-2.832	2.090
*let-7a**	-0.796	2.364	*miR-28**	-2.909	1.390
miR-30c	-0.798	1.732	*miR-9*	-2.970	2.188
miR-497	-0.801	1.632	*miR-106a*	-3.460	1.480
miR-100	-0.851	1.940	*let-7a*	-3.493	1.392

Supplemental Figures

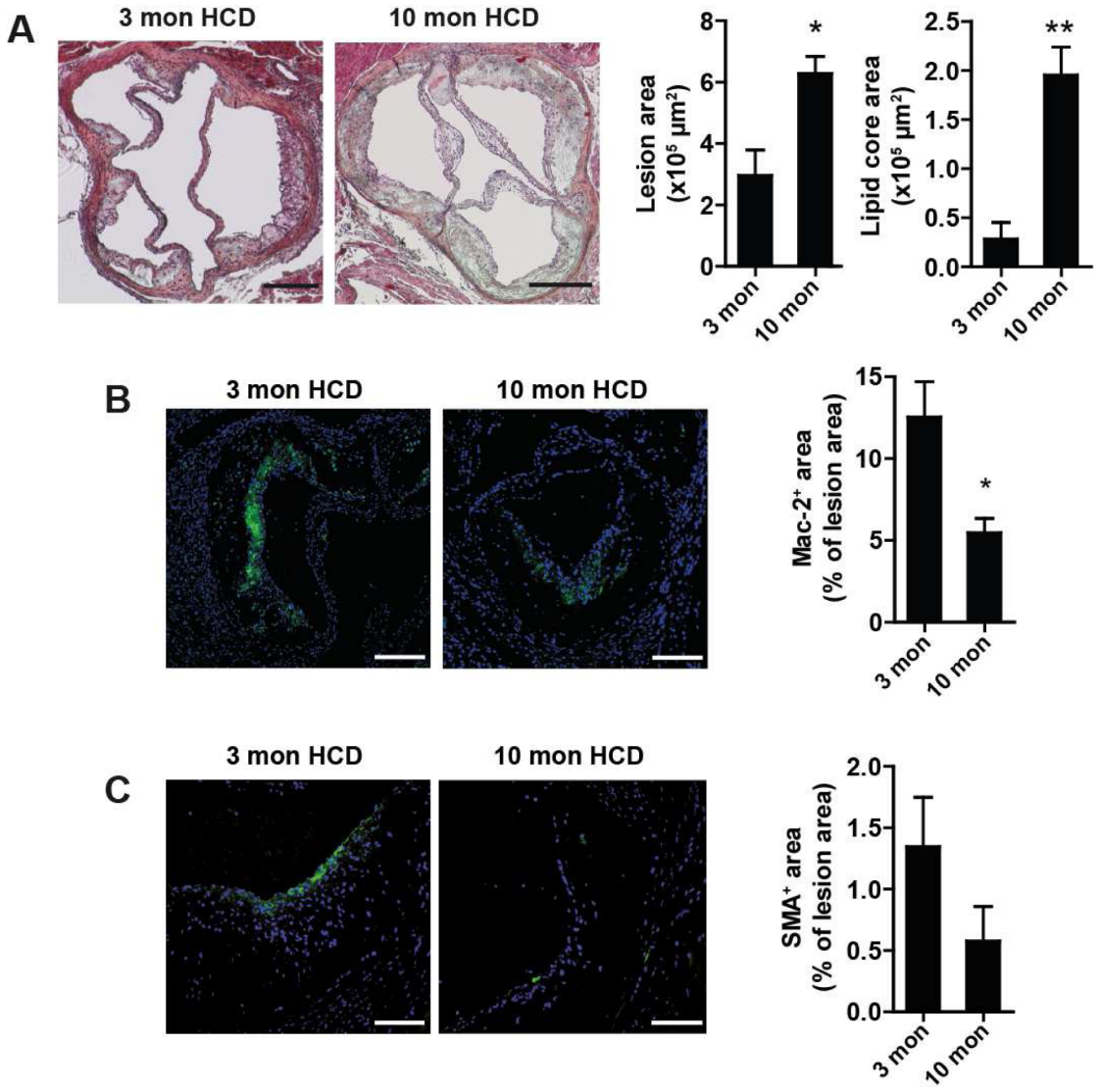

Supplemental Figure 1. Characterization of early and advanced atherosclerotic lesions in *Apoe*$^{-/-}$ mice. (A) Movat's pentachrome staining of aortic root sections from *Apoe*$^{-/-}$ mice after 3 (3 mon) or 10 months (10 mon) on a high-cholesterol diet (HCD). The lesion size and the lipid core area were quantified by planimetry. *p < 0.05; n = 3-4 mice from each group. Scale bars, 500 µm. (B) The lesional

macrophage accumulation was determined via Mac-2 immunostaining of aortic root sections. The nuclei were counterstained with DAPI. *p < 0.05; n = 3-4 mice from each group. Scale bars, 200 µm. (C) The relative SMC content was determined by immunostaining for SMA in aortic root sections from *Apoe*$^{-/-}$ mice that had been fed a high cholesterol diet (HCD) for 3 or 10 months. The nuclei were counterstained with DAPI. n = 3-4 mice from each group. Scale bars, 100 µm. The means ± the SEM are shown.

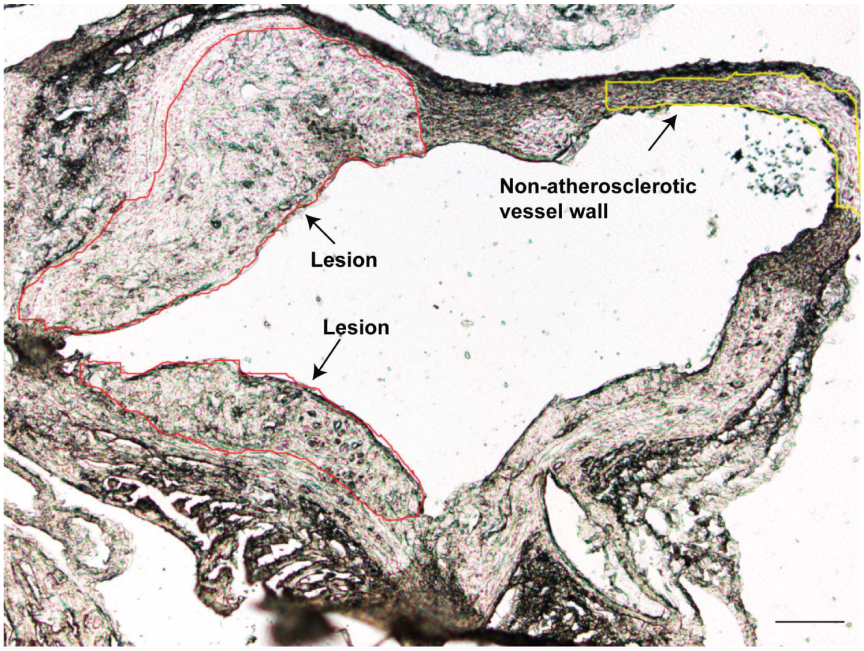

Supplemental Figure 2. Laser-microdissection of murine atherosclerotic plaques. An unstained section of the aorta of *Apoe*$^{-/-}$ mice after 3 months of a HCD is shown before the lesions were micro-dissected. Following laser microdissection, the aortic lesions outlined by red color were cut from the sections of the aortic root and used for the miRNA RT-PCR array. Non-atherosclerotic vessel wall outlined by the yellow color was cut from the same sections used as the control of miRNA RT-PCR array. Scale bars, 100 μm.

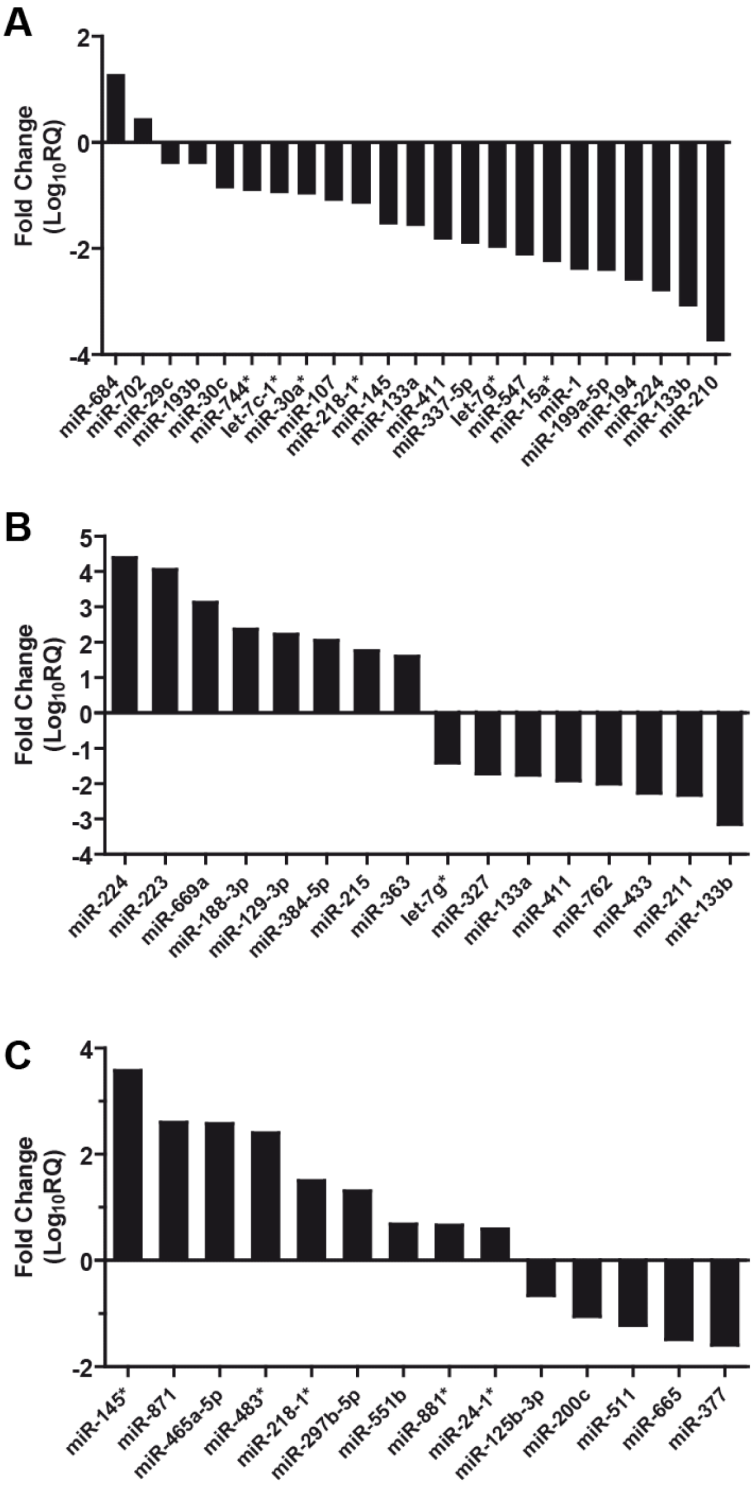

Supplemental Figure 3. Differentially expressed miRNAs during atherogenesis in *Apoe*$^{-/-}$ mice. (A) The miRNA expression profile of atherosclerotic lesions from

aortic roots was compared to that of non-atherosclerotic arterial tissues from *Apoe*$^{-/-}$ mice that had been fed an HCD for 10 months, as assessed by a qRT-PCR array of laser-microdissected samples. Significantly up- or down-regulated miRNAs are shown. $p < 0.05$; n = 3-4 mice from each group. (B) miRNAs expressed differently in advanced atherosclerotic lesions compared to early lesions from *Apoe*$^{-/-}$ mice after 10 and 3 months of an HCD, respectively, as determined by a qRT-PCR array of laser-microdissected samples are depicted. Significantly up- and down-regulated miRNAs are shown. $p < 0.05$; n = 3-4 mice from each group. (C) Changes in the miRNA expression profiles from non-atherosclerotic arterial walls after 10 months of an HCD compared to those after 3 months of an HCD, as determined by a qRT-PCR array of laser-microdissected samples are depicted. Significantly regulated miRNAs are shown. $p < 0.05$; n = 3-4 mice from each group.

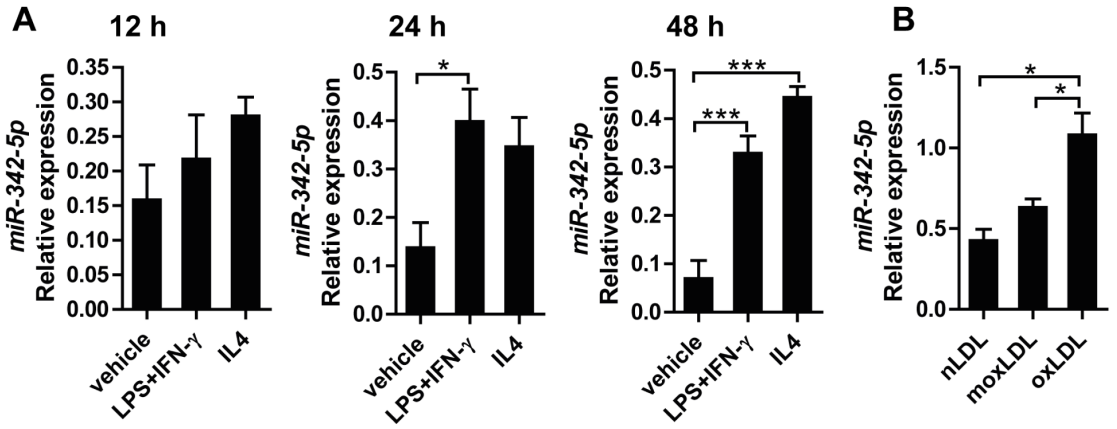

Supplemental Figure 4. Regulation of *miR-342-5p* expression in BMDMs. A. *miR-342-5p* expression at different time points (12 h, 24 h and 48 h) after LPS/IFN-γ stimulation. *p < 0.05, ***p < 0.005; n = 4. **B.** *miR-342-5p* expression was determined in BMDMs at 48 h after stimulation with nLDL, moxLDL, or oxLDL. *p < 0.05; n = 3.

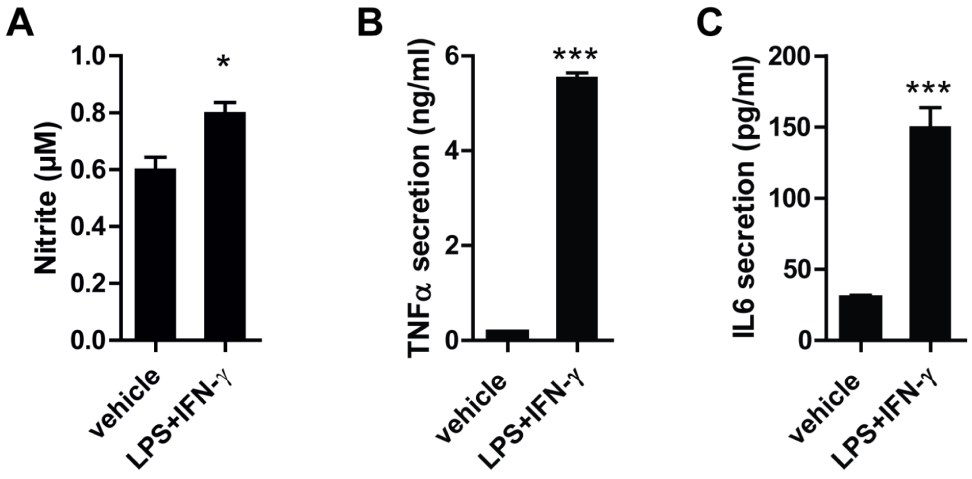

Supplemental Figure 5. Stimulation with LPS/IFN-γ induces nitrite production, TNFα and IL6 in BMDMS. The concentration of nitrite (A), TNFα (B) and IL6 (C) were determined in the culture medium of BMDMs with or without LPS/IFN-γ-stimulation. *p < 0.05, ***p < 0.005; n = 3-4.

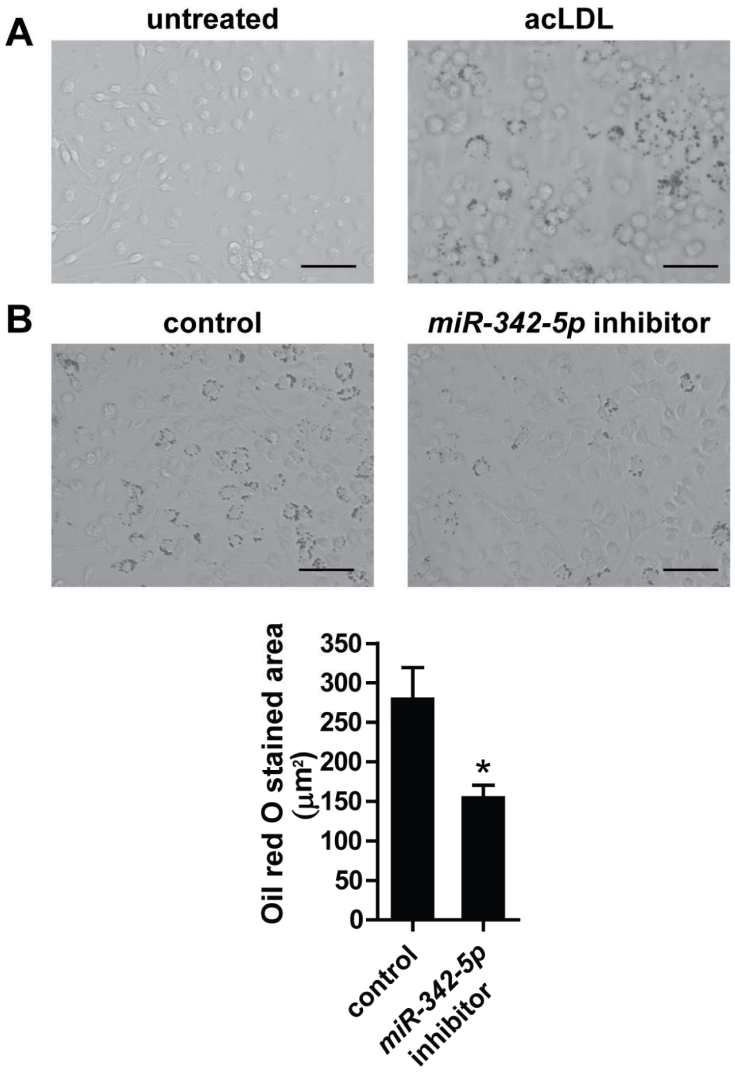

Supplemental Figure 6. *miR-342-5p* promotes lipid uptake of BMDMs. (A) The Oil red O-stained area was studied in untreated BMDMs and BMDMs treated with acLDL. (B) The effect of the *miR-342-5p* inhibitor on lipid accumulation in BMDMs treated with acLDL was compared with the effect of non-targeting LNA oligonucleotides in the control group. *p < 0.05; n = 4. Scale bars, 50 µm.

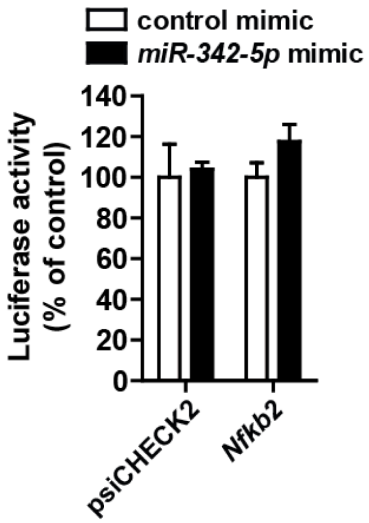

Supplemental Figure 7. *miR-324-5p* does not target the 3'-UTR of *Nfkb2.* The luciferase activity in HEK293 cells transfected with the psiCHECK-2 vector with or without the *Nfkb2* 3'-UTR was quantified 48 h after the transfection of a *miR-342-5p* or control mimic (30 nM). The graph represents the Firefly luciferase activity normalized to the control mimic. n = 4. The means ± the SEM are shown.

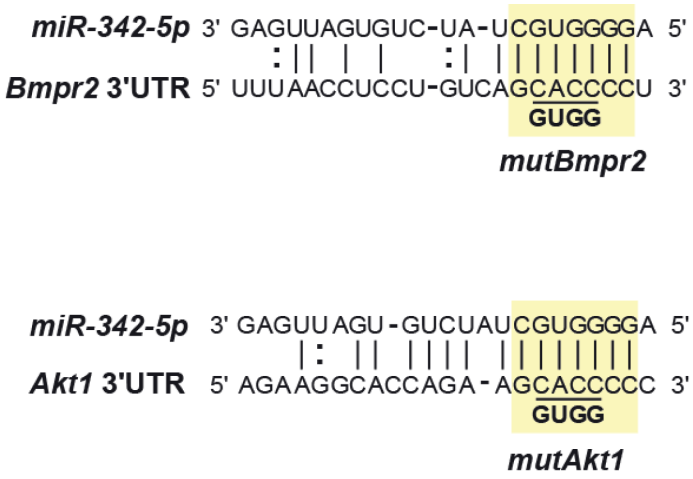

Supplemental Figure 8. Sequence alignment of *miR-342-5p* with the predicted target site in the *Bmpr2* and *Akt1* 3' untranslated regions (UTRs). Mutations in the 3'-UTRs (bold) were engineered in the region complementary to the *miR-342-5p* seed region (yellow).

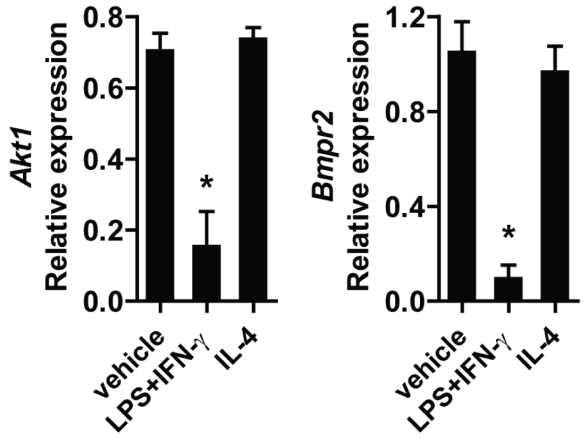

Supplemental Figure 9. The expression of *Akt1* and *Bmpr2* mRNA was quantified in unstimulated BMDMs (vehicle) and in BMDMs stimulated with LPS and IFN-γ or with IL-4. *$p < 0.05$ versus all other groups; $n = 4$.

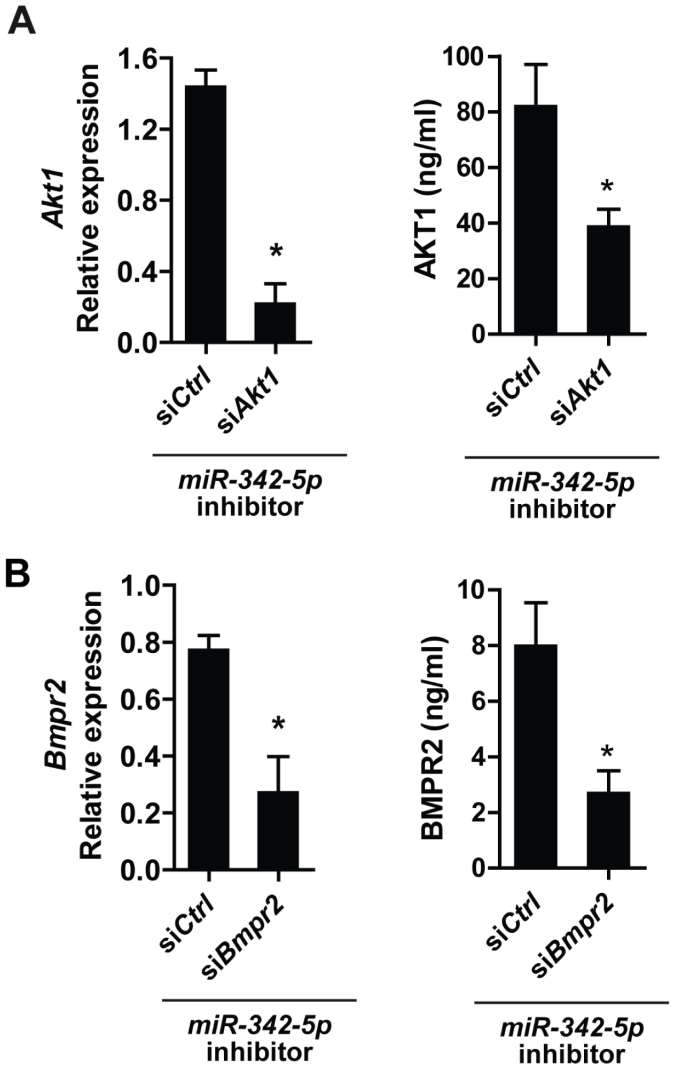

Supplemental Figure 10. Silencing of Akt1 and Bmpr2 expression in BMDMs. The suppression of Akt1 (A) and Bmpr2 (B) expression at the mRNA (left) and protein (right) level was determined in LPS/IFN-γ–stimulated BMDMs treated with the miR-342-5p inhibitor using RNA interference (siAkt1 or siBmpr2) compared with those treated with a non-targeting siRNA (siCtrl). *$p < 0.05$ versus siCtrl; $n = 4$.

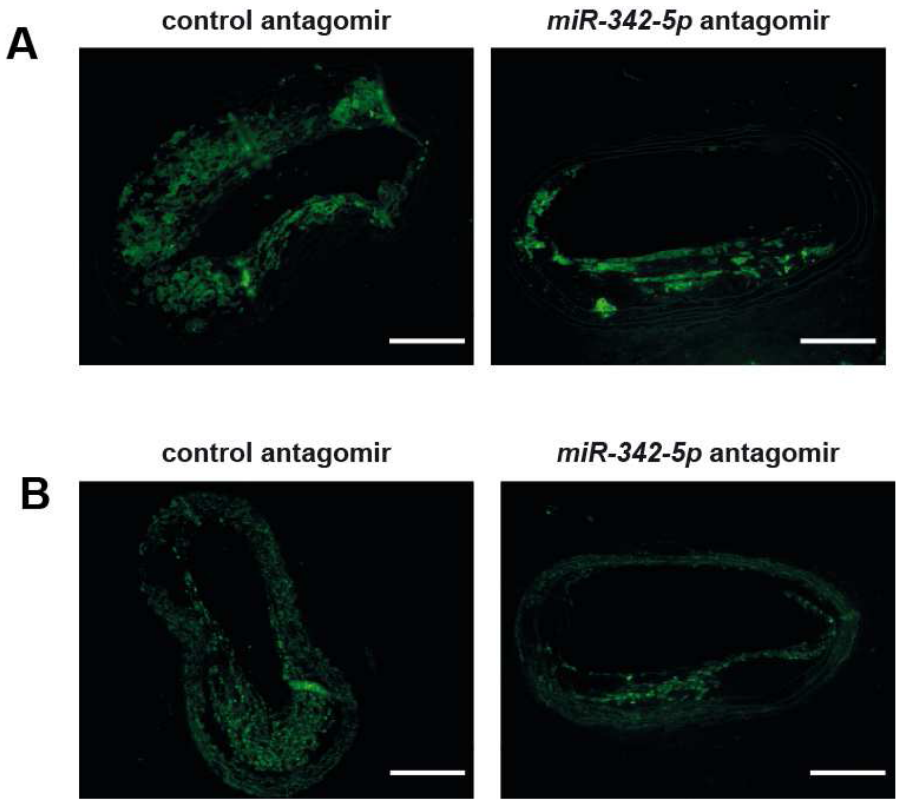

Supplemental Figure 11. The effects of a *miR-342-5p* antagomir on the cellular content of atherosclerotic lesions. (A) The relative content of macrophages (Mac-2 immunostaining) in atherosclerotic lesions from partially ligated carotid arteries was determined by immunostaining in *Apoe*$^{-/-}$ mice treated with the *miR-342-5p* antagomir or a control antagomir. Representative immunostainings are shown. Scale bars, 100 µm. (B) The relative content of SMCs (SMA immunostaining) in atherosclerotic lesions from partially ligated carotid arteries was assessed by immunostaining in *Apoe*$^{-/-}$ mice treated with an *miR-342-5p* antagomir or a control antagomir. Representative immunostainings are shown. Scale bars, 100 µm.

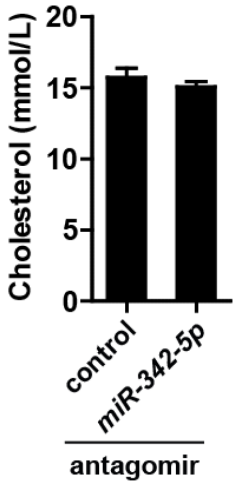

Supplemental Figure 12. *miR-342-5p* antagomir treatment and cholesterol levels. The serum cholesterol levels of *Apoe*$^{-/-}$ mice 42 days after partial carotid ligation and perivascular treatment with a *miR-342-5p* antagomir or a control antagomir are depicted. n = 5-6 mice from each group. The means ± the SEM are shown.

Supplemental references

1. Nam D, Ni CW, Rezvan A, Suo J, Budzyn K, Llanos A, Harrison D, Giddens D, Jo H. Partial carotid ligation is a model of acutely induced disturbed flow, leading to rapid endothelial dysfunction and atherosclerosis. *American Journal of physiology. Heart and circulatory physiology*. 2009;297:H1535-1543

2. Nazari-Jahantigh M, Wei Y, Noels H, Akhtar S, Zhou Z, Koenen RR, Heyll K, Gremse F, Kiessling F, Grommes J, Weber C, Schober A. Microrna-155 promotes atherosclerosis by repressing bcl6 in macrophages. *J Clin Invest*. 2012;122:4190-4202

3. Grimson A, Farh KK, Johnston WK, Garrett-Engele P, Lim LP, Bartel DP. Microrna targeting specificity in mammals: Determinants beyond seed pairing. *Mol Cell*. 2007;27:91-105

4. Betel D, Wilson M, Gabow A, Marks DS, Sander C. The microrna.Org resource: Targets and expression. *Nucleic Acids Res*. 2008;36:D149-153

5. Griffiths-Jones S, Saini HK, van Dongen S, Enright AJ. Mirbase: Tools for microrna genomics. *Nucleic Acids Res*. 2008;36:D154-158

6. Krutzfeldt J, Rajewsky N, Braich R, Rajeev KG, Tuschl T, Manoharan M, Stoffel M. Silencing of microrna in vivo with 'antagomirs'. *Nature*. 2005;438:685-689

7. van Solingen C, Seghers L, Bijkerk R, Duijs JM, Roeten MK, van Oeveren-Rietdijk AM, Baelde HJ, Monge M, Vos JB, de Boer HC, Quax PH, Rabelink TJ, van Zonneveld AJ. Antagomir-mediated silencing of endothelial cell specific microrna-126 impairs ischemia-induced angiogenesis. *J Cell Mol Med*. 2009;13:1577-1585

8. Subramanian P, Karshovska E, Reinhard P, Megens RT, Zhou Z, Akhtar S, Schumann U, Li X, van Zandvoort M, Ludin C, Weber C, Schober A. Lysophosphatidic acid receptors lpa1 and lpa3 promote cxcl12-mediated smooth muscle progenitor cell recruitment in neointima formation. *Circ Res*. 2010;107:96-105

9. Boon RA, Seeger T, Heydt S, Fischer A, Hergenreider E, Horrevoets AJ, Vinciguerra M, Rosenthal N, Sciacca S, Pilato M, van Heijningen P, Essers J, Brandes RP, Zeiher AM, Dimmeler S. Microrna-29 in aortic dilation: Implications for aneurysm formation. *Circ Res*. 2011;109:1115-1119

4 Summary

4.1 Role of endothelial Dicer in atherosclerosis

Chemokine-mediated monocyte adhesion to inflammatory ECs results in subendothelial accumulation of macrophages and initiates the formation of atherosclerotic lesions. The proinflammatory transcription factor NF-κB and the anti-inflammatory transcription factor KLF4 mediate the inflammatory activation of ECs by negatively regulating each other through competition for the binding to the coactivator p300. Dysregulation of individual miRNAs in ECs plays an important role in NF-κB-mediated endothelial inflammation during atherosclerosis. The RNase Dicer generates almost all mature miRNAs and promotes proinflammatory gene expression in ECs. However, the role of Dicer in endothelial inflammation during atherosclerosis is unknown.

Therefore, the aim of the current study is to determine the effect of endothelial Dicer knock-out on atherosclerosis using Tamoxifen-inducible Cadherin5-CreER^{T2}*Dicer*$^{flox/flox}$*apolipoprotein E*$^{-/-}$ (*Apoe*$^{-/-}$) mice fed a high-cholesterol diet. Deletion of endothelial *Dicer* in *Apoe*$^{-/-}$ mice diminished endothelial chemokine expression, monocyte adhesion to atherosclerosis-prone endothelium, lesional macrophage accumulation and reduced atherosclerotic lesion formation compared to control mice. MiRNA expression profiles in atherosclerotic arteries of *Apoe*$^{-/-}$ mice showed that *Dicer* deficiency lowers the expression levels of miR-103, -433, -301b and -652, most of which were upregulated during atherosclerosis progression. Among those downregulated miRNAs, miR-103 was most abundantly expressed in human aortic ECs (HAECs) and enriched in the RISC of ECs. Accordingly, ECs covering mouse and human atherosclerotic lesions expressed miR-103. Stimulation with moxLDL and activation of NF-κB by TNF-α upregulated the expression of miR-103 in HAECs. Gain-and-loss-of-function studies showed that miR-103 promotes the expression of the chemokines *CXCL1, CX$_3$CL1* and *CCL2* in HAECs. Moreover, overexpression of miR-103 in HAECs increased monocyte adhesion to ECs, which was reversed by blocking the CXCL1-receptor C-X-C chemokine receptor type 2 on monocytes. Genome-wide microarray analysis of atherosclerotic arteries from *Apoe*$^{-/-}$ mice showed that endothelial *Dicer* deletion induces the differential expression of genes related to the Klf4 pathway, indicating increased Klf4 signaling. *Dicer* deficiency increased Klf4 protein expression in atherosclerotic endothelium in mice. Moreover, *KLF4* was enriched in the RISC of HAECs in a miR-103-dependent manner and miR-103 inhibition increased KLF4 protein levels, indicating that KLF4 is a target of miR-103 in ECs. Inhibition of the interaction between miR-103 and *KLF4* via the known binding site in the *KLF4* 3` UTR using target site blocker oligonucleotides (KLF4-TSBs) reduced the expression of *CXCL1, CX$_3$CL1* and *CCL2* and monocyte adhesion to HAECs. Systemic treatment of *Apoe*$^{-/-}$ mice with KLF4-TSBs significantly reduced lesional macrophage accumulation, lesion formation and endothelial Cxcl1 expression, showing a proinflammatory and proatherogenic role of miR-103 by targeting KLF4.

Taken together, Dicer promotes endothelial inflammation and atherosclerosis, at least partly through miR-103-mediated suppression of KLF4. MiR-103 might act as a molecular switch for the inflammatory activation of arterial ECs by fine-tuning the functional antagonism between KLF4 and NF-κB. Therefore, inhibition of the interaction between KLF4 and miR-103 might be a promising therapeutic approach to treat atherosclerosis.

4.2 Effect of endothelial HIF-1α on miRNA expression in atherosclerosis

The transcription factor HIF-1α is expressed in various cell types of atherosclerotic lesions and its expression correlates with lesional inflammation and atherosclerotic lesion progression. Endothelial NF-κB and HIF-1α amplify each other through a positive feedback loop, thereby regulating EC functions. In addition to the transcriptional regulation of protein-coding genes, HIF-1α mediates its effects by the regulation of several miRNAs in ECs. However, it is unknown whether HIF-1α affects endothelial inflammation during atherosclerosis by regulating miRNAs.

Hyperlipidemia increased the expression and activation of Hif-1α in aortic ECs of *Apoe*$^{-/-}$ mice. To study the role of endothelial HIF-1α in atherosclerosis, we used *Apoe*$^{-/-}$ mice that express a Tamoxifen-inducible Cre-recombinase (CreER^{T2}) under the control of the EC-specific Cadherin5 promoter after feeding a high-cholesterol diet. Deletion of endothelial *Hif1a* reduced Cxcl1 expression, the lesional macrophage content and lesion formation, compared to control mice. Moreover, computed tomographic angiography showed that the luminal volume is significantly reduced in the carotid arteries of mice deficient for endothelial *Hif1a*. Stimulation of murine aortic ECs with moxLDL or with its derivative LPA 20:4 promoted Cxcl1 expression and monocyte adhesion by inducing Hif-1α expression. Blocking LPA receptors reduced the moxLDL-induced *Cxcl1* and *Hif1a* expression in murine aortic ECs, suggesting that moxLDL-derived unsaturated LPAs promote CXCL1-dependent monocyte adhesion by upregulating HIF-1α. MiRNA expression profiling in atherosclerotic carotid arteries of *Apoe*$^{-/-}$ mice showed that deficiency of endothelial *Hif1a* selectively reduces the expression of miR-19a in ECs. HIF-1α induced the expression of miR-19a in moxLDL-stimulated HAECs. Gain-and-loss-of-function studies showed that miR-19a promotes the expression of the chemokines *CXCL1* and *CCL2* in moxLDL-stimulated HAECs. Moreover, miR-19a triggered NF-κB activation and enhanced CXCL1-mediated monocyte adhesion to HAECs.

In conclusion, enhanced HIF-1α activation in atherosclerotic ECs promotes the expression of CXCL1 and increases atherosclerosis. The proatherogenic effect of endothelial HIF-1α might be due to an increased expression of miR-19a, which triggers NF-κB activation and CXCL1-dependent monocyte adhesion. Therefore, inhibition of the endothelial HIF-1α/miR-19a pathway may be a therapeutic option to treat atherosclerosis.

4.3 Role of miRNA-342-5p in atherosclerosis

Macrophages promote atherosclerosis by driving an unresolved inflammation in atherosclerotic lesions. Upregulated miRNAs during atherosclerosis, such as miR-155, play a crucial role in atherosclerosis. For instance miR-155 promotes the NF-κB-mediated inflammatory activation of macrophages during atherosclerosis. In addition to miR-155, miRNA expression profiles identified that miR-342-5p is selectively upregulated in early atherosclerotic lesions. The aim of the study is to investigate the so far unknown role of miR-342-5p in atherosclerosis.

MiR-342-5p was specifically expressed in lesional macrophages and suppressed the kinase *Akt1*, which is known to negatively regulate the expression of miR-155. MiR-342-5p-mediated suppression of *Akt1* induced *Nos2* and *Il6* expression in macrophages via the upregulation of miR-155. Inhibition of miR-342-5p in atherosclerotic *Apoe*$^{-/-}$ mice by systemic injection of antisense oligonucleotides reduced the progression of atherosclerosis and the Akt1-mediated Nos2 expression in lesional macrophages. Concomitantly, with the reduced Nos2 expression in macrophages, inhibition of miR-342-5p diminished the generation of nitrotyrosin and thus of nitrogen stress in the lesions.

Taken together, these date indicate a proinflammatory role of miR-342-5p in macrophages during early atherosclerosis. Therefore, targeting miR-342-5p might represent a promising strategy to treat atherosclerosis.

5 Zusammenfassung

5.1 Die Rolle von endothelialem Dicer in der Atherosklerose

Die Entstehung von atherosklerotischen Plaques wird durch die Chemokin-vermittelte Adhäsion von Monozyten an entzündliche Endothelzellen vermittelt. Dies führt zur subendothelialen Rekrutierung von Monozyten, die sich dort in Makrophagen differenzieren. Die entzündliche Aktivierung von Endothelzellen wird durch den proinflammatorischen Transkriptionsfaktor NF-κB und den anti-inflammatorischen Transkriptionsfaktor KLF4 gesteuert, welche sich durch die kompetitive Bindung an den Koaktivator p300 gegenseitig negativ regulieren. Es ist bekannt, dass eine gestörte Regulation von einzelnen miRNAs Entzündungsreaktionen in Endothelzellen hervorrufen kann. Das RNase Enzym Dicer ist für die Prozessierung von nahezu allen miRNAs und für die Expression von entzündungsfördernden Genen in Endothelzellen verantwortlich. Die Rolle von Dicer in der entzündlichen Aktivierung von Endothelzellen während der Atherosklerose ist jedoch nicht bekannt.

Das Ziel der vorliegenden Arbeit ist es, den Effekt eines endothelialen Dicer Knock-outs auf die Atherosklerose zu untersuchen. Dafür wurden Tamoxifen-induzierbare Cadherin5-CreER^{T2}Dicer$^{flox/flox}$/*apolipoprotein E$^{-/-}$ (Apoe$^{-/-}$)*-Mäuse mit einer cholesterinreichen Diät gefüttert. Im Vergleich zu den Kontrollmäusen, verminderte die endotheliale *Dicer*-Deletion in *Apoe*$^{-/-}$-Mäusen die Expression endothelialer Chemokine, die Adhäsion von Monozyten an Endothelzellen, die Anreicherung von Makrophagen in der Gefäßwand sowie die Ausbildung von atherosklerotischen Plaques. MiRNA-Expressionsanalysen in atherosklerotischen Arterien von *Apoe*$^{-/-}$-Mäusen zeigten, dass die Deletion des endothelialen *Dicer*-Gens vor allem die Expression der miRNAs miR-103, -433, -301b und -652 vermindert. Der Großteil dieser miRNAs zeigte eine erhöhte Expression während der Atherosklerose. Unter diesen vier miRNAs war miR-103 am stärksten in humanen aortalen Endothelzellen (HAECs) exprimiert als auch am stärksten im RISC von Endothelzellen angereichert. Ferner wurde miR-103 in Endothelzellen aus humanen und murinen atherosklerotischen Plaques exprimiert. Eine Stimulation mit moxLDL sowie eine TNF-α-induzierte Aktivierung von NF-κB steigerte die miR-103-Expression in HAECs. „Gain-and-loss-of-function"-Experimente zeigten, dass miR-103 die Expression der Chemokine *CXCL1, CX$_3$CL1* und *CCL2* in HAECs erhöht. Ferner induzierte eine Überexpression von miR-103 in HAECs eine gesteigerte Monozytenadhäsion an Endothelzellen, welche durch die Inhibition des CXCL1-Rezeptors C-X-C-Chemokine Rezeptor Typ 2 auf Monozyten gehemmt werden konnte. Eine genomweite Genexpressionsanalyse in atherosklerotischen Arterien von *Apoe*$^{-/-}$-Mäusen zeigte, dass das Fehlen von endothelialem *Dicer* eine differenzielle Genregulation von vorwiegend KLF4-regulierten Genen induziert. Dies wies auf eine gesteigerte Aktivierung des Klf4-Signalweges in diesen Mäusen hin. Zudem erhöhte der endotheliale *Dicer*-Knock-out in *Apoe*$^{-/-}$-Mäusen die Klf4-Proteinexpression in atherosklerotischen Endothelzellen. Darüber hinaus reicherte sich *KLF4* in Abhängigkeit von miR-103 im RISC von HAECs an und die Inhibition von miR-103 führte zu einer erhöhten KLF4-Proteinexpression in diesen Zellen. Diese Ergebnisse lassen darauf schließen, dass KLF4 ein Target von miR-103 ist. Das Blockieren der Interaktion von miR-103 und *KLF4* über die bekannte miR-103-Bindungsstelle in der *KLF4* 3` UTR mittels spezifischer „Target Site Blocker"-Oligonukleotide (KLF4-TSBs) reduzierte die Expression von *CXCL1, CX$_3$CL1* und *CCL2* sowie die Monozytenadhäsion an HAECs. Eine systemische Behandlung von *Apoe*$^{-/-}$-Mäusen mit KLF4-TSBs reduzierte den Makrophagenanteil in den Plaques, verminderte die Ausbildung von atherosklerotischen Plaques sowie die endotheliale Cxcl1-Expression. Diese Ergebnisse sprechen für eine proinflammatorische und proatherogene Rolle von miR-103 in Endothelzellen, welche durch die Suppression ihres Zielgens KLF4 vermittelt wird.

Zusammenfassend zeigen diese Daten, dass Dicer die endotheliale Entzündung sowie die Atherosklerose fördert. Dieser Effekt ist zumindest teilweise auf die miR-103-vermittelte Suppression von KLF4 zurückzuführen. Durch das Regulieren des funktionellen Antagonismus zwischen KLF4 und NF-κB ist miR-103 für die Feineinstellung der entzündlichen Aktivierung von arteriellen Endothelzellen verantwortlich. Deshalb stellt das Blockieren der Interaktion zwischen KLF4 und miR-103 einen vielversprechenden Ansatz für die Behandlung von Atherosklerose dar.

5.2 Die Effekte von endothelialem HIF-1α auf die miRNA-Expression in der Atherosklerose

Der Transkriptionsfaktor HIF-1α wird in verschiedenen Zelltypen atherosklerotischer Plaques exprimiert. Die Expression von HIF-1α korreliert mit der Entzündungsaktivität in atherosklerotischen Plaques sowie mit der Progression der Atherosklerose. NF-κB und HIF-1α steigern durch einen positiven Feedback-Mechanismus ihre Expression in Endothelzellen wechselseitig und regulieren dadurch Endothelfunktionen. Zusätzlich zur Regulation von Protein-kodierenden Genen, vermittelt HIF-1α einen Teil seiner Effekte in Endothelzellen durch die Regulation von miRNAs. Ziel der Studie ist die Untersuchung der bislang unbekannten Rolle von HIF-1α-regulierten miRNAs in der endothelialen Entzündung im Rahmen der Atherosklerose.

Eine Hyperlipidämie induzierte die Expression und Aktivierung von Hif-1α in aortalen Endothelzellen von *Apoe*$^{-/-}$-Mäusen. Um die Rolle von endothelialem HIF-1α in der Atherosklerose zu untersuchen, wurden *Apoe*$^{-/-}$-Mäuse, welche eine Tamoxifen-induzierbare Cre-Rekombinase (CreER^{T2}) unter der Kontrolle des Endothel-spezifischen Cadherin5 Promoters exprimieren, nach Gabe einer cholesterinreichen Diät verwendet. Im Vergleich zu Kontrollmäusen, reduzierte die Deletion des endothelialen *Hif1a*-Gens in *Apoe*$^{-/-}$-Mäusen die endotheliale CXCL1-Expression, den Makrophagenanteil in den Plaques sowie die Ausbildung von atherosklerotischen Läsionen. Mittels computertomographische Angiographie konnte gezeigt werden, dass das Fehlen von endothelialem *Hif1a* das Gefäßvolumen der Karotiden nach einer cholesterinreichen Diät signifikant vergrößert. Die durch moxLDL oder dessen Derivat LPA 20:4-induzierte endotheliale Cxcl1-Expression und Monozytenadhäsion wurde durch die gesteigerte Hif-1α-Expression vermittelt. Das Blockieren der LPA-Rezeptoren reduzierte die moxLDL-induzierte *Cxcl1* und *Hif1a*-Expression in murinen aortalen Endothelzellen. Diese Ergebnisse deuten darauf hin, dass moxLDL mittels ungesättigten LPAs die Expression von HIF-1α steigert und dadurch die CXCL1-vermittelte Monozytenadhäsion induziert. MiRNA-Expressionsanalysen aus atherosklerotischen Karotiden von *Apoe*$^{-/-}$-Mäusen zeigten, dass das Fehlen von endothelialem *Hif1a* die Expression von miR-19a in Endothelzellen selektiv vermindert. HIF-1α induzierte die Expression von miR-19a in moxLDL-stimulierten HAECs. „Gain-and-loss-of-function"-Experimente zeigten, dass miR-19a die Expression der Chemokine *CXCL1* und *CCL2* in moxLDL-stimulierten HAECs steigert. Ferner steigerte miR-19a die Aktivierung von NF-κB sowie die CXCL1-vermittelte Monozytenadhäsion an HAECs.

Zusammenfassend zeigen diese Ergebnisse, dass eine gesteigerte HIF-1α-Aktivierung in atherosklerotischen Endothelzellen die CXCL1-Expression erhöht und die Ausbildung von Atherosklerose fördert. Der proatherogene Effekt von endothelialem HIF-1α könnte dadurch bedingt sein, dass HIF-1α die Expression von miR-19a steigert und dadurch die Aktivierung von NF-κB sowie die CXCL1-vermittelte Monozytenadhäsion fördert. Demzufolge stellt die Inhibition des HIF-1α/miR-19a-Signalweges einen potentiellen Therapieansatz für die Behandlung der Atherosklerose dar.

5.3 Die Rolle von miR-342-5p in der Atherosklerose

Die chronische Entzündung in atherosklerotischen Plaques wird durch die Dysfunktion von Makrophagen gefördert. MiRNAs, die während der Atherosklerose hochreguliert werden, spielen eine wichtige Rolle in der Atherosklerose. Zum Beispiel induziert miR-155 im Rahmen der Atherosklerose NF-κB-vermittelte Entzündungsreaktionen in Makrophagen. MiRNA-Expressionsanalysen aus frühen atherosklerotischen Plaques zeigten, dass neben miR-155, auch die Expression von miR-342-5p stark erhöht ist. Das Ziel dieser Studie ist die Untersuchung der bislang unbekannten Rolle von miR-342-5p in der Atherosklerose.

In atherosklerotischen Plaques von *Apoe*$^{-/-}$-Mäusen war miR-342-5p vor allem in Makrophagen exprimiert. MiR-342-5p supprimierte die Expression der Kinase *Akt1*, von welcher bekannt ist, dass sie die Expression von miR-155 inhibiert. Die Suppression von *Akt1* durch miR-342-5p induzierte die Expression von *Nos2* und *Il6* in inflammatorischen Makrophagen vermittelt durch eine gesteigerte Expression von miR-155. Das Blockieren der miR-342-5p mittels systemischer Injektion von Antisense-Oligonukleotiden reduzierte die Plaqueprogression und die Akt1-vermittelte Nos2-Expression in Makrophagen in atherosklerotischen *Apoe*$^{-/-}$-Mäusen. Einhergehend mit der reduzierten Nos2-Expression in Makrophagen, führte die Hemmung von miR-342-5p zu einer verminderten Bildung von Nitrotyrosin und somit zu einem verminderten nitrosativen Stress in atherosklerotischen Plaques.

Zusammenfassend zeigen diese Ergebnisse, dass miR-342-5p in Makrophagen eine proinflammatorische Rolle während eines frühen Stadiums der Atherosklerose hat. Die Inhibition von miR-342-5p stellt deshalb eine potentielle Behandlungsstrategie für Atherosklerose dar.

6 Perspective

The maladaption of ECs to disturbed flow at atherosusceptible arterial bifurcations primes ECs for inflammatory activation in response to hyperlipidemic stress. The findings of the current study show that Dicer generates endothelial miRNAs, like miR-103, which promote atherosclerotic lesion formation by increasing endothelial inflammation. Thus, Dicer might be a crucial regulator of endothelial maladaption. These findings may represent a novel concept in the regulation of endothelial inflammation based on endothelial miRNAs.

Moreover, the findings of the study indicate that the half-life of miRNAs in ECs differs greatly. A subset of endothelial miRNAs, including miR-103, appears to have a low stability during atherosclerosis and their expression is highly dependent on permanent Dicer activity. This could be due to a high turnover rate of miR-103 in ECs, which might be related to its disease specific expression and minor role in cell homeostasis. It will be necessary to further investigate the regulation and function of miRNA stability in ECs to gain more insights into its role in EC homeostasis.

Inhibition of miRNAs using antisense oligonucleotides is a potential therapeutic tool and the first anti-miRNA-based drug was successfully tested in a phase 2a human clinical trial[117]. However, miRNA-specific antisense-oligonucleotides result in the derepression of multiple miRNA targets, which may cause unwanted side effects. In contrast, inhibition of one miRNA-mRNA interaction using TSBs could increase the specificity of the therapeutic effect by preventing the inhibition of other miRNA-mRNA interactions. In this study, we tested for the first time the effect of TSBs *in vivo* on atherosclerosis. Selective inhibition of the interaction between miR-103 and KLF4 reduced atherosclerosis and endothelial inflammation in the arteries of atherosclerotic mice due to the upregulation of KLF4. These novel miRNA-targeting inhibitors that block the interaction of a miRNA with a specific target, seem to be highly specific and may therefore represent in general a promising new approach for anti-miRNA-based therapeutic strategies and a promising strategy to treat atherosclerosis.

Moreover, the findings of the study provide further insights into the mutual activation of NF-κB and HIF-1α in ECs. HIF-1α-mediated upregulation of miR-19a promotes NF-κB activation, which can in turn positively feedback to HIF-1α, thereby promoting EC inflammation. MiR-19a might induce endothelial NF-κB activation by inhibiting a negative regulator of NF-κB[118]. Thus, miR-19a posttranscriptionally controls NF-κB activation, which might be more responsive to cellular changes than transcriptional controls, thereby representing a rapid and transient regulation of the NF-κB and HIF-1α activation. Therefore, targeting the mutual activation of NF-κB and HIF-1α by blocking endothelial miR-19a might be a promising therapeutic strategy to induce the inflammatory resolution in ECs during atherosclerosis.

7 References

1 Nichols, M., Townsend, N., Scarborough, P. & Rayner, M. Cardiovascular disease in europe 2014: Epidemiological update. *Eur Heart J* **35**, 2950-2959, doi:10.1093/eurheartj/ehu299 (2014).

2 Libby, P., Ridker, P. M. & Hansson, G. K. Progress and challenges in translating the biology of atherosclerosis. *Nature* **473**, 317-325, doi:10.1038/nature10146 (2011).

3 Nichols, M., Townsend, N., Luengo-Fernandez, R., Leal, J., Scarborough, P. & Rayner, M. European cardiovascular disease statistics 2012. (European Heart Network, Brussels. European Society of Cardiology, Sophia Antipolis., 2012).

4 Komajda, M., Coats, A., Cowie, M. R., Jackson, N., Svensson, A. & Vardas, P. Championing cardiovascular health innovation in europe. *Eur Heart J* **34**, 2630-2635, doi:10.1093/eurheartj/eht211 (2013).

5 Dahlöf, B. Cardiovascular disease risk factors: Epidemiology and risk assessment. *Am J Cardiol* **105**, 3A-9A, doi:10.1016/j.amjcard.2009.10.007 (2010).

6 Pammolli, F., Magazzini, L. & Riccaboni, M. The productivity crisis in pharmaceutical R&D. *Nat Rev Drug Discov* **10**, 428-438, doi:10.1038/nrd3405 (2011).

7 Stary, H. C. Lipid and macrophage accumulations in arteries of children and the development of atherosclerosis. *Am J Clin Nutr* **72**, 1297s-1306s (2000).

8 Stary, H. C. Natural history and histological classification of atherosclerotic lesions: An update. *Arterioscler Thromb Vasc Biol* **20**, 1177-1178 (2000).

9 VanderLaan, P. A. Site specificity of atherosclerosis: Site-selective responses to atherosclerotic modulators. *Arterioscler Thromb Vasc Biol* **24**, 12-22, doi:10.1161/01.ATV.0000105054.43931.f0 (2004).

10 Schober, A., Nazari-Jahantigh, M. & Weber, C. MicroRNA-mediated mechanisms of the cellular stress response in atherosclerosis. *Nat Rev Cardiol* **12**, 361-374, doi:10.1038/nrcardio.2015.38 (2015).

11 Strong, J. P., Malcom, G. T., Newman, W. P., 3rd & Oalmann, M. C. Early lesions of atherosclerosis in childhood and youth: Natural history and risk factors. *J Am Coll Nutr* **11 Suppl**, 51S-54S (1992).

12 Finlayson, R., Symons, C. & Fiennes, R. N. Atherosclerosis: A comparative study. *Br Med J* **1**, 501-507 (1962).

13 McCullagh, K. G. Arteriosclerosis in the african elephant. I. Intimal atherosclerosis and its possible causes. *Atherosclerosis* **16**, 307-335 (1972).

14 Ross, R., Wight, T. N., Strandness, E. & Thiele, B. Human atherosclerosis. I. Cell constitution and characteristics of advanced lesions of the superficial femoral artery. *Am J Pathol* **114**, 79-93 (1984).

15 Libby, P. Coronary artery injury and the biology of atherosclerosis: Inflammation, thrombosis, and stabilization. *Am J Cardiol* **86**, 3J-8J; discussion 8J-9J (2000).

16 Aird, W. C. Endothelial cell heterogeneity. *Cold Spring Harb Perspect Med* **2**, a006429, doi:10.1101/cshperspect.a006429 (2012).

17 Kwak, B. R., Back, M., Bochaton-Piallat, M. L., Caligiuri, G., Daemen, M. J., Davies, P. F., Hoefer, I. E., Holvoet, P., Jo, H., Krams, R., Lehoux, S., Monaco, C., Steffens, S., Virmani, R., Weber, C., Wentzel, J. J. & Evans, P. C. Biomechanical factors in atherosclerosis: Mechanisms and clinical implicationsdagger. *Eur Heart J* **35**, 3013–3020, doi:10.1093/eurheartj/ehu353 (2014).

18 Hamik, A., Lin, Z., Kumar, A., Balcells, M., Sinha, S., Katz, J., Feinberg, M. W., Gerzsten, R. E., Edelman, E. R. & Jain, M. K. Kruppel-like factor 4 regulates endothelial inflammation. *J Biol Chem* **282**, 13769-13779, doi:10.1074/jbc.M700078200 (2007).

19 Parmar, K. M., Larman, H. B., Dai, G., Zhang, Y., Wang, E. T., Moorthy, S. N., Kratz, J. R., Lin, Z., Jain, M. K., Gimbrone, M. A., Jr. & Garcia-Cardena, G. Integration of flow-dependent

endothelial phenotypes by kruppel-like factor 2. *J Clin Invest* **116**, 49-58, doi:10.1172/jci24787 (2006).

20 Jain, M. K., Sangwung, P. & Hamik, A. Regulation of an inflammatory disease: Kruppel-like factors and atherosclerosis. *Arterioscler Thromb Vasc Biol* **34**, 499-508, doi:10.1161/atvbaha.113.301925 (2014).

21 Ni, C. W., Qiu, H., Rezvan, A., Kwon, K., Nam, D., Son, D. J., Visvader, J. E. & Jo, H. Discovery of novel mechanosensitive genes in vivo using mouse carotid artery endothelium exposed to disturbed flow. *Blood* **116**, e66-73, doi:10.1182/blood-2010-04-278192 (2010).

22 Schober, A., Nazari-Jahantigh, M., Wei, Y., Bidzhekov, K., Gremse, F., Grommes, J., Megens, R. T., Heyll, K., Noels, H., Hristov, M., Wang, S., Kiessling, F., Olson, E. N. & Weber, C. MicroRNA-126-5p promotes endothelial proliferation and limits atherosclerosis by suppressing dlk1. *Nat Med* **20**, 368-376, doi:10.1038/nm.3487 (2014).

23 Hajra, L., Evans, A. I., Chen, M., Hyduk, S. J., Collins, T. & Cybulsky, M. I. The NF-kappa B signal transduction pathway in aortic endothelial cells is primed for activation in regions predisposed to atherosclerotic lesion formation. *Proc Natl Acad Sci U S A* **97**, 9052-9057 (2000).

24 Zhou, G., Hamik, A., Nayak, L., Tian, H., Shi, H., Lu, Y., Sharma, N., Liao, X., Hale, A., Boerboom, L., Feaver, R. E., Gao, H., Desai, A., Schmaier, A., Gerson, S. L., Wang, Y., Atkins, G. B., Blackman, B. R., Simon, D. I. & Jain, M. K. Endothelial kruppel-like factor 4 protects against atherothrombosis in mice. *J Clin Invest* **122**, 4727-4731, doi:10.1172/jci66056 (2012).

25 Gareus, R., Kotsaki, E., Xanthoulea, S., van der Made, I., Gijbels, M. J., Kardakaris, R., Polykratis, A., Kollias, G., de Winther, M. P. & Pasparakis, M. Endothelial cell-specific NF-kappa B inhibition protects mice from atherosclerosis. *Cell Metab* **8**, 372-383, doi:10.1016/j.cmet.2008.08.016 (2008).

26 Luo, R., Zhang, W., Zhao, C., Zhang, Y., Wu, H., Jin, J., Zhang, W., Grenz, A., Eltzschig, H. K., Tao, L., Kellems, R. E. & Xia, Y. Elevated endothelial hypoxia-inducible factor-1alpha contributes to glomerular injury and promotes hypertensive chronic kidney disease. *Hypertension* **66**, 75-84, doi:10.1161/HYPERTENSIONAHA.115.05578 (2015).

27 Kuschel, A., Simon, P. & Tug, S. Functional regulation of hif-1alpha under normoxia--is there more than post-translational regulation? *J Cell Physiol* **227**, 514-524, doi:10.1002/jcp.22798 (2012).

28 Manalo, D. J., Rowan, A., Lavoie, T., Natarajan, L., Kelly, B. D., Ye, S. Q., Garcia, J. G. & Semenza, G. L. Transcriptional regulation of vascular endothelial cell responses to hypoxia by hif-1. *Blood* **105**, 659-669 (2005).

29 Zhou, Z., Subramanian, P., Sevilmis, G., Globke, B., Soehnlein, O., Karshovska, E., Megens, R., Heyll, K., Chun, J., Saulnier-Blache, J. S., Reinholz, M., van Zandvoort, M., Weber, C. & Schober, A. Lipoprotein-derived lysophosphatidic acid promotes atherosclerosis by releasing cxcl1 from the endothelium. *Cell Metab* **13**, 592-600, doi:10.1016/j.cmet.2011.02.016 (2011).

30 Oynebraten, I., Barois, N., Hagelsteen, K., Johansen, F. E., Bakke, O. & Haraldsen, G. Characterization of a novel chemokine-containing storage granule in endothelial cells: Evidence for preferential exocytosis mediated by protein kinase a and diacylglycerol. *J Immunol* **175**, 5358-5369 (2005).

31 Huo, Y., Weber, C., Forlow, S. B., Sperandio, M., Thatte, J., Mack, M., Jung, S., Littman, D. R. & Ley, K. The chemokine KC, but not monocyte chemoattractant protein-1, triggers monocyte arrest on early atherosclerotic endothelium. *J Clin Invest* **108**, 1307-1314 (2001).

32 Gu, L., Okada, Y., Clinton, S. K., Gerard, C., Sukhova, G. K., Libby, P. & Rollins, B. J. Absence of monocyte chemoattractant protein-1 reduces atherosclerosis in low density lipoprotein receptor-deficient mice. *Mol Cell* **2**, 275-281 (1998).

33 Tsou, C.-L., Peters, W., Si, Y., Slaymaker, S., Aslanian, A. M., Weisberg, S. P., Mack, M. & Charo, I. F. Critical roles for ccr2 and mcp-3 in monocyte mobilization from bone marrow and recruitment to inflammatory sites. *J Clin Invest* **117**, 902-909, doi:10.1172/jci29919 (2007).

34 Weber, K. S., von Hundelshausen, P., Clark-Lewis, I., Weber, P. C. & Weber, C. Differential immobilization and hierarchical involvement of chemokines in monocyte arrest and transmigration on inflamed endothelium in shear flow. *Eur J Immunol* **29**, 700-712. (1999).

35 Zeng, L., Zampetaki, A., Margariti, A., Pepe, A. E., Alam, S., Martin, D., Xiao, Q., Wang, W., Jin, Z. G., Cockerill, G., Mori, K., Li, Y. S., Hu, Y., Chien, S. & Xu, Q. Sustained activation of xbp1 splicing leads to endothelial apoptosis and atherosclerosis development in response to disturbed flow. *Proc Natl Acad Sci U S A* **106**, 8326-8331, doi:10.1073/pnas.0903197106 (2009).

36 Nielsen, L. B. Transfer of low density lipoprotein into the arterial wall and risk of atherosclerosis. *Atherosclerosis* **123**, 1-15 (1996).

37 Cancel, L. M. & Tarbell, J. M. The role of apoptosis in ldl transport through cultured endothelial cell monolayers. *Atherosclerosis* **208**, 335-341, doi:10.1016/j.atherosclerosis.2009.07.051 (2010).

38 Nakashima, Y., Wight, T. N. & Sueishi, K. Early atherosclerosis in humans: Role of diffuse intimal thickening and extracellular matrix proteoglycans. *Cardiovasc Res* **79**, 14-23, doi:10.1093/cvr/cvn099 (2008).

39 Steinberg, D. Low density lipoprotein oxidation and its pathobiological significance. *J Biol Chem* **272**, 20963-20966 (1997).

40 Levitan, I., Volkov, S. & Subbaiah, P. V. Oxidized ldl: Diversity, patterns of recognition, and pathophysiology. *Antioxid Redox Signal* **13**, 39-75, doi:10.1089/ars.2009.2733 (2010).

41 Sata, M. & Walsh, K. Oxidized ldl activates fas-mediated endothelial cell apoptosis. *J Clin Invest* **102**, 1682-1689, doi:10.1172/jci3531 (1998).

42 Stocker, R. & Keaney, J. F., Jr. Role of oxidative modifications in atherosclerosis. *Physiol Rev* **84**, 1381-1478, doi:10.1152/physrev.00047.2003 84/4/1381 [pii] (2004).

43 Moore, K. J., Sheedy, F. J. & Fisher, E. A. Macrophages in atherosclerosis: A dynamic balance. *Nat Rev Immunol* **13**, 709-721, doi:10.1038/nri3520 (2013).

44 Sun, Y., Ishibashi, M., Seimon, T., Lee, M., Sharma, S. M., Fitzgerald, K. A., Samokhin, A. O., Wang, Y., Sayers, S., Aikawa, M., Jerome, W. G., Ostrowski, M. C., Bromme, D., Libby, P., Tabas, I. A., Welch, C. L. & Tall, A. R. Free cholesterol accumulation in macrophage membranes activates toll-like receptors and p38 mitogen-activated protein kinase and induces cathepsin k. *Circ Res* **104**, 455-465, doi:10.1161/circresaha.108.182568 (2009).

45 Zhou, J., Lhotak, S., Hilditch, B. A. & Austin, R. C. Activation of the unfolded protein response occurs at all stages of atherosclerotic lesion development in apolipoprotein e-deficient mice. *Circulation* **111**, 1814-1821, doi:10.1161/01.cir.0000160864.31351.c1 (2005).

46 Yvan-Charvet, L., Welch, C., Pagler, T. A., Ranalletta, M., Lamkanfi, M., Han, S., Ishibashi, M., Li, R., Wang, N. & Tall, A. R. Increased inflammatory gene expression in abc transporter-deficient macrophages: Free cholesterol accumulation, increased signaling via toll-like receptors, and neutrophil infiltration of atherosclerotic lesions. *Circulation* **118**, 1837-1847, doi:CIRCULATIONAHA.108.793869 [pii] 10.1161/CIRCULATIONAHA.108.793869 (2008).

47 Shenderov, K., Riteau, N., Yip, R., Mayer-Barber, K. D., Oland, S., Hieny, S., Fitzgerald, P., Oberst, A., Dillon, C. P., Green, D. R., Cerundolo, V. & Sher, A. Cutting edge: Endoplasmic reticulum stress licenses macrophages to produce mature IL-1beta in response to TLR4 stimulation through a caspase-8- and TRIF-dependent pathway. *J Immunol* **192**, 2029-2033, doi:10.4049/jimmunol.1302549 (2014).

48 Seimon, T. A., Nadolski, M. J., Liao, X., Magallon, J., Nguyen, M., Feric, N. T., Koschinsky, M. L., Harkewicz, R., Witztum, J. L., Tsimikas, S., Golenbock, D., Moore, K. J. & Tabas, I. Atherogenic lipids and lipoproteins trigger CD36-TLR2-dependent apoptosis in macrophages undergoing endoplasmic reticulum stress. *Cell Metab* **12**, 467-482, doi:10.1016/j.cmet.2010.09.010 (2010).

49 Veillard, N. R., Steffens, S., Burger, F., Pelli, G. & Mach, F. Differential expression patterns of proinflammatory and antiinflammatory mediators during atherogenesis in mice. *Arterioscler Thromb Vasc Biol* **24**, 2339-2344, doi:10.1161/01.ATV.0000146532.98235.e6 (2004).

50 Ponnuswamy, P., Ostermeier, E., Schrottle, A., Chen, J., Huang, P. L., Ertl, G., Nieswandt, B. & Kuhlencordt, P. J. Oxidative stress and compartment of gene expression determine proatherosclerotic effects of inducible nitric oxide synthase. *Am J Pathol* **174**, 2400-2410, doi:10.2353/ajpath.2009.080730 (2009).

51 Aiello, R. J., Bourassa, P. A., Lindsey, S., Weng, W., Natoli, E., Rollins, B. J. & Milos, P. M. Monocyte chemoattractant protein-1 accelerates atherosclerosis in apolipoprotein e-deficient mice. *Arterioscler Thromb Vasc Biol* **19**, 1518-1525 (1999).

52 McGillicuddy, F. C., de la Llera Moya, M., Hinkle, C. C., Joshi, M. R., Chiquoine, E. H., Billheimer, J. T., Rothblat, G. H. & Reilly, M. P. Inflammation impairs reverse cholesterol transport in vivo. *Circulation* **119**, 1135-1145, doi:CIRCULATIONAHA.108.810721 [pii] 10.1161/CIRCULATIONAHA.108.810721 (2009).

53 Tabas, I. Macrophage death and defective inflammation resolution in atherosclerosis. *Nat Rev Immunol* **10**, 36-46, doi:10.1038/nri2675 (2010).

54 Shah, P. K., Falk, E., Badimon, J. J., Fernandez-Ortiz, A., Mailhac, A., Villareal-Levy, G., Fallon, J. T., Regnstrom, J. & Fuster, V. Human monocyte-derived macrophages induce collagen breakdown in fibrous caps of atherosclerotic plaques. Potential role of matrix-degrading metalloproteinases and implications for plaque rupture. *Circulation* **92**, 1565-1569 (1995).

55 Lee, R. C., Feinbaum, R. L. & Ambros, V. The c. Elegans heterochronic gene lin-4 encodes small RNAs with antisense complementarity to lin-14. *Cell* **75**, 843-854 (1993).

56 Lee, R. C. & Ambros, V. An extensive class of small RNAs in caenorhabditis elegans. *Science* **294**, 862-864, doi:10.1126/science.1065329 (2001).

57 Lagos-Quintana, M., Rauhut, R., Lendeckel, W. & Tuschl, T. Identification of novel genes coding for small expressed RNAs. *Science* **294**, 853-858, doi:10.1126/science.1064921 (2001).

58 Lau, N. C., Lim, L. P., Weinstein, E. G. & Bartel, D. P. An abundant class of tiny RNAs with probable regulatory roles in caenorhabditis elegans. *Science* **294**, 858-862, doi:10.1126/science.1065062 (2001).

59 Ha, M. & Kim, V. N. Regulation of microRNA biogenesis. *Nat Rev Mol Cell Biol* **15**, 509-524, doi:10.1038/nrm3838 (2014).

60 Olena, A. F. & Patton, J. G. Genomic organization of microRNAs. *J Cell Physiol* **222**, 540-545, doi:10.1002/jcp.21993 (2010).

61 Ozsolak, F., Poling, L. L., Wang, Z., Liu, H., Liu, X. S., Roeder, R. G., Zhang, X., Song, J. S. & Fisher, D. E. Chromatin structure analyses identify miRNA promoters. *Genes Dev* **22**, 3172-3183, doi:10.1101/gad.1706508 (2008).

62 Polster, B. J., Westaway, S. K., Nguyen, T. M., Yoon, M. Y. & Hayflick, S. J. Discordant expression of mir-103/7 and pantothenate kinase host genes in mouse. *Mol Genet Metab* **101**, 292-295, doi:10.1016/j.ymgme.2010.07.016 (2010).

63 Kim, V. & Nam, J. Genomics of microRNA. *Trends Genet* **22**, 165-173, doi:10.1016/j.tig.2006.01.003 (2006).

64 Han, J., Lee, Y., Yeom, K. H., Nam, J. W., Heo, I., Rhee, J. K., Sohn, S. Y., Cho, Y., Zhang, B. T. & Kim, V. N. Molecular basis for the recognition of primary microRNAs by the drosha-dgcr8 complex. *Cell* **125**, 887-901, doi:10.1016/j.cell.2006.03.043 (2006).

65 Morlando, M., Ballarino, M., Gromak, N., Pagano, F., Bozzoni, I. & Proudfoot, N. J. Primary microRNA transcripts are processed co-transcriptionally. *Nat Struct Mol Biol* **15**, 902-909 (2008).

66 Lee, Y., Ahn, C., Han, J., Choi, H., Kim, J., Yim, J., Lee, J., Provost, P., Radmark, O., Kim, S. & Kim, V. N. The nuclear RNAse III drosha initiates microRNA processing. *Nature* **425**, 415-419, doi:10.1038/nature01957 (2003).

67 Okada, C., Yamashita, E., Lee, S. J., Shibata, S., Katahira, J., Nakagawa, A., Yoneda, Y. & Tsukihara, T. A high-resolution structure of the pre-microRNA nuclear export machinery. *Science* **326**, 1275-1279, doi:10.1126/science.1178705 (2009).

68 Pasquinelli, A. E. MicroRNAs and their targets: Recognition, regulation and an emerging reciprocal relationship. *Nat Rev Genet* **13**, 271-282, doi:10.1038/nrg3162 (2012).

69 Foulkes, W. D., Priest, J. R. & Duchaine, T. F. Dicer1: Mutations, microRNAs and mechanisms. *Nat Rev Cancer* **14**, 662-672, doi:10.1038/nrc3802 (2014).

70 Park, J. E., Heo, I., Tian, Y., Simanshu, D. K., Chang, H., Jee, D., Patel, D. J. & Kim, V. N. Dicer recognizes the 5' end of RNA for efficient and accurate processing. *Nature* **475**, 201-205, doi:10.1038/nature10198 (2011).

71 MacRae, I. J., Zhou, K. & Doudna, J. A. Structural determinants of RNA recognition and cleavage by dicer. *Nat Struct Mol Biol* **14**, 934-940, doi:10.1038/nsmb1293 (2007).

72 Wilson, R. C., Tambe, A., Kidwell, M. A., Noland, C. L., Schneider, C. P. & Doudna, J. A. Dicer-trbp complex formation ensures accurate mammalian microRNA biogenesis. *Mol Cell* **57**, 397-407, doi:10.1016/j.molcel.2014.11.030 (2015).

73 Cheloufi, S., Dos Santos, C. O., Chong, M. M. & Hannon, G. J. A dicer-independent miRNA biogenesis pathway that requires AGO catalysis. *Nature* **465**, 584-589, doi:10.1038/nature09092 (2010).

74 Kwak, P. B. & Tomari, Y. The n domain of argonaute drives duplex unwinding during RISC assembly. *Nat Struct Mol Biol* **19**, 145-151, doi:10.1038/nsmb.2232 (2012).

75 Winter, J. & Diederichs, S. Argonaute proteins regulate microrna stability: Increased microRNA abundance by argonaute proteins is due to microRNA stabilization. *RNA Biol* **8**, 1149-1157, doi:10.4161/rna.8.6.17665 (2011).

76 Gantier, M. P., McCoy, C. E., Rusinova, I., Saulep, D., Wang, D., Xu, D., Irving, A. T., Behlke, M. A., Hertzog, P. J., Mackay, F. & Williams, B. R. Analysis of microRNA turnover in mammalian cells following dicer1 ablation. *Nucleic Acids Res*, doi:10.1093/nar/gkr148 (2011).

77 Guo, Y., Liu, J., Elfenbein, S. J., Ma, Y., Zhong, M., Qiu, C., Ding, Y. & Lu, J. Characterization of the mammalian miRNA turnover landscape. *Nucleic Acids Res* **43**, 2326-2341, doi:10.1093/nar/gkv057 (2015).

78 Olejniczak, S. H., La Rocca, G., Gruber, J. J. & Thompson, C. B. Long-lived microRNA-argonaute complexes in quiescent cells can be activated to regulate mitogenic responses. *Proc Natl Acad Sci U S A* **110**, 157-162, doi:10.1073/pnas.1219958110 (2013).

79 La Rocca, G., Olejniczak, S. H., Gonzalez, A. J., Briskin, D., Vidigal, J. A., Spraggon, L., DeMatteo, R. G., Radler, M. R., Lindsten, T., Ventura, A., Tuschl, T., Leslie, C. S. & Thompson, C. B. In vivo, argonaute-bound microRNAs exist predominantly in a reservoir of low molecular weight complexes not associated with mRNA. *Proc Natl Acad Sci U S A* **112**, 767-772, doi:10.1073/pnas.1424217112 (2015).

80 Ghosh, S., Bose, M., Ray, A. & Bhattacharyya, S. N. Polysome arrest restricts miRNA turnover by preventing exosomal export of miRNA in growth-retarded mammalian cells. *Mol Biol Cell* **26**, 1072-1083, doi:10.1091/mbc.E14-11-1521 (2015).

81 Hartmann, P., Schober, A. & Weber, C. Chemokines and microRNAs in atherosclerosis. *Cell Mol Life Sci* **72**, 3253-3266, doi:10.1007/s00018-015-1925-z (2015).

82 Tay, Y., Rinn, J. & Pandolfi, P. P. The multilayered complexity of ceRNA crosstalk and competition. *Nature* **505**, 344-352, doi:10.1038/nature12986 (2014).

83 Friedman, R. C., Farh, K. K.-H., Burge, C. B. & Bartel, D. P. Most mammalian mRNAs are conserved targets of microRNAs. *Genome Res* **19**, 92-105, doi:10.1101/gr.082701.108 (2009).

84 Helwak, A., Kudla, G., Dudnakova, T. & Tollervey, D. Mapping the human miRNA interactome by clash reveals frequent noncanonical binding. *Cell* **153**, 654-665, doi:10.1016/j.cell.2013.03.043 (2013).

85 Bartel, D. P. MicroRNAs: Target recognition and regulatory functions. *Cell* **136**, 215-233, doi:10.1016/j.cell.2009.01.002 (2009).

86 Ebert, M. S. & Sharp, P. A. Roles for microRNAs in conferring robustness to biological processes. *Cell* **149**, 515-524, doi:10.1016/j.cell.2012.04.005 (2012).

87 Stark, A., Brennecke, J., Bushati, N., Russell, R. B. & Cohen, S. M. Animal microRNAs confer robustness to gene expression and have a significant impact on 3'UTR evolution. *Cell* **123**, 1133-1146, doi:10.1016/j.cell.2005.11.023 (2005).

88 Bernstein, E., Kim, S. Y., Carmell, M. A., Murchison, E. P., Alcorn, H., Li, M. Z., Mills, A. A., Elledge, S. J., Anderson, K. V. & Hannon, G. J. Dicer is essential for mouse development. *Nat Genet* **35**, 215-217 (2003).

89 Yang, W. J., Yang, D. D., Na, S., Sandusky, G. E., Zhang, Q. & Zhao, G. Dicer is required for embryonic angiogenesis during mouse development. *J Biol Chem* **280**, 9330-9335, doi:10.1074/jbc.M413394200 (2005).

90 Huang, T. C., Sahasrabuddhe, N. A., Kim, M. S., Getnet, D., Yang, Y., Peterson, J. M., Ghosh, B., Chaerkady, R., Leach, S. D., Marchionni, L., Wong, G. W. & Pandey, A. Regulation of lipid metabolism by dicer revealed through silac mice. *J Proteome Res* **11**, 2193-2205, doi:10.1021/pr2009884 (2012).

91 Melkman-Zehavi, T., Oren, R., Kredo-Russo, S., Shapira, T., Mandelbaum, A. D., Rivkin, N., Nir, T., Lennox, K. A., Behlke, M. A., Dor, Y. & Hornstein, E. MiRNAs control insulin content in pancreatic beta-cells via downregulation of transcriptional repressors. *Embo j* **30**, 835-845, doi:10.1038/emboj.2010.361 (2011).

92 da Costa Martins, P. A., Bourajjaj, M., Gladka, M., Kortland, M., van Oort, R. J., Pinto, Y. M., Molkentin, J. D. & De Windt, L. J. Conditional dicer gene deletion in the postnatal myocardium provokes spontaneous cardiac remodeling. *Circ* **118**, 1567-1576, doi:10.1161/circulationaha.108.769984 (2008).

93 Suarez, Y., Fernandez-Hernando, C., Yu, J., Gerber, S. A., Harrison, K. D., Pober, J. S., Iruela-Arispe, M. L., Merkenschlager, M. & Sessa, W. C. Dicer-dependent endothelial microRNAs are necessary for postnatal angiogenesis. *Proc Natl Acad Sci U S A* **105**, 14082-14087 (2008).

94 Sissons, J. R., Peschon, J. J., Schmitz, F., Suen, R., Gilchrist, M. & Aderem, A. Cutting edge: MicroRNA regulation of macrophage fusion into multinucleated giant cells. *J Immunol* **189**, 23-27, doi:10.4049/jimmunol.1102477 (2012).

95 Albinsson, S., Suarez, Y., Skoura, A., Offermanns, S., Miano, J. M. & Sessa, W. C. MicroRNAs are necessary for vascular smooth muscle growth, differentiation, and function. *Arterioscler Thromb Vasc Biol* **30**, 1118-1126, doi:10.1161/atvbaha.109.200873 (2010).

96 Suarez, Y., Fernandez-Hernando, C., Pober, J. S. & Sessa, W. C. Dicer dependent microRNAs regulate gene expression and functions in human endothelial cells. *Circ Res* **100**, 1164-1173, doi:10.1161/01.res.0000265065.26744.17 (2007).

97 Kuehbacher, A., Urbich, C., Zeiher, A. M. & Dimmeler, S. Role of dicer and drosha for endothelial microRNA expression and angiogenesis. *Circ Res* **101**, 59-68, doi:10.1161/circresaha.107.153916 (2007).

98 Hartmann, P., Zhou, Z., Natarelli, L., Wei, Y., Nazari-Jahantigh, M., Zhu, M., Grommes, J., Steffens, S., Weber, C. & Schober, A. Endothelial dicer promotes atherosclerosis and vascular inflammation by miRNA-103-mediated suppression of klf4. *Nat Commun* **7**, 10521, doi:10.1038/ncomms10521 (2016).

99 Fang, Y., Shi, C., Manduchi, E., Civelek, M. & Davies, P. F. MicroRNA-10a regulation of proinflammatory phenotype in athero-susceptible endothelium in vivo and in vitro. *Proc Natl Acad Sci U S A* **107**, 13450-13455, doi:10.1073/pnas.1002120107 (2010).

100 Loyer, X., Potteaux, S., Vion, A. C., Guerin, C. L., Boulkroun, S., Rautou, P. E., Ramkhelawon, B., Esposito, B., Dalloz, M., Paul, J. L., Julia, P., Maccario, J., Boulanger, C. M., Mallat, Z. & Tedgui, A. Inhibition of microRNA-92a prevents endothelial dysfunction and atherosclerosis in mice. *Circ Res* **114**, 434-443, doi:10.1161/circresaha.114.302213 (2014).

101 Fang, Y. & Davies, P. F. Site-specific microRNA-92a regulation of kruppel-like factors 4 and 2 in atherosusceptible endothelium. *Arterioscler Thromb Vasc Biol* **32**, 979-987, doi:10.1161/atvbaha.111.244053 (2012).

102 Son, D. J., Kumar, S., Takabe, W., Woo Kim, C., Ni, C. W., Alberts-Grill, N., Jang, I. H., Kim, S., Kim, W., Won Kang, S., Baker, A. H., Woong Seo, J., Ferrara, K. W. & Jo, H. The atypical mechanosensitive microrna-712 derived from pre-ribosomal RNA induces endothelial inflammation and atherosclerosis. *Nat Commun* **4**, 3000, doi:10.1038/ncomms4000 (2013).

103 Sun, X., Icli, B., Wara, A. K., Belkin, N., He, S., Kobzik, L., Hunninghake, G. M., Vera, M. P., Blackwell, T. S., Baron, R. M. & Feinberg, M. W. MicroRNA-181b regulates NF-kappaB-mediated vascular inflammation. *J Clin Invest* **122**, 1973-1990, doi:10.1172/JCI61495 61495 [pii] (2012).

104 Sun, X., He, S., Wara, A. K., Icli, B., Shvartz, E., Tesmenitsky, Y., Belkin, N., Li, D., Blackwell, T. S., Sukhova, G. K., Croce, K. & Feinberg, M. W. Systemic delivery of microRNA-181b inhibits nuclear factor-kappab activation, vascular inflammation, and atherosclerosis in apolipoprotein e-deficient mice. *Circ Res* **114**, 32-40, doi:10.1161/circresaha.113.302089 (2014).

105 Cheng, H. S., Sivachandran, N., Lau, A., Boudreau, E., Zhao, J. L., Baltimore, D., Delgado-Olguin, P., Cybulsky, M. I. & Fish, J. E. MicroRNA-146 represses endothelial activation by inhibiting pro-inflammatory pathways. *EMBO Mol Med* **5**, 949-966, doi:10.1002/emmm.201202318 (2013).

106 Chen, Z., Lai, T. C., Jan, Y. H., Lin, F. M., Wang, W. C., Xiao, H., Wang, Y. T., Sun, W., Cui, X., Li, Y. S., Fang, T., Zhao, H., Padmanabhan, C., Sun, R., Wang, D. L., Jin, H., Chau, G. Y., Huang, H. D., Hsiao, M. & Shyy, J. Y. Hypoxia-responsive miRNAs target argonaute 1 to promote angiogenesis. *J Clin Invest* **123**, 1057-1067, doi:10.1172/jci65344 (2013).

107 Bartoszewska, S., Kochan, K., Piotrowski, A., Kamysz, W., Ochocka, R. J., Collawn, J. F. & Bartoszewski, R. The hypoxia-inducible miR-429 regulates hypoxia-inducible factor-1alpha expression in human endothelial cells through a negative feedback loop. *FASEB J* **29**, 1467-1479, doi:10.1096/fj.14-267054 (2015).

108 Vink, A., Schoneveld, A. H., Lamers, D., Houben, A. J., van der Groep, P., van Diest, P. J. & Pasterkamp, G. Hif-1 alpha expression is associated with an atheromatous inflammatory plaque phenotype and upregulated in activated macrophages. *Atherosclerosis* **195**, e69-75 (2007).

109 Sluimer, J. C., Gasc, J. M., van Wanroij, J. L., Kisters, N., Groeneweg, M., Sollewijn Gelpke, M. D., Cleutjens, J. P., van den Akker, L. H., Corvol, P., Wouters, B. G., Daemen, M. J. & Bijnens, A. P. Hypoxia, hypoxia-inducible transcription factor, and macrophages in human atherosclerotic plaques are correlated with intraplaque angiogenesis. *J Am Coll Cardiol* **51**, 1258-1265 (2008).

110 Nazari-Jahantigh, M., Wei, Y., Noels, H., Akhtar, S., Zhou, Z., Koenen, R. R., Heyll, K., Gremse, F., Kiessling, F., Grommes, J., Weber, C. & Schober, A. MicroRNA-155 promotes atherosclerosis by repressing bcl6 in macrophages. *J Clin Invest* **122**, 4190-4202, doi:10.1172/JCI61716 (2012).

111 Androulidaki, A., Iliopoulos, D., Arranz, A., Doxaki, C., Schworer, S., Zacharioudaki, V., Margioris, A. N., Tsichlis, P. N. & Tsatsanis, C. The kinase akt1 controls macrophage response to lipopolysaccharide by regulating microRNAs. *Immunity* **31**, 220-231, doi:10.1016/j.immuni.2009.06.024 (2009).

112 Tian, F. J., An, L. N., Wang, G. K., Zhu, J. Q., Li, Q., Zhang, Y. Y., Zeng, A., Zou, J., Zhu, R. F., Han, X. S., Shen, N., Yang, H. T., Zhao, X. X., Huang, S., Qin, Y. W. & Jing, Q. Elevated microRNA-155 promotes foam cell formation by targeting hbp1 in atherogenesis. *Cardiovasc Res* **103**, 100-110, doi:10.1093/cvr/cvu070 (2014).

113 Wei, Y., Zhu, M., Corbalan-Campos, J., Heyll, K., Weber, C. & Schober, A. Regulation of csf1r and bcl6 in macrophages mediates the stage-specific effects of microRNA-155 on atherosclerosis. *Arterioscler Thromb Vasc Biol* **35**, 796-803, doi:10.1161/ATVBAHA.114.304723 (2015).

114 Du, F., Yu, F., Wang, Y., Hui, Y., Carnevale, K., Fu, M., Lu, H. & Fan, D. MicroRNA-155 deficiency results in decreased macrophage inflammation and attenuated atherogenesis in apolipoprotein e-deficient mice. *Arterioscler Thromb Vasc Biol* **34**, 759-767, doi:10.1161/atvbaha.113.302701 (2014).

115 Pankratz, F., Bemtgen, X., Zeiser, R., Leonhardt, F., Kreuzaler, S., Hilgendorf, I., Smolka, C., Helbing, T., Hoefer, I., Esser, J. S., Kustermann, M., Moser, M., Bode, C. & Grundmann, S.

MicroRNA-155 exerts cell-specific antiangiogenic but proarteriogenic effects during adaptive neovascularization. *Circulation* **131**, 1575-1589, doi:10.1161/CIRCULATIONAHA.114.014579 (2015).

116 Dueck, A., Eichner, A., Sixt, M. & Meister, G. A miR-155-dependent microRNA hierarchy in dendritic cell maturation and macrophage activation. *FEBS letters* **588**, 632-640, doi:http://dx.doi.org/10.1016/j.febslet.2014.01.009 (2014).

117 Janssen, H. L., Reesink, H. W., Lawitz, E. J., Zeuzem, S., Rodriguez-Torres, M., Patel, K., van der Meer, A. J., Patick, A. K., Chen, A., Zhou, Y., Persson, R., King, B. D., Kauppinen, S., Levin, A. A. & Hodges, M. R. Treatment of hcv infection by targeting microRNA. *N Engl J Med* **368**, 1685-1694, doi:10.1056/NEJMoa1209026 (2013).

118 Yang, F., Wang, H., Jiang, Z., Hu, A., Chu, L., Sun, Y. & Han, J. MicroRNA-19a mediates gastric carcinoma cell proliferation through the activation of nuclear factorkappab. *Mol Med Rep* **12**, 5780-5786, doi:10.3892/mmr.2015.4151 (2015).

8 Acknowledgment

First of all, I would like to express my special appreciation and thanks to Prof. Sabine Steffens for the supervision of my PhD study.

I would like to express my sincere thanks to Prof. Andreas Schober for his support, advice and trust in my work. His enthusiasm for scientific research motivated me and from his excellent scientific knowledge I could learn a lot in the last years. I also thank Prof. Christian Weber for giving me the opportunity to work at the IPEK.

I kindly thank Shamima Akhtar for the great collaboration in the HIF-1α study and Zhou Zhe for performing the *ex vivo* perfusion experiments.

I would like to acknowledge special thanks to Yuanyuan Wei for taking her time to patiently answer all my questions and precisely introducing me in the laboratory techniques especially at the beginning of my study. I could learn a lot from her great scientific knowledge.

Special thanks go out to all my other colleagues Lucia Natarelli, Mengyu Zhu, Farima Zahedi, Maliheh Nazari-Jahantigh, Ela Karshovska and Richard Blay. Thank you for your invaluable help and support whenever I needed and all the jokes that greatly enriched the everyday life in the lab! Moreover, I would like to acknowledge the excellent technical assistance of Kathrin Heyll, Claudia Geißler, Lourdes Ruiz-Heinrich and Judith Corbalán-Campos. I am very grateful being a member of such a supportive and considerate working group.
Furthermore, I thank all the other colleagues at the IPEK, especially Xavier Blanchet for his valuable advice on my Western Blot experiments.

I thank Karola Rügamer-Biese for her kind help with all administrative issues during the last years.

Heartfelt gratitude, I would like to express to my family for their support and faith in me during any time in my life and to my friends for motivating me and having enjoyable times out of the lab.